PROBLEMS IN PROCESSING OF RADAR SIGNALS

V. K. Sloka

Foreign Technology Division
Wright-Patterson Air Force Base, Ohio

10 November 1972

FTD-MT-24-920-71

FOREIGN TECHNOLOGY DIVISION

PROBLEMS IN PROCESSING OF RADAR SIGNALS

by

V. K. Sloka

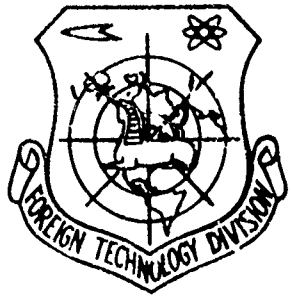

UNCLASSIFIED
Security Classification

DOCUMENT CONTROL DATA - R & D

(Security classification of title, body of abstract and indexing annotation must be entered when the overall report is classified)

1. ORIGINATING ACTIVITY (Corporate author)
Foreign Technology Division
Air Force Systems Command
U. S. Air Force

2a. REPORT SECURITY CLASSIFICATION
UNCLASSIFIED

2b. GROUP

3. REPORT TITLE

PROBLEMS IN PROCESSING OF RADAR SIGNALS

4. DESCRIPTIVE NOTES (Type of report and inclusive dates)
Translation

5. AUTHOR(S) (First name, middle initial, last name)

Sloka, V.K.

6. REPORT DATE	7a. TOTAL NO. OF PAGES	7b. NO. OF REFS
1970	277	100

8a. CONTRACT OR GRANT NO.	9a. ORIGINATOR'S REPORT NUMBER(S)
b. PROJECT NO.	FTD-MT-24-920-71
c.	9b. OTHER REPORT NO(S) (Any other numbers that may be assigned this report)
d. T70-05-02	

10. DISTRIBUTION STATEMENT

Approved for public release; distribution unlimited

11. SUPPLEMENTARY NOTES	12. SPONSORING MILITARY ACTIVITY
	Foreign Technology Division Wright-Patterson AFB, Ohio

13. ABSTRACT

Table of Contents. Preface 3. Chapter I Radar Signals and their Processing Methods 5. 2 Output Signals of Filtration Devices 30. 3 Detection of Signals on the Background of Noise and Other Signals 62. 4 Measurements of Signal Parameters 88. 5 Design Principles of Devices for Processing of Signals 103. 6 Methods for Engineering Realization of Devices for Signal Processing 145. 7 Analog Electronic Filters 160. 8 Digital Electronic Filters 192. 9 Optical Filters 221. Bibliography 248. Subject Index 253. The book deals with problems in selection of optimum radar signals and design principles of systems for their processing. The book is based on data of open Soviet and foreign literature. It was written for a wide circle of specialists working in the field of design of radio engineering systems for processing of signals; it can be useful also to post graduate and senior students of radio engineering.
AM0140207

DD FORM 1 NOV 68 1473

UNCLASSIFIED
Security Classification

14 KEY WORDS	LINK A		LINK B		LINK C	
	ROLE	WT	ROLE	WT	ROLE	WT
Radar Signal Radar Signal Analysis Radar Signal Processing Radar Detection Signal Detection Signal To Noise Ratio Electric Filter Optic Filter						

EDITED MACHINE TRANSLATION

FTD-MT-24-920-71

PROBLEMS IN PROCESSING OF RADAR SIGNALS

By: V. K. Sloka

English pages: 277

Source: Voprosy Obrabotki Radiolokatsionnykh Signalov, Sovetskoye Radio, Moscow, 1970, pp. 1-256.

Requester: FTD/PDJ

This document is a SYSTRAN machine aided translation post-edited for technical accuracy by: R. J. Zeccola.

TABLE OF CONTENTS

U. S. BOARD ON GEOGRAPHIC NAMES TRANSLITERATION SYSTEM

Block	Italic	Transliteration	Block	Italic	Transliteration
А а	*А а*	A, a	Р р	*Р р*	R, r
Б б	*Б б*	B, b	С с	*С с*	S, s
В в	*В в*	V, v	Т т	*Т т*	T, t
Г г	*Г г*	G, g	У у	*У у*	U, u
Д д	*Д д*	D, d	Ф ф	*Ф ф*	F, f
Е е	*Е е*	Ye, ye; E, e*	Х х	*Х х*	Kh, kh
Ж ж	*Ж ж*	Zh, zh	Ц ц	*Ц ц*	Ts, ts
З з	*З з*	Z, z	Ч ч	*Ч ч*	Ch, ch
И и	*И и*	I, i	Ш ш	*Ш ш*	Sh, sh
Й й	*Й й*	Y, y	Щ щ	*Щ щ*	Shch, shch
К к	*К к*	K, k	Ъ ъ	*Ъ ъ*	"
Л л	*Л л*	L, l	Ы ы	*Ы ы*	Y, y
М м	*М м*	M, m	Ь ь	*Ь ь*	'
Н н	*Н н*	N, n	Э э	*Э э*	E, e
О о	*О о*	O, o	Ю ю	*Ю ю*	Yu, yu
П п	*П п*	P, p	Я я	*Я я*	Ya, ya

* ye initially, after vowels, and after ъ, ь; e elsewhere. When written as ё in Russian, transliterate as yё or ё. The use of diacritical marks is preferred, but such marks may be omitted when expediency dictates.

FOLLOWING ARE THE CORRESPONDING RUSSIAN AND ENGLISH

DESIGNATIONS OF THE TRIGONOMETRIC FUNCTIONS

Russian	English
sin	sin
cos	cos
tg	tan
ctg	cot
sec	sec
cosec	csc
sh	sinh
ch	cosh
th	tanh
cth	coth
sch	sech
csch	csch
arc sin	$\sin^{-1}$
arc cos	$\cos^{-1}$
arc tg	$\tan^{-1}$
arc ctg	$\cot^{-1}$
arc sec	$\sec^{-1}$
arc cosec	$\csc^{-1}$
arc sh	$\sinh^{-1}$
arc ch	$\cosh^{-1}$
arc th	$\tanh^{-1}$
arc cth	$\coth^{-1}$
arc sch	sech^{-1}
arc csch	csch^{-1}
rot	curl
lg	log

This book deals with certain of the more important problems, from an engineering design standpoint, having to do with the selection of optimum radar signals and the principles underlying the development of systems for the processing of such signals. The author has discussed questions relating to the technical implementation of devices for the detection and measurement of radar signal parameters, with attention directed at the chief factors capable of causing the performance characteristics of this equipment to deviate from potentially possible values.

Also presented are the design principles involved in coherent and noncoherent signal-filtration systems and computational devices. The effect of limitation in the dynamic amplitude band of the signals to be processed on the characteristics of detection and measurement is analyzed along with a more detailed study of the structural principles embodied in analog electronic filters employing ultrasonic delay lines, discrete digital filters, as well as filters based on optical techniques of signal processing.

This book has been written with reliance on material taken from open Soviet and foreign literature. The appended bibliography will provide a source of more extensive information on whatever problem areas may have been inadequately expounded in the body of the text. The presentation is directed at a wide range of specialists working in the area of signal-processing radio system design, but will also be of interest to graduate students and students of higher technical study courses.

Foreward

In order to acquire information on the coordinates and characteristics of radar targets, the received signals at radar sites are subjected to various kinds of processing. This processing of received radar signals is effected throughout all the links of the radar, including the antenna, the receiver, the measuring units, and the computer devices, and may be characterized by the aggregate of the mathematical operations (processing algorithms) which must be carried out to determine specific signal parameters. However, despite the common mathematical essentials encountered in all the processing modes of a radar system, each individual stage has its own peculiar tasks with different instrumentation normally used. As a consequence, along with the general problem of determining the optimal algorithms for the processing of the signal as a whole - which is solved during the design phase of the radar - one is confronted with the task of selecting optimal methods of signal processing, and their implementing techniques, for each of the radar's individual stages.

The procedure whereby radar signals and the resultant data are processed can be broken down into two stages: the stage of the extraction of primary radar information and the stage of data reduction according to this primary information. The first stage is tied in with the processing (reduction) directly of the signals themselves and the extraction from these signals of the primary

radar information; this stage is customarily referred to as the primary signal-processing stage. The second stage provides for the further processing of the resultant data and is often called the secondary processing stage.

First-stage radar signal processing is handled by a number of radio devices, such as the antenna, receiver, filtering devices, and signal parameter meters. As a rule, the filtering and signal-parameter measurement equipment occupies a significant position in the overall complex of radio apparatus associated with the radar and is determinative of many of its basic characteristics. For this reason, these devices are often combined into primary signal-processing systems. Because of the sophistication and specific character of such systems, questions having to do with their rational design and performance optimization require independent analysis.

There is at the present time a sufficiently well developed theory of the synthesis and analysis of optimal radar signals and their processing methods. The key problems of this theory have been taken up in the works of Soviet scientists: S. Ye. Fal'kovich [81], V. I. Tikhonov [78], Ya. D. Shirman and V. I. Golikov [95], D. Ye. Bakman [13], A. Ye. Basharinov [6], L. S. Gutkin [23], Yu. S. Lezin [51], a team of authors under the editorial supervision of G. P. Tartarkovskiy [4], and others. Among the foreign works in this area mention might be made of the work by F. M. Woodford [16], K. Helstrom [89], and S. E. Cook [45].

However, in the design of real signal-processing systems, along with the potential capabilities as defined by the technical solutions adopted, consideration must be given to the technical difficulties encountered in the development of the actual hardware. Such factors as the sophistication, cost, dimensions, weight, and operational reliability of the systems in many cases impose limitations on the attainment of what is theoretically ideal and result in the need to modify what would otherwise be

optimal system structures. For this reason, the rational design of primary signal-processing systems capable of doing the assigned job and of simultaneously satisfying the requirements of simplicity and high performance is possible only by jointly exploiting the results of the general theory and the experience acquired in the technical implementation of individual assemblies and circuitries for such systems.

The purpose of this book is to set forth the basic methods employed in the technical implementation of the assemblies and subsystems of the primary signal-processing system, as well as to examine the major factors resulting in the deviation of real hardware characteristics from the theoretically possible.

Mr. S. S. Karinskiy collaborated in the writing of Chapter 7.

The author wishes to express his deep gratitude to S. Ye. Fal'kovich, B. N. Myateshev, and B. A. Fogel'son for their critical comments and useful advice, all of which contributed to improving the contents of this book.

1. RADAR SIGNALS AND THE METHOD OF THEIR PROCESSING

1.1. Major Tasks and Operational Modes of Systems for the Processing of Radar Signals

The acquisition of radar information is accomplished through the measurement of different parameters of the signal reflected from the target. The incoming direction (direction of arrival) of the signal (angular coordinates of the target) can be determined by measuring the difference of the phases, amplitudes, or delay time between signals as received by different antenna-equipped receivers. The range and speed of the target are determined by the measurement, respectively, of the delay time and frequency shift between the reflected and transmitted (main) signals. The extent and character of the target's motion is estimated by the results of an analysis of the phase-frequency characteristic of the reflected signals.

Various signal parameters may also be used for the resolution of the signals and their discrimination against a background of noise. Such parameters include, for example, the arrival direction of the signal, its polarization, frequency, delay time, and the like. For this purpose, either any one or several parameters simultaneously may be used.

In real radars [72] it is normally possible to discern several functionally complete systems in each of which the received radar signals are processed according to a particular parameter. Thus, for example, in the antenna and receiving systems the signals are selected according to their arrival direction and type of polarization, while in the filtration and measurement systems processing is based on such parameters as amplitude, delay time, frequency, and phase.

Considering that the problems involved in the measurement of the signals' arrival direction lend themselves to individual analysis, limited requirements can be formulated for the filtration and measurement systems which concern signal processing in the antenna-receiving system alone. The key tasks of the signal-processing system in this case will be the following:

- the detection, at the input of the receiving channels, of useful return signals to be accomplished with a high degree of reliability despite the presence at the receiver channel input of other signals and interference;

- the measurement of the parameters of reflected signals for updated target coordinate determination, to be accomplished with an assigned degree of reliability despite the presence at the receiver channel input of other signals and interference;

- the extraction of information of a noncoordinate nature, specifying the form of the target and the character of its movement, through the analysis of the fine structure of the reflected signal;

- the cleansing of primary radar information of false (spurious) signals caused by interference, for the purpose of avoiding overloads to the secondary radar information-processing systems;

- the conversion into standard message units and the codification of data acquired as a result of primary signal-processing for the introduction of such data into the secondary radar information-processing systems, the latter being normally represented by electronic digital computers.

The quality of a signal-processing system may be described by a number of indicators which reflect its informational and design-operational characteristics. The major informational indicators of a signal-processing system include the following:

- the sensitivity of the system to threshold signals;

- the resolving power of the system with respect to an assigned signal parameter;

- the accuracy of signal parameter measurement;

- the carrying capacity of the system (signal-processing and information-yield rate);

- the interference shielding (noise immunity) of the system.

The system's fundamental design-operational indicators might be:

- the reliability of the system;

- the production and operational sophistication (complexity);

- the weight and overall dimensions.

In keeping with the basic tasks to be performed by the signal-processing system, two operating conditions (modes) may be conveniently distinguished: the detection mode and the measurement mode. Depending on the tactical and technical purpose of the

radar, these modes may be combined in time or else accomplished separately [56].

By successively implementing the detection and measurement process it is possible, as a rule, to greatly simplify the structure of the measurement system. Let us consider this circumstance in greater detail by introducing the conceptual element of the system's resolution for a given parameter, taken to mean the minimal discrete value of the detuning d_i of this parameter for two signals of equal intensity at which they will be separately detected by the system with an assigned degree of statistical reliability. As will be shown below, the value of the resolution element is characterized by the region of high signal correlation for this parameter and defines, in a certain scale, the measurement accuracy for this parameter.

If the system resolves signals according to a number of parameters such as, for example, delay time τ, frequency shift Ω, and signal phase ϕ, for which the resolution elements are defined, respectively, as d_τ, d_Ω, and d_ϕ, and if there are certain *a priori* ranges of possible variation of these parameters Δ_τ, Δ_Ω, and Δ_ϕ, then the total number of the system's resolution elements will be

$$M_d = \frac{\Delta_\Sigma}{d_\Sigma}, \tag{1.1}$$

where $\Delta_\Sigma = \varphi(\Delta_\tau, \Delta_\Omega, \Delta_\varphi)$ - is the generalized range of possible parameter changes, as a function of the *a priori* regions of the individual parameters;

$d_\Sigma = \varphi(d_\tau, d_\Omega, d_\varphi)$ - is a generalized resolution element, as a function of the resolution elements of the individual parameters.

The more stringent the system's requirements for accuracy and resolution for any of the signal parameters, the smaller the resolution element d_i for that parameter must be. Reducing the

value of the resolution elements leads to a reduction in d_Σ and to a corresponding increase in the total number of resolution elements M_d.

When the region of possible signal parameter values to be measured Δ_Σ is large, requirements for high measurement and resolution accuracy result in the need to increase sharply the total number of resolution elements in the processing system, thereby substantially increasing the complexity of the system. To circumvent this contradiction, during the operation of the processing system the values Δ_Σ and d_Σ are varied in such a manner that the total number of resolution elements M_d always remains relatively small. This can be accomplished by initially, when the region of *a priori* signal parameters is large, employing a radar operating mode in which the signals and their processing systems exhibit low resolution and coarse measurement accuracy - that is, a large value for d_Σ. In this mode there is signal detection and coarse measurement of their parameters.

As the signals are detected, the system switches to a mode in which the parameters of the detected signals are refined. In this mode, signals and processing systems having higher measurement and resolution accuracy characteristics are already employed; however, since the operation in this case is based on detection-mode data, the *a priori* domain Δ_i for each of the parameters is considerably contracted and, despite the significant reduction in the value d_i, the total number of resolution elements M_d does not exceed acceptable limits.

The application of sequential methods of signal processing calls for additional time expenditures, with the consequence that systems implementing these methods possess comparatively low carrying (informational) capacity and can be used [only - *added by transator*] for limited-acquisition radars*. When processing is

*Translator's Note - The Russian term "malotselevaya RLS" literally means "a radar designed for few targets."

required for a very large number of signals simultaneously, with little time available for the processing, a parallel system-operation method must be resorted to, whereby the detection and measurement modes are combined. In this case, however, the system's accuracy and resolving power are significantly limited by factors of complexity and cost.

1.2. Radar Signals

The source of the radar information on target characteristics is that modulation of the parameters of the transmitted signals which occurs as these signals propagate and are reflected from the target. Normally, the transmitted radar signal is a narrow-band harmonic oscillation modulated in amplitude and phase. Analytically, the transmitted signal can be expressed by the dependence

$$u_з(t) = \sqrt{2P}v(t) = \sqrt{2P}A_0(t)\cos[\omega_0 t + \varphi(t) + \varphi_з] = \\ = A(t)\cos[\omega_0 t + \varphi(t) + \varphi_з]. \tag{1.2}$$

where P is the mean power of the signal;

v(t) is the normed value of the signal;

$A_0(t)$ is the law of amplitude modulation;

A(t) is the amplitude of the signal (envelope);

ω_0 is the circular carrier frequency of the transmitted signal;

$\phi(t)$ is the law of phase modulation;

$\phi_з$ is the initial phase of the transmitted signal [Translator's Note - The subscript letter "з" has the sense here of "transmitted"].

The functions v(t) and $A_0(t)$ are normalized in such a way that

$$\int_{-\infty}^{\infty} v^2(t)\,dt = \frac{1}{2} T_{э\phi},$$

$$\int_{-\infty}^{\infty} A_0^2(t)\,dt = T_{э\phi}, \tag{1.3}$$

where $T_{э\phi}$ is referred to as the effective duration of the signal.

The energy of the transmitted signal is expressed by the formula

$$E = \int_{-\infty}^{+\infty} u_э^2(t)\,dt = PT_{э\phi}. \tag{1.4}$$

The propagation and reflection of the radar signal from the target results in a time delay in the signal, as well as a change in its intensity and initial phase. With allowance for these changes, the voltage of the radio signal reflected from the target at the receiving channel input may be expressed as

$$u_{от}(t) = \varepsilon_0 \varepsilon(t) \sqrt{2P} A_0[t - \tau_э(t)] \cos\{\omega_0[t - \tau_э(t)] + \varphi[t - \tau_э(t)] + \varphi_{от}(t)\}, \tag{1.5}$$

where ε_0 is the signal attenuation factor taking into account the change in the intensity of the signal during propagation and reflection for an effective target scattering cross-section of average value;

$\varepsilon(t)$ is a coefficient taking into account random intensity fluctuations in the reflected signal;

$\phi_{от}(t)$ is the random initial phase of the reflected signal, including the initial phase of the transmitted signal and its

variations during the process of propagation and reflection [Translator's Note - Subscript letters "от" indicate "reflected"];

$\tau_з(t)$ is the delay time for the parameters of the reflected signal for a given moment of time.

The delay time is determined by the relation

$$\tau_з(t) = \frac{2R(t)}{c}, \tag{1.6}$$

where R(t) is the distance from the radar to the target at a given moment of time;

c is the propagation velocity of electromagnetic waves.

As a rule, the law governing the fluctuation in the intensity of the reflected signal and the changes of its resultant initial phase are not known *a priori*, so that these parameters of the reflected signal are random. The random change in the initial phase of the signal limits the time interval during which its coherent processing is possible. This time interval is customarily called the coherence interval of the signal. It is defined as the segment of time during which random variation in the phase characteristics of the reflected signal does not yet introduce significant changes in its parameters.

To determine the variation in the signal's parameters, with a time lag in the signal, we expand the function $\tau_з(t)$ by degrees $(t - t_0)$ for the observation interval, where t_0 is a specified fixed moment of time. Now

$$\tau_з(t) = \tau_з + (t - t_0)\tau'_з + \frac{1}{2}(t - t_0)^2\tau''_з + \\ + \frac{1}{6}(t - t_0)^3\tau'''_з + \dots. \tag{1.7}$$

where

$$\tau_3 = \frac{2R(t_0)}{c}; \quad \tau'_3 = \frac{2R'(t_0)}{c}.$$

The values $R'(t_0)$ and $R''(t_0)$ define, respectively, the radial velocity and acceleration of the target at the moment of time t_0.

The presence of a complex time dependence in the time-delay function $\tau_3(t)$ of the reflected signal leads to a transformation of its structure. Depending on whether the target is approaching or drawing away from the radar, the reflected signal is, respectively, compressed or extended in time. In general this results in a change in its carrier frequency ω_0 (Doppler effect) and also in distortions in its amplitude and phase modulation.

The Doppler frequency shift is defined as

$$\Omega_д = \omega_0 \frac{2R'(t_0)}{c} = \omega_0 \tau'_3. \tag{1.8}$$

[Translator's Note - Subscript letter "д" indicates "Doppler"]. It is not always necessary to make allowance for the amplitude and phase modulation distortions of the signal.

Amplitude modulation distortions may be disregarded, provided the change in the delay of the signal τ'_3 during the time of its processing $T_{об}$ is much less than the resolution element for that parameter d_τ, that is

$$\tau'_3 \ll \frac{d_\tau}{T_{об}} \cong \frac{1}{T_{об}\Delta W}, \tag{1.9}$$

where ΔW is the rms value of the spectrum of the signal [Translator's Note - Subscript letters "об" indicate "processing"].

Condition (1.9) is satisfied in many instances since even with the target traveling at speeds close to the first cosmic

(orbital) velocity $\left(R'(t_0) \sim 8 \cdot 10^3 \frac{\text{m}}{\text{s}}\right)$, the change in the delay time is such as to fulfill the inequality

$$T_{\text{ог}} \Delta W < 10^4. \tag{1.10}$$

The distortions in the phase modulation of the signal, which in the case of a constant radial acceleration are characterized by linear frequency modulation in the reflected signal, may be disregarded if the changes in the frequency of the signal during the time of its coherent processing $T_{\text{ког}}$ do not exceed the resolution element for the frequency d_Ω. This condition is met whenever

$$R''(t_0) \ll \frac{\pi c}{T^2_{\text{ког}} \omega_0}. \tag{1.11}$$

[Translator's Note - Subscript letters "ког" indicate "coherent."]

As will be evident from relation (1.11), the need to take into account phase modulation distortions in the radar signal occurs whenever the coherent processing time of the signal exceeds 0.01 s.

Inasmuch as in the detection and measurement mode the signal-processing time is normally limited, inequalities (1.9) and (1.11) are satisfied. Therefore, in the simplest case for the moment of time $t_0 = \tau_э$ the reflected signal can be represented by a function of time and the four parameters $\tau_э$, $\Omega_д$, $\varepsilon(t)$, $\varphi_0(t)$, that is

$$u_{\text{от}}(t) = \varepsilon_0 \varepsilon(t) \sqrt{2P} A_0(t - \tau_э) \cos[(\omega_0 - \Omega_д) t + \varphi(t - \tau_э) + \varphi_0(t)], \tag{1.12}$$

where

$$\varphi_0(t) = \varphi_{\text{от}}(t) - (\omega_0 - \Omega_д) \tau_э.$$

If the signal-observation time is sufficiently large, the presence of frequency modulation in the signal cannot be disregarded, and the reflected signal is expressed by the relation

$$u_{0т}(t) = \varepsilon_0 \varepsilon(t) \sqrt{2P} A_0 (t - \tau_з) \cos \left[(\omega_0 - \Omega_д) t - \frac{1}{2} \Omega'_д t^2 + \right.$$
$$\left. + \frac{\Omega'_д}{\omega_0} \tau_з t + \varphi(t - \tau_з) + \varphi_1(t) \right], \qquad (1.13)$$

where

$$\varphi_1(t) = \varphi_{0т}(t) - (\omega_0 - \Omega_д) \tau_з - \frac{1}{2} \Omega'_д \tau_з^2.$$

The value of $\Omega'_д$ describes the rate of change of the signal's Doppler frequency and defines the radial acceleration of the target:

$$\Omega'_д = \frac{2\omega_0 R''(t_0)}{c}. \qquad (1.14)$$

For the super-resolution mode, when the coherent processing interval of the signal and its bandwidth are considerably larger and inequality (1.10) is not satisfied, it is necessary to take into account the presence of other additional parameters in the reflected signal defined by the higher-powered terms of series (1.7).

Radar signals and the execution of their various transformations may be conveniently described through the use of complex functions [16, 81, 89]. The complex signal U(t) depicting the real signal is defined as

$$U(t) = u(t) + j\hat{u}(t). \qquad (1.15)$$

Here, $\hat{u}(t)$ is related to the signal u(t) by the Hilbert

transform, that is

$$\hat{u}(t)=\frac{1}{\pi}\int_{-\infty}^{\infty}\frac{u(z)}{t-z}\,dz. \tag{1.16}$$

The real signal u(t) is identified in this case with the real part of the complex signal by the dependence

$$u(t)=\operatorname{Re}U(t)=\frac{1}{2}[U(t)+U^{*}(t)]. \tag{1.17}$$

(Here and throughout the sign * indicates a complex conjugate value.)

The complex, energy-normed, narrow-band signal may be written in the following form:

$$V(t)=S(t)\exp[j(\omega_0 t+\varphi)], \tag{1.18}$$

where S(t) is the complex envelope or modulation function corresponding to

$$S(t)=A_0(t)\exp[j\varphi(t)]$$

and normalized so that

$$\int_{-\infty}^{\infty}|S(t)|^2\,dt=T_{эф}. \tag{1.19}$$

The energy of the signal represented by the complex function may be defined by the expression

$$E=\frac{1}{2}\int_{-\infty}^{\infty}|U(t)|^2\,dt. \tag{1.20}$$

The spectrum of the modulation function S(t) is expressed by the dependence

$$S(\omega) = \int_{-\infty}^{\infty} S(t) \exp(-j\omega t)\, dt. \tag{1.21}$$

If the reference point on the frequency and time axes is selected so that

$$\frac{\int_{-\infty}^{\infty} \omega |S(\omega)|^2 d\omega}{\int_{-\infty}^{\infty} |S(\omega)|^2 d\omega} = 0 \tag{1.22}$$

and

$$\frac{\int_{-\infty}^{\infty} t |S(t)|^2 dt}{\int_{-\infty}^{\infty} |S(t)|^2 dt} = 0, \tag{1.23}$$

then, according to [89], the dispersion of the signal's energy spectrum may be defined as

$$\Delta W^2 = \frac{\int_{-\infty}^{\infty} \omega^2 |S(\omega)|^2 d\omega}{\int_{-\infty}^{\infty} |S(\omega)|^2 d\omega} = \frac{\int_{-\infty}^{\infty} |S'(t)|^2 dt}{\int_{-\infty}^{\infty} |S(t)|^2 dt}, \tag{1.24}$$

and the dispersion of the signal's time extension ΔT in the form

$$\Delta T^2 = \frac{(2\pi)^2 \int_{-\infty}^{\infty} t^2 |S(t)|^2 dt}{\int_{-\infty}^{\infty} |S(t)|^2 dt} = \frac{(2\pi)^2 \int_{-\infty}^{\infty} |S'(\omega)|^2 d\omega}{\int_{-\infty}^{\infty} |S(\omega)|^2 d\omega}. \tag{1.25}$$

The values ΔW^2 and ΔT^2 describe, respectively, the dispersion of the spectral components of the signal in terms of frequency and of its envelope in terms of time. The parameter ΔT we shall call the rms value of the time extension of the signal.

The signals's phase structure characteristic is determined by the so-called effective phase constant ρ, which is expressed by the relation

$$\rho = \frac{2\pi \int_{-\infty}^{\infty} t\varphi'(t) |S(t)|^2 dt}{\int_{-\infty}^{\infty} |S(t)|^2 dt}. \qquad (1.26)$$

The signal characteristics discussed above (1.24), (1.25), and (1.26) are interrelated by the following inequality [89]:

$$\Delta W^2 \Delta T^2 - \rho^2 \geq \pi^2. \qquad (1.27)$$

1.3. Radar Interference

As a rule, radar signals are always accompanied by interference. The form and character of the interference affecting radar systems may differ. In terms of its origin, such interference may be natural or artificial; in terms of character, active or passive. The different kinds of active and passive interference, and also the characteristics of many of these interference types. have been discussed at considerable length in the technical literature [4, 7, 70, 78, 89].

Active and passive intereference functions independently of the signal. It is added to the signal, and the resultant oscillation in this case can be represented in the form

$$X(t) = U(t) + N(t), \qquad (1.28)$$

where X(t) is the complex resultant oscillation;

U(t) is the useful signal;

N(t) is the additive interference.

Multiplicative interference takes the form of signal distortion (modulation). Its effect is detectable only when a signal is present. Interference of this kind is described by an additional factor in the composition of the resultant oscillation - for example, an amplitude factor:

$$X(t) = \varepsilon_n(t) U(t), \qquad (1.29)$$

where $\varepsilon_n(t)$ is a time function giving rise to parasitic amplitude modulation of the signal [Translator's Note - Subscript letter "n" indicates "parasitic"].

As a consequence of its random character, interference is analytically described by random time functions which are characterized by a probability distribution density or by numerical characteristics in the form of moments of distribution. Normally, stationary or quasistationary random processes are considered, for which the statistical characteristics do not change in time.

According to its distribution law, interference is conventionally divided into two kinds: Gaussian and non-Gaussian interference.

The Gaussian variety includes interference which is described in terms of random processes with a multidimensional normal distribution law of probability density. This category covers most real interference such as, for example, internal receiver noise, cosmic and ionospheric noise, various man-made noise interference (jamming), and passive interference.

An important feature of normal processes is the fact that they are totally defined by their mixed second-order moment (correlation function) $B(\tau)$ or spectral density $N(f)$, a factor which simplifies considerably the mathematical operations involved. The spectral density of the interference power (energy spectral density) is linked to the interference correlation function by the Fourier transform [78]:

$$B(\tau) = \int_{-\infty}^{\infty} N(f) \exp(j2\pi f\tau)\, df, \tag{1.30}$$

where τ is the time shift of the correlated functions.

From (1.30), when $\tau = 0$, it follows that the interference fluctuation power equals

$$B(0) = \sigma_n^2 = \int_{-\infty}^{\infty} N(f)\, df, \tag{1.31}$$

where σ_n^2 is the dispersion of the interference [Translator's Note - Subscript letter "n" here indicates "interference"].

For broad-band interference, when the spectral intensity of the noise within the interval of the working frequency range of the signals or passband of the filtering systems remains approximately constant, one may conveniently call upon the white noise model, for which the spectral density remains constant for all frequencies. In this case we can set

$$N'(f) = \frac{1}{2} N_0 = \text{const}, \tag{1.32}$$

where N_0 is the real (located only in the positive frequency region) energy spectral density of the white noise.

For interference, transmitted by the filter, with frequency

characteristic K(f) the spectral density of the interference at the filter output is defined as

$$N(f)_{вых} = |K(f)|^2 N(f)_{вх}, \tag{1.33}$$

where $N(f)_{вх}$ is the energy spectral density at the filter input [Translator's Note - Subscript letters "вх" and "вых" indicate "input" and "output," respectively].

Now, the interference fluctuation power at the filter output will be

$$\sigma^2_{пф} = \int_{-\infty}^{\infty} |K(f)|^2 N(f)_{вх} df. \tag{1.34}$$

[Translator's Note - Subscript letter "ф" indicates "filter."]
If

$$N(f)_{вх} = \frac{1}{2} N_0,$$

then

$$\sigma^2_{пф} = N_0 K^2(f)_{макс} \Delta F, \tag{1.35}$$

[Translator's Note - Subscript letters "макс" indicate "max"]
where ΔF is the equivalent passband of the real filter, defined as

$$\Delta F = \frac{\int_{-\infty}^{\infty} |K(f)|^2 df}{|K(f)|^2_{макс}}, \tag{1.36}$$

$K(f)_{макс}$ is the maximum value of the filter transmission factor.

Setting $K(f)_{макс} = 1$, we obtain

$$\sigma^2_{пф} = N_0 \Delta F. \tag{1.37}$$

Passive interference caused by reflections from a large number of independent reflectors is usually defined [4] by a correlation function of the kind

$$B(\tau, \tau_э) \cong \mathrm{Re}\,\mu_п(\tau_э)\, r_п(\tau, \tau_э) T_{эф} \Psi(\tau, 0) \exp[j(\omega_0 + \Omega_п)\tau], \qquad (1.38)$$

where $\mu_п(\tau_э)$ is the density distribution of the intensity of the passive interference for the delay time;

$r_п(\tau, \tau_э)$ is the normalized correlation coefficient of the passive interference fluctuations (maximum value does not exceed 1);

$\Psi(\tau, 0)$ is the normalized value of the autocorrelation function for the modulation of the transmitted signal;

$\Omega_п$ is the Doppler shift on the center frequency of the interference.

Whenever for all practical purposes the spectral density of the interference is concentrated in a narrow band, as is in the case of narrow-band signals, the interference may be represented in the form of a harmonic oscillation randomly modulated in amplitude and phase [78]. In this case, the additive mixture of narrow-band signal and noise can be expressed as an amplitude- and phase-modulated oscillation:

$$x(t) = \mathrm{Re}\,X(t) = A_x(t)\cos[\omega_0 t + \varphi(t) + \varkappa_x(t) + \varphi_0], \qquad (1.39)$$

where ϕ_0 is the initial phase of the reflected signal.

$A_x(t)$ and $\kappa_x(t)$ are random functions slowly changing in time. The complex envelope for an oscillation of this kind is represented in the form

$$S_x(t) = A_x(t)\exp j[\varphi(t) + \varkappa_x(t) + \varphi_0]. \qquad (1.40)$$

1.4. Algorithms and Structural Circuits for the Optimal Processing of Radar Signals

As has already been noted above, the detection of signals and the measurement of their parameters under condition of various kinds of interference constitute the principal tasks of signal-processing radar systems. For this reason, the optimization of the system's operating algorithms must be primarily aimed at those indicators that describe the quality with which the system performs these missions.

The presence of interference and random fluctuations in the parameters of the signals to be processed carries the problem of signal detection and parameter measurement into the area of statistical solution theory, on the basis of which an optimal signal-processing system can be broken down into two basic devices: an optimal signal filtering device and a resolving (logical processing) device (Fig. 1.1).

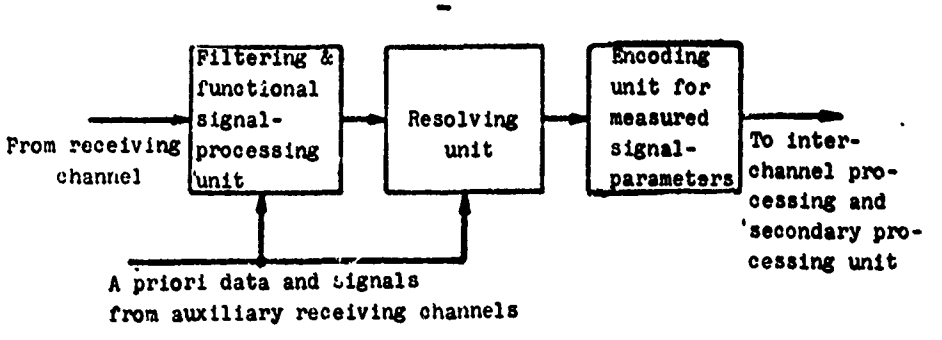

Fig. 1.1. Simplified block diagram of signal-processing.

The optimal filtering unit, which ensures the best discrimination of the signal from the interference and its resolution, must shape at its output a certain "signal relief" describing the distribution of the *a posteriori* probability. The resolving unit

must provide an analysis of this signal relief and, in accordance with the criterion selected, furnish a decision as to the existence of a signal or else make an estimate of its parameter to be measured.

The distribution of the *a posteriori* probability density for the presence of a signal P_{pc} [x(t)] in the input oscillation x(t) or for the value of any parameter to be measured in this signal corresponds, to within a constant factor, to the product of the *a priori* probability density P_{pr} and a certain function L [x(t)] referred to as the likelihood function [78], that is

$$P_{pc}[x(t)] = c_0 P_{pr} L[x(t)], \tag{1.41}$$

where c_0 is a constant coefficient.

In the case of radar systems, the *a priori* probability density distribution for the presence of a signal or the value of its parameter within a definite range of values may be assumed to be uniform. Therefore, for both signal-detection and parameter-measurement assignments the optimal filtration unit must shape at its output a signal pattern portraying either the likelihood function or a monotonic dependence of this function. Normally, this function will be a logarithmic dependence of the type ln L[x(t)].

The received radar echo signal may be represented as a function of time and a series of parameters in the form

$$Au(t, \alpha, \beta), \tag{1.42}$$

where A is a discrete random parameter which describes the presence or absence of a signal and assumes one of the values 1 or 0, respectively;

α is a random fixed parameter assumed to be unchanging during the processing time of the signal, or a set of parameters (delay

time $\tau_з$, Doppler frequency shift $\Omega_д$, rate of change of Doppler frequency shift $\Omega'_д$. The distribution of these parameters in a certain interval Δ_α is assumed to be uniform);

β is a random unfixed parameter or set of parameters (initial signal phase $\phi_0(t)$, its intensity $\varepsilon(t)$).

The probability density distributions for these parameters are regarded as known.

Parameters A and α are generally informational and are therefore frequently referred to as substantive. Parameter β does not, as a rule, carry information (non-substantive) and is excluded through averaging from the likelihood relation.

A likelihood function must be formed for all the values of the parameter α within its anticipated range of values Δ_α. Practical difficulties are normally encountered in the formation and analysis of the likelihood function for the continuum of parameter α values. For this reason, real filtering devices form the likelihood function only for a series of discrete values for parameter α (α_1, α_2, ..., α_i). If the discrete increment for the reading of the parameters has been correctly selected, the results will be acceptably close to optimal. In this way, an optimal filtering unit must shape a signal pattern to portray the aggregate of likelihood function values for a series of parameters α_1, α_2, ..., α_i.

The operating logic is somewhat differ .t in the case of the resolver for the signal-detection and parameter-measurement modes.

When the likelihood function is formed from any input oscillation containing a signal from a single target with an unknown parameter α and noise, for the detection mode the resolver compares the value of the function $\ln L(\alpha_i)$ in the anticipated range of parameters α values against a certain threshold h_0.

which is the *a posteriori* probability function of interference (Fig. 1.2). The decision as to the presence of a signal is taken for those regions of parameter α where

$$\ln L(\alpha_i) \geqslant h_0. \tag{1.43}$$

In the figure this corresponds to the region $\Delta_\alpha^0 = \alpha_4 - \alpha_8$. Now, the probability of inequality (1.43) being fulfilled in the event the signal actually exists is known as the probability of correct detection and is written as D, whereas the probability that inequality (1.43) will be satisfied with the absence of a signal at the input of the processing system is called the false-alarm probability and is designated by the letter F.

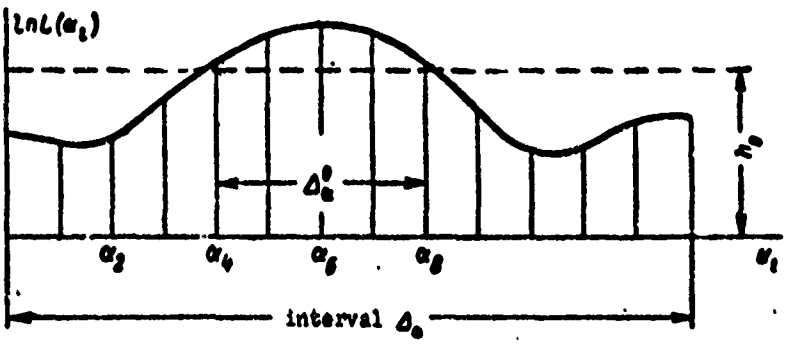

Fig. 1.2. Resolver operating logic in detection and measurement mode.

The selection of the threshold level in radar-processing systems is generally based on the Neuman-Pearson test, according to which the probability of correct detection is maximized for an assigned probability of false alarm. That characteristic which determines the dependence of the probability of correct detection on the parameters of the signal and interference for a prescribed false-alarm value is often called the detection characteristic. An enumeration of these characteristics for different detection systems is cited in the literature [81, 95]. A point to be noted is that in the signal-detection mode a rough estimate is also made of the signal's parameters (the parameter α value interval in which

the threshold is exceeded; Fig. 1.2). The measured data are used as an *a priori* interval for the fine-measurement mode for this parameter.

In the fine-measurement mode for parameter α the resolving unit analyzes the function $\ln L(\alpha_i)$ in the interval Δ^{o}_{α} and furnishes for the parameter to be measured an estimate which may be designated as α^{0}.

If the distribution functions of parameter α are symmetrical, its statistically best estimate can be obtained by the maximum likelihood method [78, 81]. In keeping with this method, the resolver must seek the maximum of function $\ln L(\alpha_i)$ in the range of values of parameter Δ^{o}_{α}. In Fig. 1.2 this estimate corresponds to α_6.

Because of the presence of interference and a variety of distortions in the signal, the estimate arrived at for the signal parameter will differ from its true value. The accuracy of a measurement system can be described in terms of measurement errors.

The form of the optimum signal-processing algorithms which characterize the operations involved in the formation of the *a posteriori* probabilities or likelihood functions is largely dependent both on the nature of the interference present in the signal mix at the input to the processing system and on the character and spatial distribution of the targets affecting the quality and parameters of the signals simultaneously received at the processing system input. The great multiplicity of interference types and possible signal-parameter distribution combinations makes the task of optimum processing in general form a difficult one in any event. At the present time, the most complete solutions for the detection, resolution, and measurement of signal parameters in the presence of noise have been formulated for only a limited kind of interference and for the simplest distrubutions in the parameters of the overlapping signals. The

major findings of this theory have been set forth in sufficient detail in [4, 6, 78, 81, 89, 95]. It follows from these studies that whenever the form and frequency of the echo signals are known and when there is no signal overlap in time at the input to the processing system, with the noise distribution close to normal, the functional diagram of a signal-processing channel to implement an optimum algorithm for signal detection or parameter measurement can be represented in the manner shown in Fig. 1.3.

The filtering unit forms a monotonic dependence on the likelihood function, with the latter in this case a function of the single information parameter $\tau_э$.

From this same diagram it will be evident that the function $\ln L(\tau_э)$ is formed by two circuitries: the coherent filtering circuit and the noncoherent signal-processing circuit. This kind of processing algorithm is optimum for the general situation when the signal is not coherent over the entire interval of its duration. It should be noted that in a number of instances coherent-noncoherent processing methods are also applied to a fully coherent signal; in this case, to simplify the processing circuits, the coherence of the signal is deliberately disregarded over a specified interval of its duration. In this way, the processing algorithm for such a signal becomes quasi-optimal.

A system for the optimum filtering of a coherent signal in t the case of Gaussian interference and known parameters $\Omega_д$ and $\Omega'_д$ must provide for the execution of a correlation operation for the oscillation x(t) incoming to its input with a certain anticipated (reference) signal $v_0(t, \tau_э)$, which is a function of the time t and the parameter $\tau_э$ describing the time lag of the signal. The output effect of the circuit can now be expressed by means of complex functions as

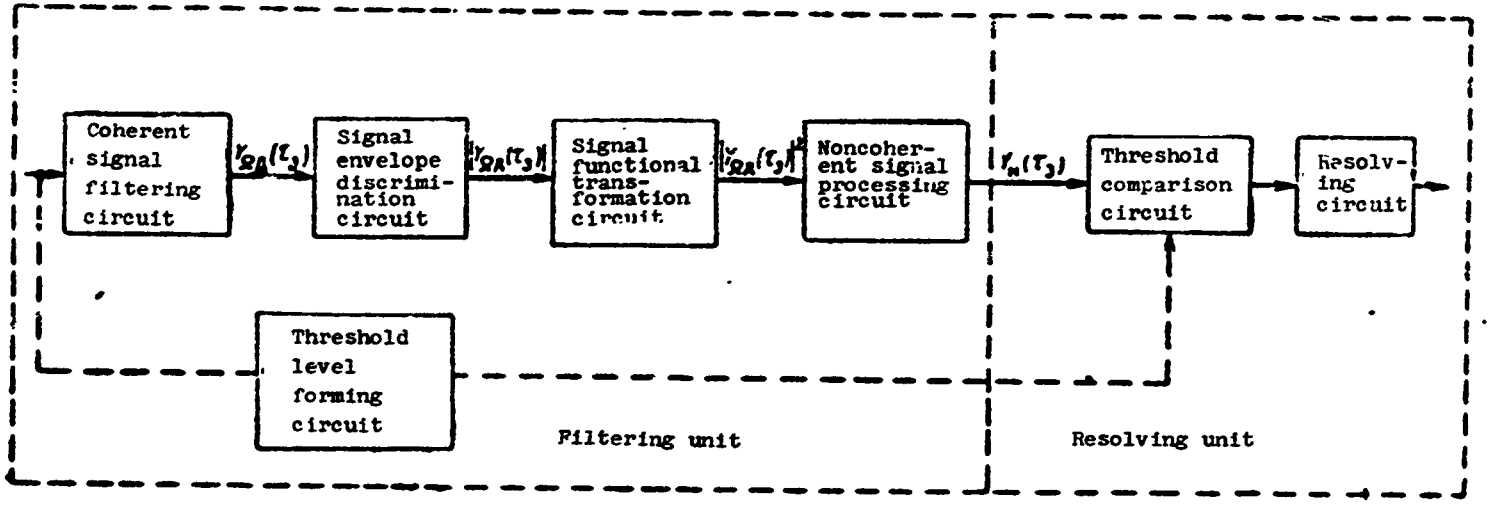

Fig. 1.3. Block diagram of a single-signal optimum processing channel.

$$y(\tau_3) = \frac{1}{2} \operatorname{Re} Y_{\Omega_д \Omega'_д}(\tau_3) =$$

$$= \frac{1}{2} \operatorname{Re} \exp[j\psi(\tau_3)] \left| \int_{-\infty}^{\infty} S_x(t) S^*_0(t - \tau_3)\, dt \right| =$$

$$= \frac{1}{2} |Y_{\Omega_д \Omega'_д}(\tau_3)| \cos[\psi(\tau_3)], \qquad (1.44)$$

where the integrands define, respectively, the complex envelope of the input oscillation (1.40) and the reference signal; $\psi(\tau_э)$ is the resultant phase of the output effect, determining its oscillation as the delay time $\tau_э$ changes.

From the output of the coherent filtration circuit the oscillation reaches the envelope detector, where its envelope $|Y_{\Omega_д \Omega'_д}(\tau_э)|$ is separated out. This operation eliminates the phase and frequency dependence of the signal. The resultant video signal is subjected to functional transformation and noncoherent processing which provides an additional improvement in the signal/noise ratio.

Normally, the noncoherent processing of the signal can be ultimately resolved to operations of the type

$$Y_н(\tau_3) = \sum_k b_k^2 |Y_{\Omega_д}(\tau_3)|_k^2 \qquad (1.45)$$

or

$$Y_н(\tau_3) = \sum_k b_k |Y_{\Omega_д}(\tau_3)|_k, \qquad (1.46)$$

where $|Y_{\Omega д}(\tau_э)|k$ is the k-th component of the envelope of the output effect of the coherent filiration circuit;

b_k is a certain weighting factor [Translator's Note - Subscript letter "н" in (1.45) and (1.46) indicates "noncoherent"].

The noncoherent signal-processing circuit performs the weighted summation of the envelopes of the signals from the output of the coherent filtering unit at specified moments of time [81, 95]. The oscillation $Y_н(\tau_э)$ from the output of the noncoherent processor is compared against the threshold and analyzed, following which a decision is made as to the reliability of either hypothesis.

Whenever the interference intensity is unknown or changes in time, the threshold level is a function of the parameters of the input signal x(t) and must be regulated, as indicated by the broken line in Fig. 1.3, by a signal from the threshold level shaping circuit [81].

In the event the parameters $\Omega_д$ and $\Omega'_д$ of the reflected signal are unknown and capable of variation within wide limits, the filtration unit must provide for the formation of a monotonic function of the likelihood ratio which will depend not only on $\tau_э$, but also on fixed discrete values of the parameters $\Omega_{дi}$ and $\Omega'_{дi}$. The result, in this case is a multichannel signal-processing system, as portrayed in Fig. 1.4. The resolver performs the threshold comparison and analysis of the output effect from the individual channel, as well as the comparison of its values between the channels. Meanwhile, as in Fig. 1.3 already considered, a determination is made for the detected signals of those regions for the parameters $\tau_э$, $\Omega_д$ and $\Omega'_д$ in which the threshold is exceeded and an estimate is provided regarding the values of those parameters.

If an oscillation containing time-overlapping signals (multiple target) reaches the input of the signal-processing system, then interference noise is generated in the detection channels because of the presence of correlations between the signals. The output effect components from some signals are imposed on the output effects of others. The processes of signal detection and parameter estimation in this case, rather than

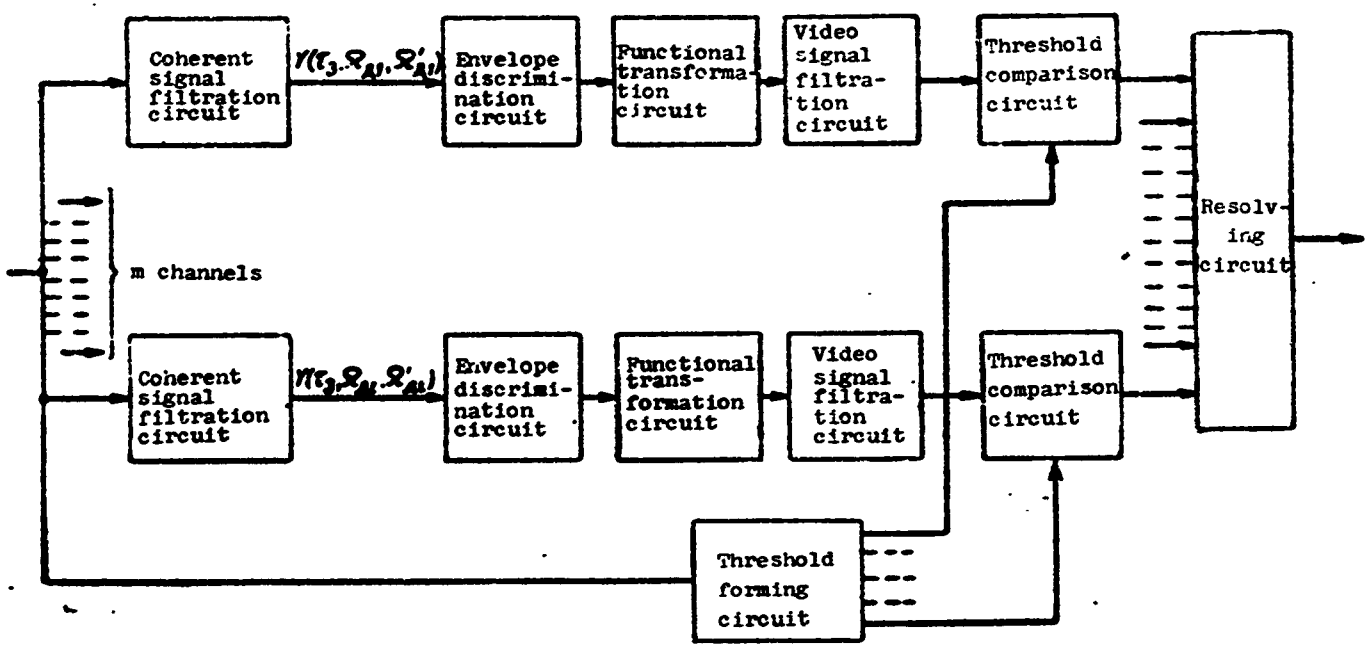

Fig. 1.4. Block diagram of a multichannel processing system.

proceeding independently for each signal individually, are also related to the interaction of these signals. The input oscillation must then be so processed as to ensure the separate detection of the signals and the estimation of their parameters - or, stated otherwise, the system must provide for the resolution of the signals.

In the discussion that follows, we shall understand by the term "signal resolution" that process as a result of which a given signal is detected or its parameters are evaluated, with assigned characteristics, when there is present at the input of the system a set of other signals whose parameters may change within specified limits. The resolving power for any parameter in this situation will be characterized by the resolution element d_i (1.1). When the number of signals and their parameters $\tau_э$ and $\Omega_д$ are known, then, as is evident from [4, 6, 89], an optimum system implementing the detection of the signal $S_1(t)$ to be resolved must form and match against a threshold an output effect proportional to a correlation intergral of the form

$$Y = \int_{-\infty}^{\infty} S_x(t) S^*_{экв}(t)\, dt, \qquad (1.47)$$

where Y is the maximum value of the output effect of the coherent filtration system for the signal to be resolved [Translator's Note - Subscript letters "экв" indicate "equivalent"];

$$S_{экв}(t) = S_1(t) - \left[\sum_{i=2}^{i=n} \eta_i S_i(t),\right.$$

$S_1(t)$, $S_i(t)$ are the complex envelopes of the signal to be resolved and the interfering signal, respectively;

η_i are weight coefficients determined by the correlation characteristics of the signal;

n is the total number of signals.

Since when dealing with radar systems the parameter values of the signal to be resolved and the interfering signals are not normally known beforehand, operation (1.47) must in this case be simultaneously performed for a large number of discrete parameter τ and Ω values. The signal-processing circuitry will now contain a large number of fairly complex channels. As a result of the fact that considerable difficulties are encountered in the design of such multichannel signal-processing systems and, because of equipment instability, the values of the correlation coefficients η_i are subject to random changes, optimal signal-resolution circuitry is used only rarely in real systems, if at all. Increasingly extensive application is being made in practical circuit arrangements of resolution algorithms employing mismatch filtering methods or nonlinear signal-processing techniques [6, 45, 71, 78].

The mismatch filtering method consists in having the characteristics of the reference signal in the filtering unit deliberately mismatched to some degree with respect to the characteristics of the anticipated signal. A reference signal is selected having the the kind of structure that will ensure that, with permissible degradation in the detection characteristics of the useful signal embedded in Gaussian noise, there will be minimal intercorrelation between the reference signal and the interfering signals within a certain range of variation in their parameters.

In the case of nonlinear processing the technique calls for nonlinear transformations of the input oscillation before it is fed to the matched filter. For a number of signal types this ensures their independent amplitude normalization, resulting in improved resolution conditions [70].

Whenever the interference distribution differs radically from the normal - for example, when the interference is of a pulsed

nature - ahead of the coherent filtering circuit an optimum signal-processing channel contains nonlinear elements and variable-parameter circuits whose function is the amplitude limiting of the input oscillations and their gating in time [2, 76]. In the simplest case, such a processing channel may appear as shown in Fig. 1.5. From the practical standpoint, this kind of processing channel arrangement is the most general since nonlinear circuits and variable-parameter circuits may also be encountered in signal-processing systems in the face of Gaussian noise as well. In this instance, the presence of such circuitries may be dictated by the need to limit the dynamic amplitude range of the oscillation to be processed for the reason that this range may far exceed the linearity interval of real circuitries for the filtering and logical processing of the signal.

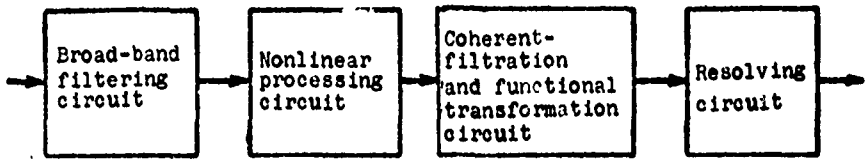

Fig. 1.5. Block diagram of processing channel with pulsed interference.

From the foregoing remarks it should be clear that optimum signal-processing algorithms require the availability of rather sophisticated devices for the filtering and logical processing of the signals, particularly if the radar's operational procedure entails variations in the character of the interference and in the parameter distribution of the echo signals. The practical implementation of these kind of complex signal-processing units is no easy matter, as a consequence of which the real equipment found in sophisticated processing systems normally execute quasi-optimal algorithms which to a permissible degree merely approach the optimal. The factors affecting the quasi-optimality of a signal-processing algorithm may be different and are largely determined by the form of the signal, the parameters of the

interference, and the structure of the processing system. For this reason, the extent to which the algorithms deviate from the optimal is best evaluated during the immediate consideration of the principles which are to govern the design and technical realization of the specific systems and the appropriate signal-processing equipment.

2. OUTPUT SIGNALS OF FILTER DEVICES

2.1. Regular Component of Oscillations at Filter Equipment Output

In most cases the output effect of the filtering devices can be represented as the sum of the regular and random components reflecting a certain functional transformation of the input oscillation:

$$Y(\tau_3, \Omega_\Delta, \Omega'_\Delta) = U_y[x(t)] + N_y[x(t)], \tag{2.1}$$

whereby the regular component $U_y[x(t)]$ is normally defined as the cross-correlation function, or its modulus, of the modulation function of the received and reference signals; that is

$$U_y(\tau_3, \Omega_\Delta, \Omega'_\Delta) = \\ = k_y \left| \int_{-\infty}^{\infty} S(t) S_0(t, \tau_3, \Omega_\Delta, \Omega'_\Delta)\, dt \right| \exp[j\psi_y(\tau_3)]. \tag{2.2}$$

The random component $N_y[x(t)]$ characterizes the cross correlation between the modulation function $S_N(t)$ of the input interference $N(t)$ and the modulation function of the reference signal; that is

$$N_y(\tau_3, \Omega_\Delta, \Omega'_\Delta) = \\ = k_y \left| \int_{-\infty}^{\infty} S_N(t) S_0(t, \tau_3, \Omega_\Delta, \Omega'_\Delta)\, dt \right| \exp[j\psi_N(\tau_3)]. \tag{2.3}$$

where k_y is a constant coefficient; $\psi_y(\tau_э)$, $\psi_N(\tau_э)$ is the resultant phase of the regular and random coefficients.

The component $U_y(\tau_э, \Omega_д, \Omega'_д)$ in this case is a regular function which defines the signal at the filtering device output when no interference is present. The random component $N_y(\tau_э, \Omega_д, \Omega'_д)$ describes the oscillation fluctuations at the output of the filtering system when no signal is present. The presence of this component leads to a distortion in the character of the regular component and causes the occurrence of additional surges in the output effect, resulting in various kinds of errors in the solution of specific problems.

By way of example, Fig. 2.1. presents a graphic representation of the envelopes of the regular and random components of a certain output effect which is a function of only the two parameters $\tau_э$ and $\Omega_д$. Parameter $\tau_э$ is depicted as a continuous function of time, while parameter $\Omega_д$ displays fixed values determined by the number of the filtering channel. The resultant output effect envelope $|Y(\tau_э, \Omega_д)|$ in each channel exhibits many overshoots caused by the regular and random components. If the regular component level is high, its peaks exceed the random surges and are recorded by the resolving device (the signals are detected). The position of these maximum values with respect to time and channels defines the value of the $\tau_э$ and $\Omega_д$ parameters of the signal, while the rate of decline of the regular component in the vicinity of its maxima describes the accuracy and resolution of the measurement system.

Since the structure of the regular component is largely responsible for the characteristics of signal detection against a background of noise and of signal parameter measurement, the function which describes this regular component is of independent interest.

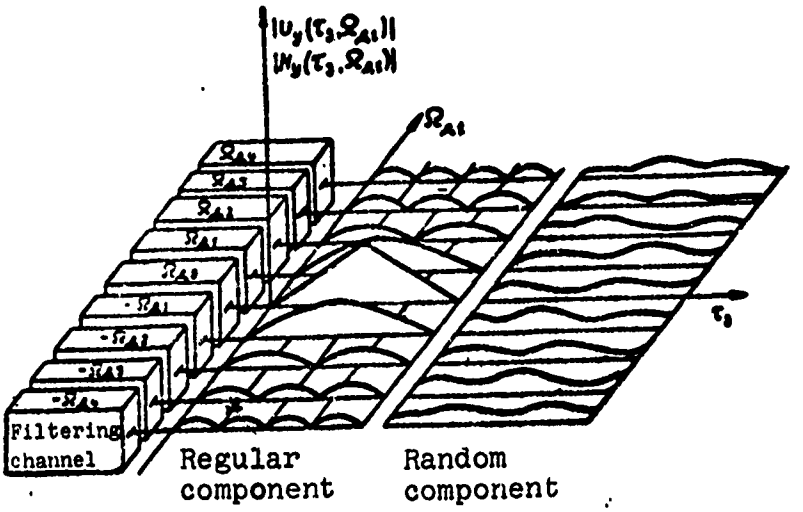

Fig. 2.1. Graphic representation of regular and random output effect components.

When the reflected signal is defined by an aggregate of fixed parameters $\tau_{э0}$ and $\Omega_{д0}$, the regular component at the output of a linear filtering system may be represented in complex form as follows:

$$U_y(\tau, \Omega) = k_y \exp[j\psi_1(\tau)] \int_{-\infty}^{\infty} S(t) S^*_0(t-\tau) \exp(j\Omega t)\, dt, \qquad (2.4)$$

where τ, Ω is the difference of the corresponding parameter of the received and reference signals

$$\tau = \tau_{э0} - \tau_э, \quad \Omega = \Omega_{д0} - \Omega_д;$$

where S(t) is the modulation function of the received signal;

$S_0(t)$ is the modulation function of the reference signal;

$$\psi_1(\tau) = (\omega_0 + \Omega_д)\tau.$$

The normed regular component (2.4) defines the cross-correlation function between the input signal u(t) and a certain reference signal $u_0(t)$, whence its designation as the signal correlation function. When the reference signal is matched with the form of the transmitted signal, expression (2.4) describes the autocorrelation function of the signal.

The integral in expression (2.4) is known as modulation correlation function and can be expressed in the form

$$\Psi_0(\tau, \Omega) = \int_{-\infty}^{\infty} S(t) S^*_0(t-\tau) \exp(j\Omega t)\, dt = \\ = \frac{1}{2\pi} \int_{-\infty}^{\infty} S^*(\omega) S_0(\omega - \Omega) \exp(j\omega\tau)\, d\omega. \qquad (2.5)$$

If the reference signal and transmitted signals are matched, the modulation correlation function (2.5) is transformed into the modulation autocorrelation function $\Psi(\tau, \Omega)$.

The square of the modulus of the signal autocorrelation function $|\Psi(\tau, \Omega)|^2$ is called the indeterminacy function, while the square of the correlation function modulus $|\Psi_0(\tau, \Omega)|^2$ we shall, by analogy with the first, refer to as the reciprocal indeterminacy function.

In accordance with Schwartz's inequality and relation (1.19), for the reciprocal indeterminacy function we can write

$$|\Psi_0(\tau, \Omega)|^2 \leq T_{э\Phi} T_{0\,э\Phi}. \qquad (2.6)$$

Now, for the indeterminacy function we have

$$|\Psi(\tau, \Omega)|^2 \leq T^2_{э\Phi} = |\Psi(0, 0)|^2. \qquad (2.7)$$

From (2.7) and (2.8) [sic] it follows that the maximum value of the reciprocal indeterminacy function does not exceed the value $T_{эф}T_{0\ эф}$, and the indeterminacy function - the value $T^2_{эф}$. The indeterminacy function acquires its maximum value at the coordinate origin and possesses the property of central symmetry; that is

$$|\Psi(\tau, \Omega)|^2 = |\Psi(-\tau, -\Omega)|^2. \qquad (2.8)$$

Inequalities (2.6) and (2.7) are used to norm the functions

$$|\Psi_0(\tau, \Omega)|^2 \quad \text{and} \quad |\Psi(\tau, \Omega)|^2. \qquad (2.9)$$

The normed functions are defined by the dependences:

$$|\Psi_0(\tau, \Omega)|^2_н = \frac{1}{T_{эф}T_{0\ эф}}\left|\int_{-\infty}^{\infty} S(t)\,S^*_0(t-\tau)\exp(j\Omega t)\,dt\right|^2. \qquad (2.10)$$

$$|\Psi(\tau, \Omega)|^2_н = \frac{1}{T^2_{эф}}\left|\int_{-\infty}^{\infty} S(t)\,S^*(t-\tau)\exp(j\Omega t)\,dt\right|^2. \qquad (2.11)$$

From this point on, only normed functions will be used, and in the interests of notational simplicity they will not be designated by a special symbol.

2.2. Basic Properties of the Indeterminacy Function

The indeterminacy function and the reciprocal indeterminacy function (2.10) and (2.11) represent surfaces of the arguments τ and Ω.

By way of example, Fig. 2.2 illustrates the indeterminacy function for a radio pulse

$$S(t) = 1(t, T)\exp(j\omega_0 t),$$

where 1(t, T) is a single, rectangular cut-off time function of duration T.

Practical filtering circuits normally have a finite number of channels tuned to a different value of the signal frequency. As a consequence, the output signals of the processing channels are defined by the section of the indeterminacy function for the corresponding frequency shifts Ω_i (Fig. 2.1).

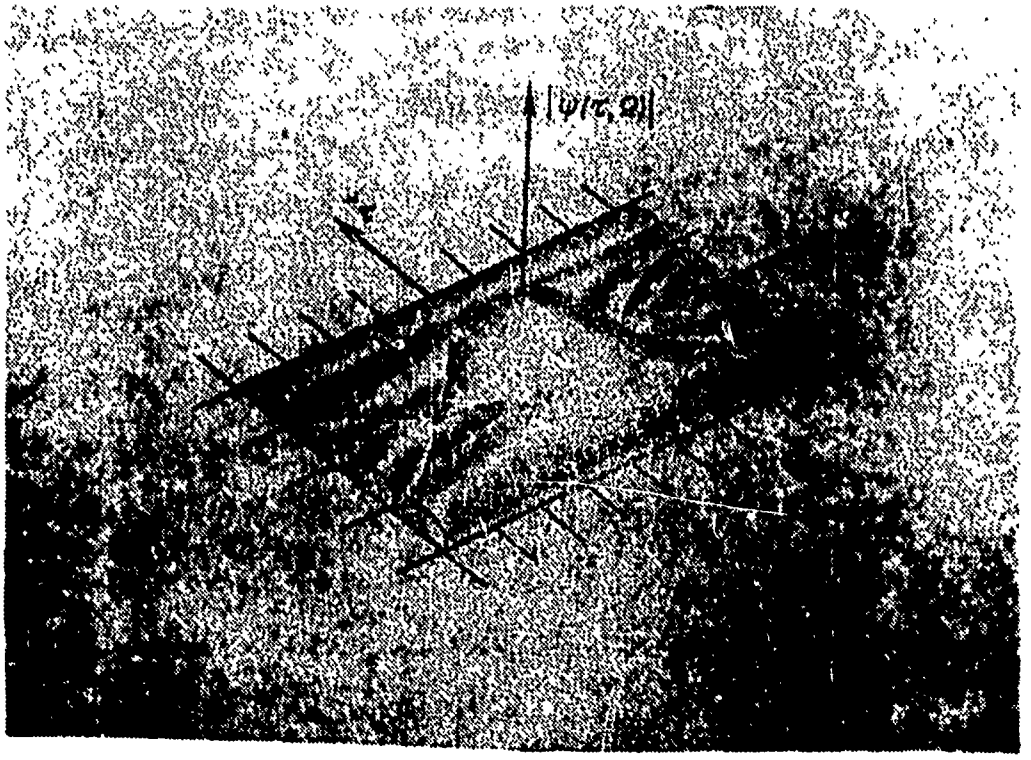

Fig. 2.2. Surface of the indeterminacy function of a squarewave radio pulse.

For analytical purposes, indeterminacy functions are usually approximated by cylindrical surfaces whose heights define the value of the function to be approximated in a given region of the

parameters τ and Ω. The functions may be conveniently represented in this event through the use of topographical methods involving lines of equal level. For a qualitative analysis a sufficient condition is the amplitude quantification of the indeterminacy functions into three levels defining the high-correlation region, the side-lobe region, and the zero-value region of the function. By expanding the indeterminacy function in the vicinity of the zero arguments into a double Taylor series and disregarding terms higher than the third order, then, with allowance for definitions (1.24) - (1.26), one obtains the following dependence:

$$|\Psi(\tau, \Omega)|^2 \cong 1 - \tau^2 \Delta W^2 - 2\tau\nu\rho - \nu^2 \Delta T^2, \qquad (2.12)$$

where ν is the frequency shift equal to $\nu = \frac{\Omega}{2\pi}$.

Relation (2.12) expresses the approximation of the central peak of the indeterminacy function. The peak section on the level representing 0.75 of the maximum defines the so-called "ellipse of uncertainity" [89]:

$$\tau^2 \Delta W^2 + 2\tau\nu\rho + \nu^2 \Delta T^2 = \frac{1}{4}. \qquad (2.13)$$

This ellipse is shown in Fig. 2.3. The width of the ellipse along the τ and ν axes defines the extent of the central peak (high-correlation interval) $\tau_н$ and $\nu_н$ of the indeterminacy function on the 0.75 level for its sections $(\tau,0)$ and $(0, \nu)$, respectively. This quantity, as we shall show below, describes the measurement accuracy of the time lag and frequency of the signal, as well as the resolving power for these parameters. In [89] it has been demonstrated that the area of the ellipse of uncertainty is limited only by an upper bond, this being expressed by the dependence

$$(\Delta W^2 \Delta T^2 - \rho^2)^{1/2} \geq 2. \qquad (2.14)$$

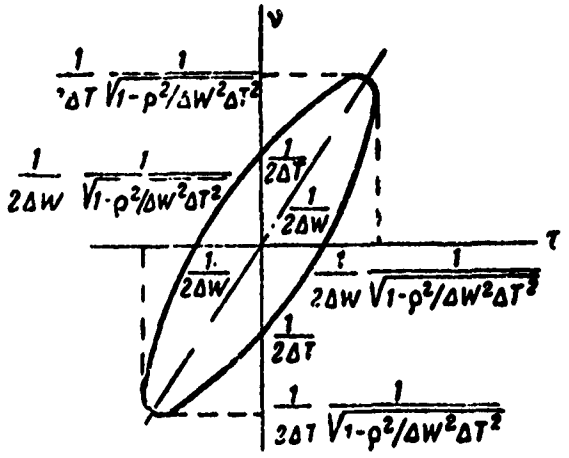

Fig. 2.3. Ellipse of "uncertainty."

By modifying the form of the signal, the area of the ellipse and also its width along the τ and ν axes may be made as small as desired.

Another important feature of the indeterminacy function, defining the resolution of signals and their processing systems, is its integral dependence as an expression of what is known as the indeterminacy principle. The essence of the indeterminacy principle consists in the fact that the space beneath the surface of the indeterminacy function and reciprocal indeterminacy function is independent of the form of the main and reference signals and, with appropriate norming, is a constant quantity.

In effect, considering that the correlation function is a Fourier transform of the product $S(t)S_0^*(t-\tau)$, on the basis of Parseval's equality we can write

$$\int_{-\infty}^{\infty} |\Psi_0(\tau, \nu)|^2 d\nu = \frac{1}{T_{эф} T_{эф}} \int_{-\infty}^{\infty} |S(t)|^2 |S^*_0(t-\tau)|^2 dt. \qquad (2.15)$$

Integrating the right and left sides of equality (2.15) for τ and substituting the variables $z = t + \tau$, we obtain

$$\iint_{-\infty}^{\infty} |\Psi_0(\tau, \nu)|^2 d\nu d\tau =$$

$$= \frac{1}{T_{0\phi} T_{0\Phi}} \int_{-\infty}^{\infty} |S(t)|^2 dt \int_{-\infty}^{\infty} |S_0(z)|^2 dz = 1, \qquad (2.16)$$

and for the indeterminacy function, respectively,

$$\iint_{-\infty}^{\infty} |\Psi(\tau, \nu)|^2 d\nu d\tau = 1. \qquad (2.17)$$

The space beneath the indeterminacy surface is like a heap of sand. By changing the form of the transmitted and reference signals, we change the configuration of the heap, but we are unable to do away with so much as a single grain of sand [30]. In this way, unlike the area of the ellipse of uncertainty, which can be varied by the structure of the signal, the volume of the indeterminacy body is independent of the signal structure.

In any analysis of the resolution and noise-immunity of processing systems a key characteristic is the sectional area of the indeterminacy cross function as defined by planes parallel to the τ and ν axes (Fig. 2.4). For example,

$$\int_{-\infty}^{\infty} |\Psi_0(\tau, \nu_t)|^2 d\tau$$

or

$$\int_{-\infty}^{\infty} |\Psi_0(\tau_t, \nu)|^2 d\nu.$$

This characteristic reflects the general character of the decay of these functions along the time-lag and frequency-shift direction. Let us designate these characteristics as $A_{\tau 0}(\nu)$ and $A_{\nu 0}(\tau)$, respectively, calling them accordingly the effective

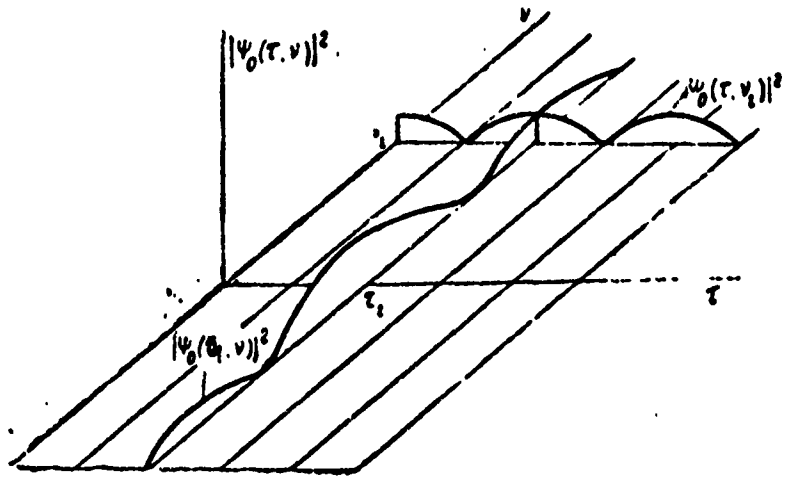

Fig. 2.4. Indeterminacy function section.

extent of the reciprocal indeterminacy function along the τ and ν axis as appropriate.

To determine the function $\Lambda_{\tau_0}(\nu)$, we shall use an expression for the normed modulation correlation function in terms of the spectral characteristics of the signal:

$$\Psi_0(\tau,\ \nu)=\frac{1}{\sqrt{T_{0\phi}T_{0\partial}}}\int_{-\infty}^{\infty}S^*(f)\,S_0(f-\nu)\exp(j2\pi f\tau)\,df. \qquad (2.18)$$

As in the case of (2.15), we may write

$$\Lambda_{\tau_0}(\nu)=\int_{-\infty}^{\infty}|\Psi_0(\tau,\ \nu)|^2\,d\tau=\frac{1}{T_{0\phi}T_{0\partial}}\int_{-\infty}^{\infty}|S^*(f)\,S_0(f-\nu)|^2\,df. \qquad (2.19)$$

Considering that the energy spectrum of the modulation equals

$$G(f)=|S(f)|^2=\int\Psi(\tau,\ 0)\exp(-j2\pi f\tau)\,d\tau, \qquad (2.20)$$

after simple operations we have

$$\Lambda_{\tau_0}(\nu)=\int_{-\infty}^{\infty}\Psi^*(\tau,\ 0)\,\Psi_1(\tau,\ 0)\exp(-j2\pi\nu\tau)\,d\tau. \qquad (2.21)$$

where $\Psi_1(\tau,\ \nu)$ is the autocorrelation function for the modulation of the signal $S_0(t)$.

In the event there is matching of the transmitted and reference signals, we have

$$\Lambda_\tau(\nu)=\int_{-\infty}^{\infty}|\Psi(\tau,\ 0)|^2\exp(-j2\pi\nu\tau)\,d\tau=$$

$$=\frac{1}{T_{эф}^2}\int_{-\infty}^{\infty}|S(f)|^2\,|S(f-\nu)|^2\,df. \qquad (2.22)$$

The area of the reciprocal indeterminacy function section with a plane parallel to the ν axis can be described by the dependence

$$\Lambda_{\nu_0}(\tau)=\int_{-\infty}^{\infty}|\Psi_0(\tau,\ \nu)|^2\,d\nu=$$

$$=\int_{-\infty}^{\infty}\Psi(0,\ \nu)\,\Psi^*_1(0,\ \nu)\exp(j2\pi\nu\tau)\,d\nu. \qquad (2.23)$$

By analcgy, for the indeterminacy function we obtain

$$\Lambda_\nu(\tau)=\int_{-\infty}^{\infty}|\Psi(\tau,\ \nu)|^2d\nu=\int_{-\infty}^{\infty}|\Psi(0,\ \nu)|^2\exp(j2\pi\nu\tau)\,d\nu=$$

$$=\frac{1}{T_{эф}^2}\int_{-\infty}^{\infty}|S(t)|^2\,|S(t-\tau)|^2\,dt. \qquad (2.24)$$

From (2.22) and (2.24) it follows, specifically, that the sectional areas of the normed indeterminacy function, which define, respectively, the so-called resolution constants [16] for time and frequency $\Lambda_\tau(0)$ and $\Lambda_\nu(0)$, will equal

$$\Lambda_\tau(0)=\frac{1}{T_{эф}^2}\int_{-\infty}^{\infty}|S(f)|^4\,df=\frac{1}{T_{эф}^2}\int_{-\infty}^{\infty}G^2(f)\,df, \tag{2.25}$$

$$\Lambda_\nu(0)=\frac{1}{T_{эф}^2}\int_{-\infty}^{\infty}|S(t)|^4\,dt=\frac{1}{T_{эф}^2}\int_{-\infty}^{\infty}A_0^4(t)\,dt. \tag{2.26}$$

Using the definition of the effective frequency interval Δ_e and effective time T_e introduced by Woodford [16], we arrive at

$$W_e=\frac{T_{эф}^2}{\int_{-\infty}^{\infty}G^2(f)\,df}, \tag{2.27}$$

$$T_e=\frac{T_{эф}^2}{\int_{-\infty}^{\infty}A_0^4(t)\,dt}. \tag{2.28}$$

Considering expressions (2.25)-(2.28), we obtain the following dependences:

$$\begin{aligned}\Lambda_\tau(0)W_e&=1,\\ \Lambda_\nu(0)T_e&=1.\end{aligned} \tag{2.29}$$

From this last expression it will be evident that the area of the indeterminacy function section along the τ and ν axes depends on the form of the signal and can be made arbitrarily small. For its reduction along the τ axis the signal must exhibit a wider and uniform energy spectrum, while its reduction along the ν axis

requires that the signal be of great extent and that its envelope be uniform.

It is to be noted that such signal characteristics as the dispersion of its time extension ΔT^2 (1.25) along with the high-correlation interval $\nu_к$ (2.13) and effective extent of the indeterminacy function $\Lambda_v(\tau)$ (2.24) for frequency depend only on the signal envelope. Therefore, for signals with different frequency or phase modulation but with identical envelopes these characteristics will be equivalent. Conversely, such characteristics as the dispersion of the signal spectrum ΔW^2 (1.29), the high-correlation interval $\tau_к$ (2.13), and the effective extent of the indeterminacy function $\Lambda_v(\nu 0)$ (2.22) for the time lag are determined only by the signal's energy spectrum and are equivalent for signals with different envelopes but with identical energy spectra. This fact is illustrated in Table 2.1.

Table 2.1.

Signal mode U(t)	$\lvert\Psi(\tau, \nu)\rvert^2$ Form of indeterminacy function	Root-mean-square value of signal spectrum and time extension		High-correlation interval (for 0.75 level)		Resolution constants	
		ΔF	ΔT	$\tau_н$	$\nu_н$	$A_\tau = \frac{1}{W_e}$	$A_\nu = \frac{1}{T_e}$
Radio pulse with Gaussian envelope $\exp\left(-\frac{\pi}{2}\frac{t^2}{T_{эф}^2}\right)\exp(j2\pi f_0 t)$	$\exp\left[-2\pi\left(\frac{\tau^2}{4T_{эф}^2}+T_{эф}^2\nu^2\right)\right]$	$\sqrt{\frac{\pi}{2}}\frac{1}{T_{эф}}$	$\sqrt{2\pi}T_{эф}$	$\sqrt{\frac{2}{\pi}}\times$ $\times\sqrt{1{,}15}T_{эф}$	$\frac{\sqrt{1{,}15}}{\sqrt{2\pi}T_{эф}}$	$\sqrt{2}T_{эф}$	$\frac{1}{\sqrt{2}T_{эф}}$
Radio pulse with square-wave envelope $\begin{cases}\exp(j2\pi f_0 t), & \lvert t\rvert\le\frac{T_{эф}}{2},\\ 0, & \lvert t\rvert>\frac{T_{эф}}{2}\end{cases}$	$\begin{cases}\left\{\frac{\sin[\pi\nu(T_{эф}-\lvert\tau\rvert)]}{\pi\nu T_{эф}}\right\}^2 & \lvert\tau\rvert<T_{эф}\\ 0 & \lvert\tau\rvert>T_{эф}\end{cases}$	$\frac{3}{2}\frac{\pi}{T_{эф}}$	$\frac{\pi}{\sqrt{3}}T_{эф}$	$(2-\sqrt{3})T_{эф}$	$\frac{1}{\sqrt{3}T_{эф}}$	$\frac{2}{3}T_{эф}$	$\frac{1}{T_{эф}}$
LFM radio pulse with square-wave envelope $\begin{cases}\exp\left[j2\pi\left(f_0+\frac{F_m}{2\Delta T}t\right)t\right], & \lvert t\rvert\le\frac{T_{эф}}{2},\\ 0, & \lvert t\rvert>\frac{T_{эф}}{2},\end{cases}$ F_m – frequency deviation	$\left\{\frac{\sin\left[\pi\left(K_{см}\frac{\tau}{T_{эф}}+\nu T_{эф}\right)\times\left(1-\frac{\lvert\tau\rvert}{T_{эф}}\right)\right]}{\pi\left(K_{см}\frac{\tau}{T_{эф}}+\nu T_{эф}\right)}\to\dots\right\}^2$ $K_{см}=F_m\Delta T$	$\sqrt{2\pi}F_m$	$\frac{\pi}{\sqrt{3}}T_{эф}$	$\frac{1}{\sqrt{\pi}F_m}$	$\frac{1}{\sqrt{3}T_{эф}}$	$\frac{1}{F_m}$	$\frac{1}{T_{эф}}$
LFM radio pulse with Gaussian envelope $\exp\left(-\frac{\pi}{2}\frac{t^2}{T_{эф}^2}\right)\exp\times$ $\times\left[j2\pi\left(f_0+\frac{F_m}{2\Delta T}t\right)t\right]$	$\exp\left\{-2\pi\left[\frac{(1+4K_{см})\tau^2}{4\Delta T^2}+T_{эф}^2\nu^2+2K_{см}\nu\tau\right]\right\}$	$\sqrt{2\pi}F_m$	$\sqrt{2\pi}T_{эф}$	$\frac{\sqrt{1{,}15}}{\sqrt{2\pi}F_m}$	$\frac{\sqrt{1{,}15}}{\sqrt{2\pi}T_{эф}}$	$\frac{1}{\sqrt{2}F_m}$	$\frac{1}{\sqrt{2}T_{эф}}$

Table 2.1. (Continued)

Signal mode U(t)	$\lvert\Psi(\tau,\nu)\rvert^2$ Form of indeterminacy function	Rcot-mean-square value of signal spectrum and time extension		High-correlation interval (for 0.75 level)		Resolution constants	
		ΔF	ΔT	τ_n	ν_n	$\Lambda_\tau = \frac{1}{\Delta F_e}$	$\Lambda_\nu = \frac{1}{T_e}$
Phase-keyed radio pulse $\left\{\begin{array}{l}\sum\limits_{i=0}^{i=N-1} l_n(t-iT_n, T_n)g_i\times \\ \times\exp(j\varphi_i t),\ \lvert t\rvert \leqslant \frac{T_{\text{эф}}}{2}, \\ 0, \quad \lvert t\rvert > \frac{T_{\text{эф}}}{2}\end{array}\right.$	$\left[\frac{\sin(\pi\nu T_{\text{эф}})}{\pi\nu T_{\text{эф}}}\right]^2\left(1-\frac{\lvert\tau\rvert}{T_n}\right)\ \lvert\tau\rvert<T_n$ $\frac{1}{N}\left[\frac{\sin(\pi\nu T_n)}{\pi\nu T_n}\right]^2\ \lvert\tau\rvert\geqslant T_n$ (approximate value)	$\frac{3\pi}{2T_n}$	$\frac{\pi}{\sqrt{3}}T_{\text{эф}}$	$(2-\sqrt{3})\,T_n$	$\frac{1}{\sqrt{3}}T_{\text{эф}}$	$\frac{7}{6}T_n$	$\frac{1}{T_{\text{эф}}}$
Sequence of radio pulses $\left\{\begin{array}{l}\sum\limits_{i=0}^{i=N} A_{\text{or}}(t)\,S_n(t-iT_n, T_n)\times \\ \times\exp(j2\pi f_0 t),\ \lvert t\rvert \leqslant \frac{T_{\text{эф}}}{2}, \\ 0, \quad \lvert t\rvert > \frac{T_{\text{эф}}}{2}\end{array}\right.$ $S_n(t)$ – modulation function of single pulse $A_{\text{or}}(t)$ – envelope of pulse burst	$\sum\limits_{i=-N}^{i=N}\lvert\Psi_n(\tau-iT_n,\ \nu)\rvert^2\times$ $\times\sum\limits_{k=-\infty}^{k=+\infty}\left\lvert\Psi_{\text{or}}\left(\tau,\ \nu-\frac{k}{T_n}\right)\right\rvert^2$ $\lvert\Psi_n(\tau,\nu)\rvert^2$ – indeterminacy function of single pulse $S_n(t)$ $\lvert\Psi_{\text{or}}(\tau,\nu)\rvert^2$ – indeterminacy function of envelope $A_{\text{or}}(t)$	single pulse $S_n(t)$	envelope $A_{\text{or}}(t)$	single pulse $S_n(t)$	envelope $A_{\text{or}}(t)$	$\frac{\Lambda_{\tau_n}}{T_n}\Lambda_{\tau_{\text{or}}}$ Λ_{τ_n} single pulse $S_n(t)$	$T_n\Lambda_{\nu_n}\times$ $\times\Lambda_{\nu_{\text{or}}}$ $\Lambda_{\tau_{\text{or}}}$ envelope $A_{\text{or}}(t)$

2.3. Indeterminacy Functions of Characteristic Radar Signals

Considered below are the indeterminacy functions for several frequently encountered radar signals.

Bell-shaped radio pulse:

$$u(t) = \mathrm{Re}\, S(t) \exp(j2\pi f_0 t) = \\ = \mathrm{Re} \exp\left[-\frac{\pi}{2}\left(\frac{t}{T_{0\Phi}}\right)^2\right] \exp(j2\pi f_0 t). \qquad (2.30)$$

According to (2.11) we can write

$$|\Psi(\tau, \nu)|^2 = \frac{1}{T_{0\Phi}^2} \left| \int_{-\infty}^{\infty} \exp\left[-\frac{\pi}{2}\left(\frac{t}{T_{0\Phi}}\right)^2\right] \times \right. \\ \left. \times \exp\left[-\frac{\pi}{2}\left(\frac{t-\tau}{T_{0\Phi}}\right)^2\right] \exp[j2\pi\nu t]\, dt \right|^2. \qquad (2.31)$$

Following the appropriate transformations we obtain

$$|\Psi(\tau, \nu)|^2 = \exp\left[-2\pi\left(\frac{\tau^2}{4T_{0\Phi}^2} + T_{0\Phi}^2 \nu^2\right)\right]. \qquad (2.32)$$

If the function $|\Psi(\tau, \nu)|^2$ is quantified in terms of amplitude, the lines of equal level will be ellipses whose axes coincide with the τ and ν axes. This indeterminacy function is represented topographically in Fig. 2.5. The remaining parameters of this signal have been cited in Table 2.1.

It is interesting to note that inequality (1.27) becomes an equality only for a signal of Gaussian form.

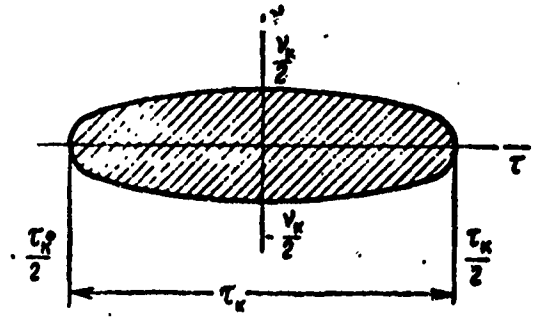

Fig. 2.5. Topographic representation of the indeterminacy function of an unmodulated signal.

Square-wave radio pulse:

$$v(t)=\begin{cases}\operatorname{Re}\exp(j2\pi f_0 t) & \text{for } -\frac{T_{э\phi}}{2}\leqslant t\leqslant\frac{T_{э\phi}}{2},\\ 0 & \text{for all other t.}\end{cases} \tag{2.33}$$

By analogy with (2.31),

$$|\Psi(\tau,\nu)|^2=\begin{cases}\left|\frac{\sin[\pi\nu(T_{э\phi}-|\tau|)]}{\pi\nu T_{э\phi}}\right|^2 & \text{when } |\tau|\leqslant T_{э\phi},\\ 0 & \text{when } |\tau|>T_{э\phi}.\end{cases} \tag{2.34}$$

For a high reading level the equal-level lines for the indeterminacy function of this pulse are also of elliptical form, and for this reason its topographic representation is similar to that of the Gaussian-pulse indeterminacy function (Fig. 2.5). The high-correlation intervals along the τ and ν axes for the 0.75 reference level in this case are, respectively,

$$\tau_к=(2-\sqrt{3})T_{э\phi};\ \nu_к=\frac{1}{\sqrt{3}T_{э\phi}}. \tag{2.35}$$

The remaining parameters of the signal are indicated in Table 2.1.

Radio Pulse with Linear Frequency Modulation (LFM)

A pulse of this kind has a rectangular or bell-shaped envelope (Fig. 2.6a, b), and its instantaneous frequency varies according to a linear law with respect to the center frequency (Fig. 2.7):

$$f = f_0 + \frac{F_m}{\Delta T} t, \tag{2.36}$$

where F_m is the maximum frequency deviation over the signal duration interval, which may be determined by the quantity ΔT.

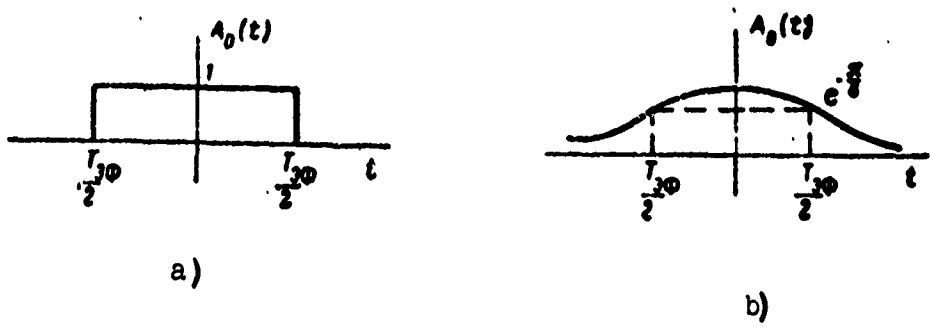

Fig. 2.6. Radio pulse envelope: a) - rectangular; b) - Gaussian.

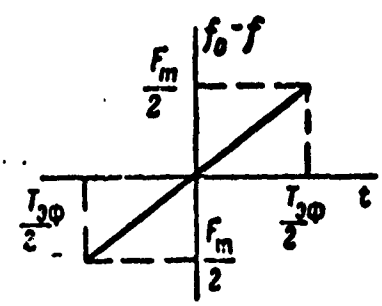

Fig. 2.7. Change in instantaneous frequency in FM radio pulse.

Analytically written, this signal appears as follows:

- for the rectangular envelope

$$u(t)=\begin{cases}\operatorname{Re}\exp\left[j2\pi\left(f_0+\frac{F_m}{2\Delta T}t\right)t\right], & |t|<\frac{T_{s\phi}}{2},\\ 0 \text{ for all other t;}\end{cases}$$

- for the Gaussian envelope

$$u(t)=\operatorname{Re}\exp\left[-\frac{\pi}{2}\left(\frac{t}{T_{s\phi}}\right)^2\right]\exp\left[j2\pi\left(f_0+\frac{F_m}{2\Delta T}t\right)t\right]. \quad (2.37)$$

For $F_m\Delta T >> 1$ the amplitude spectrum of such signals can be approximated by a rectangular function, and the phase by a parabolic dependence (Fig. 2.8) [24]:

$$S(f)=\begin{cases}S_f \text{ for } |f_0-f|<\frac{F_m}{2},\\ 0 \text{ for } |f_0-f|>\frac{F_m}{2},\end{cases} \quad (2.38)$$

$$\varphi(f)=\frac{\pi}{2}\frac{\Delta T}{F_m}(f-f_0)^2+\varphi_0. \quad (2.39)$$

The indeterminacy function for an LFM signal with rectangular and Gaussian envelope, respectively, appear as follows

$$|\Psi(\tau,\nu)|^2=\begin{cases}\left|\dfrac{\sin\left[\pi\left(K_{c\text{ж}}\frac{\tau}{T_{s\phi}}+\nu T_{s\phi}\right)\left(1-\frac{|\tau|}{T_{s\phi}}\right)\right]}{\pi\left(K_{c\text{ж}}\frac{\tau}{T_{s\phi}}+\nu T_{s\phi}\right)}\right|^2, & |\tau|<T_{s\phi},\\ 0, & |\tau|>T_{s\phi};\end{cases} \quad (2.40)$$

$$|\Psi(\tau,\nu)|^2=\exp\left\{-2\pi\left[\frac{(1+4K_{c\text{ж}}^2)\tau^2}{4\Delta T^2}+T_{s\phi}^2\nu^2+2K_{c\text{ж}}\nu\tau\right]\right\}, \quad (2.41)$$

where $K_{сж}$ is the signal compression coefficient, equal to

$$K_{сж} = F_m \Delta T.$$

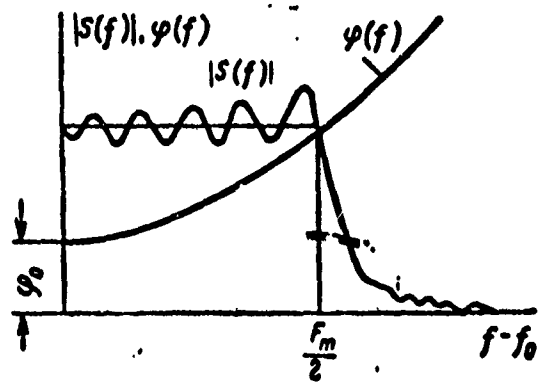

Fig. 2.8. Amplitude spectrum and phase of LFM signal.

The topographic representation of the indterminacy function for the rectangular envelope is shown in Fig. 2.9.

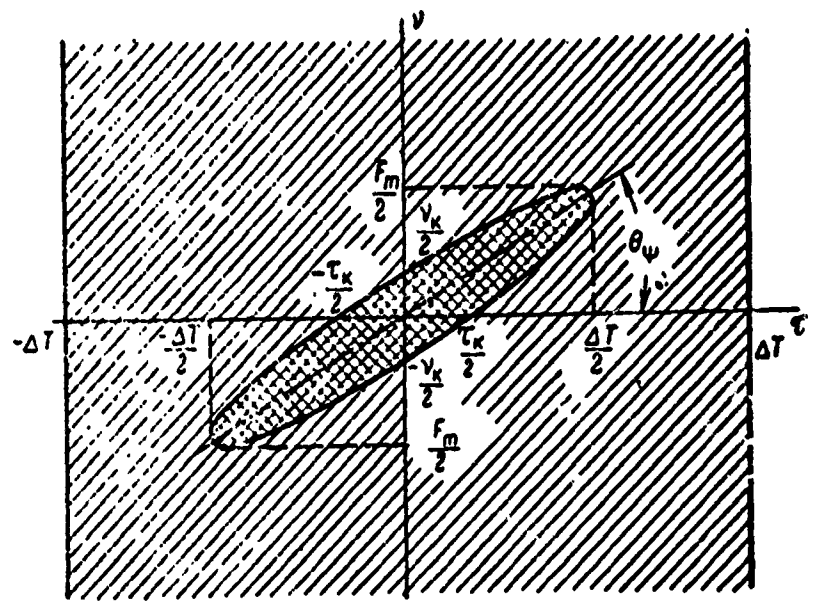

Fig. 2.9. Topographic representation of the indeterminacy function of an LFM signal.

The sectional characteristics of the indeterminacy function for the LFM signal $[\Psi(0, \nu)]^2$ along the ν axis remain the same as for the non-frequency-modulated pulses (2.30) and (2.34) since they are defined only by the signal envelope. On the other hand, there is a substantial change in the section of the indeterminacy function of the LFM signal $|\Psi(\tau, 0)|^2$ along the τ axis.

For the realistically important case of $F_m \Delta T >> 1$, the dependences of the $|\Psi(\tau, 0)|^2$ function for an LFM signal with rectangular and Gaussian envelope may be represented, respectively, in the following form:

$$|\Psi(\tau, 0)|^2 = \frac{\sin^2(\pi F_m \tau)}{(\pi F_m \tau)^2}, \qquad (2.42)$$

$$|\Psi(\tau, 0)|^2 = \exp(-2\pi F_m^2 \tau^2). \qquad (2.43)$$

These sections are shown graphically in Fig. 2.10.

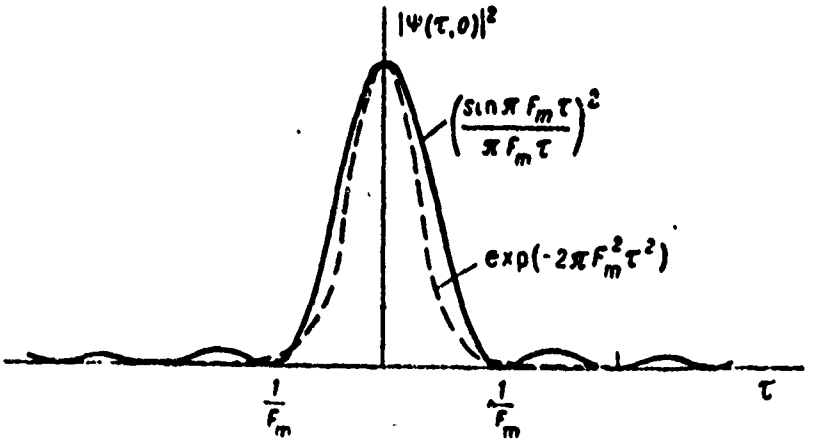

Fig. 2.10. Indeterminacy function section for LFM signals with rectangular and Gaussian envelope.

It will be clear from Equations (2.42) and (2.43), as well as from Fig. 2.10, that because of the LFM there has been a K_{cm} -fold compression of the indeterminacy function section as compared with the case of signals unmodulated in frequency. In

Fig. 2.9 this effect is marked by the rotation of the ellipse of the high-correlation region through an angle of $\theta_\psi = \text{arc tg } K_{CH}/\Delta T^2$. The larger K_{CH}, the greater the turning of the ellipse and the smaller becomes the high correlation interval along the axis τ.

As follows from Table 2.1, where there is a listing of the key characteristics of the different signals, the introduction of the frequency deviation F_m in the signal is equivalent to the compression of its duration by K_{CH} times. However, in comparison to a short pulse for which $T_{э\phi} \simeq 1/F_m$, in signals with frequency or phase modulation the value of the indeterminacy function beyond the interval $|\tau| > \pm 1/F_m$ does not become zero, as in the case of short pulses when $|\tau| > T_{э\phi}$.

The presence of secondary maxima (side lobes) in the indeterminacy function along the τ axis beyond the high-correlation region degrades the delay-time resolution of these signals. For this reason, the level of such indeterminacy-function side lobes must be kept as low as possible.

In the case of LFM signals the side-lobe level of the $|\Psi(\tau, 0)|^2$ function is largely determined by the signal envelope. Given $K_{CH} >> 1$, the $|\Psi(\tau, 0)|^2$ function of such signals can be expressed by the following approximate formula [78]:

$$|\Psi(\tau, 0)|^2 \cong \left| \int_{-\infty}^{\infty} A_0^2(t) \exp\left(j2\pi \frac{F_m}{\Delta T} \tau t\right) dt \right|^2. \qquad (2.44)$$

From this relation it will be seen that by varying the form of the LFM signal envelope a significant change can be achieved in the side-lobe level of its indeterminacy function. The dependence of the side-lobe level of the $|\psi(\tau, 0)|^2$ function for the two extreme cases of the rectangular and Gaussian envelope are illustrated by expressions (2.42) and (2.43) and in Fig. 2.10. On the other hand, however, the achievement of a main pulse with

a bell-shaped waveform is very often a difficult matter, and for this reason methods based on mismatched filtration and a correction of the frequency modulation law are also used for the reduction of the side-lobe level in the indeterminacy function of the linear frequency-modulated signal [7, 45, 78].

Phase-Keyed (PK) Pulse

A phase-keyed radio pulse is a discrete signal, normally with a rectangular envelope, whose phase abruptly changes its value at discrete moments of time according to a definite code. Because phase-keyed (PK) signals are easy to shape and to generate, they are well suited to practical application.

Analytically, a signal of this kind can be represented in the form

$$v(t)=\begin{cases}\operatorname{Re} S(t)\exp(j2\pi f_0 t)=\operatorname{Re}\left\{\sum_{i=0}^{i=N-1} 1_n(t-iT_д,\ T_д)\times\right. \\ \left.\times\exp(j\varphi_i)\right\}\exp(j2\pi f_0 t) \quad \text{for } |t|<\frac{T_{оф}}{2}. \\ 0 \qquad\qquad \text{for } |t|>\frac{T_{оф}}{2}.\end{cases} \tag{2.45}$$

where $1_п(t-iT_д,\ T_д)$ is a unit function, the duration of which is determined by the discrete value of the PK signal $T_д$ (Fig. 2.11);

ϕ_i are the discrete values of the phase code;

N is the total number of discrete elements in the signal.

In the event that ϕ_i takes on only the two values 0 or π, we have a so-called binary phase-keyed signal, whose modulation

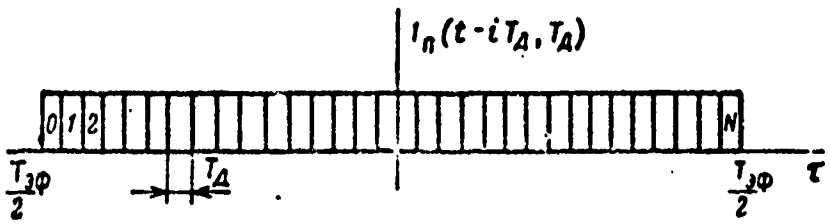

Fig. 2.11. Graphic representation of a periodically recurrent unit function.

function acquires the form:

$$S(t) = \sum_{i=0}^{i=N-1} 1_n(t - iT_д,\ T_д)\, g_i, \qquad (2.46)$$

where g_i is a series of positive and negatives ones 1, -1, -1, -1, -1, ..., determined by the assigned code sequence.

With allowance for expression (2.46), the spectrum of the PK signal will be written as

$$S(j) = S(j)_д \sum_{i=0}^{i=N-1} g_i \exp(-j2\pi j i T_д), \qquad (2.47)$$

where $S(f)_д$ is the spectrum of the elementary square-wave signal with duration $T_д$,

$$S(j)_д = \frac{\sin(\pi j T_д)}{\pi j T_д} \exp(-j\pi j T_д).$$

The indeterminacy function of a PK signal may be presented in the form [13]

$$|\Psi(kT_д + \tau,\ \nu)|^2 = \frac{|\Psi(\tau,\ \nu)|_1^2}{N^2} \left| \sum_{i=0}^{i=N-1} g_i g_{i+k} \times \right.$$

$$\left. \times \exp(j2\pi\nu i T_д) \right|^2 = \frac{|\Psi(\tau,\ \nu)|_1^2}{N^2} C_k^2(\nu), \qquad (2.48)$$

where

$$C_k^2(\nu)=\left[\sum_{i=0}^{i=N-1} g_i g_{i+k}\cos(i2\pi\nu T_д)\right]^2+$$
$$+\left[\sum_{i=0}^{i=N-1} g_i g_{i+k}\sin(i2\pi\nu T_д)\right]^2.$$

Here, N is the number of code symbols for the discrete element over the entire duration of the signal;

$|\Psi(\pi,\nu)|^2_д$ is the indeterminacy function of the elementary pulse signal of duration $T_д$;

$$|\tau|\leqslant T_д \text{ for } k=0;$$
$$|\tau|=0 \text{ for } |k|>0;$$
$$0\leqslant i\leqslant N-k-1 \text{ when } k>0.$$

The magnitude of the indeterminacy function in the interval between the discrete reference elements, when $|k|>0$, does not exceed its masimum value with respect to the nearest maxima, and for this reason it is quantized in terms of constant levels.

As is evident from (2.48), the indeterminacy function section for a PK signal for $k = 0$, $\tau = 0$, is defined by the dependence

$$|\Psi(0,\nu)|^2=\frac{1}{N^2}\left|\sum_{i=0}^{i=N-1}\exp(j2\pi\nu iT_д)\right|^2=\left|\frac{\sin(\pi\nu NT_д)}{\pi\nu NT_д}\right|^2. \quad (2.49)$$

Dependence (2.49) is analogous to the expression for the section of the indeterminacy function of the non-phase-modulated signal (2.34).

Along the time axis the indeterminacy function section is defined by the expression

$$|\Psi(kT_д + \tau, 0)|^2 = \frac{|\Psi(\tau, 0)|^2_д}{N^2} C_k^2(0) =$$

$$= \frac{|\Psi(\tau, 0)|^2_д}{N^2} \left| \sum_{i=0}^{i=N-1} g_i g_{i+k} \right|^2. \qquad (2.50)$$

By the selection of the code sequence g_i it is possible to ensure that for $k > 0$

$$\left| \sum_{i=0}^{i=N-1} g_i g_{i+k} \right| \ll N.$$

In this case, just as for the LFM signal, the section $|\Psi(kT_д + \tau, 0)|^2$ has the form of a narrow peak in the neighborhood of $k = 0$, $\tau \leq T_д$ (Fig. 2.12).

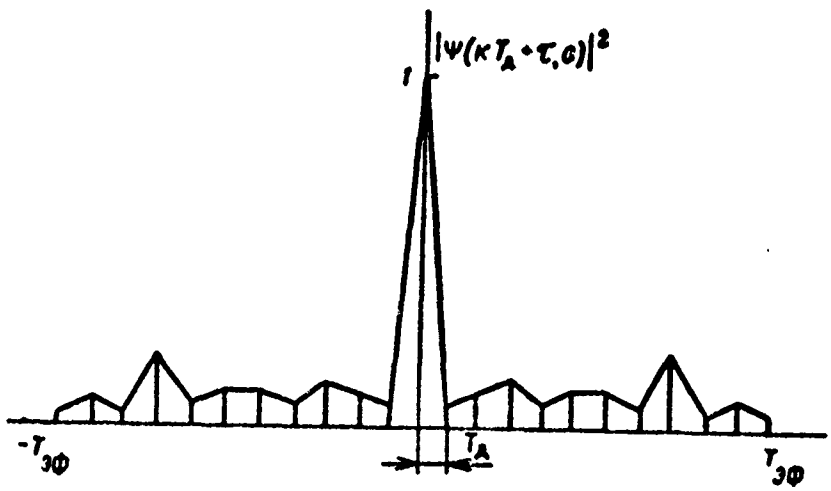

Fig. 2.12. Indeterminacy function section of a phase-keyed signal when $\nu = 0$.

In the case of "noise-like" code sequences a low indeterminacy function side-lobe level also occurs for frequency shifts of $\nu \neq 0$.

The topographic representation for the indeterminacy function of this kind of phase-keyed signal is shown in Fig. 2.13, where four approximation levels have been used: two levels in the central-peak zone

$$1 > |\Psi(\tau, \nu)|^2 \geq 0{,}75,$$
$$\frac{3}{N} < |\Psi(\tau, \nu)|^2 < 0{,}75$$

and two levels in the side-lobe region

$$|\Psi(\tau, \nu)|^2 < \frac{3}{N},$$
$$|\Psi(\tau, \nu)|^2 < \frac{1}{rN}.$$

Here, r is a specified factor, greater than one, whose specific value depends on the structure of the code.

Unlike the linear frequency-modulated (LFM) signal, the phase-keyed (PK) signal has a nearly ideal indeterminacy function with an ellipse of uncertainty of minimum area. As will be pointed out in Section 4.2 of this book, this ensures maximum accuracy in the simultaneous measurement of τ and ν.

At the present time, a large number of different code sequences are known which may be used to form phase-keyed signals. The majority of them have been discussed in the technical literature [17, 45, 67, 78, 95]. Greatest practical interest centers on Barker's and Huffman's code sequences [78] and also on the B codes [17, 95].

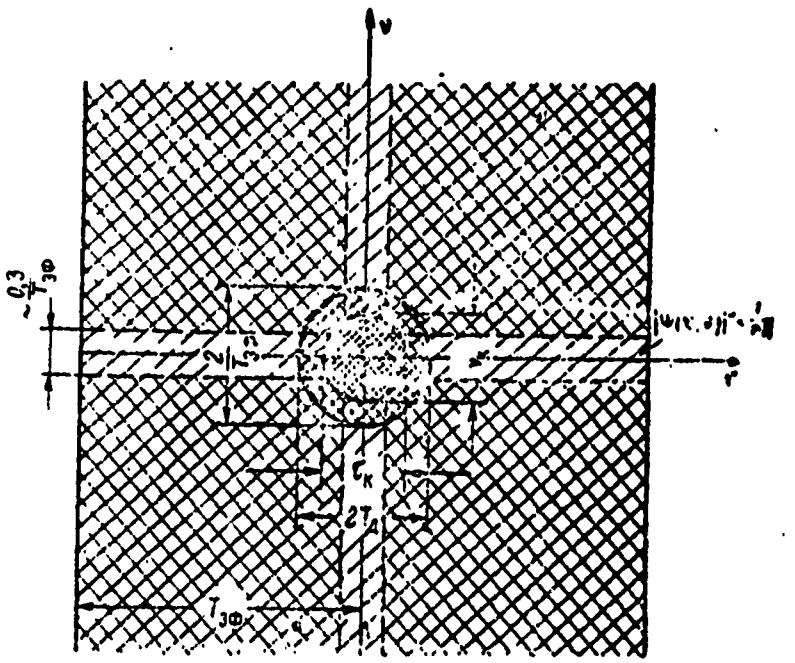

Fig. 2.13. Topographic representation of the indeterminacy function of a phase-keyed signal.

The Barker codes ensure a minimum side-lobe level $1/N^2$ in the indeterminacy function of the phase-keyed signal in the section $|\Psi(\tau, 0)|^2$, but they give rise to high secondary maxima in the sections for $\nu \neq 0$. Huffman codes make it possible to obtain side lobes of fairly uniform structure over the entire τ and ν plane, and are easily shaped by feedback shift-registers [45, 78]. B codes provide satisfactory indeterminacy function characteristics and, at the same time, permit the use of simple circuitries for the matched filtering of phase-keyed signals [17, 95].

Unlike linear frequency-modulated signals, in PK signals the side-lobe level of the indeterminacy function cannot be reduced by bell-shaped amplitude modulation or through the introduction of corrective frequency modulation. In the case of phase-keyed signals, reduction of the side-lobe level of the function $|\Psi(\tau, 0)|^2$ is achieved through selection of the code sequences (minimal code sequences) [78] or through the use of mismatch filtering.

For many practical computational purposes the level of the secondary maxima in the indeterminacy function of phase-keyed signals can be conveniently approximated by a mean value; it has been noted in [13], in this connection, that for $k \neq 0$ the following relation obtains:

$$\langle |C_k(\nu)|^2 \rangle = N - k. \tag{2.51}$$

The averaging here is carried out for the set of values for the square of the modulus $|C_k(\nu)|^2$ in the τ, ν plane.

Keeping in mind expression (2.51), the approximated value of the indeterminacy function for the PK signal can be written in the form

$$|\Psi(\tau, \nu)|^2_{\text{апр}} = \begin{cases} \left[\frac{\sin(\pi\nu T_{\text{эф}})}{\pi\nu T_{\text{эф}}}\right]^2 \left(1 - \frac{\tau}{T_{\text{д}}}\right)^2 & \text{for } |\tau| < T_{\text{д}}, \\ \frac{1}{N}\left[\frac{\sin(\pi\nu T_{\text{д}})}{\pi\nu T_{\text{д}}}\right]^2 & \text{for } NT_{\text{д}} < |\tau| \geq T_{\text{д}}, \\ 0 & \text{for } |\tau| > NT_{\text{д}}. \end{cases} \tag{2.52}$$

Radio-Pulse Train

A radio-pulse train is a discrete signal in the form of a burst of coherent radio pulses (Fig. 2.14).

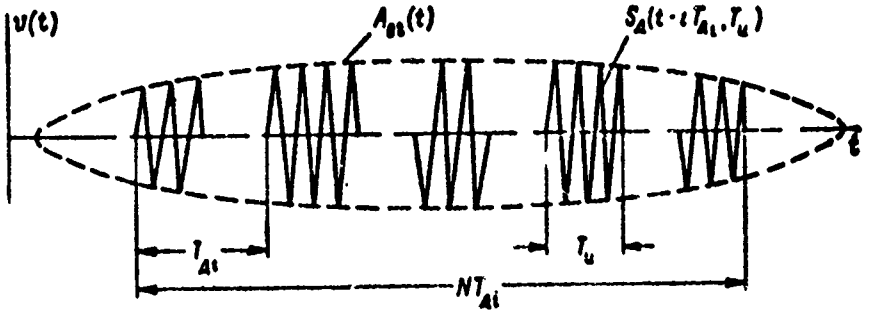

Fig. 2.14. Radio-pulse train.

Analytically, this signal may be represented by the dependence

$$u(t) = \mathrm{Re} \sum_{i=0}^{i=N-1} A_{or}(t) S_{д}(t - iT_{дi}, T_{и}) \exp[j\varphi_i(t)] \times \times \exp(j2\pi f_0 t), \quad (2.53)$$

where A_{or} defines the envelope of the pulse burst;

$T_{д\,i}$ is the time interval between the pulses;

$S_{д}(t, T_{и})$ is the modulation function of a single pulse with duration $T_{и}$;

$\phi_i(t)$ is the law of the phase modulation in the intervals between individual pulses [Translator's Note - Subscript letter "or" and "и" indicate "envelope" and "pulse," respectively].

For such a signal it is always assumed that $T_{д\,i} > 2T_{и}$. In the event the conditions

$$T_{дi} = T_{д} = \mathrm{const}, \ \varphi(t) = 0,$$

take place, the signal represents a burst of coherent radio pulses periodically recurrent in a time interval $NT_{д}$.

The modulation correlation function for this kind of signal, for different single-pulse modulation modes and different envelopes, is easily found from the formula cited in [81]:

$$\Psi(\tau, \nu) = \sum_{i=-\infty}^{i=\infty} \sum_{k=-\infty}^{k=\infty} \Psi_{д}\left(\tau - iT_{д}, \frac{k}{T_{и}}\right) \Psi_{or}\left(\tau, \nu - \frac{k}{T_{и}}\right), \quad (2.54)$$

where $\Psi_{д}(z)$ is the modulation correlation function of the elementary signal $S_{д}(t, T_{и})$;

$\Psi_{or}(z)$ is the modulation correlation function $A_{or}(t)$.

Considering that the values of the terms of the sum do not overlap in τ and overlap only negligibly in frequency, with accuracy acceptable for practical purposes we can set the following:

$$|\Psi(\tau, \nu)|^2 = \sum_{i=-N}^{i=N} |\Psi_{\text{д}}(\tau - iT_{\text{д}}, \nu)|^2 \sum_{k=-\infty}^{k=\infty} \left|\Psi_{01}\left(\tau, \nu - \frac{k}{T_{\text{д}}}\right)\right|^2. \quad (2.55)$$

Specifically, when the signals represent bursts of unmodulated, rectangular radio pulses with a common rectangular envelope, from relations (2.55) and (2.34) we obtain

$$|\Psi(\tau, \nu)|^2 = \sum_{i=-N}^{i=N} \left|\frac{\sin[\pi\nu(T_{\text{и}} - |\tau| - iT_{\text{д}})]}{\pi\nu T_{\text{и}}}\right|^2 \times$$
$$\times \sum_{k=-\infty}^{k=\infty} \left|\frac{\sin\left[\pi(NT_{\text{д}} - |\tau|)\left(\nu - \frac{k}{T_{\text{д}}}\right)\right]}{\pi NT_{\text{д}}\left(\nu - \frac{k}{T_{\text{д}}}\right)}\right|^2. \quad (2.56)$$

A topographic representation of this kind of indeterminacy function is shown in Fig. 2.15.

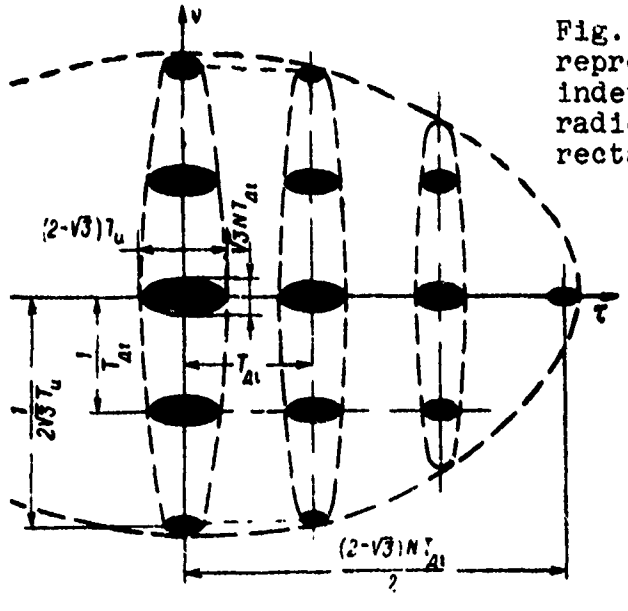

Fig. 2...5. Topographic representation of the indeterminacy function of a radio-pulse train with rectangular envelope.

If the single pulses in the burst have frequency or phase modulation - for example, LFM or PK - then the appropriate expression (2.40) or (2.48) for the unit-pulse indeterminacy function must be substituted in equation (2.55). In terms of frequency there is no change in the character of the resultant indeterminacy function, but in delay time there will occur an additional compression of its maxima (Fig. 2.16). Meanwhile, the secondary-maxima region will be preserved, for which

$$\frac{1}{N} < |\Psi(\tau, \nu)|^2 < 0{,}75.$$

When $T_{д\,i} \neq \text{const}$, that is, when the intervals between pulses do not remain constant, the result is a so-called aperiodic pulse train.

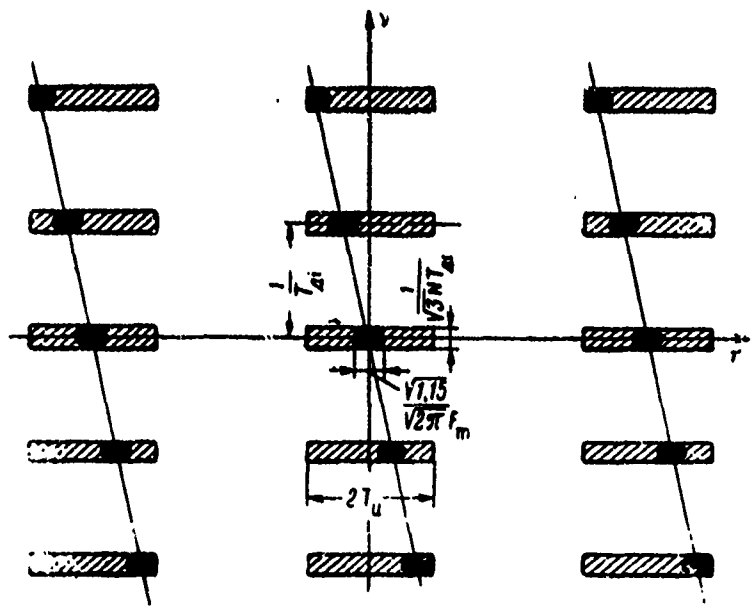

Fig. 2.16. Topographic representation of the indeterminacy function for a pulse burst with intrapulse modulation.

The aspect of the indeterminacy function for such a signal may be seen in Fig. 2.17. The secondary maxima beyond the $|\tau| > T_н$ region of the entire τ, ν plane do not exceed the value $\frac{1}{N^2}$.

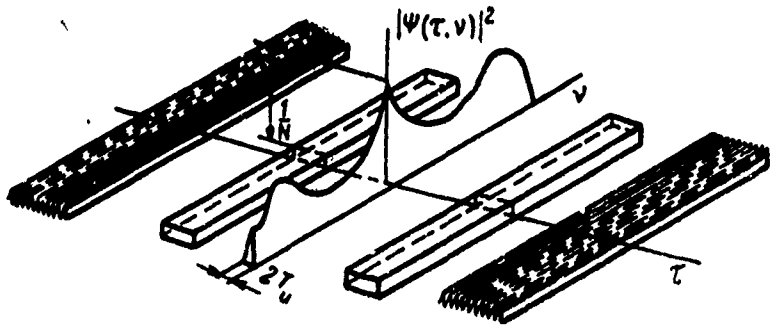

Fig. 2.17. Indeterminacy function of an aperidoic pulse train.

In section $|\Psi(0, \nu)|^2$ the indeterminacy function value is determined by the relation

$$|\Psi(0, \nu)|^2 = \frac{\sin^2(\pi\nu T_н)}{(\pi\nu T_н)^2} \left| \sum_{l=1}^{l=N} \cos(2\pi\nu l T_{дl}) \right|. \qquad (2.58)$$

As indicated by an analysis of expression (2.58), in this section the secondary maxima of the indeterminacy function may be of rather high level, reaching values of as much as 0.5. To reduce this level, irregular modulation of the pulse repetition frequency is employed [38, 78].

Radar signals may also be based on a pulse train in which T = const, and $\phi(t) \neq 0$. In this case, there is a change in the frequency or phase from pulse to pulse [67]. An example of this kind of pulse sequence might be a pulse signal with pulse-to-pulse linear frequency modulation:

$$v(t) = \mathrm{Re} \sum_{i=0}^{i=N-1} 1_{\text{п}}(t - iT_{\text{д}}, T_{\text{и}}) \exp\left(j \frac{F_m}{NT_{\text{д}}} \frac{t^2}{2}\right) \exp(j2\pi f_0 t). \quad (2.59)$$

For this kind of signal the indeterminacy function appears as follows:

$$|\Psi(\tau, \nu)|^2 = \sum_{i=-N}^{i=N} |\Psi_{\text{д}}(\tau - iT_{\text{д}}, \nu - iF_m)|^2 \times$$

$$\times \frac{\sin^2\{(N - |i|)[T_{\text{д}}\nu\pi - \pi F_m(\tau - iT_{\text{д}})]\}}{\sin^2[T_{\text{д}}\nu\pi - \pi F_m(\tau - iT_{\text{д}})]} \frac{(N - |i|)^2}{N^2}. \quad (2.60)$$

3. DETECTION OF SIGNALS AGAINST A BACKGROUND OF INTERFERENCE AND OTHER SIGNALS

3.1. Sensitivity of Detection Systems

One of the basic indicators of a signal-processing system is its sensitivity to threshold signals. This criterion describes the reliability with which the system will detect a minimum threshold signal against a background of different kinds of interference, which may be both active interference, which may be both active interference as well as interfering reflections (clutter) caused by echo signals reflected from other targets and a variety of reflectors. System sensitivity in this sense is normally defined by detection characteristics which reflect the dependence of the values D and F on the parameters of the signal and the interference.

The probability of correct signal detection D and the probability of false alarm F at the output of a single-detection channel tuned to fixed values for the parameters of the anticipated signal τ_i and Ω_i and accomplishing the detection of the

signal in one resultant resolution element $d_\Sigma = \phi(d_{\tau i}, d_{\Omega i})$, may be determined according to the distribution of the filter-circuit output effect $Y_{\tau i,\ \Omega i}$. In this case, the quantity $Y_{\tau i,\ \Omega i}$ is described by some random number. The indexes D and F are defined by the relations

$$D = \int_{Y_0}^{\infty} P_{nc}(Y_{\tau i, \Omega i})\, dY_{\tau i, \Omega i}, \tag{3.1}$$

$$F = \int_{Y_0}^{\infty} P_{n}(Y_{\tau i, \Omega i})\, dY_{\tau i, \Omega i}, \tag{3.2}$$

where $P_n(Y_{\tau i,\ \Omega i})$, $P_{nc}(Y_{\tau i,\ \Omega i})$ are the distributions in the output effect of a signal-filtering circuit tuned to the parameters τ_i, and Ω_i, when there is present at the input of this circuit, respectively, only interference ("n") or interference plus a signal ("nc"); Y_0 is the threshold level.

When as a result of the processing of an input oscillation consisting of a useful signal and fluctuating interference having definite characteristics a system ensures the assigned (or better) values of D and F, such a system is then said to be capable of detecting (discriminating) a useful signal against a background of interference. If as a result of the processing of the input oscillation there are ensured the prescribed D and F values for the useful signal and along with the fluctuation interference other signals are present in the input oscillation, the system is then said to resolve the useful signal against a background of interference and other signals. The characteristics of the interfering signals in this case are considered among the characteristics of the interference for the resolution element in question. When the parameters τ and Ω of the received signal are unknown, then, as already noted, this signal is processed for a number of fixed values for these parameters, with the resolving unit analyzing the output effect for m discrete values of the parameters τ and Ω. In other words, we have an m-channel detection

system. The output effect will be maximum in the elementary channel, whose tuning parameters are in close agreement with those of the received signal, and the probability that this signal will be detected in this channel is greatest.

If the signal characteristics and the discrete spacing of the channel tuning parameters are such that signals with different parameters are processed by the m-channel system independently, then the probability that any signal will be correctly detected by a multichannel system of this kind, assuming the interference characteristics in each resolution element are identical, does not differ from the probability that this same signal will be properly detected by a single channel having the appropriate parameters. The assumption is that the false-alarm probability now is fairly low. The value of the D index of the system in this case for any signal can be determined using equation (3.1). The false-alarm probability F_Σ in such an m-channel detection system differs from that of the separate channel F. It can be easily shown [81] that for the situation in question this probability is m times greater than the false-alarm probability of the single channel; that is,

$$F_\Sigma \approx mF. \tag{3.3}$$

When the fluctuation interference characteristics in the different resolution elements are not the same, or when there are simultaneously present in the input oscillation other cross-correlated signals, the values of D for the corresponding signal and of F in each resolution element (elementary detection channel) will differ. To evaluate the system's performance in terms of assigned D parameter values it must be checked for all resolution elements, bearing in mind the different possible variations in the characteristics of the interference and other signals.

For many kinds of interference and signal-processing systems the output effect is characterized by a normal distribution law.

In this case, the value of correct detection D for fixed F can be expressed as a function of a specified parameter

$$q^2 = \frac{m_{cn}^2[Y]}{\sigma_{cn}^2[Y]}, \qquad (3.4)$$

describing the ratio of signal power to interference power at the filter circuit output [81]. Here $m_{cn}[Y]$ and $\sigma_{cn}^2[Y]$ are the mathematical expectancy and dispersion of the output effect. When D depends uniquely on q^2, for fixed values of F the quantity q^2 completely describes the index of sensitivity of the processing system, and for this reason the form of such a system can be optimized by taking the q^2 parameter into account.

When submitting a signal-processing system to engineering synthesis major importance attaches to the determination of the sensitivity of specific signal-processing arrangements in the face of interference of various kinds, as well as to the evaluation of how this indicator changes according to the type of transmitted signal and also to the structure and working mode of the system.

3.2. Signal Resolution and Selection Against a Background of Interference by Means of Linear Filtering Circuits

As already noted above, circuitries employing matched or mismatched filtering followed by the logical processing of the filtered signal constitute one of the principal arrangements for practical signal-processing in the presence of a wide range of interference types and space-time target distribution. Generally speaking, a processing system of this kind will be quasi-optimal, but it is very largely universal and does not call for the same extraordinarily great number of channels found in the optimal resolution scheme (Section 1.4). Since the processing of the input oscillation is effected in a linear manner and its distribution law is assumed to be normal, also normal will be the distribution of the output effect of the matched or mismatched filtering circuit.

As a consequence, in a circuit of this type the quantity q^2 may serve as the parameter indicating the discrimination of the signal from the interference surrounding it, along with its resolution against a background of other signals.

Let us determine the effect which will be exerted on this quantity by a change in the characteristics of the signal and filtering circuitries. Consider the situation when along with internal receiver noises and the useful signal there is present at the processing channel output either passive interference or signals occasioned by reflections from other targets. For our analysis we shall call on the familiar relation for the signal/noise ratio at the filter system output, as derived, for example, in [4].

The parameter q^2, in this case, for resolution element $d_{\tau_{д0}}$, $d_{\nu_{д0}}$, assuming mismatched filtering, will be expressed in the form:

$$q^2 = \frac{m^2_{сп}[Y]}{\sigma^2_{сп}[Y]} =$$

$$= \frac{P_{сиг} T_{эф} |\Psi_0(0)|^2}{\frac{1}{2} N_0 + T_{эф} \int_{-\infty}^{\infty} d\nu \int_{-\infty}^{\infty} |\Psi_0(\tau_{д_0} - \tau, \nu_{д_0} - \nu)|^2 \mu_п(\tau) Q_п(\tau, \nu) d\tau}, \quad (3.5)$$

while in the event of matched filtering the same relation will appear as

$$q^2_{сог.} =$$

$$= \frac{P_{сиг} T_{эф}}{\frac{1}{2} N_0 + T_{эф} \int_{-\infty}^{\infty} d\nu \int_{-\infty}^{\infty} |\Psi(\tau_{д_0} - \tau, \nu_{д_0} - \nu)|^2 \mu_п(\tau) Q_п(\tau, \nu) d\tau}, \quad (3.$$

where N_0 is the spectral energy density of the noise;

$\mu_п(\tau)$ is the density distribution of passive interference intensity for the time lag;

$Q_п(\tau, \nu)$ is the normed spectral density (energy spectrum) of the passive interference, being the Fourier transform of coefficient $r_п(\tau, t)$;

$\tau_{з_0}$ is the delay of the useful signal;

$\nu_{д_0}$ is the Doppler frequency shift in the useful signal;

$P_{свх}$ is the mean power of the useful signal at the processing system input.

The second term in the denominator of expressions (3.5) and (3.6) defines the passive interference energy at the output of a filtering channel tuned to the useful signal in the appropriate resolution element. Let us consider how this value depends on the structure of the transmitted signal and the form of the filter's frequency characteristic.

The intensity distribution for the interference and signals in the frequency-time plane can be conveniently represented through the use of topographical methods, as shown in Fig. 3.1. (shaded area). This kind of topographical mapping makes possible a graphic analysis of the interference energy distribution at the filter unit output in the appropriate resolution element. In a specified scale, the energy of the passive interference in the resolution element will be characterized by the area of intersection of the indeterminacy function (the coordinate origin of which corresponds to the parameters of the anticipated signal) and the frequency-time distribution of the interference. In Fig. 3.1 the broken lines indicate the high-correlation regions for the indeterminacy function of an LFM signal with a modulation law

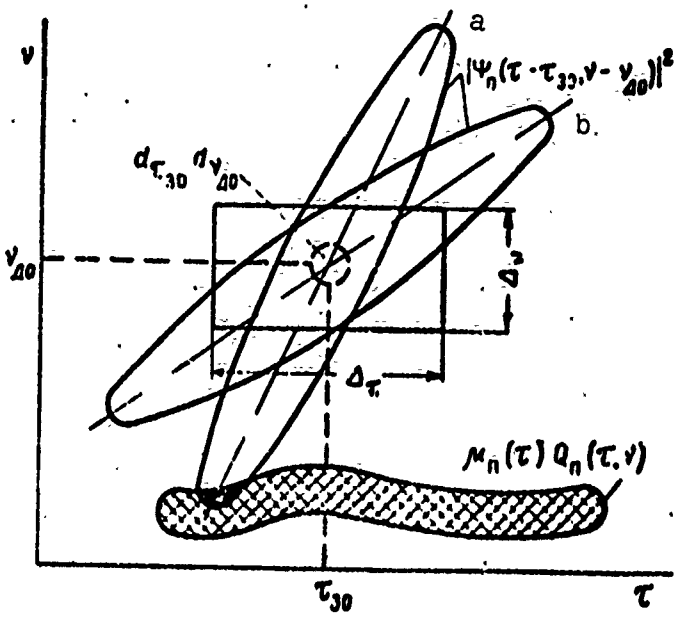

Fig. 3.1. Topographic representation of the frequency-time distribution of the interference and indeterminacy function of the signal.

curve of different inclinations (a and b). Maximum interference intensity will occur in those of the unit's resolution elements in which the high-correlation region of the indeterminacy function or reciprocal indeterminacy function of the signal overlaps to a significant extent the interference distribution region. As shown in Fig. 3.1, for the resolution element $d_{\tau_{э0}}$, $d_{\nu_{д0}}$ the interference intensity will be greater in the event the LFM signal exhibits a modulation law curve inclined in the manner of case "a." When the parameters of the anticipated signal may vary within the intervals Δ_τ, Δ_ν, the interference intensity distribution must be considered in all the resolution elements present in the region limited by the intervals Δ_τ, Δ_ν. The form of the functions $|\Psi(\tau, \nu)|^2$ and $|\Psi_0(\tau, \nu)|^2$ is meanwhile selected with an eye to the specific distribution of the interference.

For reduction of the interference level in the resolution elements found in the region of *a priori* values for delay time

Δ_τ and Doppler frequency shifts in the useful signals, the signal structure and the filter characteristics must be of the kind for which the reciprocal indeterminacy function or the indeterminacy function will intersect the interference distribution region in a zone where its value are minimal (Fig. 3.1, situation "b").

As can be seen from expressions (3.5) and (3.6), with matched filtering this can be accomplished only by varying the form of the main (transmitted) signal, while in the case of mismatch filtering the variation of the frequency-phase response of the filter can additionally be employed for interference level reduction.

However, with arbitrary changes in the frequency-phase characteristic of the filter it is possible that along with a lowering of the noise intensity at the filter output there may also be incurred a loss of power in the useful signal as well, and for this reason it is advisable to resort to mismatch filtering only in the event that for a given signal in the required region of time lags and frequency shifts Δ_τ, Δ_ν the following inequality is satisfied:

$$\frac{|\dot{\Psi}_0(0)|^2}{\int\limits_{-\infty}^{\infty} d\nu \int\limits_{-\infty}^{\infty} |\Psi_0(\tau_{3_0}-\tau, \nu_{д_0}-\nu)|^2 \mu_{11}(\tau) Q_{11}(\tau, \nu)\, d\tau} > \frac{1}{\int\limits_{-\infty}^{\infty} d\nu \int\limits_{-\infty}^{\infty} |\Psi_0(\tau_{3_0}-\tau, \nu_{д_0}-\nu)|^2 \mu_{11}|\tau| Q_{11}(\tau, \nu)\, d\tau}. \qquad (3.7)$$

This inequality (3.7) will in fact be fulfilled under specific conditions, and under these circumstances an enhanced signal/noise ratio can be achieved through the use of mismatch filtering [100].

Allowance must be made, however, for the fact that mismatch filtering results in degraded detection characteristics in the absence of passive interference - that is, when the interference is caused only by the internal noise of the receiver. In fact, from expression (13.5), with no passive interference present, we obtain

$$q_0^2 = \frac{2P_{сигн}T_{эф}|\Psi_0(0)|^2}{N_0} = q_{0\,corr}^2 |\Psi_0(0)|^2, \qquad (3.8)$$

where $q_{0\ corr}^2$ is the signal/noise ratio for a matched filter in the face of white Gaussian noise.

It follows from expression (3.8) that the value of the normed reciprocal indeterminacy function describes the reduction in the signal/noise ratio with mismatch filtering. This circumstance imposes an additional constraint on the manipulation of the filter phase response when optimizing this characteristic for passive interference.

If the reflections are caused by a point source (object), then for this situation the normed spectral density $Q_п(\tau, \nu)$ and intensity density distribution $\mu_п(\tau)$ can be expressed through delta functions, respectively, as:

$$Q_п(\tau, \nu) = \delta(\nu - \nu_i),$$
$$\mu_п(\tau) = P_i\delta(\tau - \tau_i), \qquad (3.9)$$

where P_i is the mean power of the signal reflected from a point object, at the filter system input;

ν_i is the Doppler frequency shift of the reflected signal, corresponding to the radial velocity in the movement of the object;

τ_i is the range delay of the reflected signal, describing the distance to the object.

Through the use of expression (3.9), formulas (3.5) and (3.6) can be solved to yield relations descriptive of the parameters q^2 and $q^2_{согл}$ at the output of the corresponding filter circuitries.

When the noise component caused by internal receiver noises at the filter system output is negligibly small, the following relations will define the values of q^2 and $q^2_{согл}$ in a filter channel tuned to a signal with frequency shift $\nu_{д_0}$ and time delay $\tau_{э_0}$

$$q_k^2 = \frac{P_{сиг} |\Psi_0(0)|^2}{P_ш |\Psi_0(\tau_ш - \tau_{э_0}, \nu_ш - \nu_{д_0})|^2}, \qquad (3.10)$$

$$q_{k\,согл}^2 = \frac{P_{сиг}}{P_ш |\Psi(\tau_ш - \tau_{э_0}, \nu_ш - \nu_{д_0})|^2}.$$

It is reasonable to suppose that a signal having parameters $\tau_{э_0}$ and $\nu_{д_0}$ will be resolved, provided[1]

$$q_k^2 \gg 1. \qquad (3.11)$$

Normally, two situations are distinguished:

a) resolution of signals from nearby targets;

b) resolution of signals from a single target against a background of interferential noise caused by a signal from another target.

The first case (resolution of signals from nearby targets)

[1]This condition must be met for high-quality detection and measurement of the parameters of useful signals.

occurs whenever the task is one of detecting or measuring the parameters of targets which are close either in range or speed, or simultaneously in both these parameters. The intensities of the return signals in this situation are commensurate (the usual assumption being that they are equal). The second case assumes a significant spread in target parameters, whereby, however, the intensities of the reflected signals may differ very markedly.

In the first instance, as follows from expressions (3.10), signal resolution for a particular parameter will be determined by the rate of decay of the reciprocal indeterminacy function or indeterminacy function for this parameter in the region of its central peak. The range-delay or frequency-shift interval ensuring the required q^2 value for signal resolution in this case will describe the resolving power of the system for this parameter.

For matched filtering this resolution region for range delay and frequency, in a specific scale, may be described by an indeterminacy ellipse, whose expression for the value $q^2_{corn} = \frac{4}{3}$ has been given in Chapter 1. From this expression it specifically follows that for high range-delay resolution the signals must exhibit a high frequency dispersion value ΔW^2, at the same time that good resolution for frequency is achieved through large time-dispersion values ΔT^2.

This analysis, however, is valid for the most part only for aperiodic pulses and aperiodic filter frequency characteristics, for which the reciprocal indeterminacy function or indeterminacy function represent single-peak surfaces. The presence of a periodic structure in the signals or in the filter frequency responses, with ths structure resulting in the occurrence of high secondary maxima in the indeterminacy function (2.56), leads, in the absence of *a priori* information, to a variety of ambiguities in signal parameter measurement and to worsened resolution. The

values of the resolution constants (2.25) may be employed to take this factor into account when estimating the resolving power for a particular parameter of a periodic signal. As may be seen from Table 2.1, the values of these parameters for periodic signals with high frequency or time dispersion provide a definite description of the deterioration of resolution for periodic signals.

In case "b" (resolution against a background), when the signals from the target display a considerable parameter spread but overlap in time and differ substantially in intensity, the determinant factor in their resolution is the level of secondary maxima for the functions $|\Psi_0(\tau, \nu)|^2$ and $|\Psi(\tau, \nu)|^2$.

A complete understanding of this characteristic can be had only by analyzing the entire indeterminacy or reciprocal indeterminacy function in the working region of the parameters. In many instances, however, it will be sufficient to estimate the side-lobe level in the major sections of these functions, specifically in the sections $\tau \neq 0$, $\nu = 0$ and $\tau = 0$, $\nu \neq 0$.

By way of example, following expressions (2.18), when $\nu = 0$, the value of these functions in the secondary maxima region can be analyzed by means of the relations:

$$|\Psi(\tau, 0)|^2 = \frac{1}{T_{\Sigma\Phi}^2}\left|\int_{-\infty}^{\infty}|S(f)|^2 \exp(j2\pi f\tau)\,df\right|^2,$$

$$|\Psi_0(\tau, 0)|^2 = \frac{1}{T_{\Sigma 1}T_{\Sigma\Phi}}\left|\int_{-\infty}^{\infty}S^*(f)\,S_0(f)\exp(j2\pi f\tau)\,df\right|^2. \qquad (3.12)$$

From this last expression it is evident that the form of the indeterminacy function section along the τ axis, when $\nu = 0$, is wholly determined by the signal's amplitude spectrum. If a low

side-lobe level is to be achieved in the indeterminacy function along the τ axis, the signals must exhibit smooth and broad spectra.

If difficulties of a practical nature are encountered in realizing a signal of the required waveform for the attainment of a prescribed side-lobe level, mismatch filtering methods can be used. Here, as is evident from expression (3.12), the signal form at the filter output will be defined as a Fourier transform of the product of the input signal spectrum and the filter frequency response. A prescribed side-lobe level can be secured by varying the filter frequency response.

Despite the fact that mismatch filtering normally results in a more sophisticated filter circuit, in actual practice this technique is very frequently employed. The synthesis of mismatched filters for frequency-modulated and phase-keyed signals has been discussed in detail in [7, 45, 78].

Two distinct mismatch filtering methods are encountered. In the first, the manipulation affects only the filter's amplitude-frequency response, which is selected in such wise as to give a smoothing effect for the spectral edges of the signal to be processed. The second approach presupposes a variation in the filter's phase-frequency characteristic to ensure an assigned side-lobe level. The first method is mainly applicable with frequency modulated signals and is more extensively employed, including for phase-keyed signals as well*.

It should be noted that the method based on the variation of the phase-frequency response of the filter is largely dependent on the signal frequency and, as a rule, permits side-lobe suppression in a very narrow zone of input signal frequency shifts, in the order of

$$\frac{0,05 \div 0,1}{\Delta T}.$$

*Translator's Note - This sentence appears to be somewhat garbled in the original Russian.

By applying mismatch filtering one can achieve a fairly low side-lobe level of about -40 to -50 dB in the modulation cross function, although in practical terms the achievement of this low a side-lobe level is limited by random distortions in the signal waveform incurred as it propagates, as well as by distortions caused by instability in the phase-frequency characteristics of the receiving and transmitting equipment. Analysis of the effect of these distortions on the form of the indeterminacy cross function and estimates of realistically attainable side-lobe levels are properly the subject of specialized studies and have been discussed in a limited sense in [27, 45, 78].

If reflections from several point objects are simultaneously present at the receiver input, then using expressions (3.5) and ignoring the inherent noise of the receiver, we obtain

$$q_k^2 = \frac{P_{max}|\Psi_0(0)|^2}{\sum_{i=1}^{i=n} P_i |\Psi_0(\tau_i - \tau_{i_0}, \nu_i - \nu_{i_0})|^2}, \qquad (3.13)$$

where n is the number of reflecting objects.

In the event the intensity of the signals reflected from these objects is nearly identical and one can determine the mean side-lobe level of the reciprocal indeterminacy function in the region of the *a priori* time-delay Δ_τ and frequency-shift Δ_ν values, expression (3.23) is rewritten in the following form:

$$q_k^2 = \frac{P_{max}|\Psi_0(0)|^2}{nP_0 \langle |\Psi_0(\tau, \nu)|^2 \rangle_{\Delta_\tau, \Delta_\nu}}, \qquad (3.14)$$

where P_0 is the mean power, at the filter unit input, of a signal reflected from a single object;

$\langle |\Psi_0(\tau, \nu)|^2 \rangle_{\Delta_\tau, \Delta_\nu}$ is the mean side-lobe level of the reciprocal indeterminacy function in the region Δ_τ, Δ_ν.

By assigning the minimum value $q^2_{мин}$ for which the prescribed value of D and F is realized, the maximum number of signals against the background of which the useful signal will be resolved using mismatch filtering will be

$$n_{макс} = \frac{|\Psi_0(0)|^2}{q^2_{мин}\frac{P_0}{P_{сиг}} < |\Psi_0(\tau, \nu)|^2 >}. \qquad (3.15)$$

[Translator's Note - Subscript letters "макс" and "мин" indicate "max" and "min," respectively.]

3.3. Analysis of Signal/Noise Ratio at the Output of Linear Circuits for the Characteristic Forms of Radar Signals

Whenever useful signals are received against a background of interference caused by reflection from a large number of reflectors and the intensity of the interference is markedly greater than the level of internal receiver noise, which can thus be disregarded, the signal/noise ratio will be determined by the following dependence:

$$q^2_{вых} = \frac{P_{сиг\,max} T_{эф} |\Psi_0(0)|^2}{T_{эф} \int_{-\infty}^{\infty} d\nu \int_{-\infty}^{\infty} |\Psi_0(\tau_{э_0} - \tau, \nu_{д_0} - \nu)|^2 \mu_{вх}(\tau) Q_{вх}(\tau, \nu)\, d\tau}. \qquad (3.16)$$

That this is so follows from expression (3.5).

In most cases of practical concern, the spectral density of the passive interference is concentrated around a certain frequency $\nu_п$ and is uniformly distributed within a small interval of frequencies $\Delta_{\nu_п}$ around this frequency. The density distribution of the interference intensity can be approximated by a uniform distribution in the delay interval $T_п$ and be taken as equal to

$$\mu_{\text{п}}(\tau)=\mu_{\text{п}_0}(\tau)=\begin{cases}\dfrac{P_{\text{пик}}}{T_{\text{п}}} & \text{for } 0<\tau\leqslant T_{\text{п}},\\ 0 & \text{for other } \tau,\end{cases} \tag{3.17}$$

while the distribution of the function $Q_{\text{п}}(\tau, \nu)$ may be assumed to be

$$Q_{\text{п}}(\tau, \nu)=\begin{cases}\dfrac{1}{\Delta_{\nu_{\text{п}}}} & \text{for } \nu_{\text{п}}-\dfrac{\Delta_{\nu_{\text{п}}}}{2}<\nu<\nu_{\text{п}}+\dfrac{\Delta_{\nu_{\text{п}}}}{2},\\ 0 & \text{for others } \nu.\end{cases} \tag{3.18}$$

Then, if

$$T_{\text{п}}>T_{\text{имп}} \tag{3.19}$$

and if the interference overlaps with the signal in range delay and has a frequency distinct from the frequency of the signal, as shown in Fig. 3.2, then from expression (3.16), considering that the value of the cross modulation function in the interval $\Delta_{\nu_{\text{п}}}$ undergoes little change, we obtain

$$q^2_{\text{псогл}}=\frac{P_{\text{сигн}}T_{\text{п}}}{P_{\text{п вх}}\Lambda_{\tau}(\nu_{д_0}-\nu_{\text{п}})},$$

$$q^2_{\text{п}}=\frac{P_{\text{сигн}}T_{\text{п}}|\Psi_0(0)|^2}{P_{\text{п вх}}\Lambda_{\tau_0}(\nu_{д_0}-\nu_{\text{п}})}. \tag{3.20}$$

For nonperiodic broad-band signals with a continuous spectrum, for which $\Delta W >> \nu_{д_0}$, expression (2.22) gives the approximate equality

$$\Lambda_{\tau}(\nu_{д_0}-\nu_{\text{п}})\cong\Lambda_{\tau}(0).$$

Then, for matched filtering we have

$$q^2_{\text{псогл}}=\frac{P_{\text{сигн}}W_{\text{с}}T_{\text{п}}}{P_{\text{п вх}}}. \tag{3.21}$$

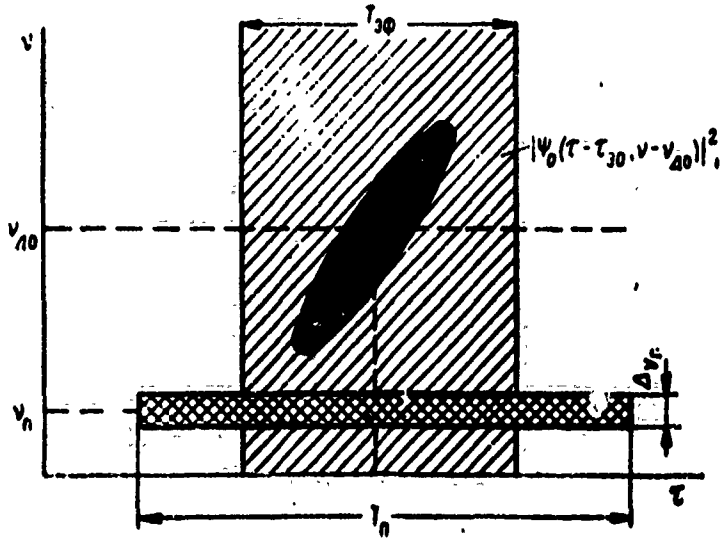

Fig. 3.2. Topographic representation of a uniform frequency-time distribution of interference.

From expressions (3.21) and (2.25), specifically, it follows that for broad-band signals with continuous spectrum with matched filtering in the case of extended passive interference $T_п > T_{эф}$ an improvement of the signal/noise ratio can be achieved only at the expense of expanding the bandwidth of the signal. This cannot be achieved by varying the mode of signal modulation. Additional improvement in this case may be obtained through the use of mismatch filtering, but, as indicated earlier, this inevitably involves energy losses in the detection of the signal against a background of receiver equipment noises. This point is well illustrated in the use of mismatched Urkovits filters [3, 89].

If the extent of the interference $T_п$ is less than the duration of the signal - that is, $T_п < T_{эф}$ - then the value $q^2_{псогл}$ is greatly affected by the modulation mode of the broad-band signals. In effect, using expressions (3.16), (3.17), and (3.18), for a phase-keyed signal for example, considering that its mean indeterminacy function level along the τ axis, when $\nu = \nu_{д0} - \nu_п$, corresponds to a quantiy of the order of

$$< |\Psi(\tau, \nu_{д_0} - \nu_д)|^2_{фм} > \cong \frac{1}{N} = \frac{1}{\Delta W \Delta T},$$

we obtain

$$q^2_{п\,согл\,(фм)} \cong \frac{P_{сех} \Delta W \Delta T}{P_{п\,вх}}. \qquad (3.22)$$

[Translator's Note - The reader will recall that the subscripts "согл," "вх," "фм," and "чм" stand for "matched," "input," "phase-keyed," and "frequency-modulated," respectively.]

From this same expression for a frequency-modulated expression we have

$$q^2_{п\,согл\,(чм)} \cong \frac{P_{сех} F_m T_п}{P_{п\,вх}}, \qquad (3.23)$$

now, when

$$\Delta W \cong F_m$$

$$\frac{q^2_{п\,согл\,(фм)}}{q^2_{п\,согл\,(чм)}} \cong \frac{\Delta T}{T_п}. \qquad (3.24)$$

The same relation occurs if, instead of an FM signal, we consider a pulse signal whose spectrum is equivalent to that of a phase-keyed signal. In this way, the smaller the extent of the interference with respect to the mean-square duration f the signal, the greater the gain in the signal/noise ratio that can be achieved through the use of a phase-keyed signal in comparison with a frequency-modulated or pulsed signal if their bandwidth is wide.

Normally, for narrow-band signals,

$$\Lambda_s(\nu_{д_0} - \nu_д) \ll \Lambda_s(0). \qquad (3.25)$$

With a Doppler frequency shift of $(\nu_{д_0} - \nu_п) \neq 0$ present in the useful signals relative to the interference frequency, this fact makes it possible, by filtering the input oscillation, to enhance considerably the signal/noise ratio.

By way of example, consider the case when the interference exhibits the characteristics (3.17), (3 18), and (3.19) and transmitted pulses of form (2.28) and (2.33) are used, the duration of which is selected so that

$$T_{\Phi} > \frac{1}{\nu_{д_0} - \nu_п}. \qquad (3.26)$$

Since in this case the spectral density of the interference is not constant in the region of the *a priori* frequency values for the useful signal, the frequency response of the filter system must satisfy the relation [78]:

$$K(f) = \kappa_f \frac{S^*(f - f_0 - \nu_{д_0})}{G_п(f - f_0 - \nu_п)\exp(-j2\pi f T_{\Phi})}, \qquad (3.27)$$

where κ_f is a normalizing factor;

T_{Φ} is the filter delay constant;

$S(f - f_0 - \nu_{д_0})$ is the spectrum of the useful signal;

$G_п(f - f_0 - \nu_п)$ is the normed interference energy spectrum, representing a Fourier transform of correlation function (1.37), which, with allowance for (3.17), is expressed as

$$G_п(f - f_0 - \nu_п) = \frac{1}{\mu_{п_0}} \int_{-\infty}^{\infty} B(t)\exp(-j2\pi f t)\,dt.$$

In practical terms, a frequency characteristic of form (3.27) can be achieved through the series connection of a band-elimination and matched filter (Fig. 3.3). Now, the square of the frequency characteristic modulus of the band-elimination filter is approximated by the dependence

$$|K(f-f_0-\nu_{\text{п}})|^2_{\text{реж}}=1-\beta_0\Delta W_{\text{п}}G_{\text{п}}(f-f_0-\nu_{\text{п}}), \qquad (3.28)$$

where β_0 is a normalizing factor for which

$$\beta_0\Delta W_{\text{п}}G_{\text{п}}(0)=1.$$

[Translator's Note - The subscript letter "реж" indicate "band-elimination."]

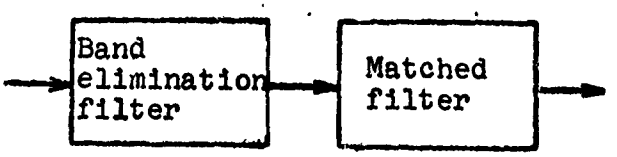

Fig. 3.3. Band-elimination filter circuit diagram.

The effective extent of the reciprocal indeterminacy function we obtain from expression (2.19) by substituting the square of the signal spectrum modulus and the resultant frequency response of the series-connected filters (Fig. 3.3):

$$\Lambda_{\text{т0}}(\nu_{\text{д}}-\nu_{\text{п}})=\frac{1}{T_{\text{эф}}T_{\text{эф}}}\int_{-\infty}^{\infty}|S(f-$$

$$-\nu_{\text{п}})|^2|K(f)|^2_{\text{реж}}|S(f-\nu_{\text{д}_0})|^2df. \qquad (3.29)$$

Figure 3.4 presents graphs of the function $\Lambda_{\text{п}}(\nu)=\frac{\Lambda_{\text{т0}}(\nu_{\text{д0}}-\nu_{\text{п}})}{T_{\text{эф}}}$ versus the frequency shift of the signal with respect to the interference $(\nu_{\text{д}_0}-\nu_{\text{п}})$ for different signal envelopes. Using the

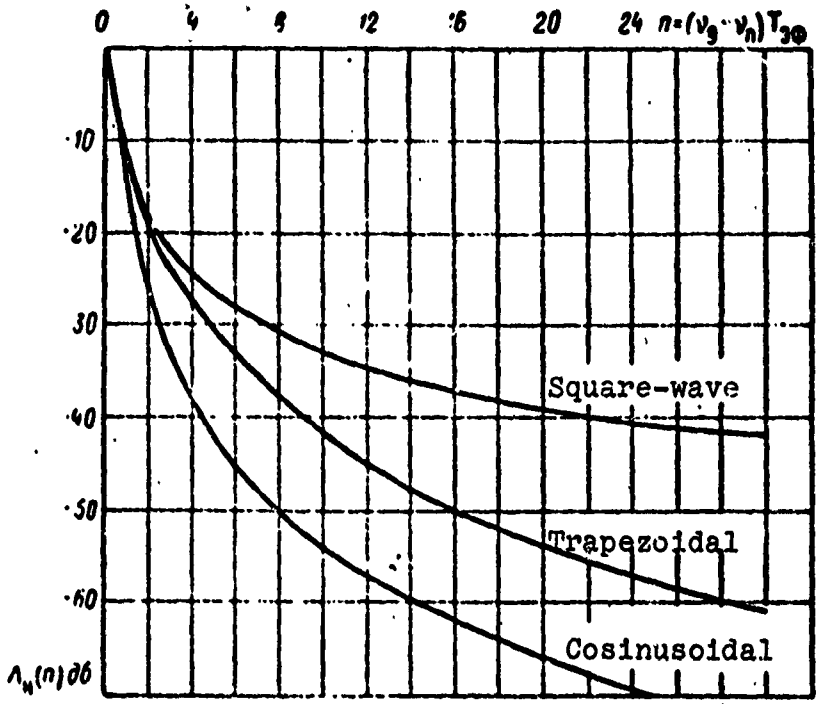

Fig. 3.4. Graph illustrating the decay of function $\Lambda_n(n)$ for a radio pulse with different envelopes.

expression for $\Lambda_n(n)$ and adopting the value $|\Psi_0(0)|^2 \approx 1$, for $\nu_{\text{с}} - \nu_n > \frac{3}{T_{эф}}$, expression (3.20) can be presented in the form

$$q_n^2 = \frac{P_{\text{с}} \times T_n}{P_{\text{ш}} \times \Lambda_n(n)\, T_{эф}}. \qquad (3.30)$$

From (3.30), using the data found in the graphs of Fig. 3.4, the required signal/noise ratio at the filter system output can easily be found for assigned frequency shifts in the signal with respect to the interference, and the optimal envelope form for the signal can thus be selected.

The ratio of relations (3.30) and (3.21) shows the improvement in signal/noise ratio achieved through the use of narrow-band signals over broad-band. This ratio appears as follows:

$$\frac{q^2_{\text{узк}}}{q^2_{\text{шир}}} = \frac{1}{\Lambda_{\text{ш}}(n)\, T_{\text{эф}} W_e}, \qquad (3.31)$$

where $q^2_{\text{узк}}$ and $q^2_{\text{шир}}$ is the signal/noise ratio for narrow- and broad-band signals, respectively. This ratio becomes greater than one - that is, an advantage is incurred in the use of narrow-band signals - when

$$\frac{1}{\Lambda_{\text{ш}}(n)} > T_{\text{эф}} W_e. \qquad (3.32)$$

Relation (3.32) is satisfied in a number of cases, and this factor ensures higher efficiency in the discrimination of useful signals against a background of passive interference through the use of narrow-band signals than with broad-band.

It should be noted that relatively free variation of signal waveform and filter system characteristics is possible only when the problem is one of signal detection. When it is a question of the measurement of signal parameters, the structure of the signal cannot be selected solely on the basis of the required signal/noise ratio since there must simultaneously be taken into account the characteristics which ensure the prescribed accuracy of measurement. Specifically, whenever requirements call for a high degree of accuracy in the measurement and resolution of range delay, it becomes virtually impossible to employ narrow-band signals of type (2.28) and (2.33). The presence of contradictions of this kind leads to severe complications of a general nature in the selection of the main and reference signal waveforms. An optimal solution is possible only in the light of all the particular features of the interference characteristics and radar operating mode, something that calls for a concrete analysis in each separate case. Individual recommendations on this subject have been given in [57, 65, 66, 71, 100].

3.4. Signal Detection with Input-Oscillation Amplitude Limiting

As already noted above, the suppression of pulse interference or compression of the dynamic amplitude range in the filtering system can be achieved through nonlinear transformations of the input oscillation. One such nonlinear transformation of the input oscillation is a nonlinear operation brought about by means of what is known as the "rigid" limiting of the oscillation amplitude. The essential effect of this limiting is to convert an input oscillation of form (1.39) into an oscillation

$$x_{\text{orp}}(t) = A_0 \cos[\omega_0 t + \varphi(t) + \varkappa_x(t) + \varphi_0], \tag{3.33}$$

where A_0 is the constant amplitude of the oscillation at the limiter output [Translator's Note - Subscript letters "orp" indicate "limited"].

A limiter endowed with this property is referred to as "ideal" since it eliminates the oscillation's amplitude modulation while completely retaining the phase modulation. In practical terms this kind of amplitude limiter can be realized in the form of the series connection of a band-pass filter eliminating all the upper harmonics of frequency ω_0 and an inertialess nonlinear element with the characteristic

$$x_{\text{н}}(t) = \begin{cases} A_0 \text{ when } x(t) > 0, \\ 0 \text{ when } x(t) = 0, \\ -A_0 \text{ when } x(t) < 0, \end{cases} \tag{3.34}$$

where $x_{\text{н}}(t)$ is the oscillation at the output of the nonlinear element.

Analysis results for the perfect limiter can be used for preliminary estimates in a number of nonlinear circuits whose amplitude characteristic differs somewhat from that given in (3.34)

(those, for example, which provide a logarithmic conversion of the amplitudes). Individual amplitude-limiting filter-system characteristics have been studied in numerous papers. In [50, 78, 85], for instance, there are discussions of the statistical and spectral characteristics of limited interference and signals, in [25, 26, 50, 93] formulas are derived defining the basic relations between signals and noise at the output of limiters, while [62, 92, 94] deal with the detection characteristics proper to such circuitries. It is worthwhile noting, however, that by and large the question of the detection, resolution, and measurement characteristics for even so individual a variety of nonlinear processing as rigid limiting has not been adequately researched from the theoretical standpoint. This lack of theoretical results is due, primarily, to the mathematical difficulties accompanying the analysis of even the simplest nonlinear circuits. Nevertheless, in the case of specific operating conditions for limiting circuits it is possible to obtain results to support certain conclusions of practical importance which may be used in the engineering synthesis of signal-processing systems.

Relying on the findings of works [50, 92, 94], let us attempt an evaluation of the basic characteristics of the detection system whose block diagram can be seen in Fig. 3.5.

Fig. 3.5. Block diagram of detection channel with limiting.

Assume the channel input (Fig. 3.5) receives an oscillation $x(t)$ consisting of the sum of the signal $u(t)$ and the interference $n(t)$. The interference $n(t)$ is normally distributed and has a constant spectral density N_0 within the passband interval of the band-pass filter ΔF. The signal $u(t)$ is actually a radio pulse of duration T, with arbitrary amplitude $A_0(t)$ and phase $\phi(t)$

modulation:

$$u(t)=\begin{cases} A(t)\cos[\omega_0 t+\varphi(t)] & \text{for } 0<t<T, \\ 0 & \text{for other } t. \end{cases} \tag{3.35}$$

At the output of the ideal limiter the input oscillation x(t) is converted to form (3.33).

In the event a signal with known parameters is detected, the coherent filter circuit performs the operation

$$y=\operatorname{Re} Y=\int_0^T x_{огр}(t)\,v_0(t)\,dt, \tag{3.36}$$

where $v_0(t)$ is a reference signal equal to $v_0(t)=A_0(t)\cos[\omega_0 t+\varphi(t)]$.

By substituting (3.33) in (3.36) we get

$$y=\frac{A_0}{2}\int_0^T A_0(t)\cos[\varkappa_x(t)]\,dt. \tag{3.37}$$

In the general situation the output effect y exhibits a complex distribution, whose form depends on the parameters of the signal and interference, with the consequence that considerable difficulty is encountered in determining the detection characteristics for arbitrary signal and interference parameters; however, for the realistically importance case when the interference spectrum determined by the band of the band-pass filter ΔF is such as to satisfy the dependence

$$\Delta F \gg \frac{1}{T}, \tag{3.38}$$

that is, when a large number of interference fluctuations occur for the duration of the signal, one may assume that the output effect y has a nearly normal distribution. This kind of normalizing is occasioned by the fact that within a period of time T the coherent filter circuit sums a large number of independent and random noise fluctuations.

Normalization of the distribution of output effect y affords a means of simplifying substantially the distribution of the signal's detection characteristics. The parameter D in this case is expressed as a function of the signal/noise ratio at the output of the circuit q^2_{orp} in the form

$$D = \Phi(q_{orp} - Y_0), \tag{3.39}$$

where Y_0 is the relative threshold;

$\Phi(z)$ is the probability integral, equal to

$$\Phi(z) = \frac{1}{\sqrt{2\pi}} \int_{-\infty}^{z} \exp\left(-\frac{t^2}{2}\right) dt. \tag{3.40}$$

This integral has been tabularized, for example, in [78].

The signal/noise ratio at the output of the arrangement shown schematically in Fig. 3.5 is determined from dependence (3.4). The mean value and dispersion of the output effect is defined from expression (3.37) as

$$m_{cu}[y] = \frac{A_0}{2} \int_0^T A_0(t) < \cos[\varkappa_x(t)] > dt, \tag{3.41}$$

$$\sigma^2_{cu}(y) = \left(\frac{A_0}{2\Delta F}\right)^2 \sum_{i=1}^{i=N} A_0^2(t_i)\, \sigma_z\{\cos[\varkappa_x(t_i)]\}, \tag{3.42}$$

where $A_0(t_i)$ and $\varkappa_x(t_i)$ are sampling values of the envelope and phase within time intervals $\frac{1}{\Delta F}$ in conformity with the discrete representation of the signal [23, 24]; $N = T\Delta F$ is the number of independent samplings.

As is evident from (3.41) and (3.42), to a significant degree the mean value and dispersion of the output effect are determined by the statistical characteristics of the function $\cos[\varkappa_x(t_i)]$.

These characteristics have been reviewed in [50, 78].

In the general case, the mean value and dispersion of function $\cos[\kappa_x(t_i)]$ are expressed by a complex nonlinear dependence on the signal/noise ratio $A^2(t)/\sigma^2_{n\,f}$ at the limiter input. However, for the case when

$$\frac{A^2(t)}{\sigma^2_{nf}} \leqslant 0{,}5, \tag{3.43}$$

the following approximation may be accepted:

$$\begin{aligned} &\langle \sin[\varkappa_x(t_i)] \rangle = 0, \\ &\langle \cos[\varkappa_x(t_i)] \rangle \approx \sqrt{\frac{\pi}{8}} \frac{A(t)}{\sigma_{nf}}, \\ &\langle \cos^2[\varkappa_x(t_i)] \rangle \approx \frac{1}{2}, \\ &\sigma^2\{\cos[\varkappa_x(t_i)]\} \leqslant \frac{1}{2}. \end{aligned} \tag{3.44}$$

Now, on the basis of (3.44), (3.42), (3.41), and (1.2), the quantity q^2_{orp} is defined as

$$q^2_{orp} \approx \frac{2\pi\Delta F_2 P_1 T_{эф}}{4\sigma_{nf}}. \tag{3.45}$$

or, with allowance for (1.36), in the form

$$q^2_{orp} \approx \frac{\pi}{4}\left(\frac{2E}{N_0}\right). \tag{3.46}$$

The detection characteristics of a circuit with limiting, when the initial phase of the signal is unknown, may be analyzed with similar methods and, as indicated by the findings of [92], with the same relation arrived at for q^2_{orp}.

Using computerized numerical computations, a determination was made in [94] of the detection characteristics for several cases marked by the nonfulfillment of conditions (3.38) and (3.43).

The graphs for such detection characteristics are shown in Fig. 3.6. From a comparison of these graphs and expressions (3.38) and (3.46) it follows that the sensitivity of the limiting circuit (Fig. 3.5) in the presence of Gaussian interference is somewhat worse in comparison with an optimum linear filtering circuit. In this same context, if condition (3.38) is satisfied, this deterioration is relatively minor and amounts to 1 - 2 dB, whereas if condition (3.38) is not met, the energy losses of the limiting circuit increase and may reach values of as much as approximately 6 dB.

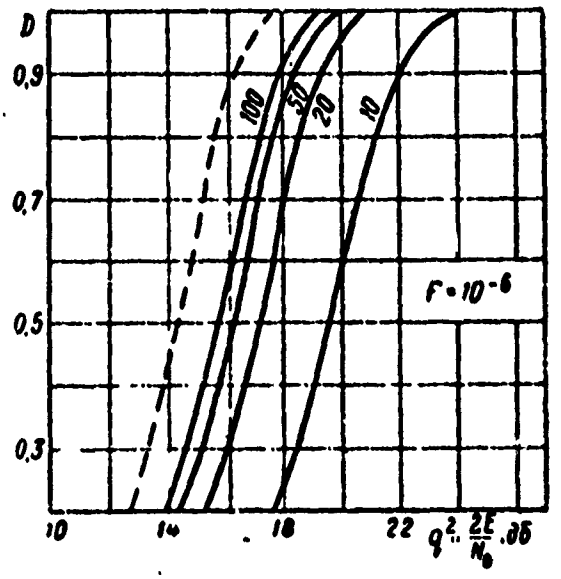

Fig. 3.6. Detection characteristics of a signal-processing circuit with limiting for different

$$\Delta F \cdot T_{э\phi}$$

——— channel with limiting;
– – – no limiting.

The foregoing detection-characteristic analysis was conducted on the assumption that only one useful signal is present in the input oscillation. Generally speaking, considerable difficulties are involved in determining the detection characteristics with allowance for the simultaneous presence of many signals (circuit detection resolution). At the present time, no general approach

to the determination of such characteristics has yet been adequately developed. For this reason, the required estimate can be made only for specific signal waveforms and interference parameters by means of computerized numerical calculations and mathematical simulation techniques. Still, in the event conditions (3.38) and (3.43) are satisfied, there are certain general conclusions which can be drawn.

For the circuit arrangement depicted in Fig. 3.5 the real value of the output effect, as a function of the parameter τ, can be represented in the form:

$$y(\tau) = \operatorname{Re} Y(\tau) = \langle \operatorname{Re} Y(\tau) \rangle + \operatorname{Re} Y^0(\tau), \tag{3.47}$$

where $\langle \operatorname{Re} Y(\tau) \rangle$ is the regular function of the parameter;
$\operatorname{Re} Y^0(\tau)$ is a centered random function.

With allowance for relations (1.44), (3.33), and (3.44), the regular function $\langle \operatorname{Re} Y(\tau) \rangle$ is defined by the expression

$$\langle \operatorname{Re} Y(\tau) \rangle = \left\langle A_0 \int_{-\infty}^{\infty} \cos[\omega_0 t + \varphi(t) + \varkappa_x(t) + \gamma_0] v_0(t - \right.$$

$$\left. - \tau)\, dt \right\rangle = \frac{A_0 \sqrt{\pi 2 P}\, T_{э\Phi}}{2\sqrt{8}\, \sigma_{nI}} \operatorname{Re} \exp(\omega_0 \tau) \int_{-\infty}^{\infty} S(t) S_0^*(t - \tau)\, dt =$$

$$= \frac{A_0 \sqrt{\pi 2 P}\, T_{э\Phi}}{2\sqrt{8}\, \sigma_{nI}} \operatorname{Re} \Psi_0(\tau, 0) \exp(\omega_0 \tau). \tag{3.48}$$

If conditions (3.38) and (3.43) are satisfied, the random function $\operatorname{Re} Y^0(\tau)$ represents a normal random process with zero mean value and a constant dispersion which, as can be easily shown, is approximately determined by the same relation as in (3.42) as well; that is, it equals

$$\langle \{\operatorname{Re} Y^0(\tau)\}^2 \rangle = \frac{A_0^2 T_{э\Phi}}{8 \Delta F}. \tag{3.49}$$

From this last expression (3.49) it is clear that the random function $Y^0(\tau)$ does not, in the case in question, depend on the presence of a signal and can therefore be regarded as a component caused by the interference alone. As a consequence, the representation of the output effect as a sum (3.47), by analogy with (2.1), may be viewed as the decomposition of this effect into a regular and random component. From expression (3.48) it will be evident that the regular output-effect component for the linear and nonlinear circuit differs only in the constant coefficient. For this reason, the circuit with limiting (Fig. 3.5) can be regarded as quasi-linear. With relation (3.43) satisfied for a signal of maximum intensity, the output effect of this kind of circuit on the sum of the signals is characterized by the superposition of the output effects of the individual signals.

With (3.38) and (3.43) unsatisfied, the quasi-linearity of the circuit in Fig. 3.5 is lost and the circuit in this event acquires nonlinear properties which result in additional distortions and loss of signal.

In this way, given a low signal/noise ratio at the limiter input (3.43) and assuming this limiter to be broad-banded (3.38), a detection channel with limiting is nearly equivalent, in terms of its characteristics, to a detection channel incorporating a linear filter circuit. The several advantages offered by limiting filter circuits (such as, for example, their high immunity to pulsed interference and the stabilization of the noise power at the input of the threshold unit) frequently make it advisable to employ these circuit arrangements in practical signal-processing systems. For example, whenever there are considerable changes in the intensity of the interference during the signal-detection process (flickering active interference, passive fluctuational interference), there must be a sufficiently rapid retuning capability for the threshold level in a detection channel with a linear filtering circuit. The presence of such threshold adjustment circuits normally leads to greater complexity in the

signal-detection system and results in additional energy losses in the detection characteristics. With a limiting feature built into the filtering channel, because of the normalized interference level for low signal/noise ratios, there is no longer any need for a tracking threshold [62] and the dynamic amplitude range of the input oscillation is significantly reduced. Because of this, the detection channel circuitry can be simplified and the requirements demanded of its components relaxed.

At the same time, it must be emphasized that because the energy spectrum of the passive interference is of the same value as the spectrum of the main (transmitted) signal, relation (3.38) will not be satisfied for all signal waveforms. Specifically, for signals with $\Delta T \Delta W \cong 1$ relation (3.38) is not fulfilled and there is an additional interference-caused suppression of useful signals leading to energy losses of the order of 6 dB (Fig. 3.6).

To eliminate this undesirable effect in systems with Doppler frequency selection the preliminary filter must ensure the rejection of those of the interference's frequency components which differ from the fundamental frequency components of the useful signals.

In the case of main pulses for which $\Delta T \Delta W >> 1$ condition (3.38) is met, and the effect of the passive interference is equivalent to broad-band noise.

4. SIGNAL PARAMETER MEASUREMENTS

4.1. Measurement Errors

The problem of measuring the parameters of signals is one of the principal problems of primary signal processing. Errors in the measurement of radar signal parameters are primarily caused by the presence of interference, the imperfection and instability of the equipment, and the inconstancy of the electromagnetic wave propagation medium.

Measurement-error calculations are based on the statistical theory of errors. In keeping with this theory, a parameter-measurement result is characterized by its estimate α^0, which differs from the true value of the parameter $\hat{\alpha}$ by the value of the error, that is

$$\nabla(\alpha)=\hat{\alpha}-\alpha^0, \tag{4.1}$$

where $\hat{\alpha}$ is the true value of parameter α.

The estimate of parameter α may be based on a single measurement or on the average results of several measurements. In terms of their character, measurement errors are usually classed as random and systematic.

Random (fluctuational) errors are mainly caused by the presence of interference and also by fast (relative to the interval within which the measurement is conducted) random fluctuations in the equipment or propagation medium. Systematic errors (bias errors) arise in connection with the nonoptimality of the measurement method and equipment calibration, as well as with drifting in the equipment parameters. Another cause of systematic errors may also be found in slow changes in the conditions of the propagation medium and in the effect of certain kinds of interference. Errors of this kind result in the displacement of each measurement's readings by a certain fixed quantity.

Slow drifting on the part of equipment or propagation environment parameters is amenable to measurement or compensation, with the result that in most situations of practical concern better calibration of the equipment or the introduction of corrective factors make it possible to reduce the systematic errors to an acceptably low level.

Fluctuational errors are the result of random causes and cannot, therefore, be reduced merely through the proper selection

of main-signal characteristics, their processing algorithms, the rational design of the equipment, and the optimal selection of its operating modes.

The systematic error is characterized by the mean value of the measurement error, that is

$$\nabla(a)_{\text{сист}} = \langle \nabla(a) \rangle = \hat{a} - \langle a^0 \rangle. \tag{4.2}$$

When in the estimation of the parameter there is no systematic error, that is

$$\hat{a} - \langle a^0 \rangle = 0, \tag{4.3}$$

the mean value of the estimate corresponds to the true value of the parameter to be measured. Such an estimate is said to be unbiased.

The spread of the measurement result values for the parameter relative to its mean value is determined by the dispersion of the error, which in the case of an unbiased estimate is equal to

$$\sigma_a^2 = \langle (\hat{a} - a^0)^2 \rangle. \tag{4.4}$$

Estimates in which the error dispersion is minimal are said to be efficient.

Signal-processing algorithms in measurement systems are normally processed on the basis of requirements for efficient and unbiased estimates. The errors caused by different factors are best analyzed separately, in line with the following breakdown:

Potential errors $\sigma^2_{\text{пот}}$ characterize the potential accuracy of signal-parameter measurement in the face of interference, when the remaining conditions are assumed to be ideal.

Propagation errors $\sigma^2_{\text{расп}}$ are occasioned by random variations in the propagation medium of the electromagnetic waves.

Equipment errors $\sigma^2_{\text{ап}}$ are caused by imperfections in the subsystems of the equipment, by the discrete nature of its readings, as well as by the mismatching and instability of its characteristics.

In the determination of the accuracy characteristics of systems and the synthesis of their optimal circuit arrangements the major emphasis is placed on the analysis of the potential errors since it is these which enable the designer to discover the principal requirements to be demanded of the structure of the signals and their processing algorithms, and also to establish the permissible specific weight of the equipment errors.

4.2. Potential Measurement Accuracy

The potential accuracy attainable in the measurement of a specified signal parameter is determinable on the basis of the static theory of estimation, which is today very well developed and has been described in a great many works, such as for example [4, 78, 81, 89, 95].

In accordance with this theory, the key signal-parameter estimation method is the method of maximum likelihood. With this method, the estimate of the true value of the parameter to be measured is taken to be that value for which the *a posteriori* probability function or the likelihood function of the signal to be estimated acquires its maximum value; that is, there is normally solved the following equation

$$\frac{d \ln L(\alpha)}{d\alpha} = 0, \tag{4.5}$$

where $L(\alpha)$ is the likelihood function for the parameter to be estimated.

Approximate solution of this equation for the case of Gaussian interference, when one of the parameters of the signal is measured while the remaining parameters are known [95], yields the following relation for the measurement-error dispersion for a high signal/noise ratio:

$$\sigma_\alpha^2 \cong \frac{-N_0}{2\left[2E|\Psi_\alpha(0)|'' - \frac{1}{2}\mathcal{E}''(\hat{\alpha})\right]}. \qquad (4.6)$$

where $|\Psi_\alpha(0)|''$ is the value of the second derivative of the modulus of the signal's normalized autocorrelation function for the parameter α to be measured with zero argument;

$\mathcal{E}''(\hat{\alpha})$ is the second derivative of the function defining the dependence of the signal energy on the parameter to be measured for its true value.

Those of the signal's parameters which are independent of its energy are usually said to be nonenergetic. According to expression (4.6), the estimate dispersion for such parameters is written as

$$\sigma_\alpha^2 \cong -\frac{N_0}{2E|\Psi_\alpha(0)|''}. \qquad (4.7)$$

Let us determine the dispersion value for the most characteristic energy-related and non-energy-related signal parameters.

In the measurement of the amplitude of a reflected signal (1.12), according to (2.11), the following dependences obtain:

$$|\Psi_A(0)|'' = 0,$$
$$\mathcal{E}''(A) = 2E. \qquad (4.8)$$

From (4.6), taking into account (4.8), we have

$$\sigma_A^2 = \frac{1}{2E/N_0}. \qquad (4.9)$$

The dispersion of the potential error in the measurement of the signal amplitude depends on the signal/noise ratio alone.

With allowance for expressions (1.24), (1.25), (2.6), and (4.8) the dispersion in the measurement errors for range delay and Doppler frequency shift will be equal, respectively, to

$$\sigma_\tau^2 = \frac{1}{\Delta W^2 2E/N_0}, \tag{4.10}$$

$$\sigma_\nu^2 = \frac{1}{\Delta T^2 2E/N_0}. \tag{4.11}$$

Whenever a number of parameters are unknown and one or several of them are being simultaneously measured, the dispersion in their estimates depends on the correlation connections between the parameters to be measured. Specifically, in the case of the simultaneous measurement of such nonenergetic parameters as range delay and signal frequency shift the estimate dispersion will equal, correspondingly,

$$\sigma_\tau^2 = \frac{1}{\Delta W^2 \frac{2E}{N_0}\left(1 - \frac{\rho^2}{\Delta W^2 \Delta T^2}\right)},$$

$$\sigma_\nu^2 = \frac{1}{\Delta T^2 \frac{2E}{N_0}\left(1 - \frac{\rho^2}{\Delta W^2 \Delta T^2}\right)}. \tag{4.12}$$

Analysis of (2.13), (4.12), and Fig. 2.3 indicates that the value of the dispersion of the potential errors for a fixed signal/noise ratio in a definite scale is defined by the value of the corresponding axes of the indeterminacy ellipse. Therefore, consideration of the indeterminacy ellipse enables us to estimate the potential measurement accuracy for a particular non-energy-related parameter as a function of the class of signal. Analysis of the indeterminacy functions for signals of different types (Figs. 2.9 and 2.13) clearly indicates that, in the measurement

of delay time for known frequency shift, signals having linear frequency modulation permit the achievement of measurement accuracy for this parameter in accordance with the spectral width of the signal following expression (4.11). This gives $\Delta T \Delta W$ better accuracy in delay time measurement in comparison with an unmodulated pulse signal of the same duration.

When the signal's frequency shift is not known but is also to be measured, there is a deterioration in the range delay measurement accuracy for the LFM signal, with this accuracy becoming the same as for the unmodulated signal of identical duration. Here also, accuracy in the measurement of frequency shift is likewise degraded by $\Delta T \Delta W$ times with respect to the signal without modulation.

It is to be noted that this line of reasoning is valid only if there is the possibility of a signal frequency shift commensurate with the frequency deviation of the frequency-modulated signal. If the frequency shift of the signal is much less than the signal's frequency deviation, then the displacement of the maximum output effect for the time lag due to a frequency shift $\Delta\nu$ in the case of a linearly frequency-modulated signal can be estimated as

$$\Delta\tau = \frac{\Delta T \Delta_\nu}{2F_m}, \qquad (4.13)$$

where $\Delta\tau$ is the output effect displacement value.

When

$$\frac{\Delta_\nu}{2F_m} \ll 1,$$

then $\frac{\Delta\tau}{\Delta T} \ll 1$, and delay-time measurement accuracy remains high as compared with the unmodulated signal.

In addition, for many radars the simultaneous measurement of frequency shift and delay time is not mandatory. The signal frequency shift value, in this case, is determined either during

the detection stage using narrow-band signals unmodulated in phase, or by scaling (recomputation) according to the target's radial velocity component obtained through range differentiation during the tracking stage.

When there is a need for the simultaneous measurement of the signal's frequency shift and delay time, the optimal approach is through the use of phase-keyed and periodic signals (2.45) and (2.53). The indeterminacy function for these signals is such that the parameter $\rho = 0$, and thus these signals ensure a high degree of measurement accuracy for both delay time and frequency shift. Similar results are also forthcoming for frequency-modulated signals governed by modulation laws more complex than the linear.

A point to be noted is that analysis of measurement accuracy based on relation (4.7) is not sufficient since it fails to take into account the ambiguity of the measurement and the deterioration of measurement accuracy in the presence of interferential-type noise caused by the mutual time overlap of signals from many targets. If these factors are to be considered, the analysis of characteristic accuracy must be undertaken in conjunction with a study of signal resolving power [4, 6].

Specifically, to reduce interferential noise from overlapping signals, as already noted in Chapter 3, it is possible to use mismatched filters. On the other hand, such mismatching results in a degraded signal/noise ratio at the filter output (3.8) and often gives rise to an expansion of the joint indeterminacy function peak for the parameter to be measured. This has a direct effect on measurement accuracy. We can estimate the measurement errors for non-energy-related signal parameters with mismatch filtering through the use of the dispersion function of the filter-circuit output effect cited in [81]:

$$\sigma_\alpha^2 = \frac{\left\langle \left[\frac{d \operatorname{Re} Y^c(\hat{\alpha})}{d\alpha} \right]^2 \right\rangle}{\left[\frac{d^2 \langle \operatorname{Re} Y(\hat{\alpha}) \rangle}{d\alpha^2} \right]^2}, \qquad (4.14)$$

where $Y^0(\alpha)$ is the centered output-effect function for the true value of the parameter to be measured.

Solving formula (4.14) for a large signal/noise ratio and with allowance for relations (2.1), (2.6), and the expression for the dispersion of an arbitrary random process at the output of a linear system whose input is affected by white noise [78] enables us to derive the following formulas for the dispersions of the range-delay and frequency-shift measurement errors:

$$\sigma_\tau^2 = \frac{1}{\frac{2E}{N_0} \Pi_\tau \Delta W_{\text{pac}}^2},$$
$$\sigma_\nu^2 = \frac{1}{\frac{2E}{N_0} \Pi_\nu \Delta T_{\text{pac}}^2}, \qquad (4.15)$$

where

$$\Delta W_{\text{pac}}^2 = \frac{\int_{-\infty}^{\infty} \omega^2 S(\omega) S_0(\omega) \exp(j\omega t_0)\, d\omega}{\left[\int_{-\infty}^{\infty} |S(\omega)|^2 d\omega \int_{-\infty}^{\infty} |S_0(\omega)|^2 d\omega \right]^{1/2}},$$

$$\Delta T_{\text{pac}}^2 = \frac{(2\pi)^2 \int_{-\infty}^{\infty} t^2 S(t) S_0^*(t) \exp(j2\pi\nu_0 t)\, dt}{\left[\int_{-\infty}^{\infty} |S(t)|^2 dt \int_{-\infty}^{\infty} |S_0(t)|^2 dt \right]^{\frac{1}{2}}},$$

$$\Pi_\tau = \frac{\Delta W_{\text{pac}}^2}{\Delta W_0^2}; \quad \Pi_\nu = \frac{\Delta T_{\text{pac}}^2}{\Delta T_0^2}.$$

[Translator's Note - Subscript letters "pac" indicate "mismatch."]

Here ΔW_0^2 and ΔT_0^2 are the dispersions of the spectrum and time extent of the signal $S_0(t)$ (1.24) and (1.25), while t_0 and ν_0 describe the values of the corresponding arguments at which the signal a' he filter circuit output takes on its maximum value.

When the level of the interferential disturbances is still commensurate with the noise level in the region of the indeterminacy function maximum of the signal whose parameter is to be measured, then this interference must be considered when determining the quantity q^2. The resultant spectral density of the interference, in this case, must contain the component of the spectral density of the interferential noise.

When nonlinear filtering circuitry of the kind shown in Fig. 3.5 is employed, the measurement-error dispersion will differ from the potential. Its value for nonenergetic parameters may also be determined, with allowance for the change in output-effect characteristics, from expression (4.14).

Because of the intricate mathematical relationships involved in the expression of the dispersion in the case of nonlinear transformations it is not possible to represent the dispersion value in the form of a simple design formula. For this reason, this quantity is normally determined by computerized numerical calculations. However, when the signal/noise ratio at the input of the broad-band limiter is low and condition (3.38) is satisfied for the circuit shown in Fig. 3.5, the filter-circuit output effect can be expressed by the sum of the regular and random components (3.47) exhibiting the statistical characteristics (3.48) and (3.49).

Since the random component $\mathrm{Re}Y^0(\tau, \nu)$ has a zero mean value and constant dispersion independent of the presence of a signal, this component can be regarded as caused by the interference alone,

that is, we can consider that

$$Y^0(\tau, \nu) = Y_п(\tau, \nu), \tag{4.16}$$

where $Y_п(\tau, \nu)$ is the circuit output effect with interference present.

Interference with uniform spectral density in a band ΔF, having passed through an ideal limiter, for all practical purposes preserves the distribution law of the spectral density [50, 85]. Thus, it is possible to reason that the spectral density of the interference at the output of the matched filter will be defined by the value

$$N_{огр} = \frac{\sigma^2[n_{огр}(t)]}{\Delta F}, \tag{4.17}$$

where $\sigma^2[n_{огр}(t)]$ is the interference power at the limiter output [Translator's Note - The subscript letters "огр," it will be recalled, indicate "limiter"].

As demonstrated in [78], the dispersion of the oscillation at the limiter output $n_{огр}(t) = A_0 \cos[\omega_0 t + \varkappa_x(t)]$ with random phase $\varkappa_x(t)$ corresponds to

$$\sigma^2[n_{огр}(t)] = \frac{A_0^2}{2}. \tag{4.18}$$

Therefore, expression (4.17) is rewritten in the form

$$N_{огр} = \frac{A_0^2}{2\Delta F}. \tag{4.19}$$

Since the dispersion of the derivative of random process is equal to the second derivative of the correlation function of this process when the value of the argument is zero [78] , and also taking into consideration expression (4.16), we can write

$$\left\langle \left[\frac{d \operatorname{Re} \dot{Y}^{*}(\tilde{\alpha})}{d\alpha} \right]^{2} \right\rangle = \left\langle \left[\frac{d \operatorname{Re} \dot{Y}_{n}(\hat{\alpha})}{d\alpha} \right]^{2} \right\rangle = B''_{\dot{y}_{n}}(0). \qquad (4.20)$$

Employing the properties of the fluctuation-interference autocorrelation function at the output of the matched filter in the presence of white noise [78] and considering (4.19) and (2.11), we get

$$B''_{\dot{y}_{n}}(0) = -\frac{A_0^2 T_{э\phi}}{8\Delta F} \operatorname{Re} \Psi''(0). \qquad (4.21)$$

According to (3.48), the quantity $\left[\frac{d^2 \langle \operatorname{Re} \dot{Y}_{i}(\hat{\alpha}) \rangle}{d\alpha^2} \right]^2$ is equal to

$$\left[\frac{d^2 \langle \operatorname{Re} \dot{Y}(\hat{\alpha}) \rangle}{d\alpha^2} \right]^2 = \frac{\pi A_0^2 2E T_{э\phi}}{32\sigma_{вf}^2} [\operatorname{Re} \Psi''(0)]^2. \qquad (4.22)$$

Now, the value of the dispersion is determined from (4.14), (4.20), (4.21), and (4.22) in the form

$$\sigma^2_{отр}(\alpha) = -\frac{1}{\frac{\pi}{4}\frac{2E}{N_0}|\Psi(0)|''} = -\frac{1}{q^2_{отр}|\Psi(0)|''}. \qquad (4.23)$$

Comparing this last expression with expression (4.8), it will be evident that, with relations (3.42) and (3.47) satisfied, there has been an approximately 1-dB decrease in the accuracy of the measuring circuit with filter limiting, this figure being in accord with the similar energy losses incurred in the detection characteristics (3.46) for limiting circuits.

As the signal/noise ratio increases, the effect of non-linearity on measurement accuracy grows smaller, so that the measurement-error dispersion tends toward the dispersion value of the potential error.

Figure 4.1 shows a graph reflecting the variation in the ratio of the measurement-error dispersion in the case of amplitude limiting to the dispersion of the potential error as a function of the signal/noise ratio.

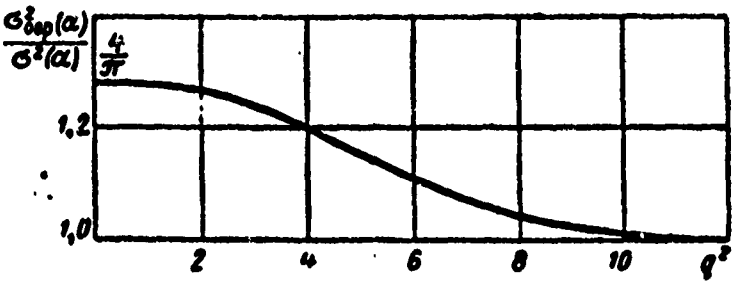

Fig. 4.1. Graph reflecting the change in the measurement-error dispersion with amplitude limiting.

4.3. Measurement Methods and Equipment Errors

As noted above, the estimation of a parameter is ultimately a matter of determining the maximum distribution value of the *a posteriori* probability or likelihood function for the parameter to be estimated. Therefore, just as in the case of detection, an optimal measurement circuit must incorporate a filtering device to shape the *a posteriori* probability distribution for the parameter in question, along with a resolving circuit for the determination of the *a posteriori* distribution maximum [1, 4].

When the parameter to be estimated is capable of changing in an interval of *a priori* values, the filter circuit must ensure that an *a posteriori* probability distribution will be formed for each of these parameter values. If the parameter is in a state of continuous change, this can normally be accomplished only if the parameter is a function of time or intensity; otherwise, the circuit will have to contain an infinitely large number of channels in each of which the distribution of the *a posteriori* probabilities will be formed for parameter values offset one from the other by

an infinitely small quantity. The resolving unit, in this case, would also be called upon to conduct an analysis of a continuous function.

In a circuit of this kind, assuming its absolute stability, the measurement errors would be the same as the potential errors. In actual practice, however, such a circuit can very rarely be designed. Normally, we are faced with a finite number of filter system channels or with a finite number of readings of the parameter's *a posteriori* probability distribution function during the analysis of this probability in the resolver.

The presence of quantification in the reading of the *a posteriori* probability distribution generates additional measurement errors, which increase in proportion to the quantiy of the discrete reading increment. In estimates of signal amplitude the usual source of such discrete-increment readings is the use of digital measurement methods whereby the signal amplitude is matched against standard reference levels (Fig. 4.2).

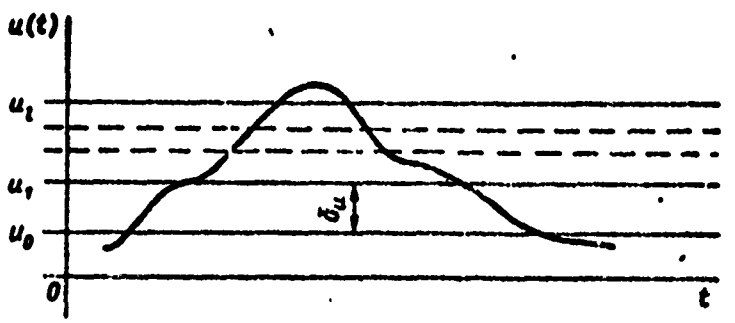

Fig. 4.2. Amplitude quantification of an analog signal.

The maximum reading error, in this case, is equal to the value of the discrete step δ_u between the reference levels:

$$\delta_u = u_i - u_{i-1}. \qquad (4.24)$$

If we assume that the values of the voltage to be measured are of equal probability within the discrete step between reference levels - that is, if the reading error is assumed to be uniformly distributed - then the dispersion error due to the quantification (discreteness) of the reading may be defined (when $\sigma_{u\ пот} > \delta_u$) as

$$\sigma^2_{\delta_u} = \frac{1}{\delta_u}\int_0^{\delta_u} x^2 dx - \left[\frac{1}{\delta_u}\int_0^{\delta_u} x dx\right]^2 = \frac{\delta_u^2}{(2\sqrt{3})^2}. \qquad (4.25)$$

[Translator's Note - The subscript letters "пот" refer to "potential."]

By fixing a definite ratio between the potential measurement error and the quantification error, we can determine from (4.25) the maximum permissible discrete reading increment:

$$\delta_{u\,макс} = 2\sqrt{3}\gamma_{доп}\sigma_{u\,пот}, \qquad (4.26)$$

where $\sigma_{u\,пот}$ is the potential rms amplitude-measurement error;

$\gamma_{доп} = \frac{\sigma_{\delta_u}}{\sigma_{u\,пот}}$ is the permissible ratio of rms errors [Translator's Note - The subscript letters "доп" indicate "permissible."]

In the measurement of non-energy-related signal parameter the discreteness of the reading may even develop at so early a point as during the filtering of the signal. The structural layout of a filtering device providing for the formation of an output effect as a function of the parameter α may be envisioned as illustrated in Fig. 1.4. The maximum measurement error value in this case is $\pm\frac{\delta_\alpha}{2}$, where δ_α is the discrete step in the spacing of the channels.

Considering, as in the case of the amplitude measurement, that the error within the interval $\pm\frac{\delta_\alpha}{2}$ is uniformly distributed,

we obtain an error dispersion equal to

$$\sigma_\delta^2 = \frac{2}{\delta_\alpha}\int_0^{\frac{\delta_\alpha}{2}} x^2 dx = \frac{\delta_\alpha^2}{(2\sqrt{3})^2}. \qquad (4.27)$$

When along with the determination of the maximum value of the signal at the channel output there are assigned the values at which the amplitude difference of the signals from two adjacent channels does not exceed a certain prescribed quantity, and when as the estimate of the signal parameter its mean value between channels is adopted, then the maximum measurement error due to the discrete character of the reading can be reduced to the value $\frac{\delta_\alpha}{2}$, and its dispersion, accordingly, to the value

$$\sigma_\delta^2 = \frac{\delta_\alpha^2}{(4\sqrt{3})^2}. \qquad (4.28)$$

To eliminate the effect of equipment errors on measurement accuracy, a fairly low value is selected for $\gamma_{доп}$. In the event the equipment errors due to quantification are commensurate with the potential errors, their contribution to the resultant measurement error can be estimated using the formula derived in [14]

$$\frac{\sigma_\Sigma^2}{\sigma_\alpha^2} \approx \frac{\delta_\alpha}{\sqrt{\pi}\,\sigma_\alpha} \qquad (4.29)$$

when

$$\frac{\delta_\alpha}{\sigma_\alpha} > 2,$$

where σ_Σ^2 is the dispersion of the resultant measurement error with allowance for the discrete nature of the readings.

By assigning the ratio of the disperion of the resultant error to the dispersion of the potential error we can determine the

maximum possible spacing of the channels for parameter α. If the permissible value of relation (4.29) is set in accordance with the prescribed measurement accuracy, then, for an *a priori* interval Δ_α for parameter α, the number of necessary channels m is defined as

$$[m = \frac{\Delta_\alpha}{\sqrt{\pi}\left(\frac{\sigma_\Sigma}{\sigma_\alpha}\right)^2 \sigma_\alpha} + 1. \qquad (4.30)$$

To ensure high measurement accuracy for a large interval of *a priori* values in the parameter to be measured, as a rule the circuit shown in Fig. 1.4 must, following expression (4.30), contain a large number of channels. Since this introduces a considerable degree of complexity in the processing system, in many instances it is simplified through the use of a consecutive method of parameter measurement.

Initially, in this method, a rough estimate is made of the parameters, following which their values are refined through measurement of the error. Normally, this error measurement is accomplished by means of a so-called discriminator, with this device estimating the deviation of the true value of the parameter from a certain specified value within the range of the error as roughly measured [56, 81]. A generalized structural diagram illustrating this kind of measurement technique may be see in Fig. 4.3.

With this measurement method the value estimate for the parameter to be measured equals

$$\alpha^0 = \alpha_{\text{макс}} + \alpha_{\text{ут}}, \qquad (4.31)$$

where $\alpha_{\text{макс}}$ is the number of the channel in which the signal is maximum;

$\alpha_{\text{ут}}$ is a correction for the rough measurement of parameter α.

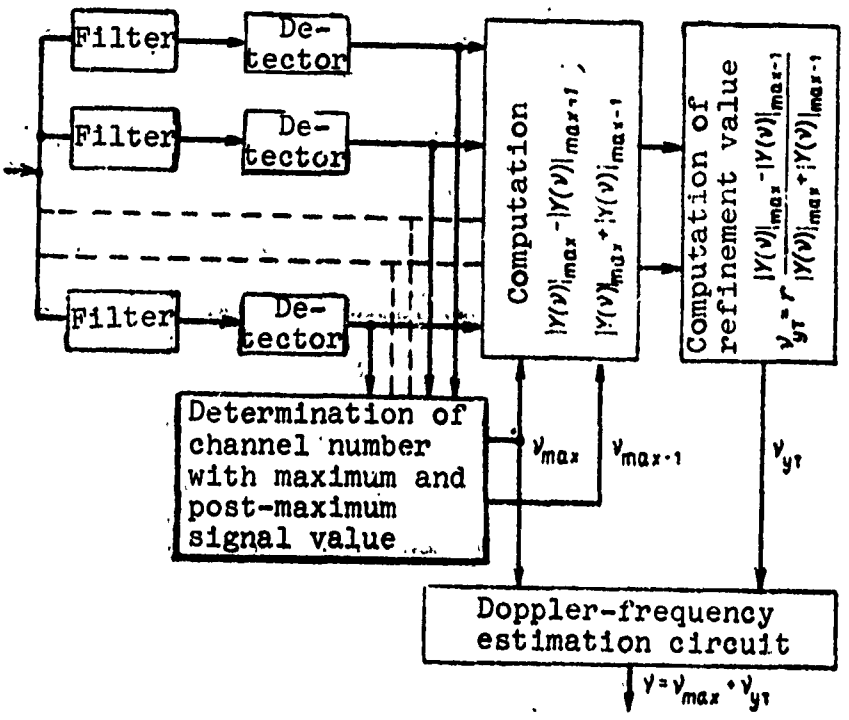

Fig. 4.3. Structural diagram of filtering and Doppler frequency measuring system with refinement feature.

In actual practice, the α_{yT} correction value is most often determined in conformity with the relation

$$\alpha_{yT} = k_d \frac{|Y(\alpha)|_{макс} - |Y(\alpha)|_{макс-1}}{|Y(\alpha)|_{макс} + |Y(\alpha)|_{макс-1}} \quad \frac{1}{2}, \qquad (4.32)$$

where $|Y(\alpha)|_{макс}$ is the value of the maximum effect received from the filter circuit following detection;

$|Y(\alpha)|_{макс-1}$ is the value of the output effect following the maximum in order of magnitude;

k_d is a constant calibration factor corresponding to the steepness of the discrimination characteristic.

With this kind of arrangement the dispersion of the measurement error will approximate the potential error for a smaller number of channels than in the case of the circuit depicted in Fig. 1.4. The value of this dispersion can be defined in the form

$$\sigma_{\alpha}^{2} = -\frac{1}{\frac{2F}{N_0}|\Psi_{\alpha}(0)|''\xi_k}, \qquad (4.33)$$

where ξ_k is a coefficient dependent on the steepness of the discrimination characteristic.

5. SIGNAL PROCESSOR DESIGN PRINCIPLES

5.1. Design Principles for Coherent Signal Filtering Devices

As already indicated, optimal signal processing is accomplished through the use of pre- and post-detector filtering (Section 1.4). A condition for predetector filtering is that the signals be coherent, and for this reason the circuits involve in this procedure are also often referred to a coherent signal-filtering circuits. Conversely, as a consequence of the fact that signals at the detector output carry only amplitude information, signal filtering after the detector is called noncoherent, and the circuits for the filtering of such signals-noncoherent filter circuits.

We shall proceed on the assumption that the principal functions to be performed by the coherent filtering unit are the operations involved in forming a correlation integral from the received oscillation with a certain reference signal (1.44) and in extracting the modulus from the result obtained. Normally, the operation of forming the correlation integral is performed by a coherent filter circuit, and that of deriving the modulus by nonlinear envelope-discrimination circuits. If the parameters of the signal are unknown, operation (1.44) must be performed for a continuous series of values for these parameters spanning the entire range of their possible variation.

Specifically, when the reflected signal is a function only of the two informational non-energy-related parameters $\tau_э$ and $\Omega_д$ (1.13), the unit providing for the coherent filtering of the signal must perform an operation of the type

$$|Y(\tau_{э_0}, \Omega_{д_0})| = \left| \int_{-\infty}^{\infty} S_x(t) S^*_0(t - \tau_{э_0}) \exp[-j(\Omega_{д_0} t dt)] \right|, \qquad (5.1)$$

where $S_x(t)$ and $S_0(t)$ are the complex envelopes of the input oscillation and reference signal, respectively;

$\tau_{э_0}$ is the anticipated delay time of the signal with respect to the moment of main pulse transmission;

$\Omega_{д_0}$ is the anticipated Doppler frequency shift of the signal with respect to zero Doppler frequency.

In the event the frequencies of the received and reference signals coincide, the filter-system output effect matches the envelope of the correlation integral only for the delay-time parameter, that is

$$|Y(\tau_{э_0})| = \left| \int_{-\infty}^{\infty} S_x(t) S^*_0(t - \tau_{э_0}) dt \right|. \qquad (5.2)$$

Systems implementing operations of type (5.1) and (5.2) may be designed using either the correlation principle or the filter principle of signal processing.

With correlation processing there is the direct computation of function (5.1) for a series of discrete values for parameters $\tau_{э_0 i}$ and $\Omega_{д_0 i}$. The degree of discreteness in the spacing of the parameters $\tau_{э_0 i}$ and $\Omega_{д_0 i}$ is determined by the permissible deterioration in the detection and measurement characteristics, and, depending on the signal parameters, may be selected for the

delay time and Doppler frequency shift of the signal, respectively, as

$$\delta_\tau = \frac{1}{\gamma_\tau \Delta W}$$

and

$$\delta_\Omega = \frac{1}{2\pi\gamma_\Omega \Delta T}. \qquad (5.3)$$

where γ_τ and γ_Ω are proportionality factors describing the permissible deterioration in the detection or measurement characteristics.

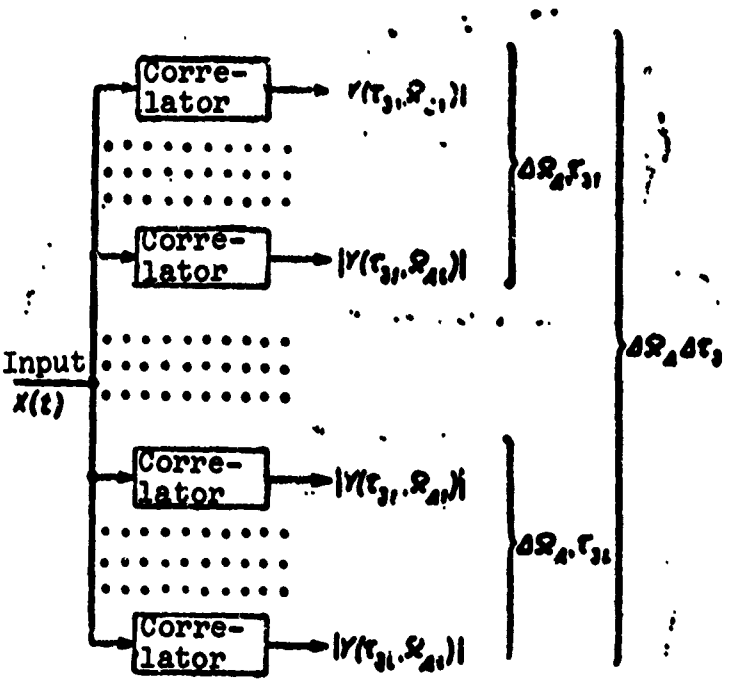

Fig. 5.1. Signal correlation processing channels.

In the event the possible range of variation for parameters τ and Ω constitutes, respectively, the values Δ_τ and Δ_Ω, the envelope of the correlation integral must be computed at

$\frac{\Delta_1\Delta_2}{2\pi\gamma_1\gamma_2\Delta W\Delta T}$ points. The block diagram of this kind of filtering system will appear as shown in Fig. 5.1. It will be seen from the diagram that this system is multichannel in design.

When signals are used for which $\Delta_1\Delta W \cong 1$ and $2\pi\Delta_2\Delta T \cong 1$, the number of channels in the correlation filter unit is small and the system can be designed in a relatively simple fashion. On the other hand, when

$$\Delta_1\Delta W \gg 1,\ 2\pi\Delta_2\Delta T \gg 1, \tag{5.4}$$

the number of channels in this circuit becomes fairly large and a considerable degree of sophistication is involved in its design.

To reduce the number of channels in the system, filter principles of signal processing are called upon. With this method of processing, the correlation integral (1.44) is formed by means of a filter which gives a response which is a mirror function with respect to the reference signal.

In effect, let the modulation function of the reference signal be $S_0(t)$ and that of the filter response, disregarding the delay constant, be $S_0(-t)$. The modulation spectrum of the input oscillation and filter response, in this case, will be expressed, respectively, as $S_x(\omega)$ and $S_0^*(\omega)$, while the modulation spectrum of the filter output signal will equal

$$S_y(\omega) = S_x(\omega)S^*_0(\omega). \tag{5.5}$$

Now, the filter-output oscillation envelope will appear as

$$|\Gamma(\tau_{3_j})| = \left| \frac{1}{2\pi} \int_{-\infty}^{\infty} S_1(\omega) \exp(j\omega\tau_{3_0})\, d\omega \right| =$$

$$= \left| \int_{-\infty}^{\infty} S_x(t)\, S^*_0(t - \tau_{3_j})\, dt \right|. \qquad (5.6)$$

Thus, a filter having a complex response envelope $S_0(-t)$ provides the continuous formation of a correlation integral for the parameter τ_3 for a specified Doppler frequency value in the reference signal.

To cover the range of Doppler frequencies Δ_Ω, a set of such filters is required having a discrete tuning increment δ_Ω (Fig. 5.2). Because of the reduced number of channels there will be somewhat fewer filters in this case than in the correlation circuit, their number being $\gamma_\Omega \Delta_\Omega \Delta T$.

In certain situations, the so-called correlation-filter processing principle [95] may be employed in the processing of complex multidimensional signals. The essential feature of this principle consists in the successive (sequential) computation of integral (5.2) first by the correlative and then by the filter method. The reference-signal modulation function in this case is represented by the product of the two signals:

$$S_0(t) = S_1(t) \cdot S_2(t). \qquad (5.7)$$

With the envelope of the correlation expressed in the form

$$|\Gamma(\tau_{3_0})| = \left| \int_{-\infty}^{\infty} S_x(t)\, S^*_1(t - \tau_{3_0})\, S^*_2(t - \tau_{3_0})\, dt \right| =$$

$$= \left| \int_{-\infty}^{\infty} S_{x_1}(t)\, S^*_2(t - \tau_{3_0})\, dt \right|, \qquad (5.8)$$

where

$$S_{x_1}(t) = S_x(t)\, S^*_1(t - \tau_{3_0}).$$

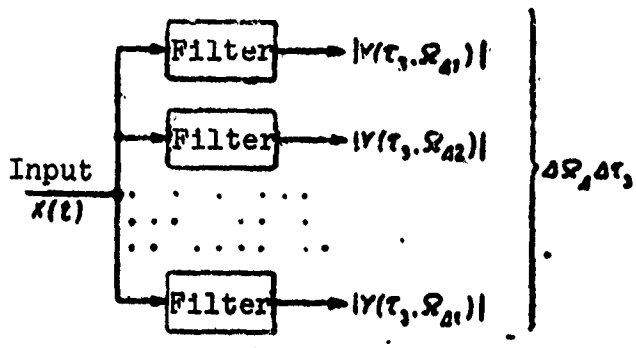

Fig. 5.2. Signal filter processing channels.

At the input of the circuit the incoming signal is multiplied by the reference signal envelope and the result is filtered by a filter matched with a signal whose modulation function corresponds to

$$\frac{S_0(t)}{S_1(t)}.$$

Inasmuch as a signal with this kind of modulation function can be much simpler than the initial reference signal, simpler filters can be used in this situation.

Let us consider the characteristic of the real circuits required to implement correlation-type and filter-type signal processing. To this end, we shall express the correlation integral of the two real signals

$$y(\tau) = \int_{-\infty}^{\infty} v_1(t)\, v_2(t - \tau)\, dt \qquad (5.9)$$

by their complex modulation functions. Let

$$v_1(t) = \operatorname{Re} S_1(t) \exp[j(2\pi f_0 t + \varphi_1)],$$
$$v_2(t) = \operatorname{Re} S_2(t) \exp[j(2\pi f_0 t + \varphi_2)]. \qquad (5.10)$$

Using the well known formula from the theory of complex functions

$$\operatorname{Re} z_1 \operatorname{Re} z_2 = \operatorname{Re}\left[\frac{z_1 z_2}{2} + \frac{z_1 z_2^*}{2}\right]$$

and bearing in mind that the result of the integration of a rapidly oscillating process over a fairly large time interval tends toward zero, we obtain

$$\int_{-\infty}^{\infty} v_1(t)\, v_2(t-\tau)\, dt = \frac{1}{2} \operatorname{Re}\{\exp j[2\pi f_0 \tau + (\varphi_1 - \varphi_2)] \times$$
$$\times \int_{-\infty}^{\infty} S_1(t)\, S_2^*(t-\tau)\, dt\} = \frac{1}{2}\left|\int_{-\infty}^{\infty} S_1(t)\, S_2^*(t-\tau)\, dt\right| \times$$
$$\times \cos[2\pi f_0 \tau + \varphi_1 - \varphi_2 + \varphi_a(\tau)], \qquad (5.11)$$

where $\varphi_a(\tau) = \arg \int_{-\infty}^{\infty} S_1(t)\, S_2^*(t-\tau)\, dt.$

In keeping with dependence (5.11), the correlation integral of the real input oscillation x(t) with the real reference signal $v_0(t)$ will be defined by the expression

$$y(\tau) = \int_{-\infty}^{\infty} x(t)\, v_0(t-\tau)\, dt = \frac{1}{2} |Y(\tau)| \cos[2\pi f_0 \tau +$$
$$+ \varphi_x - \varphi_0 + \arg Y(\tau)], \qquad (5.12)$$

where

$$x(t) = \operatorname{Re} S_x(t) \exp\{j(2\pi f_0 t + \varphi_x)\};$$
$$v_0(t) = \operatorname{Re} S_0(t-\tau) \exp\{j[2\pi f_0 (t-\tau) + \varphi_0]\}.$$

From expression (5.12) it follows that the correlation integral of real radio signals with carrier frequencies f_0 will be an oscillating function with the same center frequency (Fig. 5.3). The values of this function for the time delay

$$\tau = -\frac{\varphi_x - \varphi_s + \arg Y(\tau)}{2\pi f_0} \tag{5.13}$$

will be in accord with the required values of the envelope $|Y(\tau)|$.

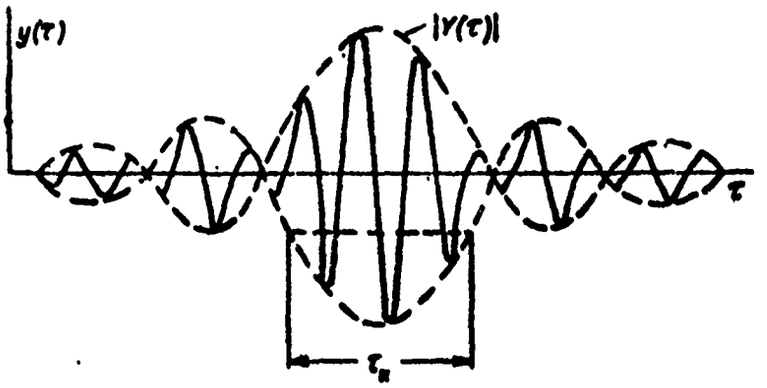

Fig. 5.3. Correlation function diagram.

In practical filtering circuits one of the means of discriminating the envelope is through the quadrature conversion of the input oscillation.

Considering that the real oscillation x(t) can be expressed as

$$x(t) = \frac{1}{2}\{S_x(t)\exp[j2\pi(f_0 - \nu)t] + S^*_x(t)\exp[-j2\pi(f_0 - \nu)t]\}, \tag{5.14}$$

relation (5.2) for the continuous value of the parameter τ can be rewritten in the form

$$|Y(\tau)| = \left|\int_{-\infty}^{\infty} x(t)\,S^*(t-\tau)\exp[-j2\pi(f_0-\nu)t]\,dt\right|. \tag{5.15}$$

Placing the phase factor $\exp(-j2\pi\nu\tau)$ under the integral sign and performing simple operations, we obtain

$$|Y(\tau)| = \left| \int_{-\infty}^{\infty} x(t) S^*(t-\tau) \exp(-j2\pi f_0 t) \times \right.$$
$$\left. \times \exp[j2\pi\nu(t-\tau)]\, dt \right|.$$

Calling on a familiar relation from the theory of complex functions, we get

$$|Y(\tau)| = \sqrt{[\mathrm{Re}\, Y(\tau)]^2 + [\mathrm{Im}\, Y(\tau)]^2}, \qquad (5.16)$$

where

$$\mathrm{Re}\, Y(\tau) = \int_{-\infty}^{\infty} x(t)\, \mathrm{Re}\{S^*(t-\tau)\exp(-j2\pi f_0 t) \times$$
$$\times \exp[j2\pi\nu(t-\tau)]\} = \int_{-\infty}^{\infty} x_c(t) A_c(t-\tau)\, dt +$$
$$+ \int_{-\infty}^{\infty} x_s(t) A_s(t-\tau)\, dt = I_{cc}(\tau) + I_{ss}(\tau),$$
$$\mathrm{Im}\, Y(\tau) = \int_{-\infty}^{\infty} x_s(t) A_c(t-\tau)\, dt -$$
$$- \int_{-\infty}^{\infty} x_c(t) A_s(t-\tau)\, dt = I_{sc}(\tau) - I_{cs}(\tau), \qquad (5.17)$$

$$x_c(t) = x(t)\cos(2\pi f_0 t);$$
$$x_s(t) = x(t)\sin(2\pi f_0 t);$$
$$A_c(t-\tau) = A_0(t-\tau)\cos[2\pi\nu(t-\tau) - \varphi(t-\tau)];$$
$$A_s(t-\tau) = A_0(t-\tau)\sin[2\pi\nu(t-\tau) - \varphi(t-\tau)].$$

Finally we obtain

$$|\dot{Y}(\tau)| = \sqrt{[I_{cc}(\tau) + I_{ss}(\tau)]^2 + [I_{sc}(\tau) - I_{cs}(\tau)]^2}. \qquad (5.18)$$

Expression (5.17) and (5.18) can be used in the circuit design of practical filtering systems.

Figure 5.4 illustrates the block diagram of a filtering unit for the correlation technique of signal processing in the time lag range of $0-\tau_1$. Whenever along with the delay time the Doppler frequency shift $\nu_д = 2\pi\Omega_д$ is also unknown, in each delay channel this circuit must contain supplementary quadrature channels tuned to the anticipated Doppler frequencies of the signal $\nu_1, \ldots, \nu_i$.

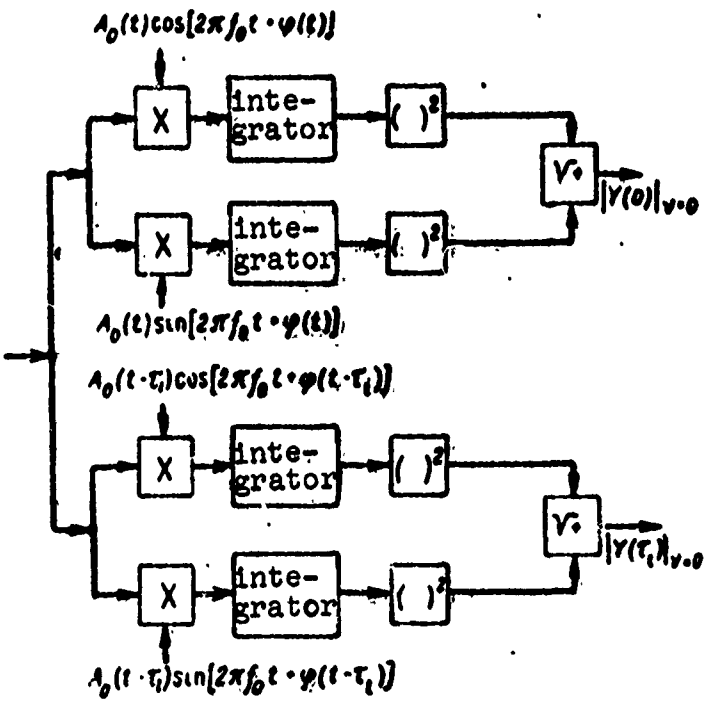

Fig. 5.4. Block diagram of quadrature correlation processing of the signal.

The block diagram for the filter method of processing in the video-frequency band is shown in Fig. 5.5. Filters Cv_i and Sv_i are video-frequency filters with responses

$$K_{cv_i}(t) = A_0(T_\phi - t)\cos[2\pi v_i(T_\phi - t) + \varphi(T_\phi - t)], \qquad (5.19)$$
$$K_{sv_i}(t) = A_0(T_\phi - t)\sin[2\pi v_i(T_\phi - t) + \varphi(T_\phi - t)],$$

where T_ϕ is a specified filter delay constant.

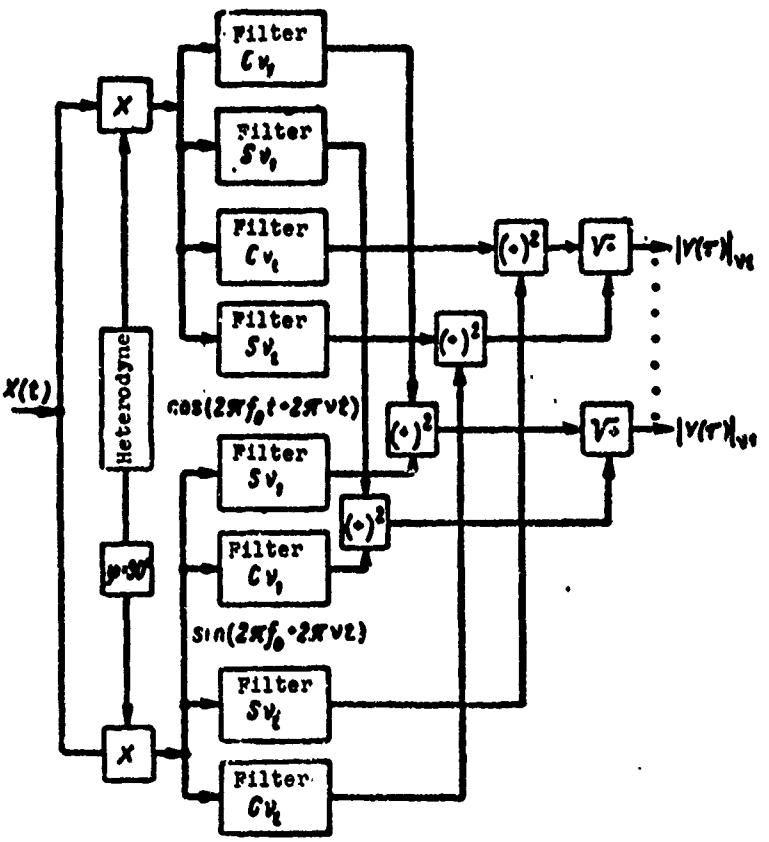

Fig. 5.5. Block diagram of quadrature filter processing of the signal.

Another method of separating out the envelope of the correlation integral in practical circuit arrangements is through the detection of the signal at the output of the circuit in which it has been coherently filtered. This approach is applicable only in the case of filter or correlation-filter signal processing. Here, the filter output provides a continuous value for the function $y(\tau)$, with the value $|Y(\tau)|$ formable only through simple detection of function $y(\tau)$. A block diagram of a filtering device implementing this approach is shown in Fig. 5.6.

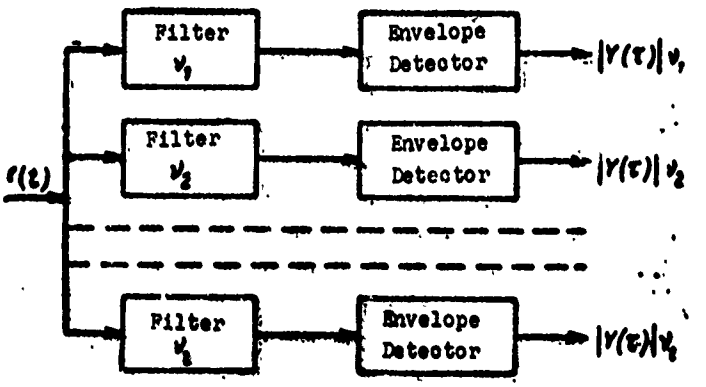

Fig. 5.6. Block diagram of filter processing of signal.

Each filter in this circuit is tuned to different signal frequencies differing from each other by the value ν_i. All told, the circuit covers a signal frequency-shift range of $\Delta_\nu = i\nu_i$. The individual filter's real response in this arrangement will be

$$K_i(t) = \mathrm{Re}\, S(T_\phi - t) \exp\{j[2\pi(f_0 + \Omega_i)(T_\phi - t)]\}. \qquad (5.20)$$

In the correlation-filter processing method, by analogy with (5.12), the correlation integral for real signals can be expressed in the form

$$y(\tau) = \int_{-\infty}^{\infty} x_1(t)\, v_2(t-\tau)\, dt = \frac{1}{2}|Y(\tau)| \cos [2\pi (f_0 - f_1) t + \\ + \varphi_x - \varphi_s + \arg Y(\tau)], \tag{5.21}$$

where

$$x_1(t) = \operatorname{Re} S_x S_1 (t-\tau) \exp \{j [2\pi (f_0 - f_1) t + \varphi_x]\},$$
$$v_2(t) = \operatorname{Re} S_2(t) \exp \{j [2\pi (f_0 - f_1) t + \varphi_s]\}.$$

A knowledge of $x_1(t)$ can be acquired through the multiplication of the real signals

$$x(t) = \operatorname{Re} S_x(t) \exp [j (2\pi f_0 t + \varphi_x)]$$

and

$$v_1(t) = \operatorname{Re} S_1(t) \exp [j (2\pi f_1 t + \varphi_0)] \tag{5.22}$$

followed by the filtering of the signal with the difference frequency $f_0 - f_1$.

On the basis of these considerations, a practical block diagram for signal processing by the correlation-filter method for the range of parameters τ and ν will appear as shown in Fig. 5.7.

The filters in each correlation channel are tuned to different signal frequencies offset by the quantity ν_i. For each filter the real response will be

$$K_i(t) = \operatorname{Re} S_2(T_\phi - t) \exp [j 2\pi (f_0 - f_1 - \Omega_i)(T_\phi - t)]. \tag{5.23}$$

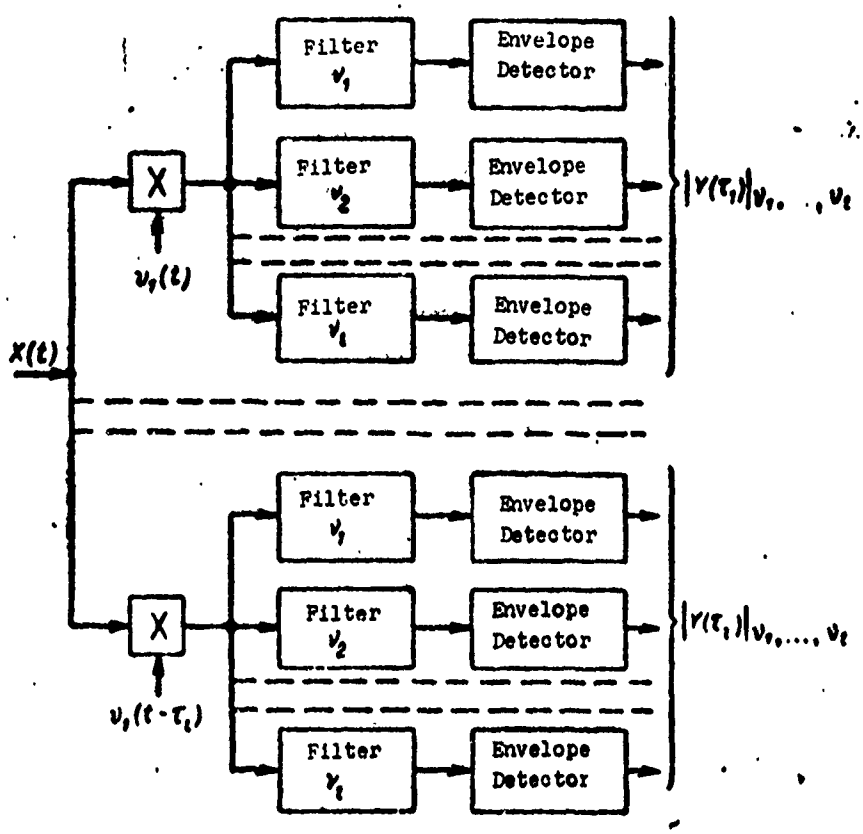

Fig. 5.7. Block diagram of correlation-filter processing of the signal.

5.2. Design Principles for Noncoherent Signal-Filtering Devices

Noncoherent signal-filtering systems are designed for the processing of signals following their detection. This processing, in concert with coherent filtering, implements an optimal algorithm whenever the coherence of the signal (the *a priori* knowledge of its phase variation law) does not extend to its entire duration [81, 95].

The structural arrangement of the noncoherent filtering device is largely determined by the character of the signal and the form of its coherent processing algorithm.

In the event the signal to be processed is representable in the form of the sum of the elementary signals

$$v(t)=\sum_{k=1}^{k=N}\operatorname{Re}\sqrt{\frac{b_k}{T_{эф}}}\,S_k'(t)\exp(j2\pi f_k t), \tag{5.24}$$

for which the coherence occurs only within a time interval corresponding to their duration T_k (where, for simplicity's sake, T_k = const), noncoherent signal-processing for a specified value of the parameter Ω_i can be resolved to operations of the kind

$$Y_н(\tau)_{\Omega_i}=\sum_{k=1}^{k=N} b_k\,|Y_{\Omega_i}(\tau-kT_k)|=$$

$$=\sum_{k=1}^{k=N} b_k\sqrt{\frac{b_k}{T_{эф}}}\left|\int_{-\infty}^{\infty}S_x(t)S_k(t-\tau-kT_k,\Omega_i)\,dt\right|, \tag{5.25}$$

$$Y_н(\tau)_{\Omega_i}=\sum_{k=1}^{k=N} b_k^2\,|Y_{\Omega_i}(\tau-kT_k)|^2.$$

[Translator's Note - The subscript letter "н," it will be recalled, indicates "noncoherent."]

Quadratic summation is taken for low signal/noise ratios or for a fluctuating signal. Linear summation is optimal for a nonfluctuation signal with a large signal/noise ratio.

A device implementing operations of form (5.25) for a number of fixed parameter values Ω_i can be designed in accordance with the block diagram shown in Fig. 5.8. Each elementary signal is coherently filtered by its own filter, following which the envelope of the signal is discriminated. The elementary video signals are delayed, functionally transformed, and summed with their appropriate weighting factors.

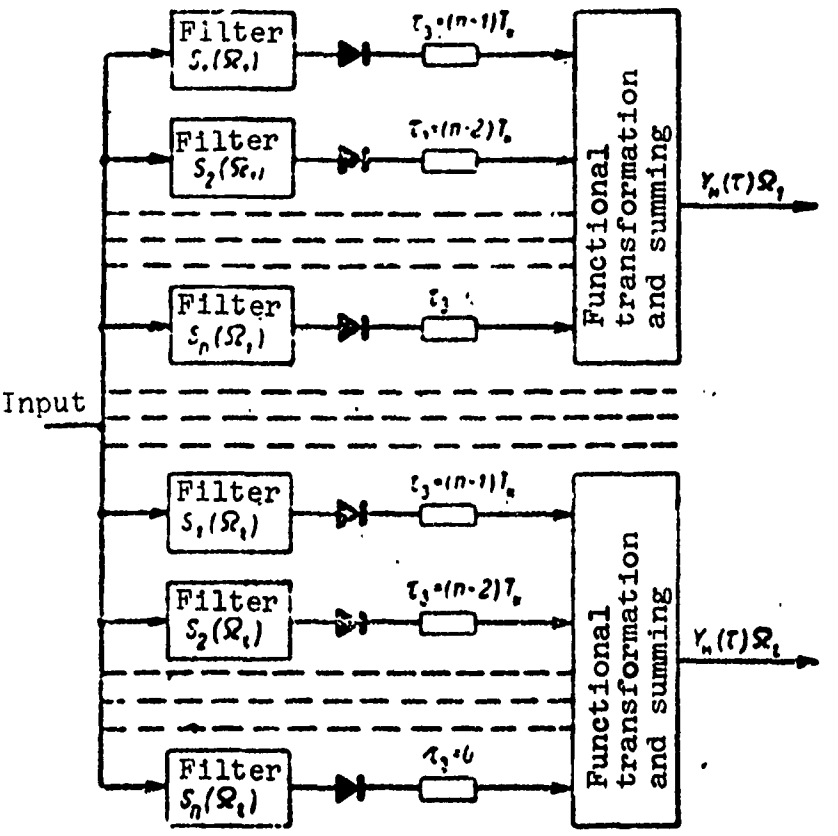

Fig. 5.8. Block diagram of the noncoherent processing of orthogonal signals.

When the elementary radio signals are similar - that is, when the condition

$$\int_{-\infty}^{\infty} S_i(t)\exp(j2\pi f_i t)\,S^*_j(t)\exp(-j2\pi f_i t)\,dt = T_{эф}, \tag{5.26}$$

is satisfied for all i and j - the coherent filtering of all the elementary signals can be accomplished by a single common filter, and their weighted summation by a video-frequency filter.

Figure 5.9 shows the block diagram for this kind of signal processing for a numer of parameters Ω_i. In this circuit the response of the coherent filter is selected to mirror the elementary signal $S_j(t)$, while the response of the video filter

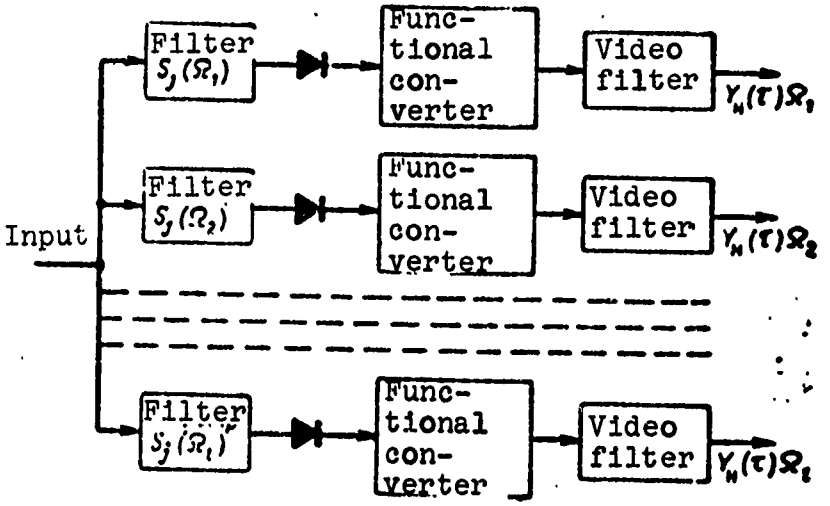

Fig. 5.9. Block diagram of the noncoherent processing of uniform signals.

is set in accordance with the envelope $|Y_{\Omega_1}(\tau-kT_H)$.

Along with the filtering methods of noncoherent signal processing illustrated in Fig. 5.9, correlation techniques may also be used. The system schematics in this case will resemble those found in devices applying these methods to coherent signal filtering (Section 5.1).

Quite frequently in actual radar practice partial noncoherent filtering is also employed for the processing of a fully coherent signal as well. This is normally done whenever information regarding the signal's frequency parameters is not necessary, but the signal's structure and parameters are such that a relatively sophisticated multichannel system (Figs. 5.6, 5.7) would be required for its coherent filtering. By reducing the interval of coherent filtering, it becomes possible to expand the band of the coherent filter, thus permitting effective operation with significantly fewer frequency channels.

The application of partial coherent filtering with subsequent noncoherent processing in the case of a fully coherent signal marks a retreat from an optimal algorithm in favor of simplified circuitry, resulting accordingly in degraded detection and resolution characteristics and impaired signal-parameter measurement accuracy. Nevertheless, for a number of signals, provided optimal ratios are selected between the duration of the coherent and noncoherent filtering, these sacrifices may be inconsequential and altogether acceptable. As an example of partial coherent filtering followed by the noncoherent processing of the signal we might cite the application of this method in the filtering of a long, unmodulated radio pulse (2.28) and (2.23), or of a burst of coherent radio pulses (2.53). In the case of a wide anticipated range of Doppler frequency shifts, when $\Delta_{\text{д}} \gg \frac{1}{\Delta T}$, fully coherent filtration for signals of this kind requires the use of multichannel systems.

If, referring to the circuit shown in Fig. 5.9, the frequency band of the coherent filter is far greater than the quantity $\frac{1}{\Delta T}$, the range of anticipated frequencies can be covered with considerably fewer coherent filters. The filter device circuitry in this case will incorporate fewer channels and will be less complex. The deterioration in detection characteristics, which is normally expressed in an increase in the required equivalent parameter q^2 to ensure specified D and F values, will depend, in this kind of circuit, on the signal/noise ratio at the envelope detector input. This deterioration can be computed using the appropriate formulas, which can be found, for example, in [81, 95].

For assigned values D and F, and identical and fixed intensities of elementary signals to be coherently processed, the increase in the quantity q^2 is a function of the ratio $n = \frac{T_{эф}}{T_{ког}}$, where $T_{эф}$ in this case is the effective duration of the entire signal, and $T_{ког}$ is the time interval of its coherent processing.

Figure 5.10 presents a graph illustrating the increase in q^2 (energy losses) as a function of the ratio $n = \frac{T_{эф}}{T_{кор}}$ for prescribed parameters D and F From this graph it is clear that for a ratio of $n = \frac{T_{эф}}{T_{кор}}$ of not more than 10 the energy losses are minor and amount at most to 1-2 dB or thereabouts.

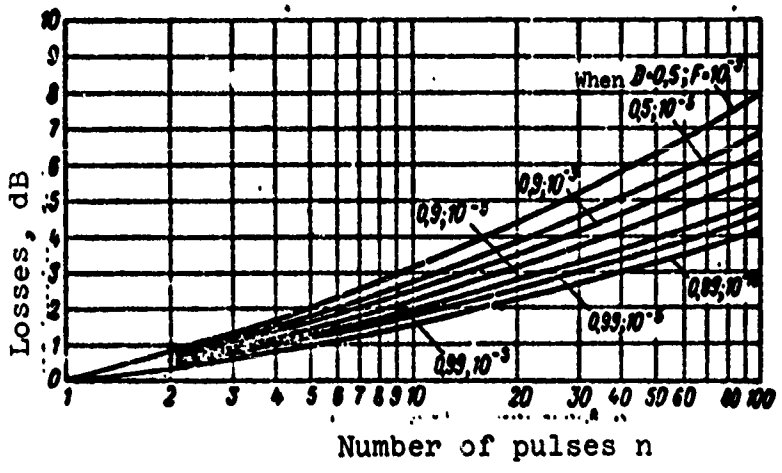

Fig. 5.10. Losses in noncoherent filtering.

Along with a deterioration in resolving power for signal frequency, which we are consciously disregarding in the case at hand, the noncoherent processing of a fully coherent signal may also be accompanied by a deterioration in its delay-time resolution and in the accuracy with which this parameter is measured. In large measure, the degree of this impairment is determined by the structure of the signal and must be estimated on an individual basis for each concrete signal according to expressions (3.1) and (4.15). It will be shown by analysis of expression (4.15), when the elementary signals satisfy the condition

$$\int_{-\infty}^{\infty} S_i(t)\exp(j2\pi f_i t)\,S^*_j(t)\exp(-j2\pi f_j t)\,dt = \begin{cases} T_{i\text{эф}} & \text{for } i=j, \\ 0 & \text{for } i\neq j, \end{cases} \tag{5.27}$$

that [81] with these signals processed by the circuit depicted in Fig. 5.8 delay-time measurement accuracy will be determined by the spectral characteristics of the elementary signals ΔW_i and by a certain equivalent quantity $q^2_{экв}$ characterized by the signal's total energy allowing for energy losses.

The dispersion of the delay-time measurement error in this case will be defined as

$$\sigma_\tau^2 = \frac{1}{\Delta W_i^2 q^2_{экв}}. \qquad (5.28)$$

For such signals the delay-time resolution characteristic will also be mainly determined by the form of the modulation function $S_i(t)$ [31].

In the case of signals satisfying conditon (5.26) the accuracy and unambiguity of lag time measurement will be determined by the high-correlation interval and the secondary maxima of the convolution function between the resultant envelope of the signal at the coherent filter output and the video filter response, that is, the function

$$Y_н(\tau) = \int_{-\infty}^{\infty} |Y(t)| K_{вид}(\tau - t)\, dt,$$

where $K_{вид}(t)$ is the response of the video filter [Translator's Note - The subscript letters "вид" indicate "video."]

Most advantageous from this standpoint are signals of the kind

$$v(t) = \sum_{i=1}^{i=N} \mathrm{Re}\, S_i(t - iT_i - T_{0i}),$$

which represent an aperiodic sequence of elementary signals $v_i(t)$ with phase or frequency modulation. The wide spectrum of these elementary signals ensures that they will be compressed in time

with a low side-lobe level at the output of the coherent filter, while the fact that they are arranged aperiodically in time means that it is possible to achieve a $Y_H(\tau)$ function of satisfactory form.

Figure 5.11a, shows a schematic representation of a compound phase-keyed signal, which is in reality a burst of five phase-keyed pulses unevenly time-staggered at intervals of τ_1-τ_4. Each pulse of the burst is phase-keyed by an M-tuple code with N = 31, for which the duration of the elementary discrete step corresponds to the value $T_д$. In Fig. 5.11b, we see a graph of the function $Y_H(\tau)$ for such a signal

The use of partial coherent filtering with subsequent non-coherent processing according to the circuit arrangement shown in Fig. 5.9 for multidimensional signals of type (2.37) and (2.45) provides a means of processing these signals within a wide range of Doppler frequencies by means of simple, low-channel-capacity circuits. For a relative low $\Delta T\Delta W$ value, the energy losses associated with the degradation of the signal/noise ratio at the detector output will be minor. On the other hand, when conventional band-pass filters with a band ΔW are employed as the coherent filters in the Fig. 5.9 circuitry, the elimination of the signal's frequency and phase modulation envelope at the detector output gives rise to a function $|Y(\tau)|$ of such form that there is a substantial deterioration in delay-time measurement accuracy and in the system's resolving power for this parameter. This shortcoming can very largely be overcome if the coherent filter used has a special frequency response to provide for the conversion, at the detector input, of the signal's phase and frequency modulation into amplitude modulation [30].

Specifically, in the case of phase-keyed signals, the basis of this kind of filter might be a delay line with adder, the effect of which would be to synthesize a response of the form

$$K(t)=\delta(t)\pm\delta(t-T_s). \qquad (5.29)$$

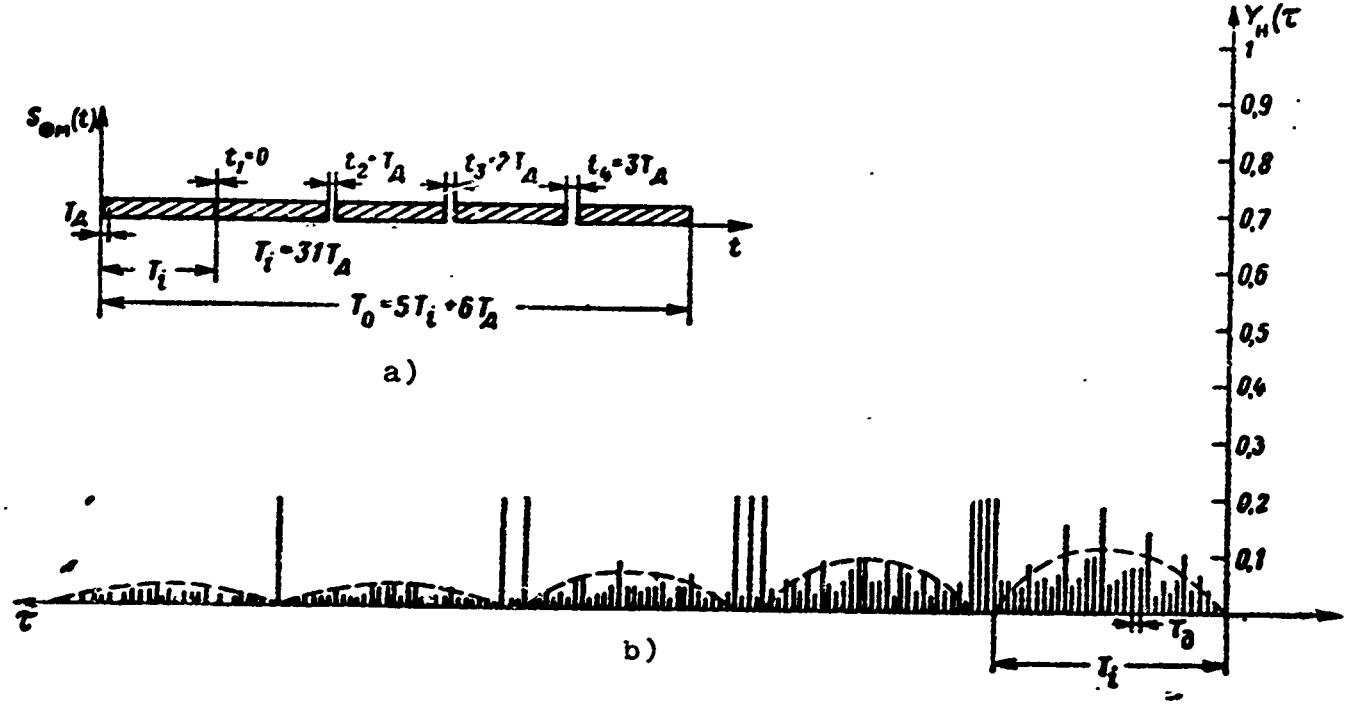

Fig. 5.11. Graph of function $Y_H(t)$ for compound phase-keyed signal.

The noncoherent processing of the phase-keyed signal in this event could be handled over the two-channel system illustrated in Fig. 5.12a. By way of example, let us determine the signal component of the output effect with this circuit for a signal of specific type. Let the input receive a phase-keyed signal of the kind described by (2.45) with modulation function (2.46), having a delay time $\tau_э$ and Doppler frequency shift $\nu_д$, that is

$$v(t)_{фм} = \operatorname{Re} A_0 \left\{ \sum_{i=0}^{i=N-1} 1_и(t - \tau_э - iT_д, T_д) g_i \right\} \times \times \exp[j2\pi(f_0 + \nu_д)(t - \tau_э)]. \quad (5.30)$$

[Translator's Note - The subscript letters "фм," it will be recalled, stand for "phase-keyed."]

For the sake of simplicity we set: $f_0 = 10k/T_д$; $T_э = T_д$; g_i is the M-tuple code; k are numbers of the natural series 1, 2, ... Now, without allowance for the $\tau_э$ shift in the time reading and considering the detector to be near, for the signal following detection at the video filter input we can write

$$Y_н(t)_1 = |v(t)_{фм} + v(t - T_д)_{фм}| - |v(t)_{фм} - v(t - T_д)_{фм}| = = A_0 \cos 2\pi\nu_д T_д \sum_{i=1}^{i=N} 1_и(t - iT_д, T_д) g_{i+m} + \frac{A_0}{2}[1_и(t, T_д) + + 1_и(t - NT_д, T_д)]. \quad (5.31)$$

The signal $Y_н(t)_1$, as follows from expression (5.31), is a video code signal of the kind shown in Fig. 5.12b, whose code corresponds to the code of the input signal, that is, the same M-tuple but offset with respect to the original by m symbols and with certain distortions at the beginning and end. In the case of a large number of code symbols, N >> 1, one may ignore

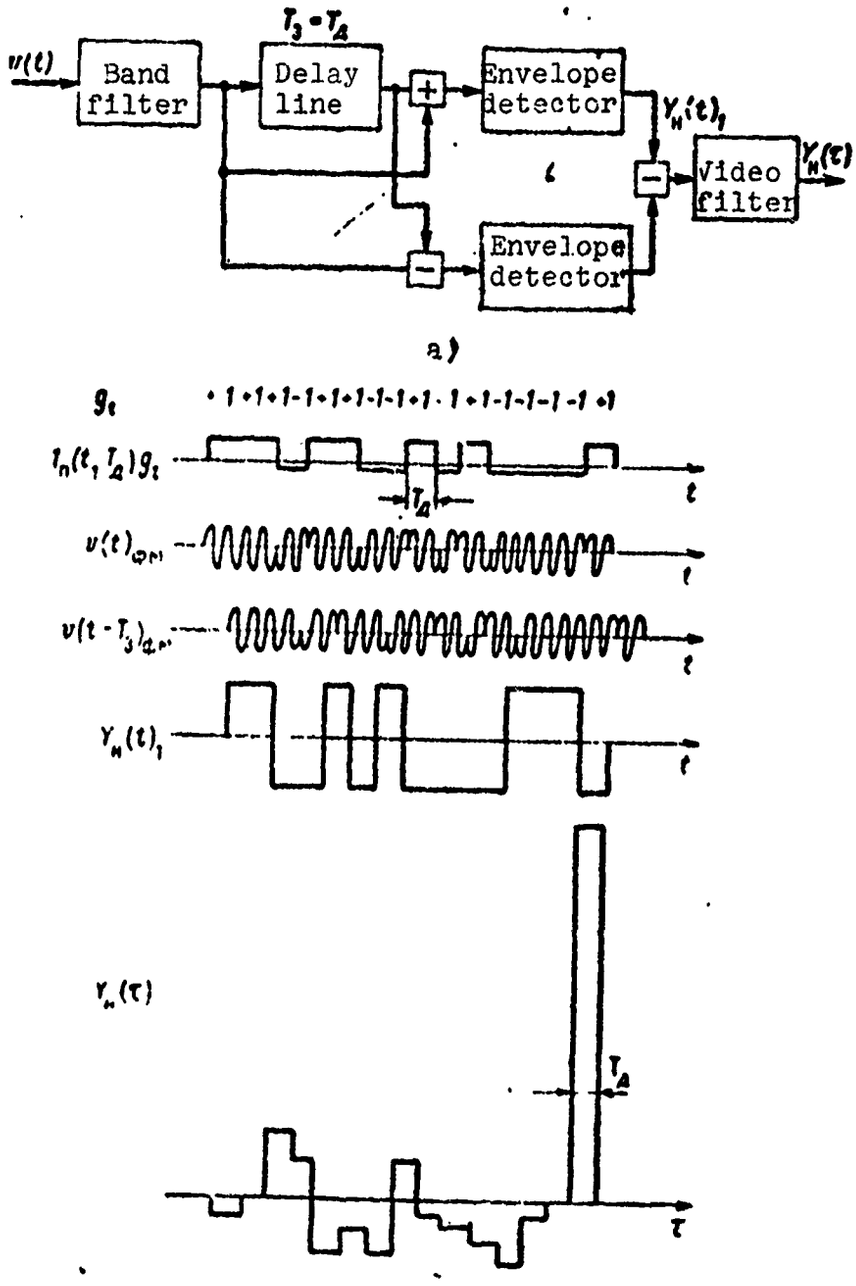

Fig. 5.12. Noncoherent processing of phase-keyed signal.

these distortions and consider that the detector signal $Y_H(t)_1$ has the same code structure as the original signal $v(t)_{\phi M}$. It is to be observed, however, that this kind of signal conversion is valid only for phase-keyed signals coded by M-tuples. For other code sequences there may be an alteration in the structure of the video signal, with respect to the original signal, which must be taken into account in the further processing of this signal. If the video filter is matched with the video signal $Y_H(t)$, then its output signal will for all practical purposes repeat the waveform of the autocorrelation function envelope of the phase-keyed input signal of Fig. 5.12b, equalling

$$Y_H(\tau) = |\Psi(\tau)|_{\phi M} \cos(2\pi \nu_д \tau_д). \qquad (5.32)$$

The reduction in output effect with the coherent filtering circuit detuned in frequency for a phase-keyed signal can be determined from dependence (2.49). If we compare expressions (2.49) and (5.32), we see that with the phase-keyed signal processed noncoherently by the circuit in Fig. 5.12, the signal frequency separation with respect to the circuit may be approximately $\frac{N}{4}$ times greater than when it is coherently processed. The energy losses here are a function of the ratio $\frac{\tau_{0\phi}}{2\tau_д} = \frac{N}{2}$ and, for prescribed values of D and F, can be determined from the graph shown in Fig. 5.10. Since the width of the maximum signal $Y_H(\tau)$ along the time-delay axis at the output of the Fig. 5.12a circuit corresponds to the high-correlation interval of the indeterminacy function of the phase-keyed input signal, there is a minor deterioration of time-delay measurement accuracy with the signal noncoherently processed in this manner.

5.3. Methods of Compressing the Dynamic Amplitude Range of the Input Oscillation and of Normalizing the Interference Intensity

Depending on the nature of the interference and the operating conditions of the radar, there may be a variation in the

interference intensity as the signals are processed. An optimal signal-processing algorithm, in this case, provides for supplementary processing of the input oscillation ahead of its optimal filtration, and also for the modification of the threshold level in keeping with the fluctuating intensity of the interference [99].

In practical terms, a minor change in the intensity of the interference over the duration of the signal will occur in a number of instances. In this event, the preliminary processing of the input oscillation can be eliminated, with the normalizing operation for the interference intensity simply a matter of changing the threshold setting. For nonstationary Gaussian interference with uniform spectral density the threshold level, as demonstrated in [81], is a function of a certain quantity Z, defined by the dependence

$$Z^2=\frac{1}{\Delta F_n T_{об} \langle N_0 \rangle}\int_{t}^{t+T_{об}} x^2(t)\,dt, \qquad (5.33)$$

where $\langle N_0 \rangle$ is the mathematical expectancy, assigned *a priori*, of the spectral density of the interference;

ΔF_n is the spectral width of the interference.

Whenever the intensity of the received signal may be assumed to have Rayleigh distribution, the threshold level for changing intensity is defined by a simple dependence [81] of the type

$$Y_0(\tau_3)\cong\beta_0 Z, \qquad (5.34)$$

where β_0 is a constant normalizing coefficient.

With allowance for expressions (5.33) and (5.34), the threshold level may be formed by a single channel, in the way shown in Fig. 5.13.

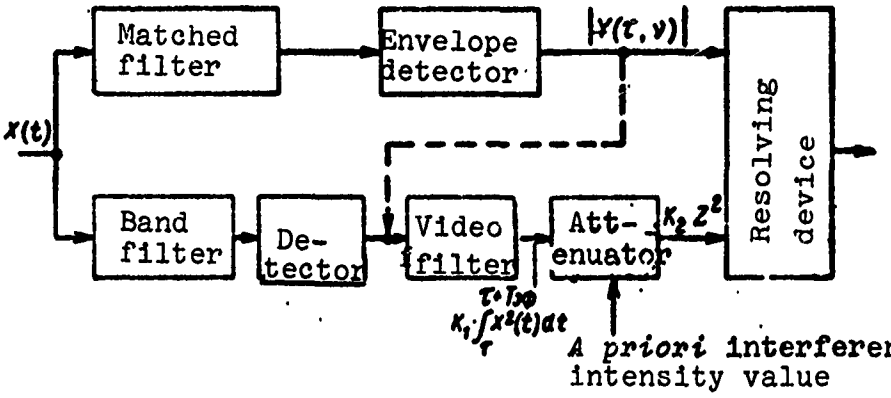

Fig. 5.13. Block diagram showing formation of threshold level.

When the band of the matched filter $\Delta W_{ф}$ is broad enough, so that

$$\Delta W_{ф} T_{изф} \gg 1, \tag{5.35}$$

the need for a special band-pass filter in the threshold-level shaping channel is eliminated, and this channel's video filter can be directly connected to the envelope detector output, as indicated by the broken line in Fig. 5.13.

With changing interference intensity the implementation of an optimal solution algorithm is unaffected by whether there is adjustment of the threshold level $Y_0(\tau_з)$ or whether there is a proportional change in the output effect $Y(\tau)$ with respect to the fixed threshold. For this reason, when the interference intensity is subject to variation, adjustment of the main-channel transmission factor will also be optimal, in which case the control signal will be a function of the quantity Z. Normally, the control of the transmission constant in the signal filtering and processing channel is accomplished at the channel input. A simplified block diagram of the signal-processing channel for this case in shown in Fig. 5.14.

In the design of real instrumentation, along with the task of norming the noise intensity one must also solve the problem

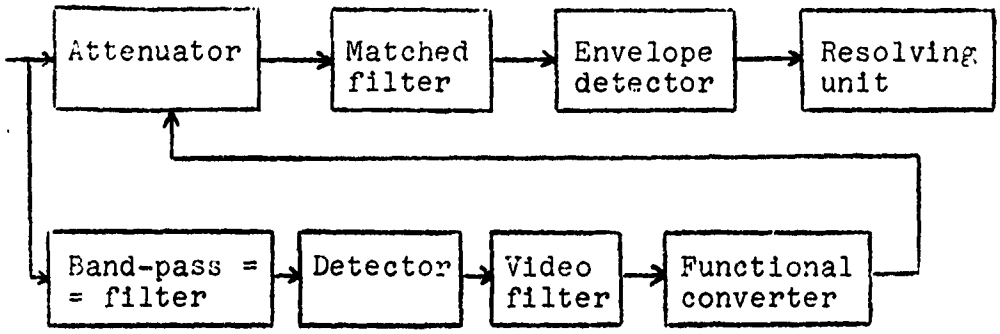

Fig. 5.14. Block diagram showing normalization of interference level.

of compressing the dynamic range of oscillation amplitudes at various points in the signal-processing system. This is because, depending on the type of target and its spatial position with respect to the radar, the level of the echo signals may vary within considerable limits. In practical terms, the dynamic range of echo-signal amplitude variation

$$\Delta_{A_{вх}} = 20 \lg \frac{A_{макс}}{A_{мин}} \qquad (5.36)$$

may constitute a significant value in the order of 60-100 dB.

Actual circuit arrangements for the filtering and functional processing of signals have a limited transmission capability in terms of the dynamic working range of amplitudes these systems can handle. Oftentimes this range is far below what is called for. To match the dynamic amplitude range of input signals to the operative dynamic band of the real instrumentation, the amplitude range of the signals to be processed is compressed at various points in the processing system.

If the signals are to be processed in the presence of Gaussian interference, the optimal approach is to compress the dynamic amplitude band of these signals only at the filter system output since this gives a one-to-one functional conversion of the *a posteriori* distribution, which, provided the threshold level is appropriately compensated, leads to no

degradation in signal-parameter detection and measurement performance. Nevertheless, with this method of dynamic band compression the range does remain considerable at the filter system input; moreover, if the filtering device is of the multi-channel variety (Figs. 5.6, 5.7), the band must be compressed simultaneously at the output of all the filtering channels, causing additional inter-channel mismatching because of equipment errors in the compression operation to reduce the range. In practical terms, therefore, it is more expedient that the dynamic range of amplitudes be compressed at the filter input. With this technique, not only is the input oscillation range matched with the technical specifications of the filter systems, but it is compressed in a circuit common to all the channels with the result that there is no additional mismatching in the characteristics of the individual channels. Moreover, by compressing the dynamic range at the filter input it is also often possible to normalize the interference intensity at the same time. This combining of functions is a specific advantage of compression by means of a nonlinear circuit affording a rigid limitation of the input oscillation amplitude (Fig. 1.5).

It will be appreciated from expression (4.19) that there is a normalizing of the spectral density of the interference at the limiter output, with the result that its dispersion at the filter output remains constant regardless of the noise level at the input of the signal-processing channel. In this case, the dynamic amplitude range of the signals at the output of the filter device, with respect to the interference level, is

$$\Delta_{A_{вх}} = 10 \lg \Delta T \Delta W - \Pi_{\phi},$$

where Π_{ϕ} indicates the losses encountered in practical filtering circuits.

If the nonlinear circuit has a logarithmic amplitude response, the interference intensity is normalized only for a specific type of circuit connection.

Let a nonlinear circuit with a logarithmic amplitude response effect a logarithmic transformation of the amplitude of a signal reaching its input:

$$u_{вх}(t) = A(t)\cos[\omega_0 t + \varphi(t)],$$

so that at the output of the circuit in question this signal is converted to the form

$$u_{вых}(t) = c_{ln}[\ln A(t)]\cos[\omega_0 t + \varphi(t)], \tag{5.37}$$

where c_{ln} is a constant conversion coefficient.

If the envelope distribution follows the Rayleigh law, the envelope dispersion for the oscillation $u_{вых}(t)$ at the output of the circuit with logarithmic amplitude characteristic will be

$$\sigma_A^2 = \langle[c_{ln}\ln A(t)]^2\rangle - \langle c_{ln}\ln A(t)^2\rangle = \frac{c_{ln}^2\pi^2}{24}, \tag{5.38}$$

and the mean value of the envelope of the same signal $u_{вых}(t)$ will be

$$\langle u_{вых}(t)\rangle = \langle c_{ln}\ln A(t)\rangle = \frac{k_{ln}}{2}[\ln\sigma_{вх}^2 + c_э], \tag{5.39}$$

where $c_э$ is Euler's constant. [Translator's Note - The subscript letters "вх" and "вых," it will be recalled, represent "input" and "output," respectively.]

From expressions (5.38) and (5.39) it is evident that in the logarithmic conversion of a radio-frequency oscillation the dispersion of the envelope of the oscillation is normed.

When the logarithmic circuit is connected ahead of the coherent filtering unit (e.g., in place of the limiter in Fig. 1.5), there will be logarithmic-law compression of the oscillation's dynamic amplitude band, but there will be no normalizing of the interference intensity at the resolver input since the total noise power at the filter system output is not normed. However, if the logarithmic circuit is connected at the output of the coherent filter unit, as illustrated in Fig. 5.15, then by virtue of the normalization of the envelope dispersion (5.38) the interference fluctuation intensity at the resolver input will be stabilized. A differentiating network is normally employed, in this case, to separate the fluctuation and constant component at the output of the noncoherent signal-processing system.

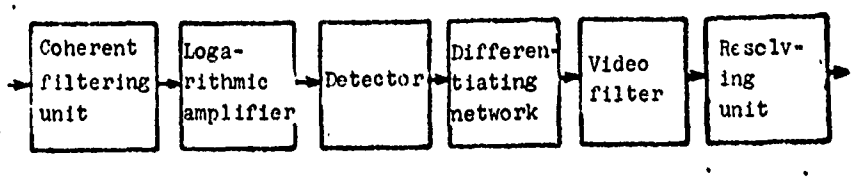

Fig. 5.15. Block diagram showing the normalization of interference intensity through the use of a logarithmic amplifier.

The logarithmic network may be connected ahead of the filtering circuit primarily in noncoherent signal processing for the purpose of normalizing the interference intensity and compressing the dynamic amplitude range at the filter input.

We see, therefore, that the nonlinear conversion of the signal amplitude at the input of the filter system affords a number of practical advantages over the compression of the dynamic range at the output of these systems.

In the general case, this kind of nonlinear conversion, in the presence of Gaussian noise, violates the optimal signal-processing algorithm and may lead to a deterioration in detection,

resolution, and measurement of signal parameters (Chapters 3 and 4). Nevertheless, under specific conditions, (3.38) and (3.43), such nonlinear conversion in the form of the limitation or taking of the logarithm of the oscillation amplitudes at the filter system input results in only minor degradation in detection and measurement performance, and may therefore be acceptable for practical purposes in many instances.

5.4. Design Principles of Resolution Devices and Devices for the Logical Processing of Signals

The primary tasks of the resolution device (resolver), regardless of the operating mode of the signal-processing system, are the twin tasks of threshold comparison and filter-system output effect analysis. In the detection mode the resolver effects a comparison of the output effect envelope $|Y(\tau,\Omega)|$ with the threshold, determining the regions of the parameters τ and Ω within which the threshold has been exceeded. In the fine-grain parameter measurement mode the resolver searches out the maximum of the function $|Y(\tau, \Omega)|$ in those regions of parameters τ and Ω where the value $|Y(\tau, \Omega)|$ has exceeded the threshold. Whenever the filter-system output effect depends on only one parameter which is also a time function (for example, the parameter $\tau_э$), the threshold comparison and output-effect analysis are accomplished sequentially by single-channel systems.

Thus, for example, in the detection mode, the signal envelope from the filter-system output is fed to the threshold unit (Fig. 5.16). Signals exceeding the threshold Y_0 are converted by the amplifier-limiter into standard-amplitude pulses $u_{огр}$ whose duration corresponds to the time during which the oscillation $|Y(\tau)|$ exceeds the threshold (Fig. 5.17). The resultant pulses are differentiated, $u_{диф}$, and their delay $\tau_{1н}$, $\tau_{1к}$, $\tau_{2н}$, $\tau_{2к}$ relative to the beginning of the time reading is determined by the time-interval clock [Translator's Note - The subscript letters "н" and "к" stand for "beginning" and "end," respectively].

Fig. 5.16. Block diagram of a single-channel resolving unit for the detection mode.

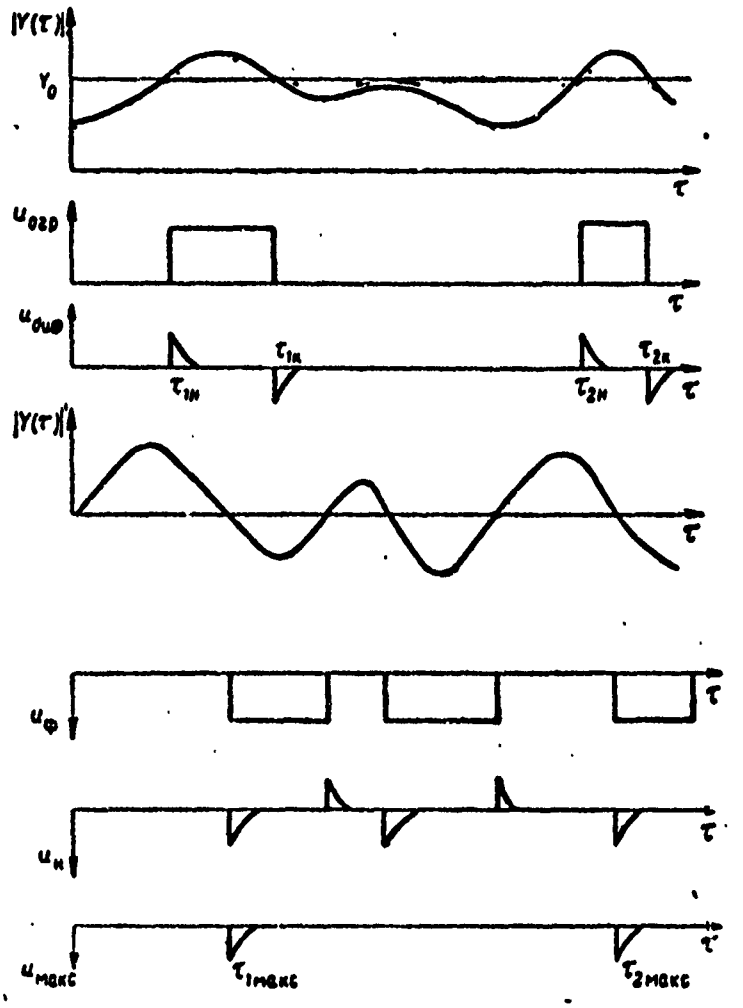

Fig. 5.17. Time diagrams illustrating the operation of a single-channel resolving unit in the detection and measurement mode.

The maximum value of the function $|Y(t)|$ in the measurement mode is determined by differentiating the signal $|Y(t)|$, followed by the fixing of the moment at which the resultant derivative passes through zero. The block diagram of the resolving unit for this situation is shown in Fig. 5.18. The differentiated oscillation $|Y(\tau)|$ reaches the input of the zero-transition hold circuit, in which the negative half-waves of the oscillation $|Y(\tau)|'$ are converted by the amplifier-limiter to standard-amplitudes pulses $u_{ф}$ (Fig. 5.17). Further, these pulses are differentiated and from them are formed the zero-transition pulses $u_{н}$. In the peak-pulse shaping circuit the time intervals defined by the pulse $u_{огр}$ are gated, and from the pulse train $u_{н}$ those pulses are segregated which correspond to the peak positions of the function $|Y(\tau)|$ in those regions where this function exceeds the threshold $u_{макс}$. The time-interval metering unit clocks the time lag of these pulses $\tau_{1макс}$ and $\tau_{2макс}$ with respect to the beginning of the time count, which describes the parameter $\tau_{э}$ to be measured.

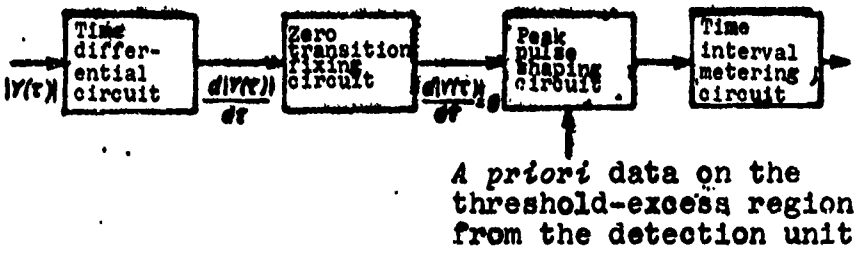

Fig. 5.18. Block diagram of time parameter measurement.

When the output effect is a function of more than one parameter - for example, $\tau_{э}$ and Ω_{0} - its distrubution for one of these parameters is discretely represented in the form of the values of the oscillations from the outputs of the individual filter system channels (Fig. 2.1). The resolving unit, in this case, must make a threshold comparison of the output oscillations from each channel. Since now a single signal may exceed the threshold in several channels, there is formed a threshold excess region. By way of illustration, Fig. 5.19 shows the topographic representation

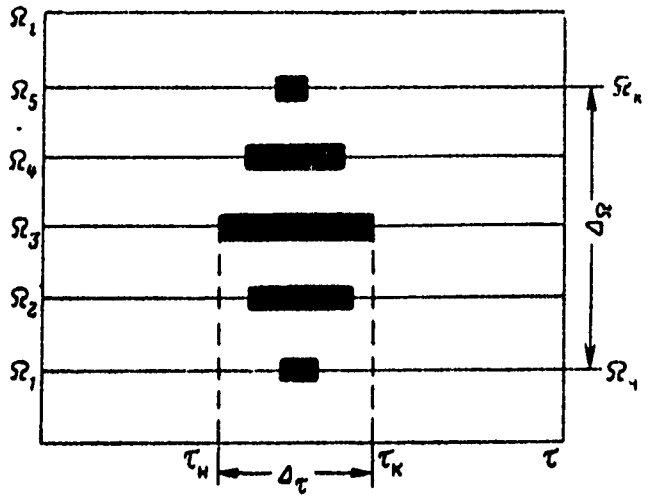

Fig. 5.19. Topographic representation of the threshold excess intervals in the case of multichannel filtering.

of the threshold excess region for the two-dimensional output effect $|Y(\tau, \Omega_i)|$. In the detection mode the resolver must determine the boundaries of the region τ_H, τ_K, Ω_H, Ω_K. This operation can be accomplished by means of a parallel-action computer circuit designed to simultaneously compute instances of threshold excess both by time and channel, while at the same time recording the values of the appropriate τ and Ω_i parameters. In the measurement mode, on the other hand, the resolver works to ascertain the maximum value of $|Y(\tau, \Omega_i)|$ in the threshold excess region. This is normally accomplished by seeking the maximum reading for those values of the function $|Y(\tau \quad \Omega_k|$ which satisfy a system of equations of the type

$$\sum_{k=1}^{k=l} \frac{d\,|Y(\tau, \Omega_k)|}{d\tau} = 0, \qquad (5.40)$$

that is, a successive search is made for the maximum values of the signal for the sections of function $|Y(\tau, \Omega_i)|$ along the Ω axis, with the minimum value then singled out from the aggregate of values derived for the function $|Y(\tau_m, \Omega_k)|$.

In practical terms, a resolving unit capable of performing these operations turns out to be a fairly complex piece of equipment because of the need to store and sort through a large quantity of different values for the function $|Y(\tau, \Omega_i)|$. In the circuit arrangements usually encountered in real applications, a resolver designed to analyze a multidimensional output effect can be simplified by averaging this effect or by transforming it on a space-time basis.

Averaging the output effect for all parameters except τ has the effect of transforming it into a time function, and this in turn makes it possible subsequently to effect the analysis for the delay time alone using single-channel systems of the kind shown in Figs. 5.16 and 5.18. The output-effect analysis for the averaged parameters is accomplished, in this case, only for those of its sections in which the parameter τ maximizes the averaged value of the function $|Y(\tau)|$. Specifically, when the output function depends on the two parameters τ and Ω, the averaging of its values for frequency can be resolved to the nonlinear summing of the signals from the channel outputs of the filter system [81], in which event the block diagram of the resolving unit for the measurement mode will appear as illustrated in Fig. 5.20.

The signal $|Y(\tau)|_{<\Omega>}$ at the input of the time-differentiation circuit represents the frequency-averaged output effect of the multichannel filter system. Following the time differentiation of $|Y(\tau)|_{<\Omega>}$, the parameter-estimate circuit for τ is used to produce delay-time values τ^0 for which the oscillation $|Y(\tau)|_{<\Omega>}$ takes on maximum values. For time sections corresponding to the value τ^0 a determination is made, by means of the circuits which provide a differentiation for Ω and estimation for Ω, of those parameter Ω values which maximize the function $|Y(\tau^0, \Omega)|$.

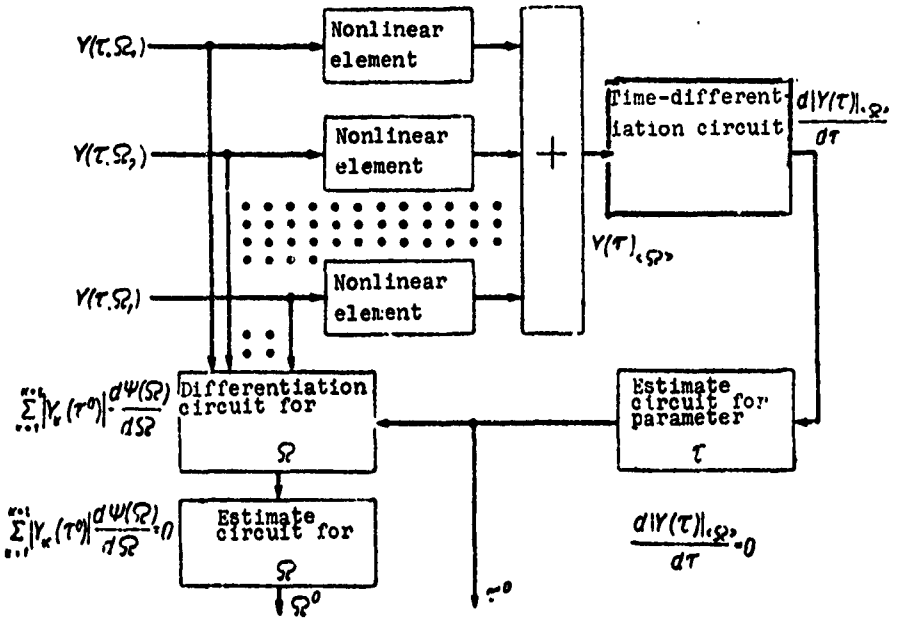

Fig. 5.20. Block diagram illustrating parameter measurement with averaging for frequency.

A point to bear in mind is that the application of the output-effect averaging method based on any one parameter permits the realization of potential measurement accuracy only in the event the signal processed has originated from a single target [81]; otherwise, output effect averaging may result in a deterioration of processing system resolution since in the case of numerous radar signals an indeterminacy function averaged for any particular parameter will have a structure worse from the standpoint of resolution than its individual sections for that same parameter.

The space-time conversion of the output effect also has as its purpose the reduction of the entire information to a single channel. Considering that within the time interval $\Delta t \ll \tau_{кор}$ the function $Y(\tau, \Omega_i)$ undergoes little change, the latter can be represented by its sampling values within the time intervals Δt. The resultant sampling values for all channels are then combined into a single channel by means of time-division multiplexing.

The space-time conversion operation is normally performed by a commutator switch sequentially connecting the individual filter system outputs to its output. By way of illustration, Fig. 5.21 presents diagrams of the space-time output effect conversion when this effect is represented by a certain regular component corresponding to the envelope of the autocorrelation function $|\Psi(\tau, \Omega_i)|$ for a square-wave radio-frequency pulse (2.34). As a result of the limited operating speed of the commutator, the same channel is connected within a time interval

$$T_{\text{оп}} \geqslant i(T_{\text{ком}} + T_{\text{пер}}), \tag{5.41}$$

where $T_{\text{ком}}$ is the duration of the connection of the channel;

$T_{\text{пер}}$ is the duration of the switching of the channels.

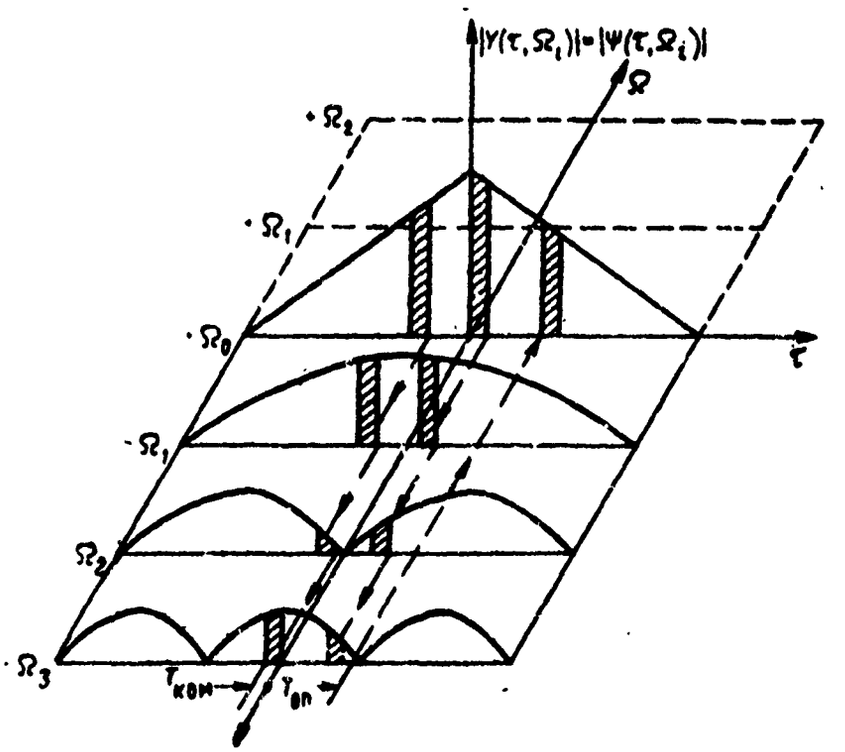

Fig. 5.21. Output effect space-time conversion diagrams.

The output effect of the separate channels takes on the form of pulse trains staggered in time. These sequences are combined at the commutator output, as shown in Fig. 5.22. Once they have been combined in a single channel, the pulse sequences, characterizing the sampling values of the output effects of all the channels, reach a single-channel resolving unit which determines the threshold crossings and separates out the maximum value of the pulse sequence $Y(t)_{пр}$ (Fig. 5.23) [Translator's Note - The subscript letters "пр" represent "converted."] The position in time of the maximum-value sampling with respect to the origin of the coordinates determines the value of the parameter $\tau_э^0$, and its delay with respect to the operating cycle of the commutator - the parameter $\Omega_д^2$ (Fig. 5.22).

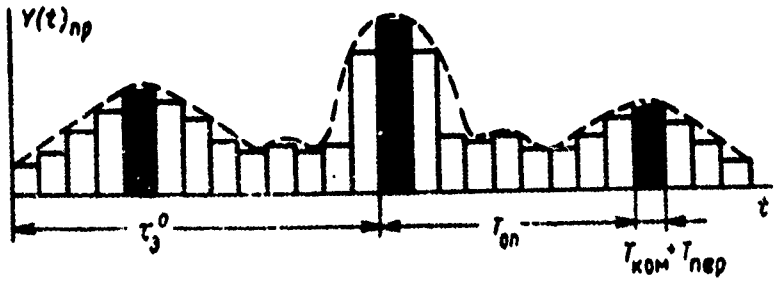

Fig. 5.22. Time diagram of converted output effect. Designation: ком = commutator; пер = switching; оп = interrogation.

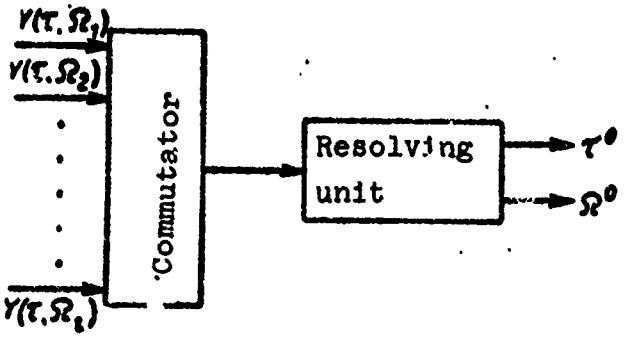

Fig. 5.23. Block diagram of resolving unit with space-time conversion.

Since the time quantification of the output effects is not time-locked with the arrival of the echo signal, the space-time conversion is the source of additional deterioration in the signal-detection and parameter-measurement characteristics. The resultant reduction in the signal/noise ratio because of the discrete arrangement of the frequency channels along with the discrete element in the time factor will be described, according to (3.8), by the normed indeterminacy function $|\Psi(\tau_j, \Omega_j)|^2$, where τ_j and Ω_j define the reading error in the maximum value of this function for the j-th measurement. Meanwhile, the maximum energy losses in the detection characteristics, measured in decibels, can be determined from the formula

$$\Pi_\delta = 10 \lg \frac{1}{\left|\Psi\left(\frac{\delta_\tau}{2}, \frac{\delta_\Omega}{2}\right)\right|^2}, \tag{5.42}$$

where δ_τ, δ_Ω represents the discrete sampling increments.

The average energy losses will be expressed in the form

$$\Pi_{\delta cp} = 10 \lg \frac{1}{\int_0^{\frac{\delta_\tau}{2}} \int_0^{\frac{\delta_\Omega}{2}} P(\tau, \Omega) |\Psi(\tau, \Omega)|^2 \, d\tau d\Omega}, \tag{5.43}$$

where $\Pi_{\delta cp}$ are the average energy losses due to quantification in decibels;

$P(\tau, \Omega)$ is the probability density in the distribution of the samples with respect to the maximum value of the function $|\Psi(\tau, \Omega)|^2$.

On the assumption that the sample distribution density with respect to the maximum is uniform and that the time samples are independent with respect to the frequency samples, expression

(5.43) is rewritten in the form

$$\Pi_{\text{cpl}} = 10 \lg \frac{1}{\frac{4}{\delta_\tau \delta_\Omega} \int_0^{\frac{\delta_\Omega}{2}} \int_0^{\frac{\delta_\tau}{2}} |\Psi(\tau, \Omega)|^2 \, d\tau / \Omega}. \qquad (5.44)$$

Specifically, when the discrete element in the spacing of the channels is sufficiently small $|\Psi(0, \Omega_j)|^2 \cong 1$, and the energy losses are determined only by the time samplings, in the case of the matched filtering of a square-wave radio pulse, with allowance for expression (2.34), these losses can be computed by means of the following formula

$$\Pi_{\text{cpt}} = 10 \lg \frac{1}{1 - \frac{\delta_\tau}{2T} + \frac{\delta_\tau^2}{12T^2}}. \qquad (5.45)$$

When $\delta_\tau = \frac{T}{2}$, average energy losses amount to a value of about 1.3 dB. Deterioration in measurement accuracy for the parameters τ and Ω, when space-time conversion is employed, will be caused not only by the reduction in q^2, but also by the discreteness in the reading of the parameter to be measured. The degree to which measurement accuracy is impaired by this factor can be additionally estimated by expression (4.27).

Along with the operations of signal detection and parameter measurement, the resolver must also perform a varying logical processing of the derived data. The end purpose of this processing is the purging of the primary radar information of spurious data originated as the result of the passage of different interference through the processing channel.

The signal is logically processed by matching some particular one of its characteristics, acquired as the result of the optimal

processing of the input oscillation, against an anticipated attribute. Based on the findings of this processing, the data whose characteristics fail to match those anticipated are subsequently sifted out [14, 72, 82]. The attributes used to effect this discrimination of signals may be the extent of the signal, its spectrum, direction of arrival, and so forth.

This kind of logical processing is conducted according to the block diagram shown in Fig. 5.24. The auxiliary channel passes signals whose parameters lie outside the parameter region of the useful signals, for example, outside the region of the useful signal's frequency band, extent interval, or arrival direction. In the comparison circuit a comparison is made between signal intensity in the primary and auxiliary channel, and in the event the output effect from the auxiliary channel is exceeded, the resolver input is blanked by the blanking-pulse shaping circuit.

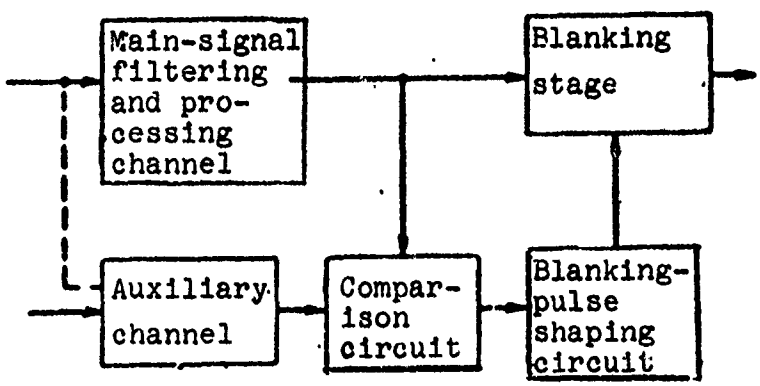

Fig. 5.24. Generalized block diagram of logical signal processing.

It is important to note that this type of logical signal processing at the filter system output is not optimal and in certain conditions results not in the improvement, but in the disruption of primary radar information. For this reason, it is recommended for use in limited circumstances when , for one reason or another, optimal methods for the resolution of useful signals against an interference background are not feasible.

5.5. Information Encoding and Transmission in Signal Processing Systems

When transmitting information between distinct processing systems and when introducing such information into the electronic computers responsible for the secondary processing of the data, it is convenient from a practical standpoint that this information be converted into a discrete form whereby a continuous message is represented by means of some code or other in the form of a sequence of standard signals. Among the technical facilities which provide for the transmission of digital information one normally finds: a conversion-encoding device which accomplishes the required conversion of the form of the message to be transmitted; a communications line (link or circuit); and a device for the reception of the information which converts the received message to a form suitable for the user. As a rule, digital information is encoded by means of a binary code using only the two symbols "1" and "0." These signals are easily reproduced by the presence or absence of a (usually pulsed) signal.

Various types of codes may be used as a binary code for message encoding. The simplest of these, which are employed when there is no interference or operational malfunctions on the transmission link, are the positional binary code (ordinary binary code) and the cyclic code (Gray code).

The positional binary code is formed by a positionally arranged power series for the number 2. Thus, for example, the number 11 can be represented in the form

$$11 = 1 \cdot 2^3 + 0 \cdot 2^2 + 1 \cdot 2^1 + 1 \cdot 2^0 \leftrightarrow 1011.$$

The digits 1 and 0 standing ahead of the powers of the number 2 are characteristic of the binary positional code. The digital configuration (number of units) of this code p is

determined by the value of the greatest degree n_{max} in the positional series and can be found as

$$p = n_{max} + 1. \tag{5.46}$$

Whenever the value of a message to be encoded is capable of assuming an intermediate position between the individual digit positions of the binary code, then, because of the considerable variations in the structure of the code, serious encoding errors may arise as some numbers shift to adjacent values. In order to eliminate these errors, cyclic codes are employed, in which the transition to adjacent values is accompanied by symbol changes in only one of the digital positons of the code. A cyclic code can be derived from a positional and vice versa. To make the transition from a positional binary code to a cyclic, a modulus operation is performed for the code offset by one place and not offset; for example

$$\begin{array}{r} 1101 \\ +\ 110\,(1) \\ \hline 1011 \end{array}.$$

Whenever the encoded messages are to be transmitted in the face of various kinds of interference and/or transmission equipment malfunctions, so-called correcting codes are used. Into the structure of such codes are introduced control (check) symbols which, by creating code redundancy, make possible its verification and correction. The basic types of these codes, along with the methods for their formulation, are discussed in [21, 28]. The key characteristics of the converter involved in the transformation of an analog value into a discrete code are its resolution, digital configuration (word length), and operating speed.

The conversion resolution $\delta_{пр}$ is defined by the ratio

$$\delta_{пр} = \frac{\Delta_\alpha}{2^p - 1}, \tag{5.47}$$

where Δ_α is the variation range of the analog value.

The resolution of a converter describes the error introduced by encoding, which, following (4.27), for uniformly spaced discrete increments, is

$$\sigma_{\text{код}} = \frac{\delta_{\text{пр}}}{2\sqrt{3}}. \qquad (5.48)$$

If the encoding error is assigned, the required digital configuration of the converter can be easily found from (5.47) and (5.48):

$$p \geq \log_2\left(\frac{\Delta_\alpha}{2\sqrt{3}\,\sigma_{\text{код}}} + 1\right). \qquad (5.49)$$

It should be noted that the resolving power of real converters is limited by the practical capabilities of the equipment. Specifically, practical amplitude-to-code converter circuitries have a minimum resolution $\delta_{\text{пр min}}$ determined by the limiting sensitivity of the comparison circuits. With allowance for equipment instability of various kinds, the limiting sensitivity of modern electronic comparison circuitry is about 0.03 V. If the converter is to provide the required operating accuracy, the following condition must be satisfied:

$$\delta_{\text{пр}} \geq (2 \div 3)\,\delta_{\text{пр мин}}. \qquad (5.50)$$

[мин = min]

Whenever practical considerations dictate the selection of a larger value for $\delta_{\text{пр}}$, the scale of the quantity Δ_α must be increased in order to preserve conversion precision; however, this increase is also limited, in real equipment, by the range of linear transmission for the parameter α. For example, conventional converter circuits in actual use will permit a ratio of

$$\frac{\Delta_A}{\delta_{\text{пр мин}}} \cong 30 \div 40 \text{ dB}.$$

With allowance for condition (5.50) and relation (5.48), such converter circuits make possible the encoding (measurement) of signal amplitude with an rms error of the order of 1-0.5% with a code length of p = 6-7.

If there is a need to boost the amplitude measurement accuracy, converters can be used which offer a high-speed digital gain control feature by means of which the range Δ_A can be considerably expanded.

A variety of principles may be used in the design of practical converter circuitries. Fundamental among these principles of consecutive computation, readout, comparison, and subtraction [21, 28]. The selection of a particular principle is based on practical considerations and converter specifications.

Two techniques are employed for the extraction and transmission of the code from the converter - a parallel and a consecutive.

In the first instance, each digital position of the code is extracted simultaneously with the others to its own transmission line (Fig. 5.25a). With consecutive extraction there is one transmission line and the code bits are arranged consecutively in time (Fig. 5.25b).

With parallel extraction, the converter speed $t_{код}$ must be somewhat less than the correlation interval of the analog quantity to be converted, that is

$$t_{код1} < \frac{1}{\Delta W}. \qquad (5.51)$$

With consecutive extraction, the converter speed requirement increases as the code length grows larger:

$$t_{код2} < \frac{1}{\Delta W p}. \qquad (5.52)$$

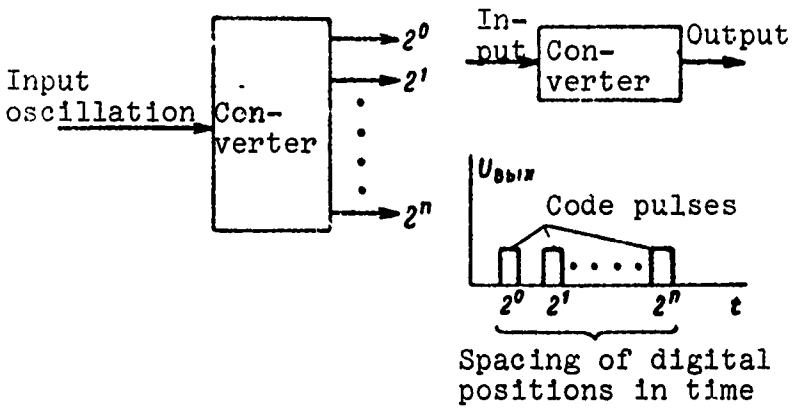

Fig. 5.25. Parallel and consecutive code detection. Designation: $U_{вых}$ = output voltage.

Today's practical circuitries for discrete semiconductor converters provide speeds of about 20 nanoseconds. With parallel code extraction, this permits the encoding of analog data whose spectrum does not exceed 20 MHz.

The reception of transmitted digital information is the function of decoding and matching devices, whose basic tasks are the storage of the transmitted information, the conversion of this information to a form suitable for the customer, and its delivery to the customer at the required moments of time. The principles underlying the design of such decoding and matching devices have been set forth in sufficient detail in [21, 28, 34, 43].

6. METHODS FOR THE TECHNICAL REALIZATION OF SIGNAL-PROCESSING DEVICES

6.1. Basic Techniques in the Technical Realization of Signal-Processing Devices

The major types of practical signal-filtering and processing systems may be conveniently classified according to their operating modes, structural features, and the kinds of physical instrumentation they employ.

In terms of operating mode, these devices can be subdivided into those which filter and process the oscillations received at their input without the preliminary memorization (storage) of these oscillations, and those in which signal processing occurs after the storage and time-scale alteration of the input oscillation. In systems of the first type the integration and execution of other operations with the signals takes place in instantaneous real time, while a characteristic feature of the second type is the possibility of significantly varying the time scale for the operations to be performed.

In terms of structural features (design techniques), two groups of signal-processing devices are conventionally distinguished: those of the analog type and those of the digital type. It is characteristic of the first group that they are designed around analog elements, while systems of the second group are designed predominantly on the basis of discrete digital-engineering components.

The principal physical devices incorporated in signal-processing systems are a large variety of electronic, electron-acoustic, magneto-electronic, electron-optical, acousto-optical, and other radio and physical circuits. By virtue of the highly specific nature of the technology involved in the design and use of equipment employing different electromagnetic wavebands, this attribute provides a convenient means of differentiating between two types of system: the electronic and the optical. Systems of the first type employ electronic, electron-acoustic, and magneto-electronic circuitry, using radio-frequency and acoustic oscillations as the basic information carriers. Devices of the second type are designed principally around electron-optical and acousto-optical components in which the data are for the most part carried on signals of the optical waveband.

6.2. Real-Time Signal-Processing Systems

Systems of this type filter and process the oscillations directly received at their input without any preliminary alteration of their time scale. All three methods of signal processing can be employed for the implemenation of this class of filtering device: the correlation method, the correlation-filtering method, and the filtering method.

Purely correlative signal-filtering techniques, according to tne structural scheme shown in Fig. 5.1, are comparatively uncommon in radar systems. Normally, these methods are used in single-target radars in which there is the possibility of a time-consecutive search for the frequency of the signal and its delay time. Whenever the requirement is for the simultaneous processing of numerous signals over a wide range of frequency and time-delay variation, practical considerations militate against the use of correlation-type filter circuits as necessitating the operation of a large number of channels with great variety in reference signal parameters.

More extensive possibilities for the practical design of filter systems are afforded, in this case, by the application of correlation-filter and filter methods. By way of example, Fig. 6.1 shows a block diagram of a practical system of signal processing, in a range of delay time and Doppler frequency shift, in which the signal filtering operation is accomplished according to the correlation-filtering method [3, 57, 90]. The system is designed to detect and measure signal parameters. The circuitry contains i time channels, in each of which the input oscillation is multiplied by the appropriate reference signal (5.8) and (5.22). Following the multiplier stage, the IF signals travel across a band-elimination filter and dynamic range compression circuit to a filter unit consisting of m filtering channels which provide frequency coverage of the entire possible

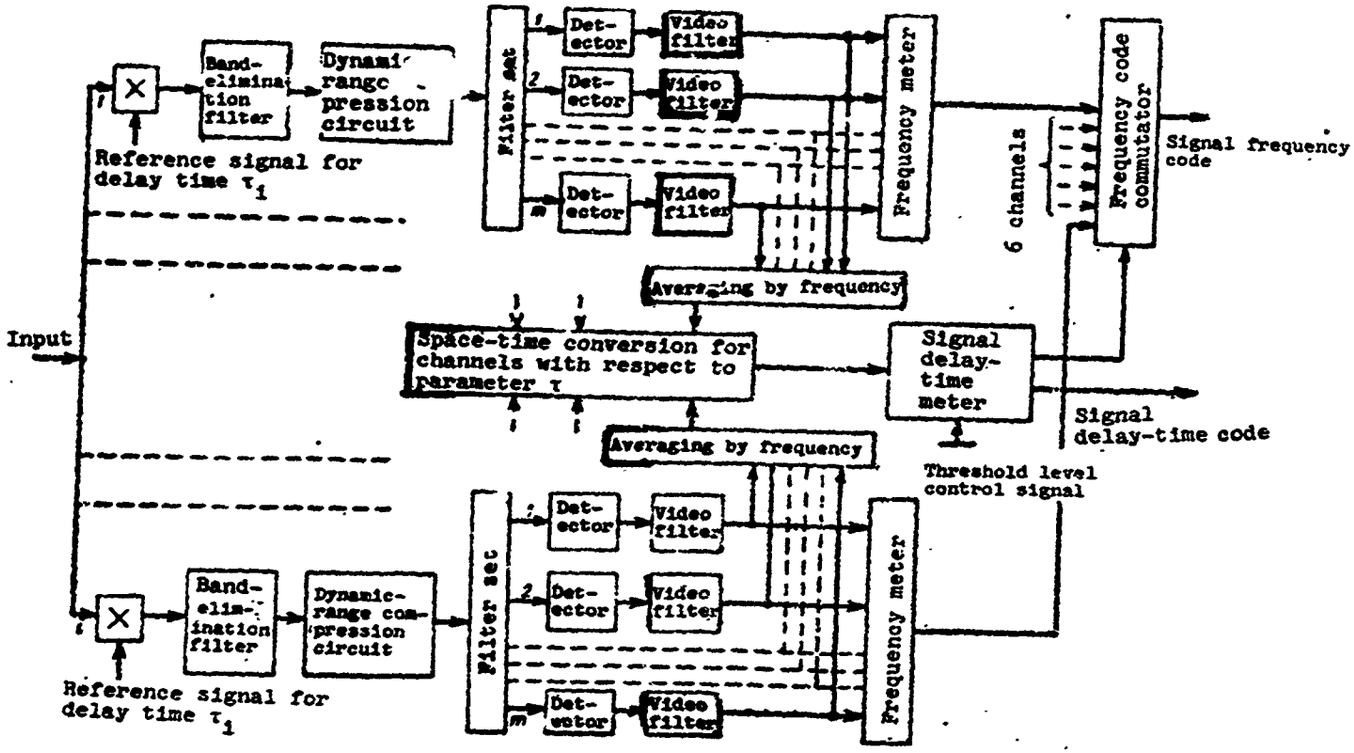

Fig. 6.1. Block diagram of signal-processing system employing the correlation-filtering method.

Doppler frequency range of the received signals. As a rule, the preliminary multiplication of the input oscillation by the reference signal makes it possible to simplify considerably the structure of the individual filters of the set (5.23)

In each time channel, according to the intensity distribution of the signals, the signal frequency is metered at the output of the set of m video filters. The signal delay-time measurement is made after the output effects in the time channels have been averaged for frequency and the information from all the time channels has been combined by means of space-time conversion (Chapter 5). The data on the frequency estimate for the signal from each time channel reach the frequency code commutator, where the code is discriminated from that time channel only in which the signal was detected.

In the filtering of signals whose parameter value ρ approaches zero - signals of type (2.45) - the discrete element in the alignment of the time channels δ_τ for the delay time must not exceed the interval $\tau_к$. Now, if $\delta_\tau = \frac{\tau_к}{2}$, the system's energy losses due to the quantification will be in the order of 1.3 dB (5.45).

Filtering and signals for which $\rho \gtrsim \Delta W \Delta T$ - signals of the kind (2.37) - is possible for a considerably greater time-lag spacing of the reference signals. The discrete spacing element δ_τ, in this case, may be increased to a value of $\frac{T_{эф}}{2}$ with no appreciable energy loss, resulting in a significant reduction in the number of time channels in the filtering of such signals. It is important to remember, however, that this approach entails an ambiguity in the measurement of the frequency-time distribution of the signal (Section 3.2), which can be eliminated only by subsequent modification of the modulation law in the main (transmitted) and reference signal. Thus, for

example, in [90] it is suggested that the measurement ambiguity be eliminated through the alternate use of a main pulse without frequency modulation of type (2.33) and a main signal with linear frequency modulation of type (2.37). Now, during the radar's first working cycle t_1 (Fig. 6.2) a determination is made, based on the measured frequency deviation of the reflected signal from the reference ν_1, of the signal's Doppler frequency shift $\nu_д$, while in the second cycle t_2 the signal delay time is uniquely measured as

$$\tau_з = T_{з0} + \frac{\nu_1 - \nu_д \Delta T}{F_m},$$

where $T_{з0}$ is the delay of the reference signal;

$\frac{F_m}{\Delta T}$ is the rate of change in the frequency of the frequency-modulated signal.

In practical terms, the use of correlation-filtering methods of processing is normally recommended either for the filtering of fairly complex signals where the design of matched filters represents an arduous technical problem or whenever the anticipated range of Doppler frequencies of the signal is commensurate with the latter's spectrum, while the signals have parameters for which $\Delta T \Delta W >> 1$.

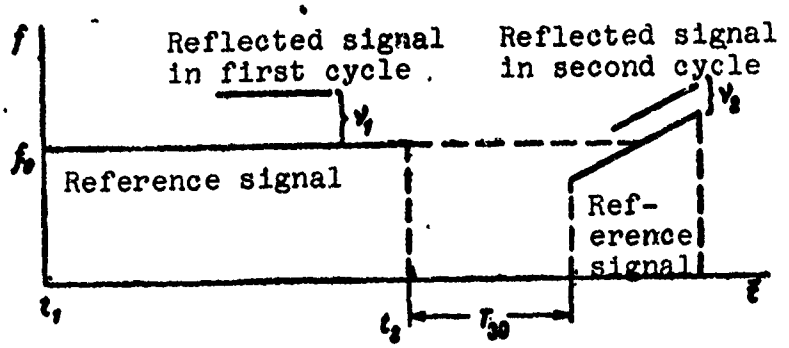

Fig. 6.2. Graph of the frequency change in a retunable signal-processing system.

In many other situations, practical filtering circuits can be based on filter methods of signal processing. Such signal-filtering techniques call for the availability of only one time channel, and they do not require special circuitry to multiply the input oscillation by the reference signal. In structural terms, the signal-processing circuit in this case (Fig. 6.3) represents a particular version of the circuit shown in Fig. 6.1. Figure 6.2 shows in somewhat greater detail the frequency and time-delay metering unit, designed in accordance with the arrangements depicted in Figs. 4.2 and 5.18.

The metering unit in the circuit depicted in Fig. 6.3 measures the frequency, for each time section, only for one maximum signal and does not resolve the signals for this parameter. When possibly several signals differing in frequency may be present in a single time section and an independent ν parameter measurement is required for each of them, the frequency measuring circuit must select a prescribed number of maximum values for ν, calculating for each of them the appropriate correction factor. As already noted, in most cases output-effect averaging results in a deterioration of processing-system resolution, and for this reason when processing signals from a multiple target, the discrimination of the peak values for τ in the resolving unit is performed in each frequency channel, as indicated in Fig. 6.4.

When any signal parameter is known with accuracy to the high-correlation interval and the requirement is merely to refine the value of this parameter, the measurement circuitry normally employs discrimination methods. By way of example, Fig. 6.5 shows a signal-processing system with frequency refinement. In this circuit the signal frequency is measured by estimating its deviation from a certain value of a frequency ν_0, which is the center frequency of the discriminator. When the frequency deviates from ν_0, the discriminator output produces a signal which is proportional to the value $\nu_{y\tau}$ defining this deviation. [Translator's Note - The subscript letters "yτ" stand for "refined."]

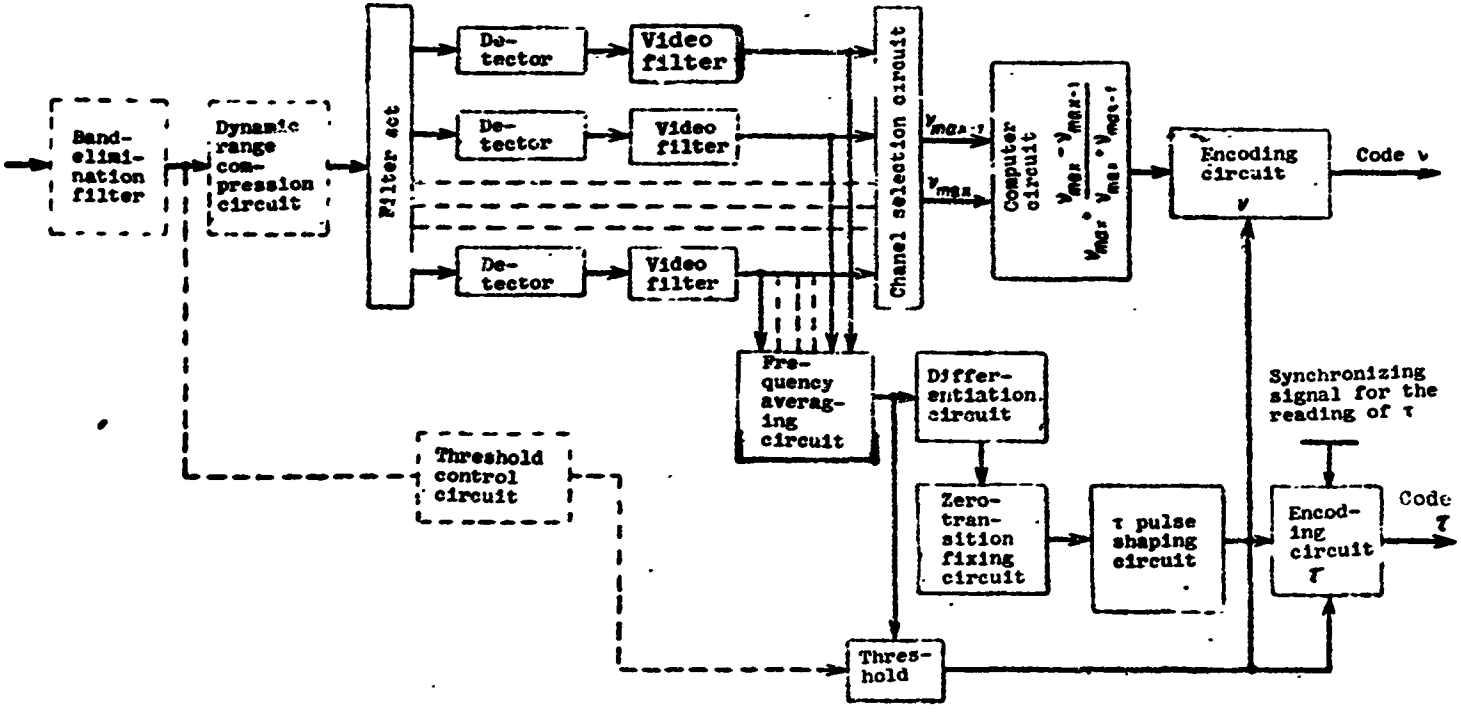

Fig. 6.3. Block diagram of signal-processing system employing the filter method.

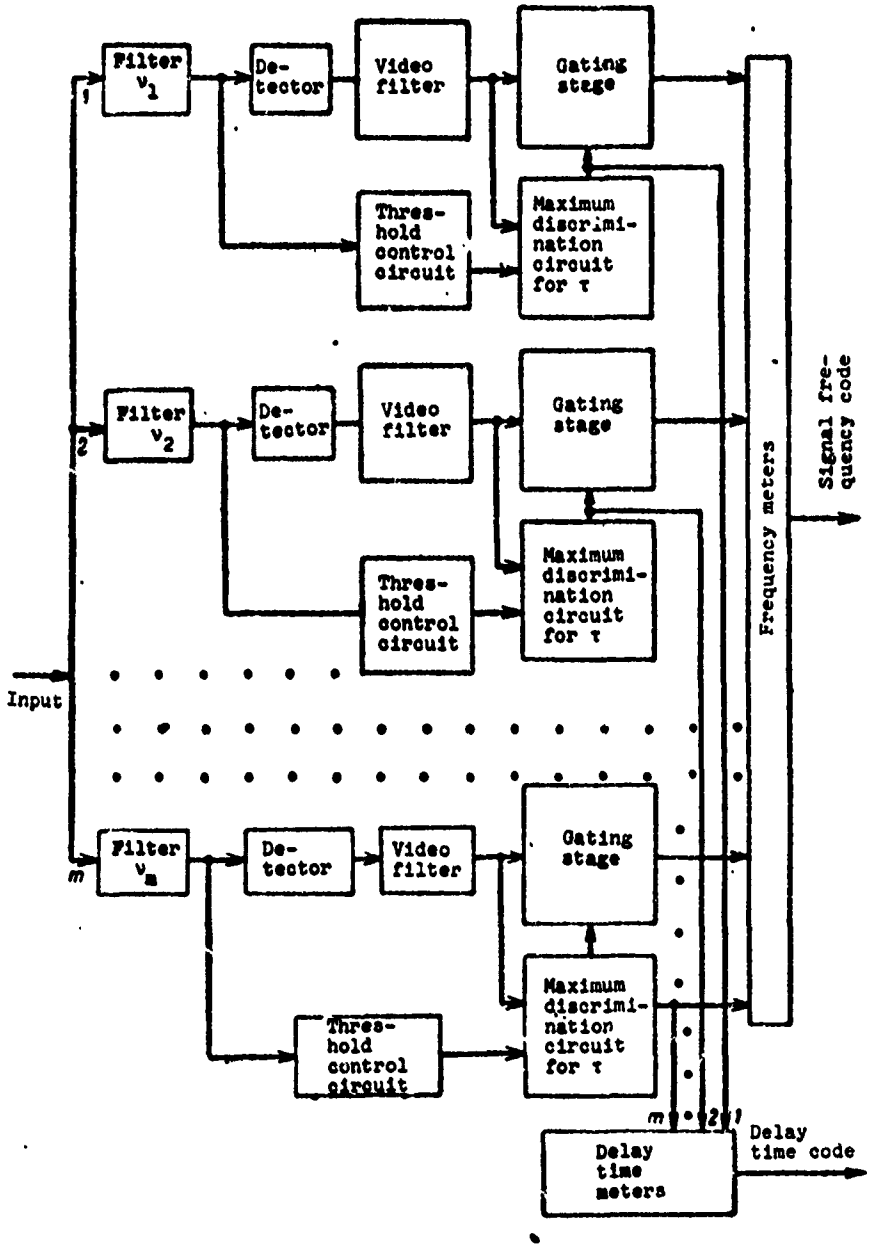

Fig. 6.4. Block diagram of signal-processing system in the presence of a multiple target.

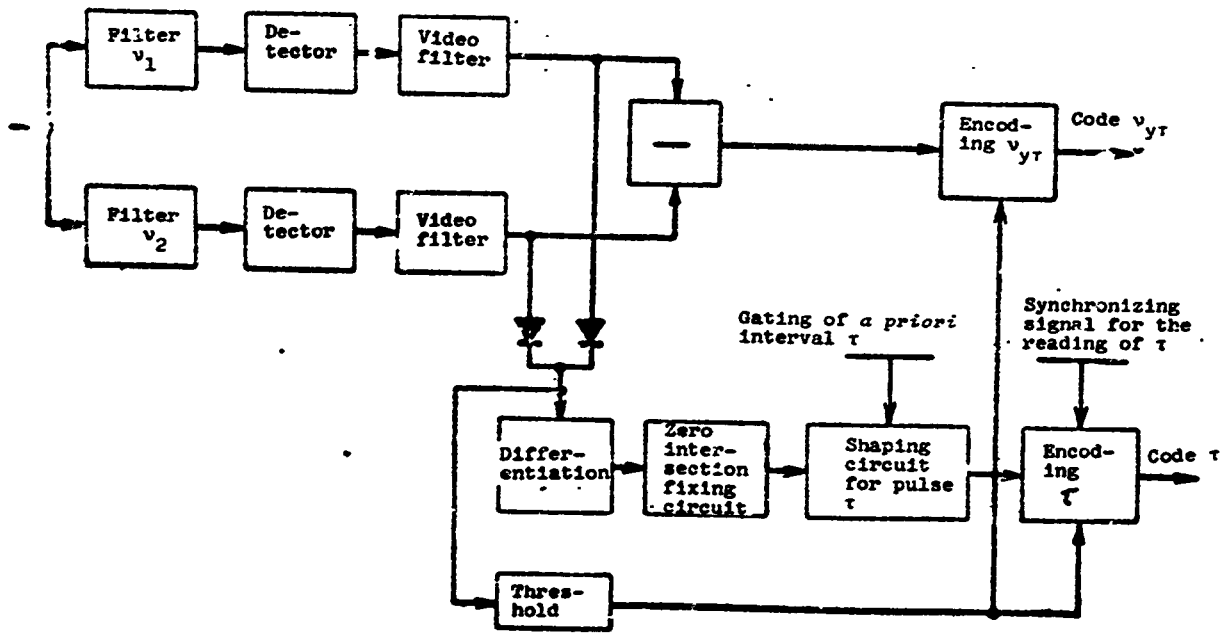

Fig. 6.5. Block diagram of discrimination meter.

For systems operating in real time and providing input-oscillation processing without preliminary storage, the monopulse method of signal processing, whereby there is no consecutive retuning of the detection or measurement circuit parameters, is a characteristic feature. However, in the case of radars having target tracking modes involving the fairly prolonged illumination of a single target over many operating cycles of the radar, there may be changes in the parameters of the processing system during tracking as they adapt themselves to values ensuring optimal signal processing conditions. The process of this system alignment is usually referred to as "target lock-on." For example, with the protracted illumination of a single target the operation of selecting the maximum values of the function $|Y(\tau, \Omega)|$ and of computing the correction factors for these values is not effected on a parallel-time basis, as indicated in Fig. 6.3, but sequentially (consecutively).

During the initial operating cycles a determination is made of the maximum values of the function $|Y(\tau, \Omega)|$, while subsequent cycles provide for the use of the discrimination circuits to measure the corrections for the values of the appropriate parameters. In many cases, this kind of consecutive signal processing results in simplified filtering and measuring equipment.

6.3. Signal Processing with Time-Scale Conversion

In certain cases, signals are processed with preliminary memorization and alteration of the time scale of the input oscillation. A simplified block diagram of this type of signal processing system is shown in Fig. 6.6. Signal processing with preliminary storage and time-scale modification is usual is situations when the extent of the signal is sufficiently long and there are practical difficulties in the design of filtering systems capable of ensuring long-term integration, or in the event that the received signal is to be multiply repeated for subsequent processing.

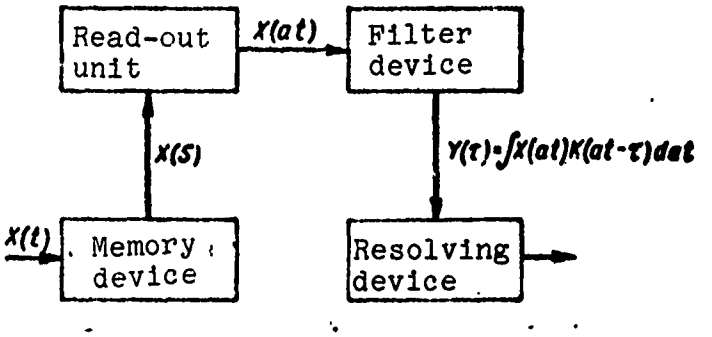

Fig. 6.6. Block diagram of the filtering and processing of a signal with preliminary storage.

Storage methods may be conventionally divided into two kinds: dynamic and static. In the case of dynamic storage, as the converted oscillation is filtered and logically processed, the signals already accumulated (stored) are erased in the memory unit and newly received signals are recorded. In static storage, there is no erasure of oscillations already recorded, but fresh incoming signals are stored in new cells of the memory unit.

Dynamic storage is normally employed when the reception of the oscillation at the memory input is continuous in time. Provided the operating modes of the memory are properly matched with those of the remaining units of the system, it is possible to achieve a time-continuous filtration and logical processing of the signals with a certain small and regular delay in the release of data regarding the oscillations reaching the system input. Static storage is common when the input oscillation is limited in time. The filtering and logical processing of such statically memorized oscillations may take place repeatedly and with a relatively extended delay time.

Many methods exist for the implementation of read-out and memory units. One of the more common is the method of dynamic storage and time-scale compression by means of a feedback delay line. A block diagram of a device implementing this method is shown in Fig. 6.7.

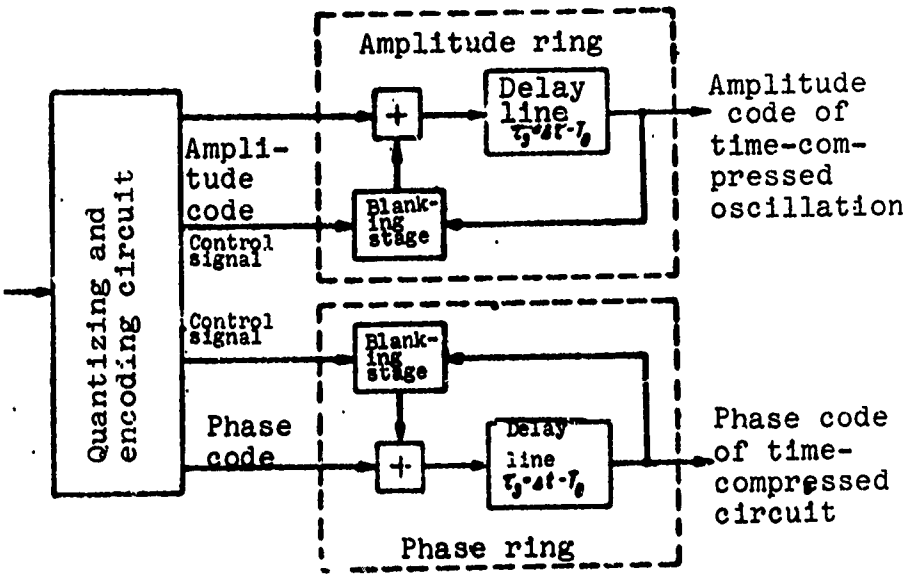

Fig. 6.7. Block diagram of dynamic storage unit with delay line.

By means of a quantizer, the input oscillation x(t) is transformed into time samples carrying information on the amplitude and phase of the signal. In accordance with the signal quantizing theory, the time interval between samplings is selected as

$$\Delta t < \frac{1}{2\Delta W_{вх}},$$

where $\Delta W_{вх}$ is the rms value of the energy spectrum of the input oscillation.

The value of the oscillation's amplitude and phase at the moment of the time sampling is represented, by means of an encoding circuit, in the form of a time code for the amplitude and phase, which occupies in time an interval T_0. Figure 6.8a shows a schematic representation of the input oscillation, and Fig. 6.8b the pulses of the time intervals within which is arranged the amplitude code; there will also be a similar pulse sequence of time intervals for the phase code as well. The pulse code for the amplitude and phase reaches the appropriate storage ring

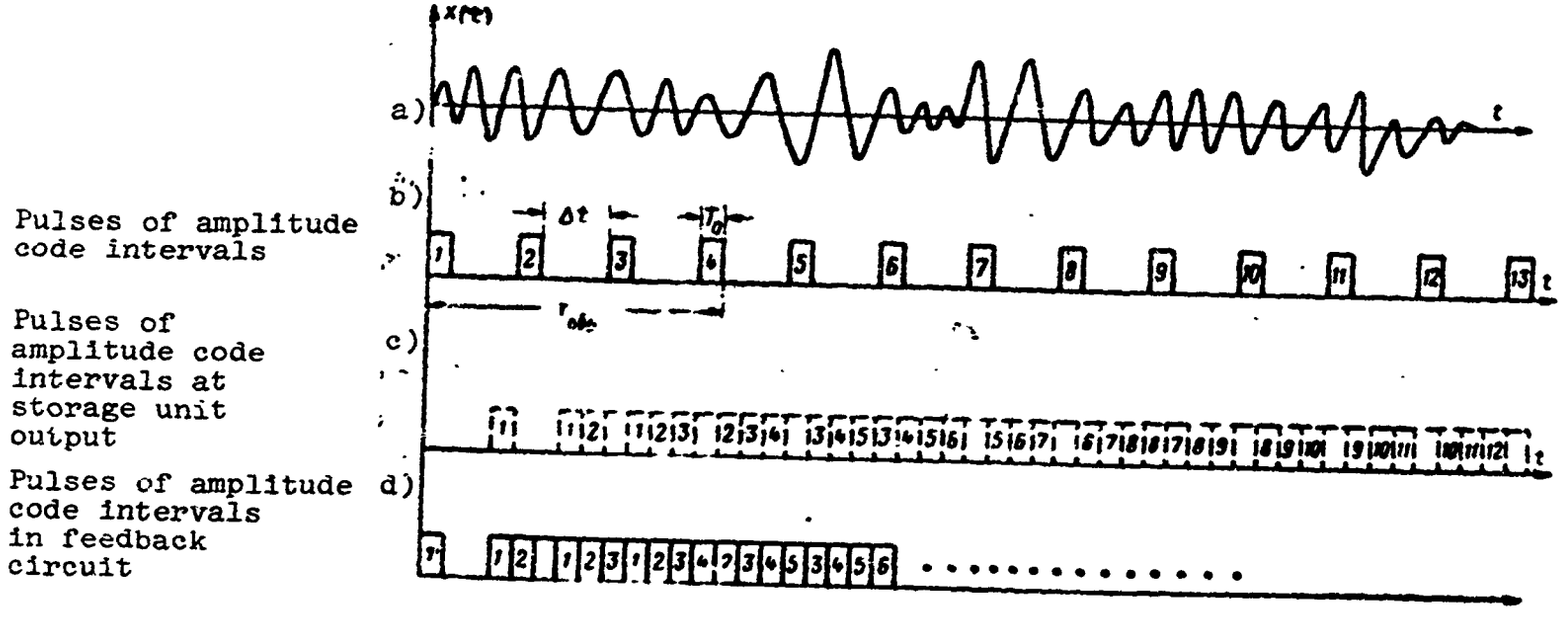

Fig. 6.8. Schematic representation of signal time scale conversion.

(Fig. 6.7). Since the operation of these storage rings is identical, we shall consider only one of them, specifically the amplitude storage ring.

The time interval T_0 accommodating the code is chosen in keeping with the dependence

$$T_0 < \frac{\Delta t^2}{T_{обр} - \Delta t}.$$

where $T_{обр}$ is the processing time interval of the input oscillation.

The delay time duration in Fig. 6.7 is set as equal to $\Delta t - T_0$. Now, within a time interval equal to $T_{обр} - \Delta t$ there will occur at the input of the delay line a sequence of time codes corresponding to the parameters of the time samples of the oscillations over the period $T_{обр}$ as arranged in the time interval Δt (Fig. 6.8a). If within the time $T_{обр}$ the arrival of the oscillation ceases, then the sum of the codes carrying all the required information regarding the amplitude or phase of the signal $x(t)$ will circulate in the appropriate ring of the delay line.

In the event the oscillation continues to reach the input of the system, provision must be made in the feedback circuit for a blanking stage to break the circuit at the instant the next time code reaches the beginning of the dealy line from the quantizer and encoder. This will be accompanied by the automatic regular erasure of the stored signal and the recording of the newly arriving signal (Fig. 6.8c, d). In this way, codes for the amplitude and phase of the time-compressed signal will be formed at the output of the appropriate storage ring in the system pictured in Fig. 6.7, with the time scale of the input signal changed by $T_{обр}/\Delta t$ times. The resultant codes may be converted to an analog signal or else directly used for the filtering and logic processing of the input oscillation.

Another method of storing (memorizing) and converting the time scale of an input signal involves the writing and reading of the signals at different rates. This is a more general method and one which may be employed for both the dynamic and the static storage of signals. A system implementing this method may be schematically represented as shown in Fig. 6.9.

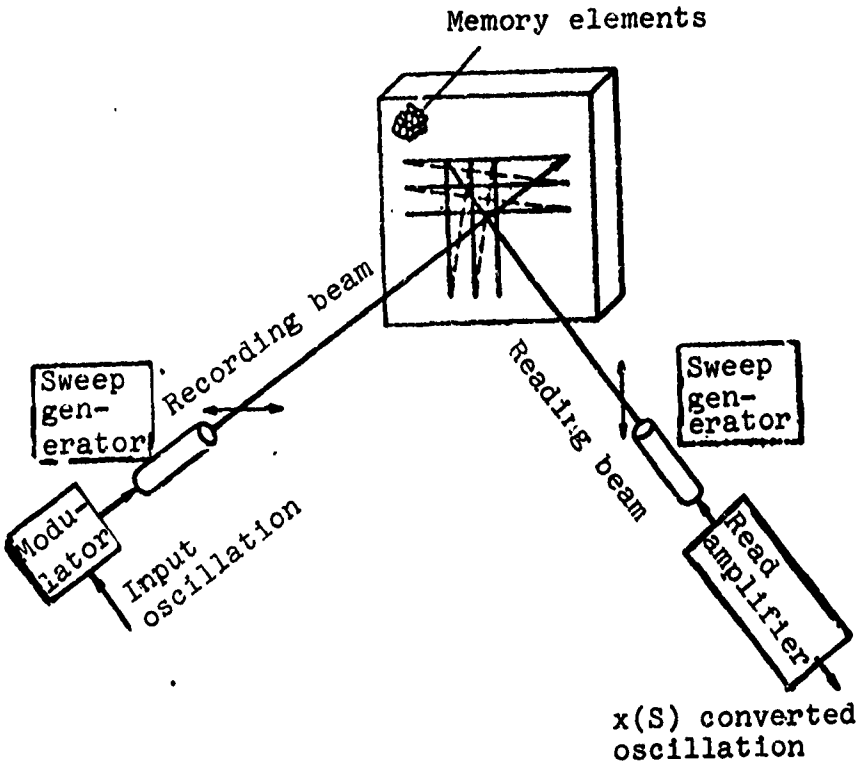

Fig. 6.9. Schematic representation of a storage and readout device.

The recording beam causes the oscillation reaching the input to be recorded on the storage element mosaic. The recording rate $V_{зап}$ is determined by the recording resolution and the correlation time of the input signal and can be established as

$$V_{зап} \geq \frac{1}{\tau_{кор}} \left[\begin{array}{c} \text{Number of storage} \\ \text{elements per second} \end{array} \right]. \qquad (6.1)$$

The read-out function is accomplished by the reading beam at any rate that can be realistically achieved. The direction of this read-out is selected based on an optimum structure for the converted signal.

In the practical design of devices of this kind a large number of different physical mechanisms may be used, based on the principles of magnetic, electrostatic, and quantum-optical signal recording and reading.

7. ANALOG ELECTRONIC FILTERS

7.1. Basic Types of Analog Electronic Filters

Analog electronic filters serve as the basis for the design of analog electronic filtering devices. Depending on the filter's required response structure and its operating mode, an analog filter of this kind may be the simplest type of electronic radio circuit or a highly sophisticated device containing a large number of various elements and physical mechanisms [45, 51].

Analog electronic filters are usually divided into the following basic types:

1. filters using oscillatory and aperiodic radio circuits;

2. filters using phase and dispersion-type radio circuits;

3. filters using delay lines.

Each of these filter varieties is normally used for the filtering of a definite class of signals and for the design of filtering devices with different frequency response form.

7.2. Electronic Filters Using Oscillatory and Aperiodic Radio Circuits

In the majority of cases, filters of this type are employed for coherent and noncoherent filtering devices for signals in which the product ΔWAT is comparatively small. Such signals include those which are not subject to complex modulation laws and whose amplitude spectra lend themselves to approximation by the simplest kind of functions.

Structurally, filters of this kind are synthesized for the required frequency or pulse characteristic through the use of methods involving the multiple-series connection of single- and two-pole networks whose resultant transfer function approximates the required filter response with an assigned degree of accuracy. This method for the approximation and composition of structural filter circuits on the basis of elementary networks has been examined in detail in a number of special papers, including [5, 39, 77]. The basis of such one- and two-pole systems may be a variety of reactive and resistive elements, as well as numerous types of electronic-acoustic networks. Depending on the major elements they incorporate, the filters are appropriately named: LC, RC, electromechanical, piezoceramic, quartz filters, etc., etc. Filter-design techniques calling for different oscillatory systems, the principles underlying the technical execution of their components, and also their key characteristics have been discussed in [1, 10, 53, 58, 86].

In any practical filtering device the selection of a particular filter type is determined both by requirements having to do with the electrical characteristics and by requirements in the area of stability, ease of manufacture, operating features, and cost. For example, LC and RC filters call for no special production technology and can be easily tuned; however, given their sophisticated multipolar structure they prove to be unwieldy in tuning and, unless special heat-stabilization measures

are adopted, they exhibit a relatively low stability of 10^{-3}. Quartz filters, while they offer high stability (10^{-6}), require a special manufacturing technology, are difficult to adjust, and are relatively costly. The piezoceramic and electromagnetic kind feature intermediate stability characteristics (10^{-4}), are more compact in design than the LC filters and less costly than the quartz type. They too, however, require a special production technology and present problems in retuning.

The frequency responses of unipolar and multipolar filters provide an approximation of a prescribed characteristic only with a certain error, for which reason the detection and resolution of the filtering systems will be worse than the potential characteristics. The deterioration in the signal/noise ratio in this regard can be determined, in accordance with dependence (3.8) and (2.18), according to the formula

$$\frac{q^2}{q^2_{cor.a}} = |\Psi_0'(00)|^2 = \frac{\left[\int_{-\infty}^{\infty} S^*(f) S_0(f)\, df\right]^2_{макс}}{\int_{-\infty}^{\infty} |S(f)|^2 df \int_{-\infty}^{\infty} |S_0(f)|^2 df}, \qquad (7.1)$$

where $S(f)$ and $S_0(f)$ is the spectrum of the signal modulation function and the filter response, respectively.

Figure 7.1 presents a graph illustrating, for several of the simplest filters, the change as a function of filter structure, in the bandwidth value ΔF_0 ensuring minimum deterioration in the parameter q^2 when filtering a radio pulse with rectangular envelope. The band ΔF_0 is read on the -3 dB level.

Table 7.1 lists the basic characteristics of a number of filters, along with the energy losses caused by their mismatching with respect to a radio signal with right-angled envelope.

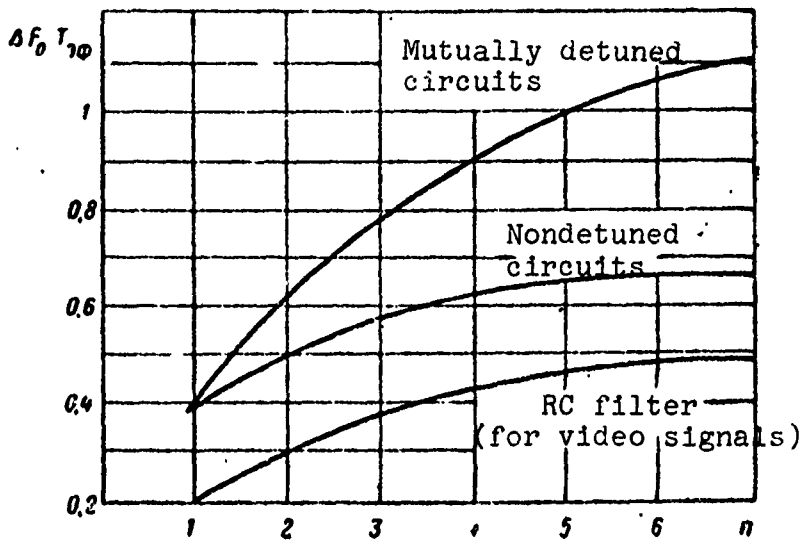

Fig. 7.1. Graph of the filter band ΔF_0 vs the number of circuits.

Table 7.1.

Form of filter frequency response	$\Delta F_0 T_{э\phi}$	Energy losses, dB
Gaussian	0.72	0.65
Series connection of five single resonance circuits	0.67	0.65
Square-wave	1.37	(8
System of coupled circuits with critical coupling	1.2	0.65
Single resonance circuit	0.4	0.9

A filter's frequency response can be brought into closer agreement with the required characteristic by adding to the complexity of the filter. Thus, for example, for filters whose pulse characteristic has the form

$$K(t) = (1 + b_2 t + \ldots + b_n t^{n-1}) \exp(-b_1 t), \qquad (7.2)$$

corresponding to the presence in the resulting transmission characteristic of this filter of one real n-th order pole and n - 1 prime nulls [24, 39], the energy losses in the filtering

of a square-wave radio pulse, for n = 3, 4, will be considerably less than in the case of the simplest filters. The parameter values of the pulse characteristic for this situation are cited in Table 7.2.

Table 7.2.

n^m	$b_1T_{э\phi}$	$b_2T_{э\phi}$	$b_3T^2_{э\phi}$	$b_4T^3_{э\phi}$	Energy losses, dB
3	4,5	—2,9	35	—	0,4
4	6,2	14	—74	284	0,3

For the filtering out of signals in the Doppler frequency band Δ_ν, common practice calls for the use of a set of filters with overlapping frequency characteristics (Fig. 7.2). The number of filters in the set is fixed by the permissible measurement error and by the permissible deteriorations in the detection characteristics due to the discrete spacing of the filters (4.3, 5.4). The graph in Fig. 7.3 illustrates how the energy losses are affected by the discrete value in the arrangement of the filters when a square-wave radio pulse is filtered by a set single- and twin-circuit filters.

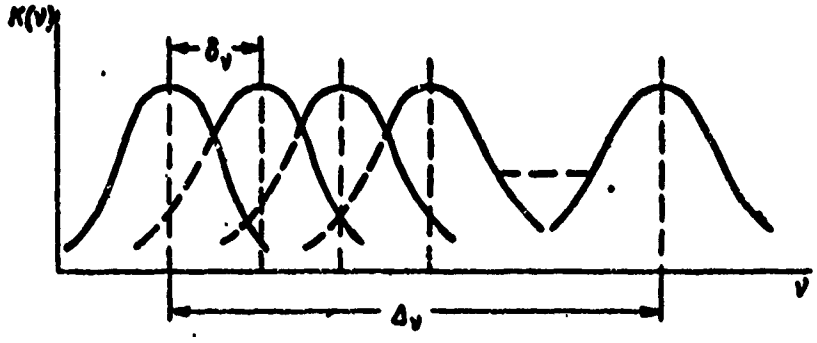

Fig. 7.2. Frequency characteristic of a set of filters.

Band-elimination filters for coherent signal-filtering devices may be designed on the basis of the same oscillatory systems used in matched and mismatched filters. However, as a

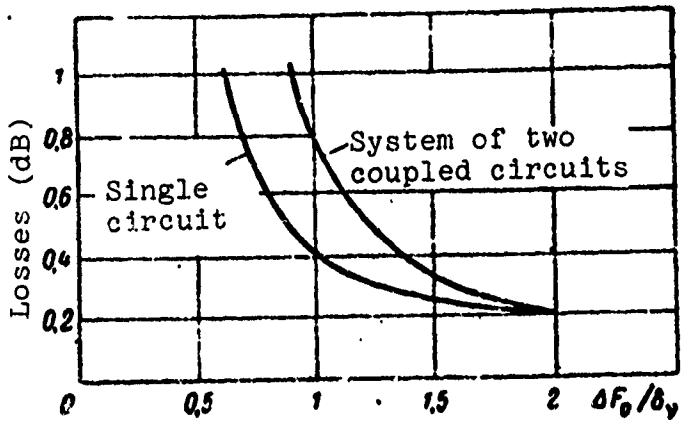

Fig. 7.3. Graph illustrating dependence of losses on spacing of filters.

rule, more stringent requirements with respect to the rectangularity factor are demanded of the characteristics of band-elimination filters, with the result that such filters more often employ electromechanical, piezoceramic, and quartz oscillatory systems. The basic parameters of a number of band-elimination filters using different types of oscillatory systems are cited in Table 7.3. The meanings of the parameters are explained by Fig. 7.4 and by the following relations:

$B_0 = 20 \lg K_{пр}$ is the filter's transfer constant in the transmittance band;

$\Delta B = 20 \lg \frac{\Delta K}{K_{пр}}$ is the nonuniformity of the filter transfer constant in the transmittance band;

Δf_0 is the filter's nontransmittance band at the level of its transfer constant;

Δf_1 is the filter's nontransmittance band at the suppression level;

$\frac{\Delta f_0}{\Delta f_1}$ is the rectangularity factor;

$B_{под} = 20 \lg \frac{K_{пр}}{K_2}$ is the filter's suppression factor.

Table 7.3.

Type of filter's oscillatory system	f_0 MHz	$\frac{\Delta f_0}{\Delta f_1}$	$B_{под}$, dB	ΔR, dB	R_0, dB
Piezoceramic	0,01—1	1—3	30—50	3—5	5—15
Electromechanical	0,001—1	2—4	30—60	3—6	5—15
Quartz	0,1—100	2—4	30—100	2—4	3—10

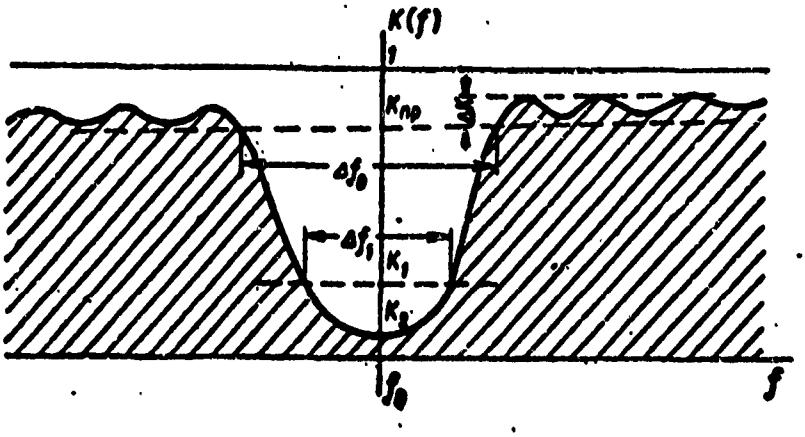

Fig. 7.4. Frequency response of band-elimination filter.

7.3. Electronic Filters Using Phase and Dispersion Circuits

This type of filter can be used to filter signals whose amplitude spectrum undergoes little change throughout their frequency band but whose phase spectrum exhibits a monotonic nonlinear frequency dependence. An example of this kind of signal is a frequency-modulated radio pulse (2.37) the spectral characteristic of which, following formulas (2.38) and (2.39), can be approximated, with a degree of accuracy adequate for practical purposes, by the following expression:

$$S(f) = S_f \exp j\varphi(f). \qquad (7.3)$$

The appearance of such an approximated frequency response has been shown in Fig. 2.8.

A filter whose frequency response represents a complex-conjugate function with respect to the spectrum of this kind of signal can be synthesized in the form of a series connection of conventional band filters, with an amplitude-frequency characteristic approximating the spectrum S_f, and a phase filter having a uniform amplitude and quadratic phase-frequency characteristic. Dispersion-type radio circuits can be employed as this kind of phase filter - specifically, the cascade connection of the branches of nonminimal-phase networks (Fig. 7.5).

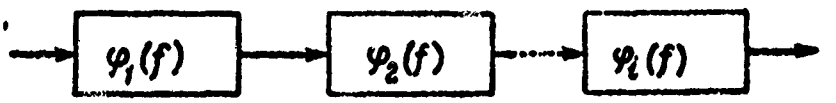

Fig. 7.5. Cascade connection of phase networks.

Each such section (branch) is actually a bridge circuit, as structurally represented in Fig. 7.6. The amplitude-frequency response of these sections is uniform over an extensive frequency range, while the phase-frequency response vaires according to different laws of change within individual frequency segments. By combining the parameters of the inductances and capacitances of the individual sections, a network having the required phase-frequency characteristic can be synthesized [24]. However, if the compression factor K_{CW} is greater than 10, a filter of this kind will require an extraordinarily large number of sections, resulting in considerable technical difficulties in its manufacture and alignment. Moreover, the presence of mismatching and distortions in the individual sections leads to significant degradation in its resultant response.

From the practical standpoint it is more expedient to employ electronic-acoustic networks featuring dispersive properties for

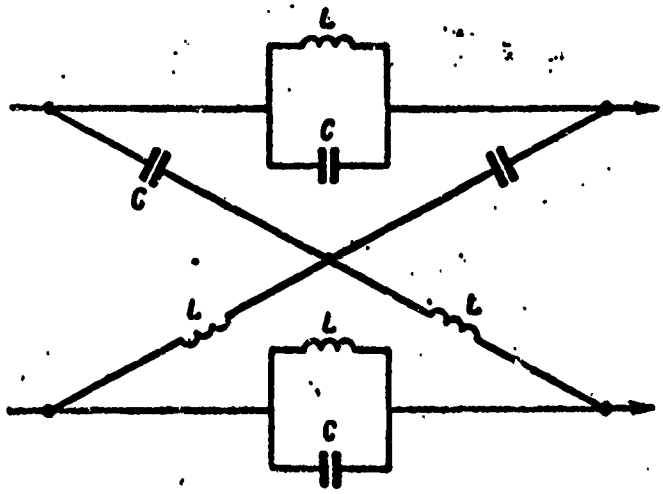

Fig. 7.6. Phase-network bridge circuit.

such a phase filter. These networks my be metal sound-conductors of variable thickness, as well as a variety of acoustic lines with the excitation and output systems in the form of an array of radiating elements (§ 7.5).

Whenever the parameters of such dispersion circuits cannot be immediately matched with the required filter characteristics, these circuits are connected in parallel or in series [45, 78] (Figs. 7.7 and 7.8).

The arrangement shown in Fig. 7.7 has n parallel channels, at the input of each of which is connected a band filter Φ_i with a passband ΔF. The center tuning frequencies of these filters correspond to the value $f_0 + \Delta F(n - 1)$, that is, they differ from each other by the quantity ΔF. The dispersion network in each channel exhibits a uniform amplitude-frequency response within the passband of the band filter, while the phase characteristic of the network is related to the filter's center frequency in each channel in the following manner:

$$\varphi_i(f) = \frac{\pi |f - f_0 + \Delta F(i-1)|^2 T_{\text{disp}}}{\Delta F n}. \qquad (7.4)$$

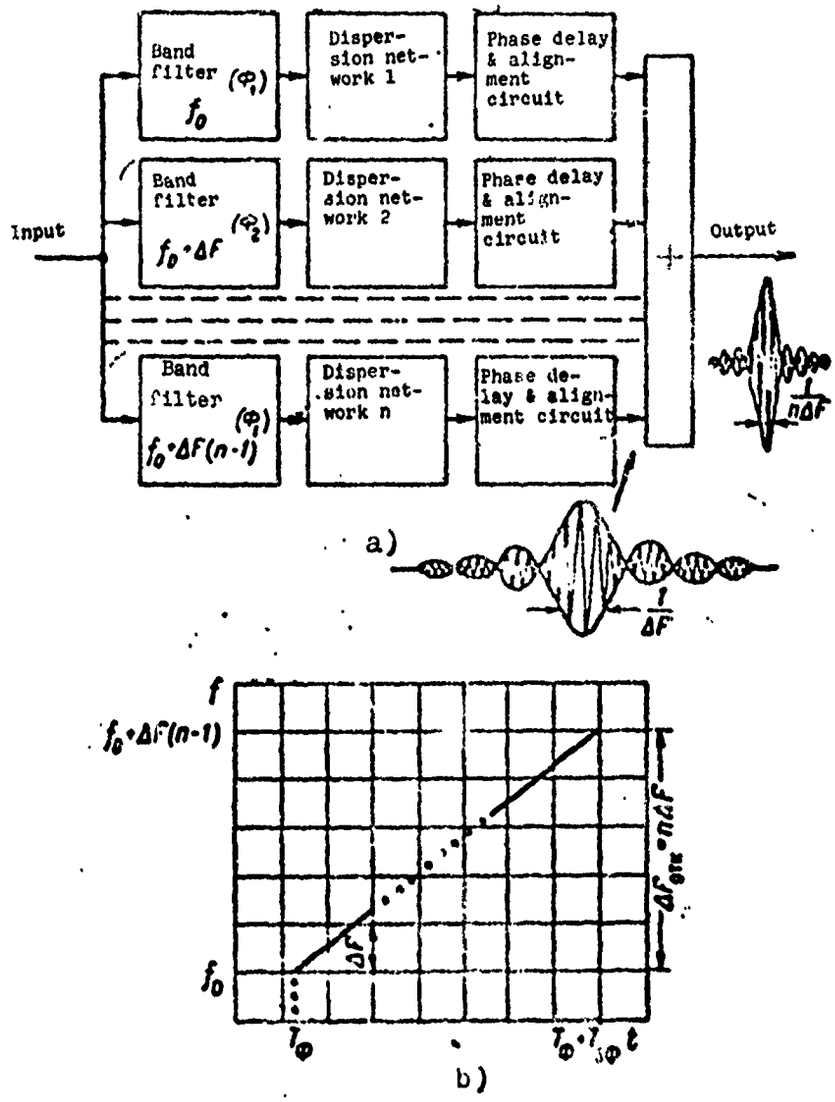

Fig. 7.7. Parallel connection of dispersion networks: a) structural diagram of filter; b) graph showing the change in response frequency with dispersion networks connected in parallel.

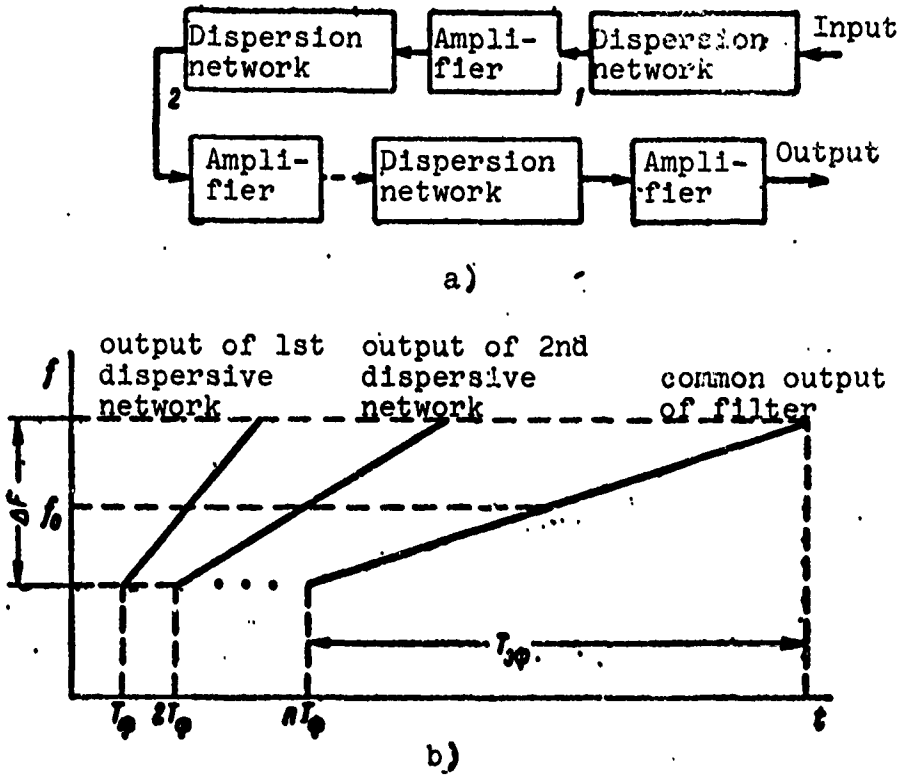

Fig. 7.8. Series connection of dispersion networks: a) structural diagram of filter; b) graph showing the change in response frequency with dispersion network connected in series.

Such a filter has a response of duration $T_{э\phi}$, whose spectral width is

$$\Delta F_{отв} = n\Delta F. \tag{7.5}$$

Figure 7.7b shows a graph of the frequency variation in the responses of the individual channels and of the overall filter. The time T_{ϕ} describes the initial delay of the filter. The compression factor of a linear frequency-modulated signal by each channel of the system depicted in Fig. 7.7 will be

$$K_{сжк1} = \Delta F \frac{T_{э\phi}}{n}, \tag{7.6}$$

while the resultant compression coefficient for this entire system is determined by the quantity

$$K_{сж1} = \Delta F T_{э\phi} n = n^2 K_{сжк1}. \tag{7.7}$$

In the case of the series-connected circuit (Fig. 7.8a) the amplitude-phase characteristic of each dispersive network will also have a frequency band of ΔF, with the phase characteristic corresponding to

$$\varphi(f) = \frac{\pi (f - f_0)^2 T_{эф}}{\Delta F n}. \tag{7.8}$$

The duration and spectral width of the response for the filter in this case also are

$$\tau_{отк} = T_{эф},$$
$$\Delta F_{отк} = \Delta F. \tag{7.9}$$

A graph illustrating the change in the response frequency at various points in the series-connected arrangement can be seen in Fig. 7.8b.

For the individual dispersive network the compression factor is

$$K_{сжат1} = \Delta F \frac{T_{эф}}{n}. \tag{7.10}$$

while the resultant compression factor for the series connection is defined as

$$K_{сжат} = \Delta F T_{эф} = n K_{сжат1}. \tag{7.11}$$

Relations (7.7) and (7.11) indicate that, with the dispersive networks connected in series or in parallel, the required values for the resultant compression factor as well as for the frequency band and duration of the response can be achieved even when the parameters of the dispersive circuits differ markedly from this required figure.

7.4. Electronic Filter Using Delay Lines

This class of filters is the most universal in that it permits the realization of a response of virtually any structure. On the other hand, the complexity and cost of these filters is comparatively

high, as a consequence they are normally used exclusively for the filtration and rejection of complex signals with a large ΔWΔT product. A generalized block diagram of a filter employing a multibranch delay line is shown in Fig. 7.9.

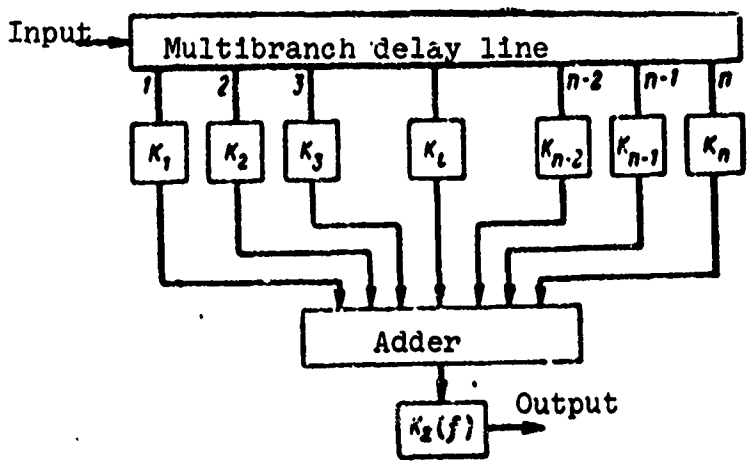

Fig. 7.9. Block diagram of a multi-branch delay-line filter.

When synthesizing a filter matched with a broad-band signal whose principal spectral components fall with the frequency interval 0-f_{max}, the following parameters of the system shown in Fig. 7.9 are selected:

$$K_z(f)=\begin{cases}\frac{1}{2f_{макс}} & \text{for } |f|<f_{макс},\\ 0 & \text{for } |f|>f_{макс},\end{cases} \qquad (7.12)$$

$$K_i=b_i,$$

$$\Delta\tau_0=\frac{1}{2f_{макс}}.$$

The resultant pulse response of the circuit will be

$$K(t)=\sum_{i=0}^{n} b_i \frac{\sin \pi (2f_{макс}t-i)}{\pi (2f_{макс}t-i)}. \qquad (7.13)$$

Expression (7.13) is in fact the well known Kotelnikov series [24], which in this case approximates the prescribed response, with the required accuracy, in the form of a sequence of time samplings interspaced by the time $\Delta t = 1/2\, f_{макс} = \Delta\tau_д$ and having the amplitude b_i.

If the signal is filtered on the intermediate frequency $f_{пр}$, then $f_{макс}$ will show a large value, thus requiring the use in the delay line of a very large number of branches closely spaced at intervals of

$$\Delta W \ll f_{пр}. \qquad (7.14)$$

Here, the filter response can be represented as

$$K(t)=A_\phi \cos[2\pi f_{пр}t+\varphi(t)], \qquad (7.15)$$

where $A_\phi(t)$ is the response envelope;

$\phi(t)$ is the instantaneous phase of the high-frequency duty cycle of the response.

A filter with this kind of response can also be synthesized using the circuit shown in Fig. 7.9, having the characteristics:

$$K_\Sigma(f)=\begin{cases}\frac{1}{\Delta W} & \text{for } f_{мин}<f<f_{макс},\\ 0 & \text{for } f_{макс}<f<f_{мин},\end{cases} \qquad (7.16)$$

$$K_i = A_{\phi i}\exp\varphi_i.$$

$$\Delta\tau_д=\frac{1}{\Delta W}.$$

where $f_{макс}$ and $f_{мин}$ are the cut-off frequencies in the spectrum of the signal.

Meanwhile, the pulse response can be written in the following form [24]:

$$K(t)=\sum_{i=0}^{i=n} A_{\phi i}\frac{\sin\pi(\Delta Wt-i)}{\pi(\Delta Wt-i)}\cos\left(\pi f_{пр}t-\frac{\pi i f_{пр}}{\Delta W}-\varphi_i\right), \qquad (7.17)$$

corresponding to the representation of the response by a sequence of n amplitude samplings with amplitude $A_{\phi i}$ and phase ϕ_i having a period of $\Delta t = \frac{1}{\Delta W}$. In this event, the number of delay-line branches for a filter whose response has an effective duration T_e is only $n = T_e\Delta W$ and is independent of the value of the intermediate frequency.

Whenever there is a need for a set of filters tuned to different frequencies, such a filter set can be synthesized using a single multibranch delay line; however, several adders will now be required (Fig. 7.10). Moreover, the synthesis of a filter with a broad-band response of form (7.13) will require that for each Doppler frequency shift there be a variation in the transfer coefficients b_i, while in the case of a filter offering a narrow-band response (7.17) only the phase shifts ϕ_i need be changed.

In this way, the block diagrams shown in Figs. 7.9 and 7.10 offer a means of synthesizing a filter matched with either a broad-band or narrow-band signal of any structure. The complexity of the filter (number of delay lines or delay-line branches), meanwhile, is proportional to the value of the product ΔWT_e, where ΔW and T_e are, respecitvely, the rms value of the frequency band and the effective filter response time interval (1.24) and (2.26).

In specific cases for certain discrete signals the overall block diagram of the filter represented in Fig. 7.9 may be somewhat modified for the purpose of reducing the total number of

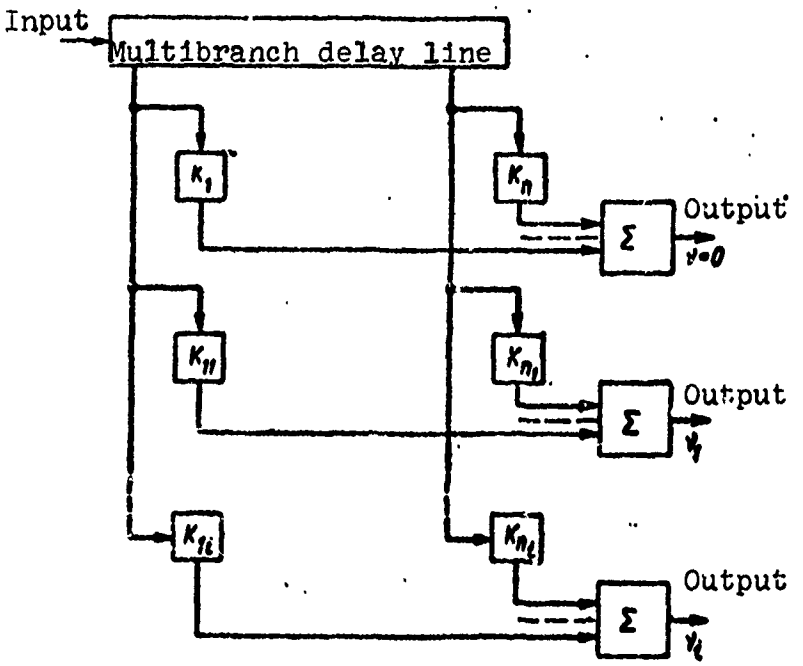

Fig. 7.10. Block diagram of a filter using a delay line with several frequency channels.

delay lines. For example, if the modulation function of a discrete phase-keyed signal (2.46) can be represented in the form of a sum

$$S(t)=\underbrace{\sum_{j=0}^{j=m-1}\cdots\sum_{i=0}^{i=q-1}\sum_{k=0}^{k=p-1}}_{s_{\text{сум}}} g_{k,\,i,\,\ldots,\,j}\,1_n(t-kT_{\text{д}}-$$

$$-ipT_{\text{д}}-\ldots-jpgT_{\text{д}},\ T_0), \qquad (7.18)$$

where $q_{k,\ i,\ \ldots,\ j}$ may be a positive or negative unit or zero depending on the indices k, i, ..., j, the filter synthesizing a response of this type may be designed on the basis of the block diagram shown in Fig. 7.11.

Each delay circuit contains a number of delay lines which corresponds to the number of minus unit terms of the individual sum of expression (7.18) and ensures the delay of the unit

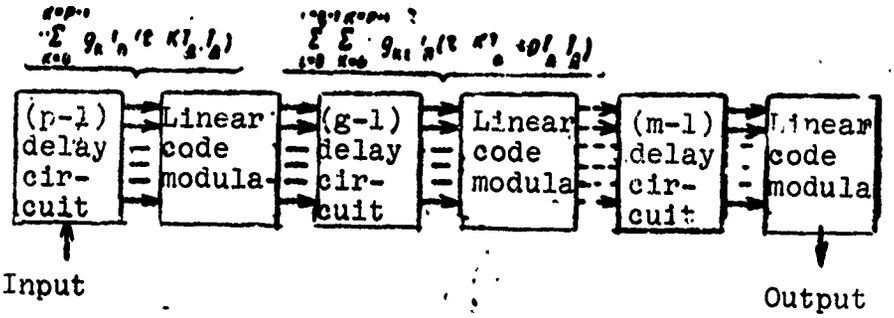

Fig. 7.11. Block diagram of cascade filter using delay lines.

function ln (t-...) in accordance with the instantaneous index. The linear code modulator effects the modulation of the coefficient $q_{k, i, \ldots, j}$ in conformity with the selected code. This kind of modulator is shown in block diagram in Fig. 7.12.

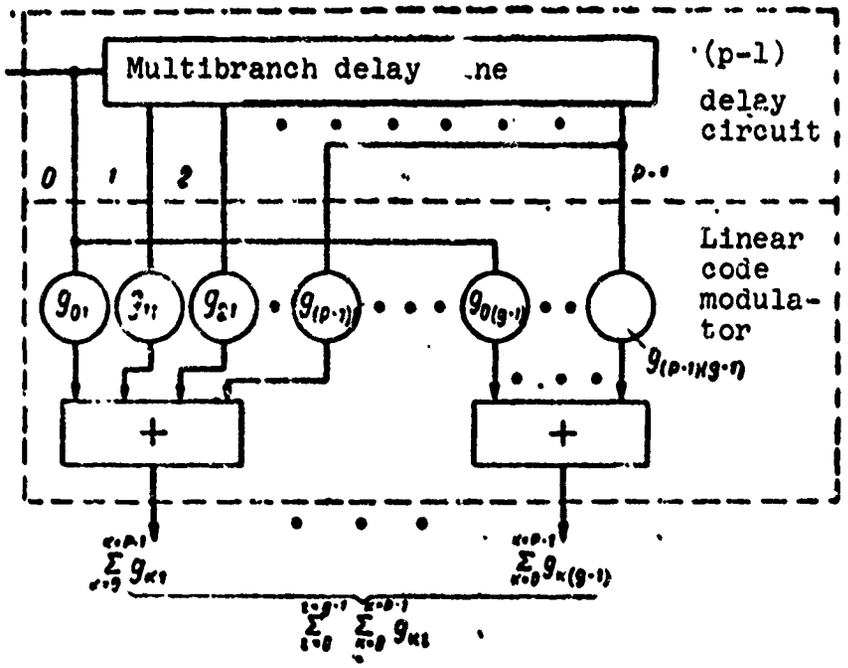

Fig.7.12. Block diagram of one delay network and linear code modulator.

The total number of code symbols in the response of the cascade filter in Fig. 7.11 is

$$N = pg, \ldots, m; \tag{7.19}$$

with the equality

$$p = g = m \qquad N = p^z \tag{7.20}$$

and the total number of delay lines will correspond to the value

$$n_3 = z(p-1) = \log_p N(p-1). \tag{7.21}$$

In the event that

$$p = g = m = 2, \tag{7.22}$$

the sum (7.18) describes a so-called two-code sequence (Reed code [63]). The block diagram of a filter designed to synthesize a response in accordance with these codes is even further simplified and will appear as shown in Fig. 7.13. The circuit contains only $n_3 = \log_2 N$ delay lines and permits the synthesis of a response consisting of $N = 2^{n_3}$ code symbols.

The arrangement pictured in Fig. 7.13 is also useful when synthesizing a response representing the modulation function of a phase-keyed, B-code-encoded signal [17]; only now the branches of the filter are connected not in accordance with the law of a linear rise in the delay (as in the case of the Reed codes [Fig. 7.13]), but according to a definite code characterizing the subcode law of the B-code [95].

Delay-line filters are extensively employed also for the filtering of periodic signals representing a variety of radio pulse trains (2.53). Since the spectra of these signals possess a comblike structure, the filters used in association with them are known as comb filters. The theory and design technique of

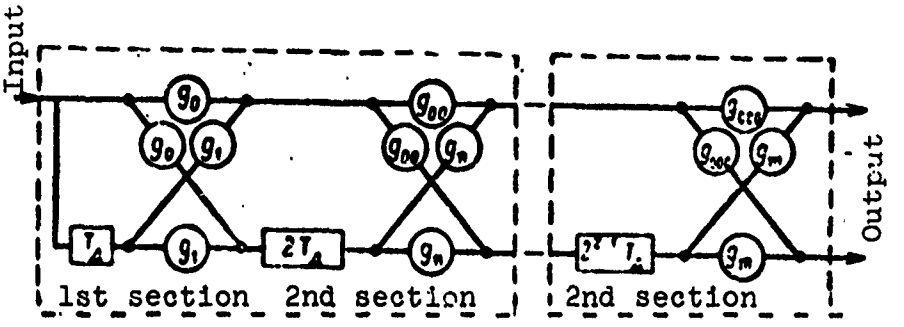

Fig. 7.13. Block diagram of a discrete filter with Reed code response.

discrete comb filters incorporating delay lines have been set forth in sufficient detail in [51, 72, 79, 84]. As encountered in actual practice, the circuit arrangements of these filters normally contain a cascade connection of the delay line sections with first- and second-order couplings (Fig. 7.14).

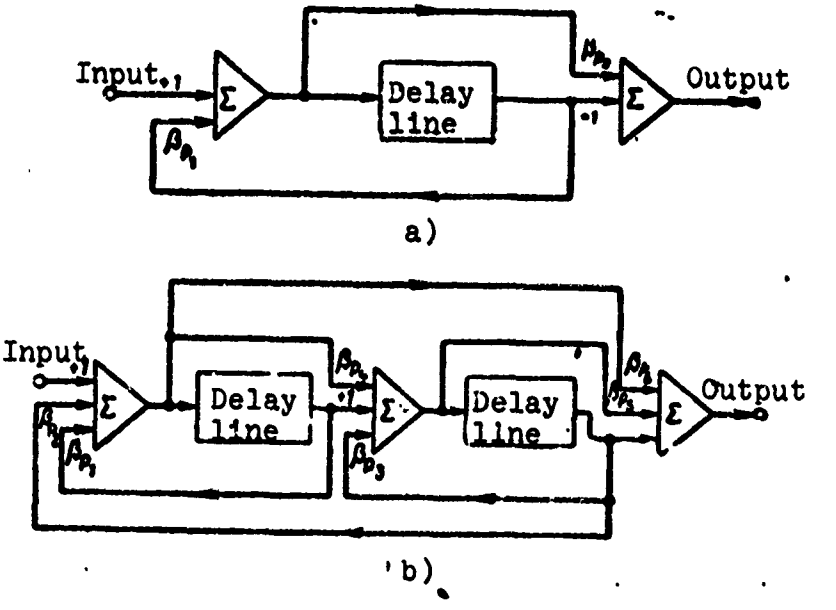

Fig. 7.14. Block diagram of a discrete comb filter: a) section with 1st-order couplings; b) section with 2nd order couplings.

By selecting the proper coupling factors β_{pi}, the required filter frequency characteristic or prescribed response can be synthesized. By way of example, Fig. 7.15a shows the block diagram of a two-cascade comb filter based on delay lines, and Fig. 7.15b its frequency characteristic for a single frequency-variation period.

By connecting a discrete comb filter in series with a filter having an aperiodically structured frequency characteristic (for example, on the basis of the simplest kind of oscillating system), it is possible to obtain a resultant aperiodic frequency characteristic with the required rectangularity without the use of multiply-coupled oscillatory systems. Filter systems of this kind can be used for high-quality band elimination and for optimum filtration of signals with a low $\Delta W \Delta T_e$ product.

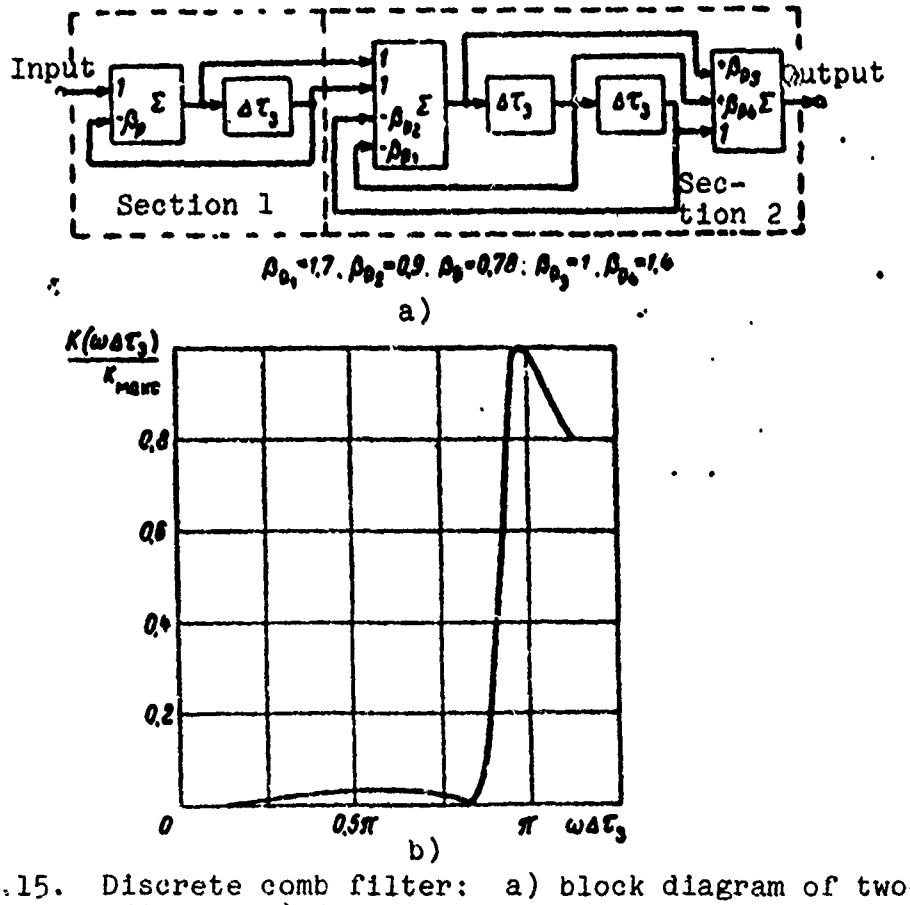

Fig. 7.15. Discrete comb filter: a) block diagram of two-section comb filter; b) frequency response of two-section comb filter

7.5. Types of Delay Lines and their Basic Characteristics

Delay lines for electrical signals [DL] (ЛЗ) can be designed both on the basis of transmission lines for electrical (electromagnetic) waves as well as the conversion of an electrical signal into a mechanical (acoustic) signal and the acquisition of a time delay associated with the propagation of this mechanical (acoustic) signal in an elastic medium, followed by the reconversion of the acoustic wave back into an electric signal by means of a receiving-end converter (transducer). The schematic representation of this kind of acoustic delay line is shown in Fig. 7.16a.

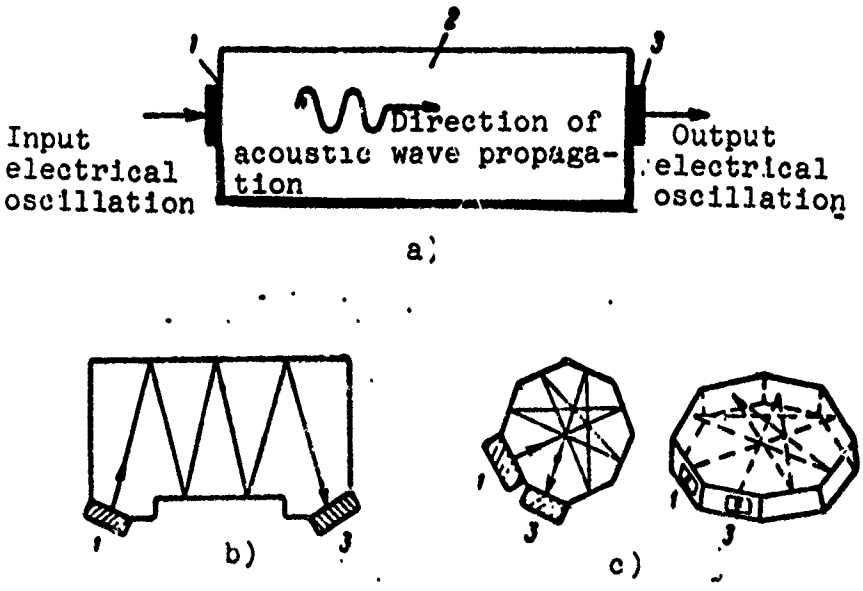

Fig. 7.16. Schematic representation of an ultrasonic delay line: 1 - input transmitting converter; 2 - acoustic elastic medium (sound conductor); 3 - output (receiving) converter.

Delay lines utilizing electrical signal transmission lines are referred to as electrical (electromagnetic) delay lines [EDL] (ЭЛЗ), at the same time that delay lines based on acoustic transmission networks are known as ultrasonic delay lines [UDL] (УЛЗ). Inasmuch as the propagation velocity of sound (acoustic) waves is $V_{ак}$ = 2-5 km/s and is approximately 10^5 times less than the

velocity of electromagnetic oscillations, the use of acoustic media in delay lines makes possible significant reductions in the size and weight of the associated instrumentation.

The basic parameters of electrical and ultrasonic delay lines are cited in Table 7.4.

Table 7.4

Type of line	Delay time $T_{зад}$ [μs]	Frequency of transmitted signal $f_{а_к}$, MHz	Band $\Delta W_{лэ}$ MHz	Losses, dB	Q-factor $Q = T_{зад}\Delta W_{лэ}$
Electrical:					
coaxial cable	0.04	10^4-10^2	10^4-10^2	–	400
delay cable	2-5	10^2-10	5	10	10-25
delay lines with bunched parameters	0.01-10	300-0.5	100-0.1	3-5	1
Acoustic non-waveguide UDL:					
monocrystal	$1\text{-}5\cdot10^3$	10^4-10	100-5	–	10^2-$25\cdot10^4$
metallic	$1\text{-}2\cdot10^3$	20-10	10-0.5	–	$10\text{-}2\cdot10^3$
Waveguide UDL:					
(wire or strip type)	$10\text{-}2\cdot10^4$	5-0.1	10-0.05		$100\text{-}10^3$

A key delay-line characteristic is the parameter $T_{зад}\Delta W_{зад}$, which is known as the Q-factor of the line, where $T_{зад}$ and $\Delta W_{зад}$ is the time delay and passband of the delay line. It is evident from the table that the Q-factor of a UDL may be in the

tens of thousands and is many times superior to the Q-factor of the EDL. On the other hand, however, electrical delay lines are free of the losses associated with wave-type conversion and, therefore, display a transmission factor of close to one, a point which makes their use preferable to that of UDL in short-response video filter-circuit arrangements or in vernier tuning circuits for delay and phase adjustment in Doppler-filter adders (Fig. 7.10).

As a rule, only ultrasonic delay lines are employed for a more-than-10-microsecond delay of electrical signals, for the reason that the use of electrical delay lines for these purposes is inexpedient by virtue of the fact that at these delay times such devices are cumbersome and restricted to a narrow passband.

The conversion of the electrical into an acoustic signal in the UDL is accomplished by electromechanical transducers featuring resonance properties. Since the resonance frequencies of these transducers normally lie outside the video frequency region, ultrasonic delay lines afford distortion-free retardation of radio signals only, while great distortion is incurred in the delay of video signals.

In terms of the number of branches, ultrasonic delay lines can be divided into two groups: lines with unit delay and multi-branch delay lines. From the stnadpoint of the acoustic (elastic) wave-propagation mechanism, UDL are classified as belonging to the *waveguide* type, in which the elastic wave propagates virtually without divergence along the guiding surfaces of a mechanical waveguide, and the *non-waveguide* type, in which there occurs the usual divergent propagation of the elastic wave energy. Since waveguide propagation requires that the transverse dimensions of the waveguide be of the same order as the wavelength, waveguide ultrasonic delay lines can be used only in the low-frequency range of signals ($f_{ак}$ = 0.1) MHz-5 MHz). UDL of the non-waveguide class are free of this limitation and can be employed for frequencies

ranging from several MHz to several GHz. Ultrasonic delay lines at frequencies above 100 MHz are commonly referred to as hypersonic.

The key parameters of a delay line are: the delay time, the transmittable signal bandwidth, the electrical signal transmission factor, and the spurious signal level.

The delay time in a UDL is determined by the length of the path $l_{ак}$ traveled by the acoustic wave and by its propagation velocity $V_{ак}$:

$$\tau_{зад}=\frac{l_{ак}}{V_{ак}}. \qquad (7.23)$$

[Translator's Note - The subscript letters "зад" and "ак" stand for "delay" and "acoustic," respectively.]

The path trajectory of an ultrasonic beam in a non-waveguide UDL may be either a straight (Fig. 7.16a) or a broken (Fig. 7.16b, c) line. In waveguide-type UDL the propagation trajectory of the acoustic wave is always a straight line.

The transmission frequency band of the signal in the UDL is characterized by the resultant frequency characteristic, whose form is fundamentally fixed by the frequency characteristics of the receiving- and transmitting-end transducers. The UDL transducer is described both by its electrical as well as by its mechanical properties [87], so that its frequency response depends both on the frequency parameters of the circuits which are coupled to it and on its own acoustical band.

As a first approximation, the acoustical band of a mechanically unloaded transducer $\Delta W_{пр}$ can be estimated by the expression

$$\Delta W_{пр}=\frac{f_в-f_н}{f_р}, \qquad (7.24)$$

where f_a is the antiresonance frequency;

f_p is the resonance frequency.

The frequency f_p is found from a transcendental equation; for example, in the case of a longitudinal-wave plate transducer, if its area is far greater than its thickness, from the equation

$$x \operatorname{ctg} x = k_m^2,$$

while the frequency f_a is determined from the relation

$$f_a = \frac{V_{пр}}{2d_{пр}},$$

where

$$x = \frac{\pi}{2} \frac{f_p}{f_a};$$

k_m is the electromagnetic coupling coefficient of the transducer material;

$d_{пр}$ is the geometrical dimension of the transducer in the wave radiation direction (thickness);

$V_{пр}$ is the speed of sound in the transducer material.

Table 7.5 above lists the basic parameters for the most commonly encountered piezoelectrical UDL transducers employed in engineering practice. The piezoceramic materials for the transducers have been cited in the literature [22].

The transmission coefficient of the entire ultrasonic delay line is determined by the signal energy losses associated with the double conversion of the signal ($2B_{пр}$), the losses caused by the absorption of the acoustic signal in the material of the acoustic line ($B_{погл}$), and also by the losses related to the divergence of the acoustic beam during propagation - the diffraction

Table 7.5

Material	Crystal structure	Density $\mu_{пр}$ · g/cm³	Speed of sound $V_{прод}$ × 10^5 cm/s		Electromechanical coupling coefficient	
					Longitudinal wave $к_{m1}$	Transverse wave $к_{m2}$
Quartz crystal SiO_2	Hexagonal	2.65	5.7	3.3	0.098	0.137
Piezo-ceramic TsTS-19	"	7.6	4	2.3	0.5	0.7-0.6
Cadmium sulfide	"	4.82	4.41	1.75	0.262	0.188
Lithium niobate $LiNbO_3$	Trigonal	4.71	7.43	3.71	0.5	0.54

losses ($B_{расх}$). The resultant losses can be expressed in the form of a sum

$$B_{\Sigma} = 2B_{пр} + B_{пога} + B_{расх}. \qquad (7.25)$$

Depending on the type of UDL, the transducer characteristics, and the signal frequency, the specific weight of a specifice loss component may vary considerably.

Losses due to dcuble signal conversion may be estimated from the following relation

$$2B_{пр} = 4k_m^2 \frac{Z_{пр}}{Z_{зв}} \left(\frac{2Z_{зв}}{Z_{зв} + Z_{нагр}} \right)^2 \frac{Q_0 c_{пр}}{\pi (c_{пр} + c_{вх})}, \qquad (7.26)$$

where $Z_{гр} = V_{пр}\mu_{пр}$ is the acoustic impedance of the transducer;

$Z_{зв} = V_{зв}\mu_{зб}$ is the acoustic impedance of the acoustic delay line;

$Z_{нагр} = V_{нагр}\mu_{нагр}$ is the acoustic impedance of the load;

$c_{пр}$, $c_{вх}$ are the electrical capacitances of the transducer and electrical input circuit;

Q_0 is the Q-factor of the electrical input circuit;

$\mu_{пр}$, $\mu_{зв}$, $\mu_{нагр}$ is the density of the acoustic media.

The principal parameters of equation (7.26) for some typical acoustical materials are cited in Tables 7.5 and 7.6. Ultrasonic wave absorption in the delay line is the outgrowth of several physical processes and is related by a complex dependence to the the working frequency, the type of ultrasonic wave, and the quality of the material [55]. To estimate these losses, Table 7.6 gives the values of specific absorption $\Delta B_{погл}$ dB/cm for a longitudinal wave.

Table 7.6

Material	$\mu_{зв}\cdot10^3$, kg/m³	$V_{зв}\cdot10^3$, m/s	$V_{нагр}\cdot10^3$, m/s	$Z_{зв}\cdot10^6$, kg/m²s	$Z_{нагр}\cdot10^6$, kg/m²s	$\Delta B_{пога}$·dB/cm
Aluminum	2.69	6.4	3.04	17.3	8.2	$5\cdot10^{-4}$ when $f_{ак}$ = 1 MHz
Magnesium	.74	5.77	3.05	10.0	5.3	
Iron	7.7	5.95	3.24	46.4	25.3	$1.5\cdot10^{-3}$ when $f_{ак}$ = 1 MHz
Nickel	8.7	6.04	3.0	53.5	26.6	$2\cdot10^{-3}$ when $f_{ак}$ = 0.2 MHz
Melted quartz	2.2	5.97	3.7	13	8.29	

[Translator's Note: The subscript letters "зв," "нагр," "погл," and "ак" stand for "sound line," "load," "absorption," and "acoustic," respectively.]

The diffraction losses associtated with the divergence of the ultrasonic beam in the non-waveguide UDL may be defined as

$$B_{\text{расх}} = \frac{S_{\text{пр}}}{l_{\text{зв}}\lambda_{\text{зв}}}, \qquad (7.27)$$

where $S_{\text{пр}}$ is the area of the transducer;

$\lambda_{\text{зв}}$ is the length of the acoustic wave.

Diffraction losses connected with the half-waveguide character of the propagation process also occur in the strip-type ultrasonic waveguide delay line. These losses equal

$$B_{\text{расх}} = \frac{H_{\text{пр}}}{\gamma l_{\text{зв}}\lambda_{\text{зв}}}, \qquad (7.28)$$

where $H_{\text{пр}}$ is the length of the transducer.

Spurious UDL signals are caused primarily by the multipath propagation of the ultrasonic wave. The principal method of abating these signals is through the use of a variety of absorptive coatings applied to the nonworking surfaces of the UDL sound conductor. The use of these coatings makes it possible to achieve a level of spurious signals of -(30-40) dB with respect to the level of the main delayed signal.

We shall consider, by way of example, certain of the more typical types of ultrasonic delay lines and their major characteristics.

Waveguide UDL for Sheer Waves

A block diagram of a strip-type waveguide UDL is shown in Fig. 7.17a. Excitation and reception are accomplished through the use of "needle-type" sheer-wave piezoceramic transducers connected to the end surfaces of an acoustic strip line.

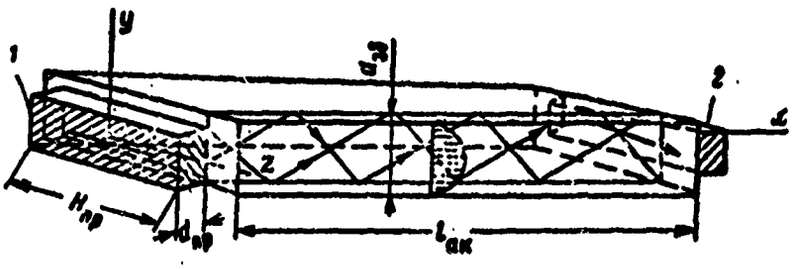

a)

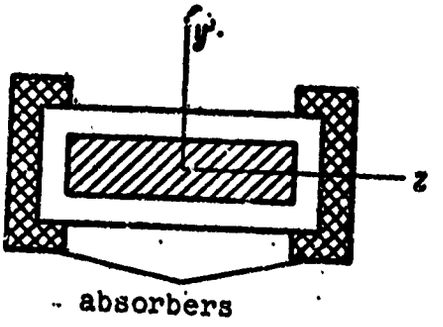

b)

Fig. 7.17. Block diagram of waveguide ultrasonic delay line: 1 - input transducer; 2 - output transducer.

The ultrasonic wave generated by transmitting transducer 1 propagates in plane YX (transverse, sheer wave) in the direction of the X axis by means of multiple reflections from the drive surfaces XZ (waveguide propagation). Non-waveguide propagation of the excited wave occurs in plane XZ. The beam-divergence losses during propagation are determined from relation (7.28).

Absorptive coatings must be applied to the narrow sides of the acoustic line to eliminate the false signals associated with the multipath propagation in plane XZ. (Fig. 7.17b). A transverse sheer wave propagates without dispersion-caused distortion at frequencies below

$$f_{кр} = \frac{V_{зв}}{2d_{зв}}, \qquad (7.29)$$

where $f_{кр}$ is the critical (cut-off) frequency;

$d_{зв}$ is the thickness of the acoustic line.

In addition to the strip-type waveguide variety of ultrasonic delay line, fairly extensive use is also made of wire waveguide UDL for longitudinal and torsional waves [55, 97]. All these UDL types feature comparatively low losses. The basic parameters of typical ultrasonic delay lines of this type for an acoustic line (sound conductor) consisting of AMG6M material are cited in Table 7.7.

Table 7.7

Type of UDL	Transducers	$T_{зад}$, μs	$f_{ак}$, MHz	$\Delta W_{ЛЗ}$, MHz	B_{Σ} dB
Strip UDL, transverse waves	"Needle-type" of TsTS-19	$5 \cdot 10^3$	1	0.3	40
Wire UDL, longitudinal waves	"Columnar-type" of TsTS-19	$2 \cdot 10^4$	0.5	0.05	40
Wire UDL, torsional waves	Toroidal of TsTS-19	10^4	0.5	0.1	45

Non-Waveguide Ultrasonic Delay Lines

This UDL type [73, 98] employs both the direct propagation of various wave classes as well as multiple-reflection propagation (Fig. 7.16b, c).

To ensure minimal divergence losses, these lines normally employ large-aperture transducers with $S_{пр} << \lambda^2_{зв}$, with metals or monocrystals having a low acoustic-wave propagation velocity used as the material of the acoustic lines.

The basic parameters of typical UDL of this type with constant delay are listed in Table 7.8.

Table 7.8

Acoustic line configuration	Acoustic line material	Transducer type	Transition layer type	Electrical parameters			
				$T_{зад}$, μs	$f_{ак}$, MHz	$\Delta W_{лЗ}$, MHz	B_{Σ}, dB
Polyhedron	Magnesium alloy MDZ-1	Piezoelectrical crystal, Y section	Indium	10^3	20	4	50
"	NaCl monocrystal			$2.5 \cdot 10^3$	20	3	60
"	Kbr monocrystal	Piezoceramic	Indium	$5 \cdot 10^3$	20	5	50
Polyhedron	Fused quartz SiO_2	Piezoelectrical crystal, Y section	Glue	10^3	10	5	50
Rod	Fused quartz SiO_2	CdS diffusion transducer		25 10	50 100	50 70	52 60
	Sapphire Al_2O_3			5	10^3	100	70

Hypersonic delay lines of this class employ monocrystals as the material of the sound duct: sapphire (Al_2O_3), rutile (TiO_2), lithium niobate ($LiNbO_3$), as well as sodium-iron (ZhIG) and sodium-aluminate (AIG) garnets. The transducers employed in these systems consist of a film of some piezo-semiconductive material, for example, cadmium sulfide (CdS).

The block diagram of a hypersonic delay line can be seen in Fig. 7.18 and its principal characteristics in Table 7.8. A typical feature of such lines is the presence of severe absorption losses, which normally increase in proportion to the frequency of the sound $f_{ак}$ (Fig. 7.19). This results in a great limitation of the possible dimensions of the acoustic line and, consequently, of the delay factor.

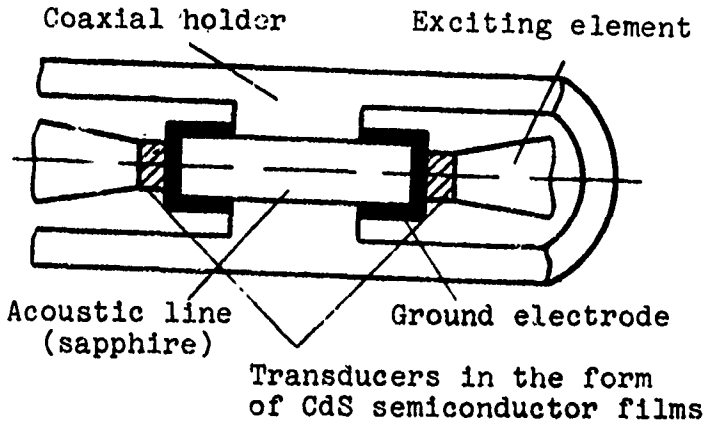

Fig. 7.18. Block diagram of a hypersonic UDL.

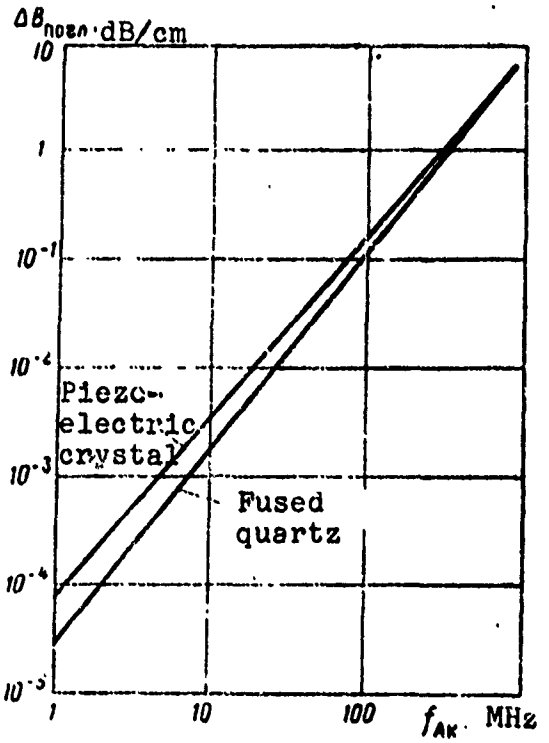

Fig. 7.19. Graph of absorption losses versus frequency.

Multibranch UDL

The multibranch ultrasonic delay line of simplest design is the magnetostriction type. In this kind of line the forward and back conversion of the electrical signal into an acoustic (elastic) wave is based on the phenomenon of magnetostriction, which consists in the alteration of the geometric dimensions of a specimen of ferromagnetic material located in an alternating magnetic field [8]. Although the deformation occasioned by the magnetostriction is comparatively small, in the order of 10^{-6}, the electromagnetic coupling coefficient for such materials as nickel reaches $k_m = 0.25$, which is comparable with the k_m of piezoelectric transducers. Since the magnetostriction effect is reversible, it can be exploited for the design of UDL. By virtue of the fact that magnetostriction transducers require no rigid acoustic coupling with the sound duct, this principle is particularly convenient in the creation of multibranch ultrasonic delay lines. Figure 7.20 shows such a multibranch longitudinal-wave magnetostriction UDL. Constant magnetic biasing is employed to ensure that such transducers operate in a linear mode. The characteristic parameters of this class of UDL, with inductive transducer and nickel acoustic line, are cited in Table 7.9.

Table 7.9.

$\tau_{зад}$, μs	$f_{вч}$, MHz	$\Delta W_{дз}$, MHz	B_Σ, dB
10^2	5	1,0	80
10^3	1,0	0,3	80
10^4	0,5	0,05	60

At the present time, wide use is being made, in the 10-30 MHz band, of multibranch surface-wave piezoelectric crystal UDL [40, 54, 98] of the type shown in the diagram in Fig. 7.21. A major feature of this delay line is the combination of the functions of the transducers and sound ducts in a single

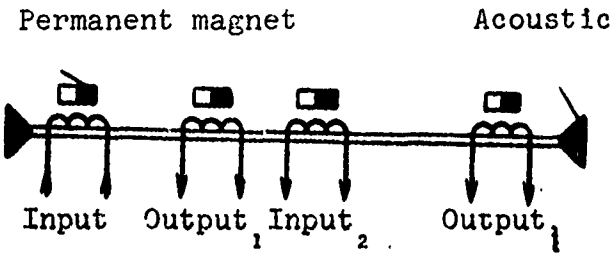

Fig. 7.20. Block diagram of a magnetostriction delay line.

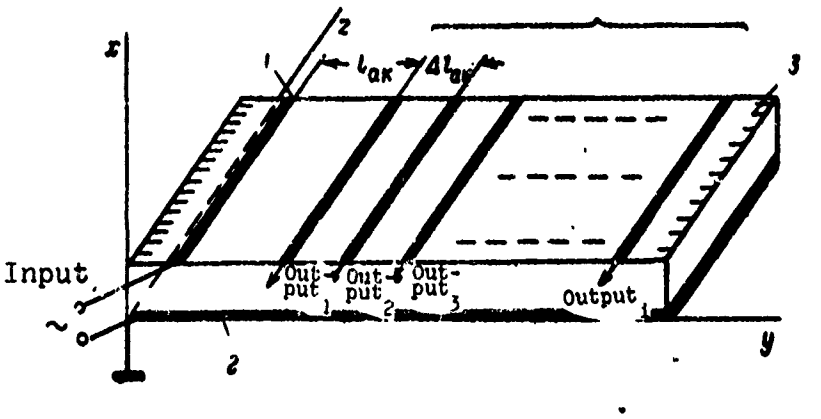

Fig. 7.21. Block diagram of multibranch surface-wave piezoelectric crystal UDL: 1 - input electrode; 2 - ground electrode; 3 - absorber.

piezoelectric crystal (e.g., in a piezoelectric quartz crystal X-section plate). When the input radio signal is delivered to the actuating electrode pair (upper thin electrode 1 and solid ground electrode 2), several modes of acoustical vibrations, including also a surface wave, are excited in the sound duct because of the reverse piezoelectric effect. The nonoperative oscillation types are absorbed by special absorbers (3), while the surface wave, propagating along the surface of the crystal plate, reaches the receiving electrodes (4) and is converted, through the forward piezoelectric effect, back into radio signals delayed by $T_{зад_i} = \frac{l_{ак} - i\Delta l_{ак}}{V_{акп}}$ ($V_{акп}$ is the velocity of the surface wave). Such lines may have a large number of branches (as many as 100 or more), but, because of the low k_m coefficient of the piezoelectric crystal and the nonresonance method of ultrasonic excitation and reception, they exhibit fairly high losses B_Σ(70-80 dB).

Table 7.10 lists the typical parameters of this kind of UDL for an X-section piezoelectric crystal.

Table 7.10

$f_{зад}$, MHz	Number of branches	$T_{зад}$,	B_Σ, dB	$\Delta f_{пз}$, MHz
10	30	15	70	2—3
20	70	60	86	6—8

Dispersive ultrasonic delay lines (DUDL) take the form of an acoustic network in which the delay of the signals is independent of their frequency. A distinction is made between wave-guide type dispersive UDL using the dispersive properties of normal ultrasonic waves in mechanical waveguides, and multi-element (lattice) surface-wave dispersive UDL in which the dispersion is artificially brought about by means of a complex multi-element transmitting and receiving transducer. In the mechanical

waveguides the majority of acoustic wave modes exhibit a propagation rate which is a function of the frequency of the driving signal. This factor is at the basis of the design of the waveguide variety of dispersive UDL. The characteristic specifications of these DUDL with transducers of TsTS-19 material are reflected in Table 7.11.

Table 7.11.

Acoustic line material	$f_{ав}$, MHz	$\Delta F_{отв}$, MHz	$\tau_{отв}$, μs	B_Σ, dB
Al	1	0,2	10⁴	30
H 45XT	10	2,5	200	60
H 45XT	45	10	40	70

To a significant degree the dispersion-characteristic parameters of the waveguide-type ultrasonic delay line are determined by the material of the sound duct and for all practical purposes cannot be controlled. This circumstance complicates severely the design of DUDL lots having an assigned dispersion characteristic and consistent performance.

More universal in this regard are the dispersive UDL with lattice-type transducers [54]. Figure 7.22a shows one of the possible configurations of this kind of delay line operating with surface waves. The system employs two groups of lattice-type strip electrodes arranged on the surface of a piezoelectric quartz crystal. The spacing between adjacent strips T_d determines the resonance frequency of the acoustic signal. By introducing the appropriate variation law in the spacing of the strips, a prescribed dispersion characteristic for the DUDL can be achieved (Fig. 2.22b).

The basic characteristic of a number of strip-type dispersion UDL with X-section piezocrystal are shown in Table 7.12.

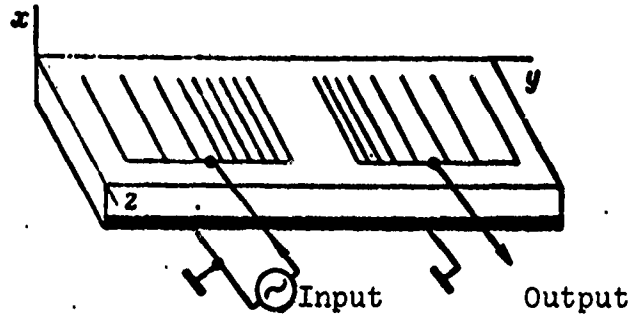

a)

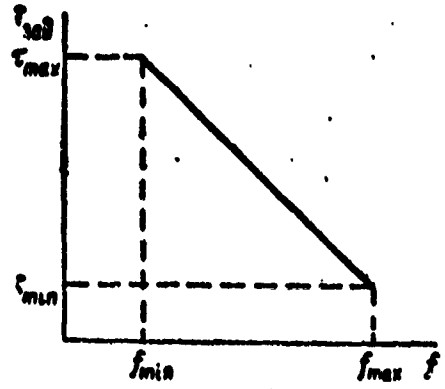

b)

Fig. 7.22. Lattice-type dispersive UDL: a) block diagram; b) dispersion characteristic.

Table 7.12.

$f_{вх}$, MHz	$\Delta F_{отв}$, MHz	$\tau_{отв}$, μs	B_Σ, dB	$K_{см}$
10	3	40	70	120
20	5	50	70	250
50	30	50	80	1500

8. DIGITAL ELECTRONIC FILTERS

8.1. General Block Diagram of Digital Filtering Device

In discrete form the coherent-filtering operation of an input signal, with allowance for expressions (1.39), (5.17), and (5.18), can be expressed as follows:

$$Y(n\Delta t)_{\Omega} = c_{u}\left\{\left|\sum_{j=1}^{j=N} A_{xm}(t_j)\,A_0(t_j - n\Delta t)\times\right.\right.$$
$$\times\cos[-\Omega n\Delta t + \varphi_{xl}(t_j) - \varphi(t_j - n\Delta t) +$$
$$+\varkappa_{xl}t_j + \varphi_{0l}]\Big|^2 + \Big|\sum_{j=1}^{j=N} A_{xm}(t_j)A_0(t_j - n\Delta t)\sin[-\Omega n\Delta t + \varphi_{xl}(t_j) -$$
$$\left.\left. - \varphi(t_j - n\Delta t) + \varkappa_{xl}(t_j) + \varphi_{0l}]\right|^2\right\}, \qquad (8.1)$$

where c_u is a constant normalizing coefficient;

t_j is the reference time moment;

Δt is the time interval between samplings.

The values of the amplitude $A_{xm}(t_j)$ and phase $\phi_{xl}(t_j) + \kappa_{xl}(t_j) + \phi_{0l}$ of the input signal at the moment of the time reading t_j are discretely measured with m and l quantization levels, respectively.

The operation involving the signal's noncoherent processing, considering its discreteness in time and quantification in amplitude, can be represented as

$$Y_u(n\Delta t)_{\Omega_i} = \sum_{k=1}^{k=M} b_k^2\,|Y_{\Omega m_i}(n\Delta t - kT_k)|^2. \qquad (8.2)$$

Figure 8.1 shows one of the possible circuit configurations providing for coherent and noncoherent signal filtering on the basis of digital methods.

By means of the amplitude-phase quantizer the input oscillation is converted into a set of discrete quantities characterizing in code form the sampling value of the amplitude and phase of the input. The quantizing is conducted uninterruptedly within time intervals of Δt, with the input-signal amplitude quantized over m levels and the phase over l levels. The set of discrete quantities, describing in binary code the discrete representation of the input oscillation, is stored successively in the memory (storage) units. The outputs of the memory elements storing the amplitude code (m levels) are summed for each equidistant phase level, whereupon the resultant values reach the weighting adder, at which point the aggregate of the signal's amplitude and phase values are summed and functionally converted in accordance with expression (8.1). The output of the functional weighting adder provides a discrete distribution of the output effect $|Y(n\Delta t)|_{\Omega_i}$ for i frequency channels.

Should there be a need for further noncoherent processing, the signals from each frequency output are subjected to additional processing of the form (8.2) in i parallel channels. In each channel the oscillation $|Y(n\Delta t|\Omega m_i$, incoming discretely in time, is quantized for amplitude, with the quantized values stored for the period of the noncoherent processing. This operation is accomplished by the amplitude quantizers and memory units, respectively (Fig. 8.1). Following this, the discrete values stored undergo a weighted processing in conformity with (8.2). From the output of the appropriate weighting adders the output effect $Y_H(n\Delta t)_{\Omega_i}$ reaches the resolver.

If there are a great number of amplitude and phase quantizing levels, the digital filtering device designed in accordance with the circuit arrangement presented in Fig. 8.1 will be quite

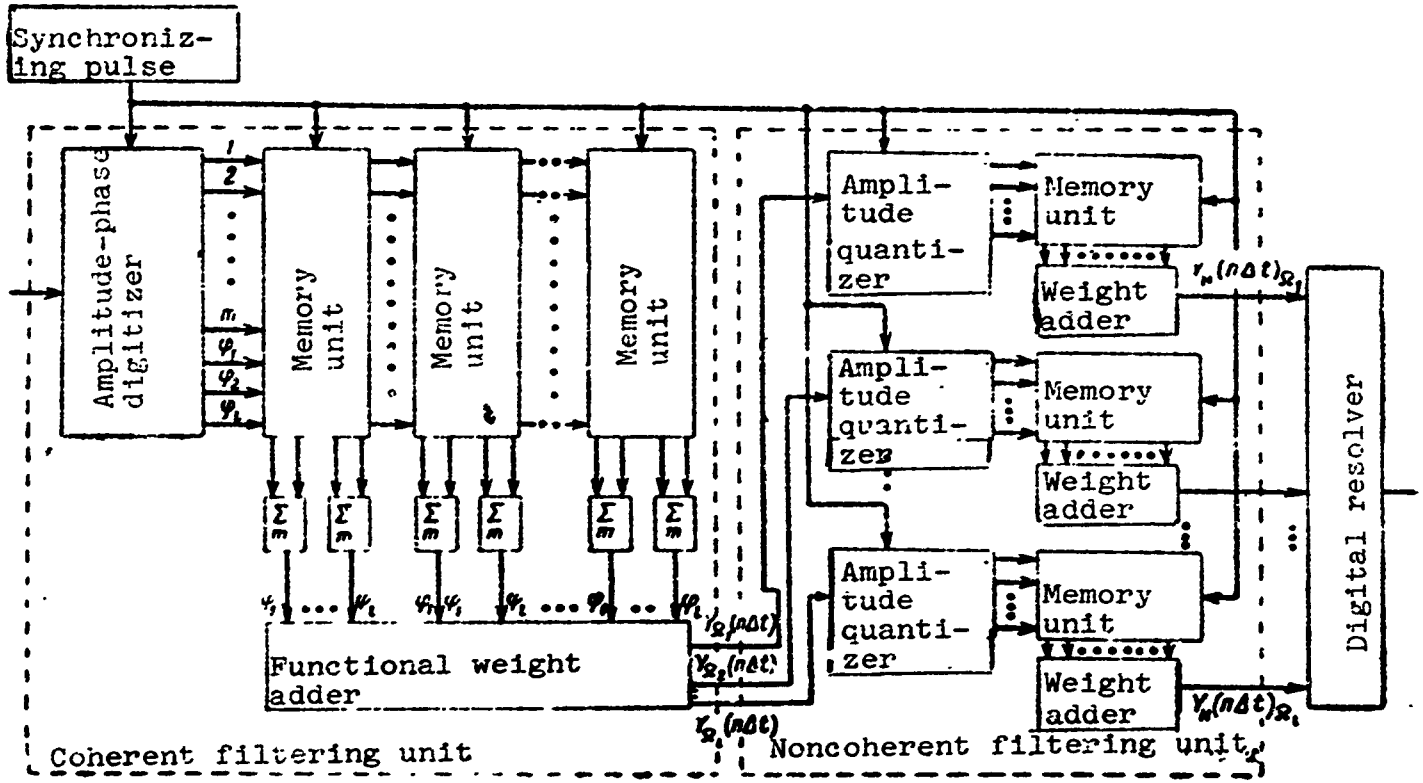

Fig. 8.1. Block diagram of a signal digital-processing channel.

complex. Because of this, in the practical design of digital systems for signal filtering and logical processing the aim is to keep the signal quantizing levels to an acceptable minimum. This permissible minimum value may be selected in accordance with the permissible degradation in detection, measurement, and resolution characteristics regarded as tolerable under given operating conditions.

When the interference is Gaussian in character and there is no signal overlap in time, the degradation in the characteristics of signal detection and parameter measurement as a function of the number of amplitude quantizing levels is relatively minor. For the limiting case of binary amplitude quantizing (rigid limitation) the energy losses amount to some 1-2 dB (Sections 3.4, 4.2). The dependence of energy losses on the number of phase quantizing levels in this situation is more pronounced; the nature of this relationship has been revealed in [91]. Energy losses do not exceed 1-2 dB with phase quantizing over 4 to 8 levels.

If the signals do overlap in time and there is also present narrow-band or non-Gaussian interference, limiting the amplitude quantizing levels may lead to additional worsening in detection and measurement characteristics. To a significant extent the character and magnitude of this impairment is determined by the form of the signals and the nature of the noise, and must be analyzed for each specific situation on an individual basis. By assigning the permissible energy losses and resolution characteristic degradation, the designer can arrive at a definite miminum value for the amplitude and phase quantizing levels.

For the purpose of substantially simplifying the equipment in practical design assignments, a limit of two amplitude quantizing levels and four or eight phase levels is often selected. This approach results in the retention of satisfactory detection and measurement performance by digital signal-processing systems in

many situations of realistic importance. The block diagram of a digital signal-processing channel with binary amplitude quantification is shown in Fig. 8.2.

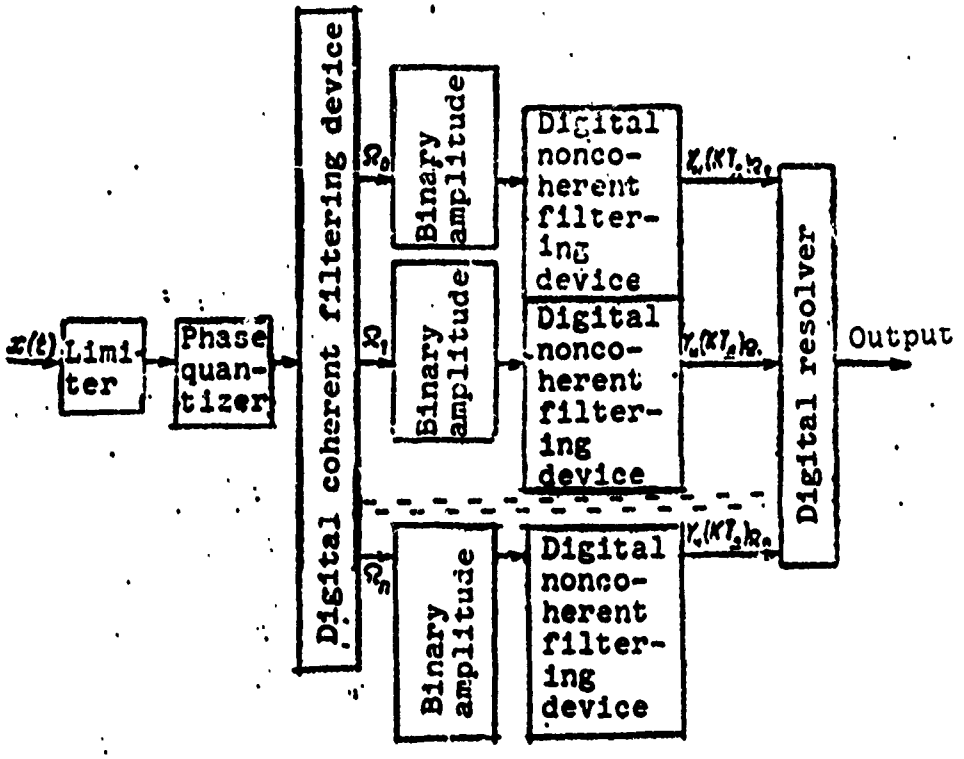

Fig. 8.2. Filtering and noncoherent processing channel for binary signal-amplitude quantification.

8.2. Digital Coherent Filtering Device with Binary Amplitude Quantification

For the purpose of arriving at a practical arrangement for a digital coherent filtering unit with binary amplitude quantification let us consider dependence (5.17).

With the input signal subject to binary amplitude quantification, its analytical expression $x_{бк}(t)$, according to (1.39), can be represented in the form

$$x_{бк}(t) = A_0 \cos [2\pi (f_0 - \nu) t + \varphi(t) + \varkappa_x(t) + \varphi_0]. \qquad (8.3)$$

[Translator's Note - The subscript letters "бк" stand for "binary quantification."]

Now, considering relations (5.17) and (8.3), we can write

$$\begin{aligned}
I_{cc}(\tau) &= \int_{-\infty}^{\infty} x_{бк}(t)_c A_c(t-\tau)\,dt = \frac{A_0}{2} \int_{-\infty}^{\infty} \cos [\theta(t)_v]\, A_c(t-\tau)\,dt;\\
I_{ss}(\tau) &= \int_{-\infty}^{\infty} x_{бк}(t)_s A_s(t-\tau)\,dt = \frac{A_0}{2} \int_{-\infty}^{\infty} \sin [\theta(t)_v] A_s(t-\tau)\,dt;\\
I_{cs}(\tau) &= \int_{-\infty}^{\infty} x_{бк}(t)_c A_s(t-\tau)\,dt = \frac{A_0}{2} \int_{-\infty}^{\infty} \cos [\theta(t)_v]\, A_s(t-\tau)\,dt;\\
I_{sc}(\tau) &= \int_{-\infty}^{\infty} x_{бк}(t)_s A_c(t-\tau)\,dt = \frac{A_0}{2} \int_{-\infty}^{\infty} \sin [\theta(t)_v]\, A_c(t-\tau)\,dt;
\end{aligned} \qquad (8.4)$$

where

$$\theta(t)_v = [\varphi(t) + \varkappa_x(t) + \varphi_0 - 2\pi\nu t].$$

Expressing the integrands by amplitude samplings recurring within an interval of $\Delta t = \frac{1}{\Delta F}$, in keeping with the theory of the discrete representation of a signal, and integrating, we can obtain

$$I_{cc}(n\Delta t)=\frac{A_0}{\Delta F}\sum_{i=1}^{N}\cos[\theta_t(t_i)_v]A_c(t_i-n\Delta t);$$

$$I_{ss}(n\Delta t)=\frac{A_0}{\Delta F}\sum_{i=1}^{i=N}\sin[\theta_t(t_i)]A_s(t_i-n\Delta t);$$

$$I_{cs}(n\Delta t)=\frac{A_0}{\Delta F}\sum_{i=1}^{i=N}\cos[\theta_t(t_i)_v]A_s(t_i-n\Delta t); \qquad (8.5)$$

$$I_{sc}(n\Delta t)=\frac{A_0}{\Delta F}\sum_{i=1}^{i=N}\sin[\theta_t(t_i)_v]A_c(t_i-n\Delta t);$$

where $\theta_t(t_i)$ is the discrete value of the phase (l quantification levels) at the moment of time t_i;

$N = \frac{\Delta T}{\Delta t}$ is the number of samplings for the duration of the signal.

A block diagram of a system permitting the implementation of signal processing in accordance with expressions (5.18) and (8.5), as shown in [41], can be represented in the form shown in Fig. 8.3.

By means of the limiter the input oscillation x(t) is subjected to binary quantification in amplitude and reaches two quadrature channels, in each of which, by means of a phase detector, it is multiplied by a harmonic reference oscillation of fixed frequency f_0. Following this multiplication, the phase-detector output will yield a signal whose form, with accuracy to within a constant factor, is determined for the cosine and sine channels, respectively, by the relation

$$x_{6x}(t)_c=\cos[\theta(t)],$$
$$x_{6x}(t)_s=\sin[\theta(t)]. \qquad (8.6)$$

By means of the digitizer and amplitude quantizer, these oscillations are converted into a sequence of zeros and ones

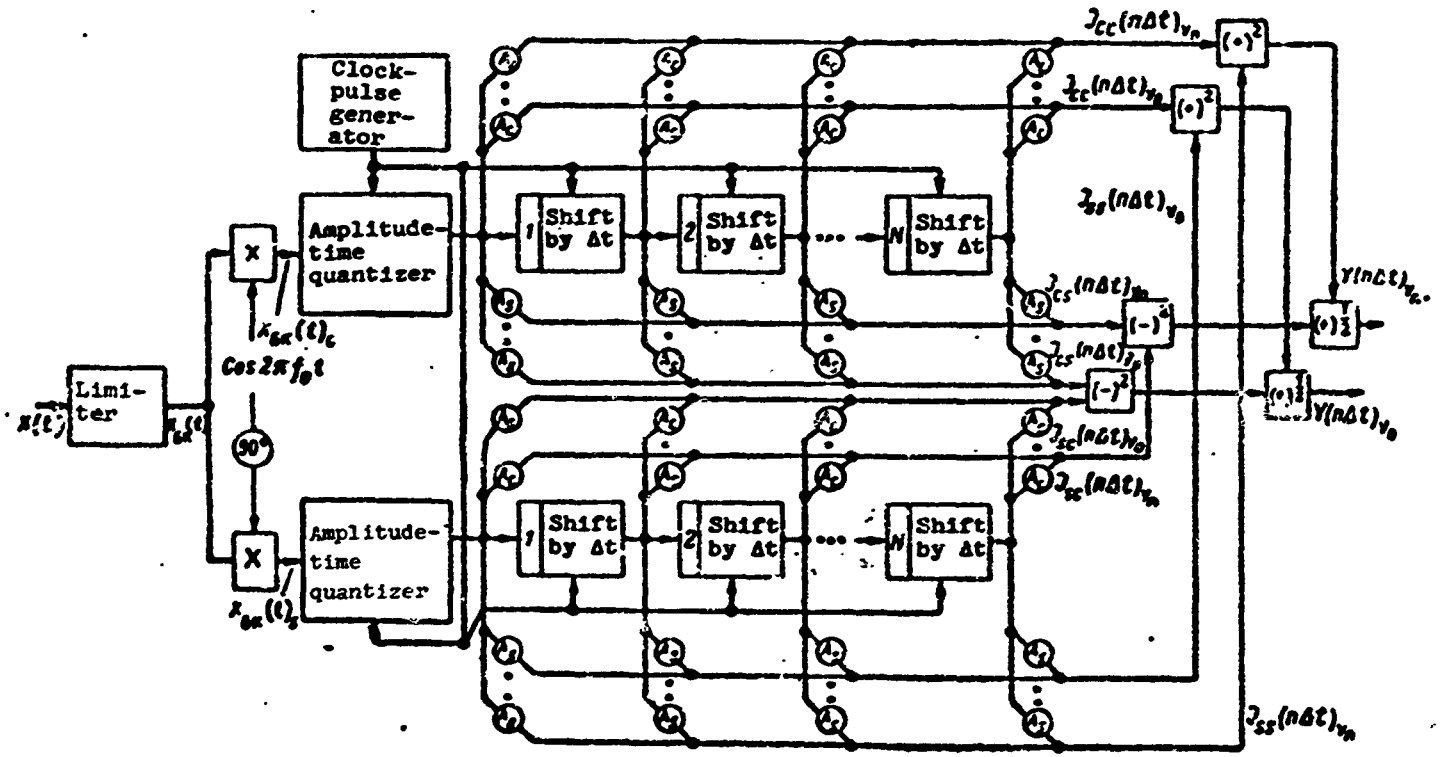

Fig. 8.3. Block diagram of a digital coherent filtering device with binary amplitude quantification.

occurring at time intervals of Δt which represent, in the symbols of a binary p-place positional encoding system, the oscillation amplitudes $x_{бк}(t)_{c,s}$. Figure 8.4 presents graphs illustrating the four-level quantification of the oscillation amplitudes $x_{бк}(t)_{c,s}$, corresponding to eight-level quantification of the input-signal phase. We shall designate this set of code sequences for p positions, describing in discrete form the amplitude of the oscillation $x_{бк}(t)_{c,s}$, as

$$x_{бк}(t)_c \to \left\{ \sum_{n=-\infty}^{n=+\infty} 1_c(n\Delta t) \right\}_p,$$

$$x_{бк}(t)_s \to \left\{ \sum_{n=-\infty}^{n=+\infty} 1_s(n\Delta t) \right\}_p. \qquad (8.7)$$

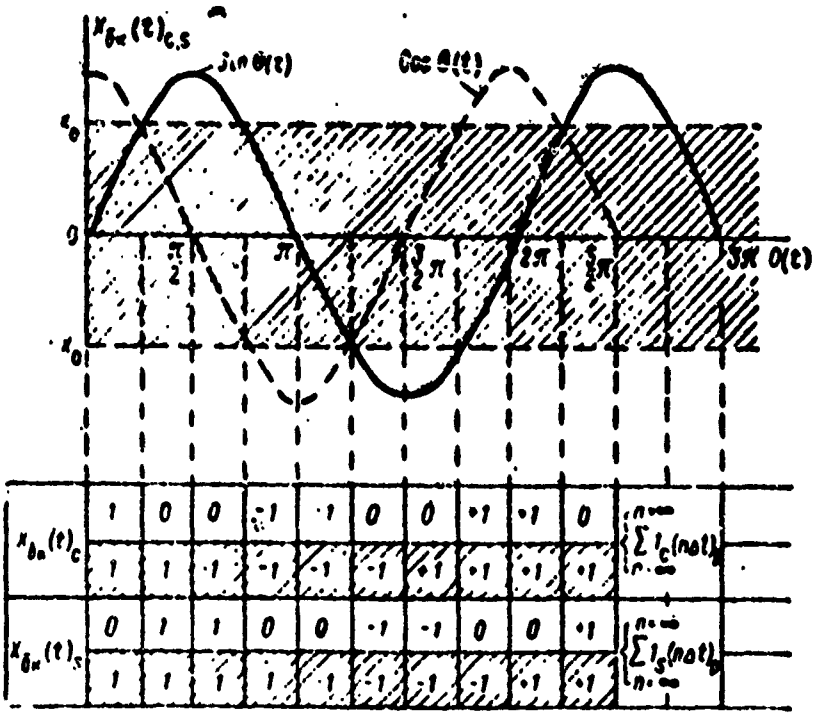

Fig. 8.4. Quantification of an amplitude-limited signal.

These code sequences (8.7) reach the appropriate shift-registers, which produce a time delay of the sequences. The weighted summing of the code sequences from the output of N series-connected shift-register elements, each of which delays the sequence for a period Δt, yields an operation of the form

$$I(n\Delta t)=\sum_{i=1}^{i=N}\left\{\sum_{n=-\infty}^{n=+\infty}1(n\Delta t-i\Delta t)\right\}_{p}A_{0}(i\Delta t),$$

where $A_0(i\Delta t)$ is the weight factor of the i-th shift-register output.

With $A_0(i\Delta t) = A_{c,s}(N\Delta t-i\Delta t)$ and the substitution of the variable $n\Delta t-i\Delta t = t_i$ at the output of the shift-register adder in the appropriate quadrature channel, we have

$$I_{c.\frac{c}{s}}(n\Delta t)=\sum_{i=1}^{i=N}\left\{\sum_{i=-\infty}^{i=+\infty}1_{c}(t_{i})\right\}_{p}A_{\frac{c}{s}}(t_{i}-n\Delta t+N\Delta t),$$

$$I_{\frac{c}{s}}(n\Delta t)=\sum_{i=1}^{i=N}\left\{\sum_{i=-\infty}^{i=+\infty}1_{s}(t_{i})\right\}_{p}A_{\frac{c}{s}}(t_{i}-n\Delta t+N\Delta t). \qquad (8.8)$$

From this last expression it is clear that the operation performed by the device pictured in Fig. 8.3, with accuracy to within the constant delay $N\Delta t$, corresponds to an operation of the kind (8.4), in which the analog values $\cos[\theta(t)_{\nu}]$ and $\sin[\theta(t)_{\nu}]$ have been replaced by the corresponding code sequences of zeros and ones.

The weighting function $A_{\frac{c}{s}}(i\Delta t)$ corresponds to the sampling value of the amplitude over time intervals $i\Delta t$ of the analog functions, which are the mirror functions with respect to $A_c(t-\tau)$ and $A_s(t-\tau)$ (5.18).

For the formation of the output effect $|Y_\nu(n\Delta t)|$, in accordance with expression (5.17), the signals from the appropriate adders are summed and functionally converted.

In actual practice, with a view to simplifying the equipment, in many cases [41, 80] a limit of two quantification levels for the oscillation $x_{6н}(t)$ is imposed, while the phase is coded in conformity with the algorithm

$$1 > \begin{matrix}\cos\\ \sin\end{matrix} [\theta(t)_\nu] \geqslant 0 \rightarrow x_{6н}(t)_{\frac{c}{s}} = 1,$$
$$-1 < \begin{matrix}\cos\\ \sin\end{matrix} [\theta(t)_\nu] < 0 \rightarrow x_{6н}(t)_{\frac{c}{s}} = 0. \qquad (8.9)$$

Now, at the quantizer output of each quadrature channel, single sequences of zeros and ones $\sum_{l=-\infty}^{l=+\infty} 1_0(t_l)$, $\sum_{l=-\infty}^{l=+\infty} 1_0(t_l)$ will occur. These sequences can be delayed by means of a simple single-channel shift-register.

For situation (8.9), the phase $\theta(t)_\nu$ in each quadrature channel is quantified over four levels in conformity with Table 8.1.

For signals having a rectangular envelope without phase modulation (2.33) the following equalities are fulfilled:

$$A(t-\tau)=1,$$
$$\varphi(t-\tau)=0.$$

Now, for such signals with phase quantification over four levels dependence (8.8) is transformed to the expression

$$I_{c,\frac{c}{s}}(n\Delta t)=\sum_{i=1}^{i=N} 1_c(t_i)\begin{matrix}\cos\\ \sin\end{matrix}[2\pi\nu(t_i-n\Delta t+N\Delta t)],$$

$$I_{s,\frac{c}{s}}(n\Delta t)=\sum_{i=1}^{i=N} 1_s(t_i)\begin{matrix}\cos\\ \sin\end{matrix}[2\pi\nu(t_i-n\Delta t+N\Delta t)]. \qquad (8.10)$$

Table 8.1.

Phase value interval	Attributed phase value	cos θ(t)	Phase code	sin θ(t)	Phase code
$0\div\frac{\pi}{2}$	$\frac{\pi}{4}$	$\frac{\sqrt{2}}{2}$	1	$\frac{\sqrt{2}}{2}$	1
$\frac{\pi}{2}\div\pi$	$\frac{3}{4}\pi$	$-\frac{\sqrt{2}}{2}$	0	$\frac{\sqrt{2}}{2}$	1
$\pi\div\frac{3}{4}\pi$	$\frac{5}{4}\pi$	$-\frac{\sqrt{2}}{2}$	0	$-\frac{\sqrt{2}}{2}$	0
$\frac{3}{4}\pi\div 2\pi$	$\frac{7}{4}\pi$	$\frac{\sqrt{2}}{2}$	1	$-\frac{\sqrt{2}}{2}$	0

For phase-keyed signals (2.45), when $\gamma = 0$, dependence (8.8) takes on the form

$$I_{c,\frac{c}{s}}(n\Delta t)=\sum_{i=1}^{i=N} 1_c(t_i)\,g(t_i-n\Delta t+N\Delta t),$$

$$I_{s,\frac{c}{s}}(n\Delta t)=\sum_{i=1}^{i=N} 1_s(t_i)\,g(t_i-n\Delta t)+N\Delta t). \qquad (8.11)$$

In conformity with expressions (8.10) and (8.11), the block diagram given in Fig. 8.3 may be used for the synthesis of the structural circuitry of a digital filter for narrow-band (2.33) and phase-keyed (2.45) signals.

8.3. Detection Characteristic and Measurement Accuracy of Systems Employing a Digital Filter with Binary Amplitude Quantification

As already indicated above, the quantification of the input-oscillation parameters in the digital filter causes some degradation in the detection and measurement characteristics of signal-processing systems. When the number of phase quantification levels for the input signal is large, the effect of phase quantification on the deterioration of detection and measurement performance, given average measurement accuracy, can be disregarded. The energy losses in this event will be determined solely by the amplitude quantification parameters and, in the case of binary quantification, may be estimated from the characteristics obtained for systems with rigid amplitude limiting (Sections 3.4, 4.2).

When the number of phase quantification levels is held to a relatively small value, the influence of such phase digitizing on the detection and measurement characteristics cannot be disregarded, and in this case the resultant energy losses must be determined with allowance for this factor.

For the energy losses with consideration of the phase quantification, the statistical characteristics of the output effect parameters must be expressed by random quantities which reflect the quantizing process.

The phase of the input oscillation in the digitizer shown in Fig. 8.3 is quantized over l levels, that is, it takes on one of l values depending on its magnitude at the moment t_i (Fig. 8.5). To the quantized value of the phase $\theta_l(t_i)$ we can assign the value

$$\theta_l(t_i) = \frac{\pi}{l}(2m-1), \quad \text{if} \quad \frac{2\pi}{l}(m-1) < \theta(t_i) < \frac{2\pi}{l}m, \text{ where } m = 1,2,3,\ldots,l.$$

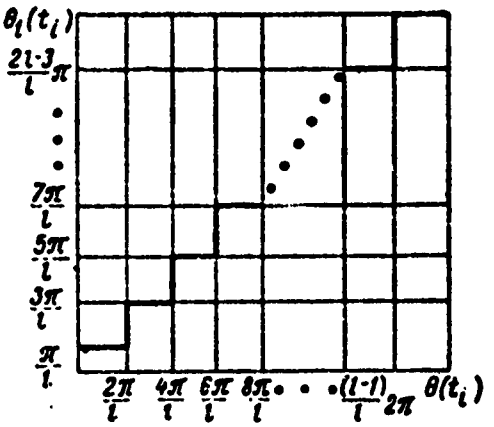

Fig. 8.5. Phase quantification graph.

As follows from dependence (8.5), the output effect of a digital filter with binary amplitude quantification is a function of the discrete random variable $\theta_l(t)$, the probability of which for level l at moment t_i is expressed as

$$P_{il} = \int_{\frac{2\pi}{l}(m-1)-\gamma(t_i)}^{\frac{2\pi}{l}m-\gamma(t_i)} P[\varkappa_x(t_i)]\, d\varkappa_x(t_i), \qquad (8.12)$$

where $P[\kappa_x(t_i)]$ is the distribution density of the continuous phase $\kappa_x(t_i)$,

$$\gamma(t_i) = \varphi(t_i) - 2\pi\nu t_i + \varphi_0.$$

The solution of relations (8.12) for an output effect with statistical characteristics of this kind, for the general case of signal and noise parameters, leads to complex analytical formulas which are normally solved only by means of an electronic digital computer.

However, whenever the input signal frequency band is large, $\Delta t << T_{эф}$, that is, when condition (3.38) is satisfied and the signal/noise ratio at the input of the digital filter is low

(3.43), the energy losses due to phase quantification can then be estimated using relatively simple analytical expressions [91]. In fact, with the fulfillment of condition (3.43), the distribution density of the phase $\kappa_x(t_i)$, as has been shown [78], is defined by the relation

$$P[\varkappa_x(t_i)] = \frac{1}{2\pi} + \frac{q_i \cos \varkappa_x(t_i)}{2\sqrt{2\pi}}. \tag{8.13}$$

With allowance for expressions (8.12) and (8.13), the probability P_{zi} will be

$$P_{ii} = \int_{\frac{2\pi}{l}(m-1)-\gamma(t_i)}^{\frac{2\pi}{l}m-\gamma(t_i)} \left[\frac{1}{2\pi} + \frac{q_i \cos \varkappa_x(t_i)}{2\sqrt{2\pi}}\right] d\varkappa_x(t_i) =$$

$$= \frac{1}{l} + \frac{\sin\frac{\pi}{l}}{\sqrt{2\pi}} q_i \cos \varkappa_x(t_i). \tag{8.14}$$

Since within the interval of a single discrete increment the phase distribution may be taken as approximately uniform, the equivalent phase probability-density $\theta_z(t_i)$ in the intervals $\frac{2\pi}{l}(m-1) \div \frac{2\pi}{l} m$ may be assumed equal to

$$P[\theta_i(t_i)] = \frac{1}{2\pi} + q_{i\,экв} \cos[\theta_i(t_i) - \gamma(t_i)]. \tag{8.15}$$

where

$$q_{i\,экв} = \frac{\sin \pi/l}{2\sqrt{2\pi}\,\pi/l} q_i.$$

From equation (8.15) it will be evident that, when the signal/noise ratio is low, the law of the phase distribution density does not change as the phase is quantized. The

quantification of the phase results merely in a decrease of the equivalent signal/noise ratio. Therefore, for the case in question those relations, derived in Sections 3.4 and 4.2 for the determination of the detection characteristics and measurement accuracy, in which the only change concerns the substitution of $q_{i\ эив}$ for $q_{огр}$ as the parameter value, will apply. The resultant energy losses in this situation, with allowance for the phase quantification, have been cited in the graph shown in Fig. 8.6.

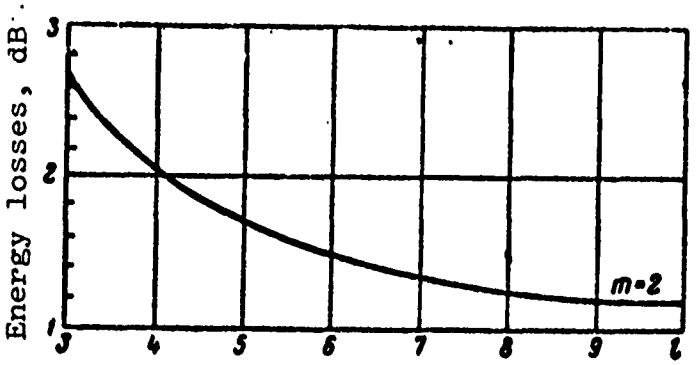

Fig. 8.6. Phase quantification loss graph.

This reasoning is also valid with respect to the resolving power of such digital filters. It is to be noted, however, that the time quantification of the input oscillation presupposes that the level of its spectral components is negligibly small outside the frequency band ΔF. This circumstance calls for band filtration in the ΔF frequency interval of the signal reaching the digital-filter input. Provided the frequency response of the band filter displays good rectangularity, this requirement can be satisfactorily met. If the frequency characteristic shows a bell-shaped waveform, the ΔF value will for all practical purposes match the filter frequency band as read on the 0.1 level and below.

In the event that condition (3.43) is not satisfied, the relations defining the detection characteristics and the accuracy of measurement take on considerable added complexity and become parametric in character [91]. As a consequence, the energy-loss

evaluation for a high signal/noise ratio is accomplished using numerical methods.

With a high signal/noise ratio there is a disruption in the quasilinearity of the digital devices with binary amplitude quantification, resulting in degraded resolution of time-overlapping signals. Quantitative formulas describing detection-performance and measurement-accuracy indicators with mutually overlapping signals and binary amplitude quantification for coherent processing turn out to be rather complicated, for which reason we shall restrict ourselves at this point to the qualitative aspect of the problem alone. For the sake of simplicity we shall assume a sufficiently large signal/noise ratio permitting the disregarding of the noise component in the input oscillation, while also considering that there is total overlapping in the signal envelopes. The oscillation at the filter-unit input, in this case, in the presence of two signals, can be expressed in the form

$$\begin{aligned} x(t) &= A_1(t)\cos[\omega_0 t + \varphi_1(t) + \varphi_{01}] + \\ &+ A_2(t)\cos[(\omega_0 + \Omega_0)(t-\tau) + \\ &+ \varphi_1(t-\tau) + \varphi_{02}] = A_1(t)\cos[\beta_1(t)] + A_2(t)\cos[\beta_2(t)] = \\ &= A_1(t)\cos[\beta_1(t)] + A_2(t)\cos[\beta_1(t) + \beta_0(t)], \end{aligned} \tag{8.16}$$

where

$$\beta_0(t) = \beta_2(t) - \beta_1(t).$$

By analogy with (1.39), we represent the oscillation (8.16) as

$$x(t) = A_\Sigma(t)\cos[\beta_1(t) + \theta_\Sigma(t)], \tag{8.17}$$

where

$$A_{\Sigma}(t) = \sqrt{\{A_1(t) + A_2(t)\cos[\beta_0(t)]\}^2 + A_2^2(t)\sin^2[\beta_0(t)]};$$

$$\theta_{\Sigma}(t) = \operatorname{arctg}\frac{(A_2(t)/A_1(t))\sin[\beta_0(t)]}{1 + (A_2(t)/A_1(t))\cos[\beta_0(t)]}.$$

After limitation, oscillation (8.17), conformably with (3.33), acquires the form

$$x_{orp}(t) = A_0\cos[\beta_1(t) + \theta_{\Sigma}(t)]. \tag{8.18}$$

When $[A_2(t)/A_1(t)] << 1$, relation (8.18) is transformed [24] to the expression

$$x_{orp}(t) = A_0\left\{\cos[\beta_1(t)] + \frac{A_2(t)}{2A_1(t)}\cos[\beta_2(t)] - \right.$$
$$\left. - \frac{A_2(t)}{2A_1(t)}\cos[2\beta_1(t) - \beta_2(t)]\right\}. \tag{8.19}$$

A comparison of expression (8.19) with expression (8.16) will reveal that the oscillation is somewhat modified following limitation. There has been a two-fold deterioration in the amplitude ratio of the weak signal to the strong - that is, the nonlinear conversion has resulted in a 6-dB suppression of the weak signal. A spurious signal has appeared in the oscillation, the amplitude of which is comparable with that of the weak signal.

Depending on the form of the input signals, the structure of this spurious signal will differ. For example, in the case of narrow-band signals of form (2.33), for which $\phi_1(t) = 0$, $\phi_2(t) = 0$ and which have different Doppler frequencies $\beta_1(t) = (\omega_0 t + \phi_{01})$, $\beta_2(t) = \omega_0 t + \Omega_0 t + \phi_{02} + (\omega_0 + \Omega_0)\tau$, the structure of the spurious signal $\nu_м(t)$ will be determined from (8.19) by the dependence

$$v_M(t) = \frac{A_2(t)}{2A_1(t)} \cos[(\omega_0 - \Omega_0)t + \varphi_M], \qquad (8.20)$$

where ϕ_M is the constant phase shift: $\phi_M = \phi_{02} + (\omega_0 + (\omega_0 + \Omega_0)\tau$.

As is clear from expression (8.20), the spurious signal retains the structure of the input signals and has a frequency which mirrors the frequency $\omega_8 + \Omega_0$. Therefore, at the filter-device output there will be present, together with the central peaks in the output effect caused by the useful signals, a peak occasioned by the spurious signal. This has been schematically represented in Fig. 8.7.

For signals with linear frequency modulation (2.37) having an identical Doppler frequency shift but delayed with respect to each other by $\Delta\tau$,

$$\beta_1(t) = \omega_0 t + \frac{2\pi F_m}{\Delta T} t^2,$$

$$\beta_2 = \omega_0(t - \Delta\tau) + \frac{2\pi F_m}{\Delta T}(t - \Delta\tau)^2 + \varphi_{02}.$$

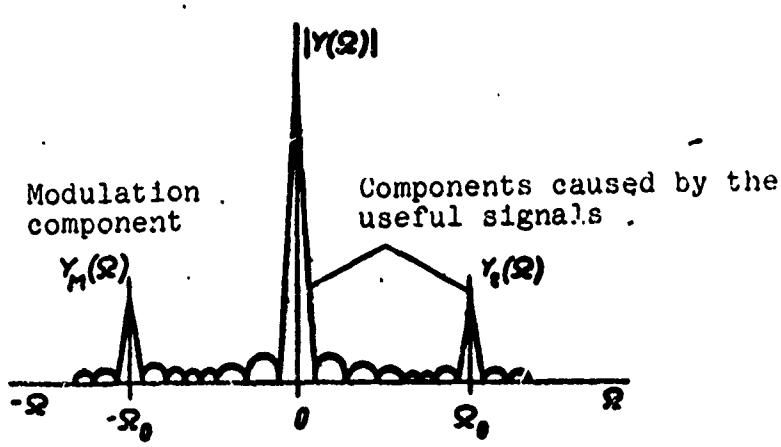

Fig. 8.7. Schematic representation of the output effect of a digital filtering unit in the presence of two overlapping signals.

Thus, the structure of the spurious signal will appear as

$$v_м(t)=\frac{A_2(t)}{2A_1(t)}\cos\left[\omega_0 t+\Delta\omega t+\frac{2\pi F_m}{\Delta T}t^2-\varphi_{м1}\right], \qquad (8.21)$$

where

$$\Delta\omega=\frac{4\pi F_m}{\Delta T}\Delta\tau; \quad \varphi_{м1}=\varphi_{02}+\frac{2\pi F_m}{\Delta T}\Delta\tau^2-\omega_0\tau.$$

It will be seen from expression (8.21) that the structure of the spurious signal corresponds to the input signal; however, the signal $v_м(t)$ exhibits a frequency shift $\Delta\omega$ with respect to the strong signal. At the filter-system output this leads to a time shift in the peak of the spurious signal relative to the peak of the strong signal. Following (4.13), this time shift will equal $\Delta\tau \approx \Delta T\Delta\omega/2F_m$, for which reason the peak of the spurious signal will lead in time the maximum value of the strong signal by the amount $\Delta\tau$. The filter-circuit output effect in this case will show a form similar to that represented in Fig. 8.7, with the sole difference that the parameter τ will correspond to the parameter Ω and the parameter $\Delta\tau$ to the parameter Ω_0.

In the case of phase-keyed signals (2.[illegible]) having an identical Doppler shift but mutually delayed by the value $\Delta\tau$ we shall have

$$\beta_1(t)=\omega_0 t+\frac{\pi}{2}1_n(t-iT_д, T_д)(g_i+1),$$

$$\beta_2(t)=\omega_0(t-\Delta\tau)+\frac{\pi}{2}1_n[\tau-(i+k)T_д, T_д](g_{i+k}+1)+\varphi_{02}.$$

Here, according to (7.46) and (8.19), the spurious signal will be defined by the relation

$$v_м(t)=\frac{A_2(t)}{2A_1(t)}\sum_{i=0}^{i=N-1}\cos\{\omega_0 t+\pi 1_n(t-iT_д, T_д)\times$$

$$\times(g_i+1)-\frac{\pi}{2}1_n|t-(i+k)T_д, T_д|(g_{i+k}+1)-\varphi_{м2}\Big\}=$$

$$=\frac{A_2(t)}{2A_1(t)}\sum_{i=0}^{i=N-1}\cos\Big\{\omega_0 t+\frac{\pi}{2}1_n|t-(i+$$

$$+k)T_д, T_д|(g_{i+k}+1)-\varphi_{м2}\Big\}, \qquad (8.22)$$

where $\phi_{м2} = \phi_{02} + \omega_0\Delta\tau$.

From this last expression it follows that the spurious signal totally matches the weak signal in structure, but that, unlike this weak signal, it has a different initial phase, which depends on the relative delay between the input signals and on the difference in their initial phases. As a consequence, the effect of the spurious signal in this case will be reflected only in the severe fluctuation of the amplitude of the weak signal as the value $\Delta\tau$ changes. On the other hand, with phase-keyed signals there will be no appearance of additional peaks in the output effect, as in the case of narrow-band or frequency-modulated signals.

In this way, then, binary quantifying of the input oscillation in a digital filter often results, in the case of severely overlapping and intensive signals, in the emergence of false peaks in the filter-unit output oscillation. As the time overlap between the input signals decreases and their amplitudes are equalized, these effects will abate; however, even in this case they must be taken into account in any determination of the detection and measurement characteristics of systems with digital filters.

8.4. Elements of the Coherent Digital Filter

A digital coherent filtering device may be designed using the standard elements of digital engineering. To a considerable degree the parameters of these elements determine the resultant characteristics of the device.

The key element of the digital coherent filter is the phase discriminator, which is responsible for the conversion of the phase characteristics of the oscillation to be filtered into a pulse code. The methods used in the design of the phase discriminator are similar to those underlying the creation of various digital phase meters and time-interval meters. Among the more important of these techniques mention might be made of the method of quantizing the amplitude of the signals at the output of the sine and cosine channel detector (as, for example, in Fig. 8.4), as well as the method of reading the moments when a harmonic oscillation passes through zero relative to a certain pulse reference train [62].

In the last-mentioned case, a measurement is made of the time intervals τ_0 between the moments of zero transition by the input oscillation and the time-reference pulses shaped from a reference signal (Fig. 8.9). The value τ_0 here describes the phase of the input oscillation [62] with respect to the reading moment t_1. The cosine or sine value of this phase can be obtained through the appropriate nonlinear conversion.

By way of example, Fig. 8.8 shows one of the possible practical circuit arrangements which will implement this method. By means of limitation and differentiation, the zero-pulse shaping circuit forms from the input oscillation a pulse train u_0 (Fig. 8.9). This pulse sequence reaches the inputs of trigger circuits (flip-flops) which shape pulses of duration equal to the time interval τ_0 to be measured. Depending on the value of the phase shift relative to the reading moment, different pulse trains u_- or u_+ are shaped, this being accomplished by virtue of the different polarity of the u_0 pulses and the reset pulses. When pulses of both polarities occur within the reading interval - for example, 0 - t_1 - the positive pulses are automatically erased by the negative signals from the negative-pulse discrimination circuit. The pulses u_- and u_+ reach the coincidence stages, to whose second inputs is fed the pulse sequence u_{c4}. Counters 1 and

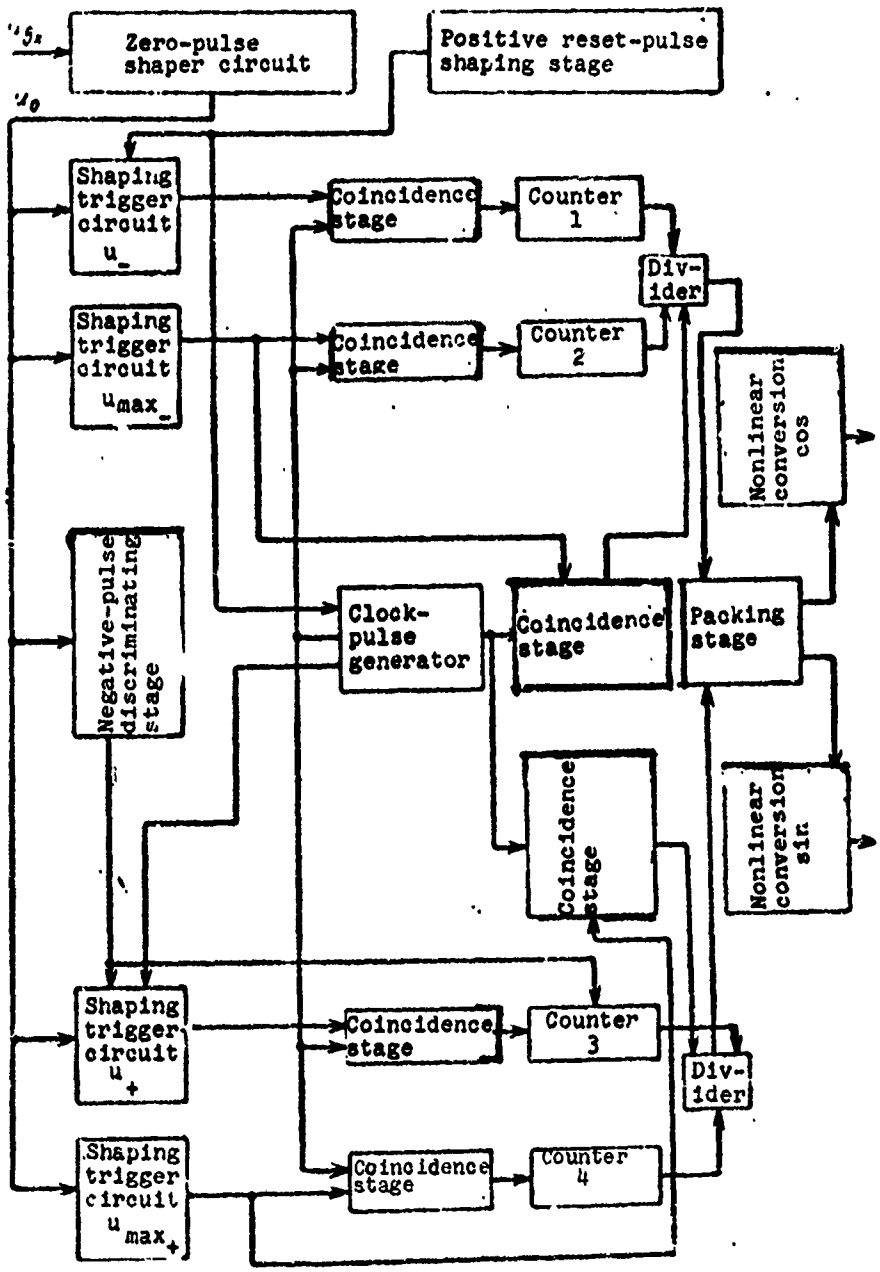

Fig. 8.8. Block diagram of a phase meter operating according to the "zero" reference method.

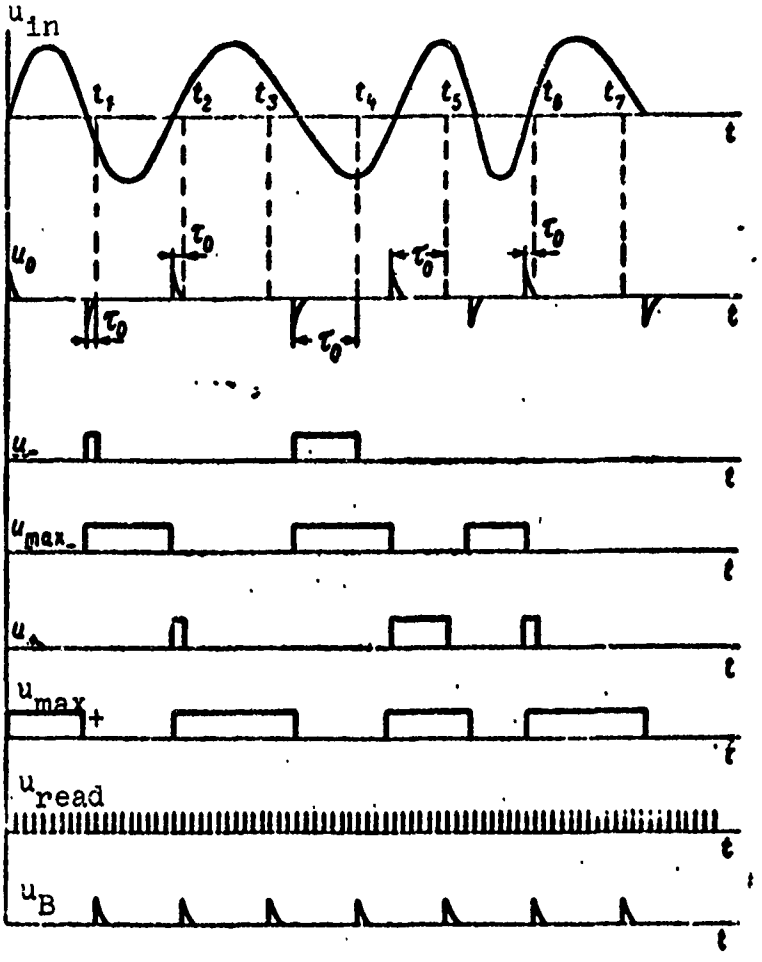

Fig. 8.9. Signal diagrams for the "zero"-reading phase meter.

3 count the number of pulses, which is proportional to the duration of the intervals τ_0. For normalization of the measured value τ_0, the derived result is divided in the divider by a quantity corresponding to the real-time input-oscillation period; this period is measured by counters 2 and 4. From the divider the information regarding the phase of the input signal is extracted at moments of time corresponding to the presence of pulses $u_в$. This information reaches the combination packing stage. Following this, the cosine and sine values of the measured phase can be obtained by the nonlinear conversion circuits. The discrete element in the phase measurement in Fig. 8.8 is determined by the period u_{c4} and can be made quite small.

The key parameters of the phase discriminator are its response speed and the accuracy with which the discrete value of the phase can be read in the dynamic amplitude range of the input oscillation. These two parameters are closely interrelated inasmuch as the reading accuracy of the discriminator declines as its response speed rises.

In the case of detection and coarse-measurement systems, because of their limited sensitivity to the value of the discrete phase step (Section 8.3), considerable errors are permissible in the quantification of the phase. For example, phase-reading errors corresponding to an angle of 25° result in such systems in additional energy losses of no more than 0.2 dB.

For fine-measurement systems the phase-reading requirements are far more stringent so that in this case the design principles of the phase quantifier and its circuit parameters must be selected in strict accordance with the permissible errors.

The shift-register of the digital filter may be designed with a variety of discrete memory elements working at the required operational rates. In most instances, these elements will take the form of different types of flip-flop circuits, capacitive storage cells, and magnetic matrixes [80].

The weighted summing operation at the shift-register output is accomplished by a weighting adder, which may be based on the analog or digital principle. The analog weighting adder is in fact a resistive or capacitive linear matrix which performs the weighted adding of the pulsed voltages directly from the appropriate shift-register outputs - for example, as shown in Fig. 8.4. A block diagram of the digital adder is shown in Fig. 8.10. The pulses from the output of the shift-register memory elements open the appropriate coincidence stages, to the secondary inputs of which are delivered the weight code sequences. Once they have passed through these coincidence stages, the codes are summed in the common adder, resulting in the execution of operation (8.8).

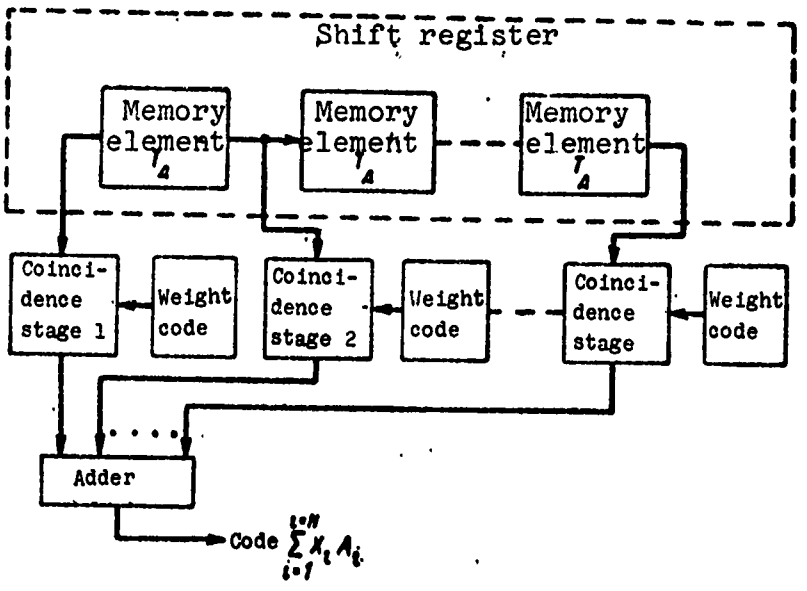

Fig. 8.10. Block diagram of digital adder.

The code-summing operation represented in Fig. 8.10 must be carried out during the time interval $T_д$. This requires that the digital adding circuit operate at a fast rate or else that it be designed according to the multichannel principle.

The accuracy and stability of an analog weighting adder is determined by the accuracy and stability of the matrix branches as well as by the accuracy and stability of the output pulses, of current or voltage, from the shift-register memory elements. The accuracy of the digital adder is a function of the number of places in the weighting code. The number of digital positions in a binary code describing with relative error the required analog value will be defined, according to expression (5.49), by the formula

$$p = \log_2\left(\frac{100}{2\delta_{доп}} + 1\right), \tag{8.23}$$

where $\delta_{доп}$ is the permissible relative conversion error expressed as a percentage.

Weighted-adding distortion in the digital coherent filter results in its frequency characteristics being mismatched with respect to the signal, with this giving rise to additional energy losses and possibly causing a deterioration in the resolving power of the device.

Functional adders designed to perform summing and squaring operations may also be based on analog or digital circuitries. In the first instance, various semiconductor devices with square-law characteristics may be employed; in the second, functional digital transducers.

A point to be kept in mind is that all the component elements incorporated in the digital coherent filter are of comparatively simple design and can therefore be produced with a high degree of technological ease.

8.5. Digital Noncoherent Signal-Processing Device

Noncoherent signal processing following coherent filtration can be essentially resolved to operations of type (8.2). These operations can be accomplished by digital devices featuring multi-level signal amplitude quantification over each of the frequency channels, with their subsequent storage and weighted processing, as indicated in the block diagram of Fig. 8.1. Practically speaking, however, binary amplitude quantification is employed in most cases involving the use of digital noncoherent signal-processing methods. Although it is true that the transition to binary amplitude quantification does lead to corresponding energy losses, in most cases of real importance these losses are of relatively low magnitude - in the order of 1-1.5 dB [37, 43] - and may therefore be acceptable. The use of binary amplitude quantification makes possible significant simplification of the structural lay-out of the digital unit effecting the noncoherent processing of the signal.

One possible block diagram of such a system with binary amplitude quantification can be seen in Fig. 8.11. The system has i channels, each of which provides noncoherent processing of the signal from the output of a separate frequency channel in the coherent filtering unit. The amplitude quantizer provides two-level quantification of the amplitude of the input oscillation. An amplitude exceeding the threshold $u_{по}$ (Fig. 8.12a) is assigned a value of 1, with a zero (0) assigned to its below-threshold values. The sequence of zeros and ones with a time interval Δt (Fig. 8.12b), determined by the clock-pulse frequency, reaches the shift-register consisting of $M = T_{обр}/\Delta t$ memory elements, where $T_{обр}$ is the time of the noncoherent processing of the signal. From the shift-register output the delayed pulse sequence undergoes weighted adding in conformity with the algorithm (8.2):

$$Y_н(n\Delta t) = \sum_{k=1}^{k=M} 1_н(n\Delta t - kT_k) b_k. \qquad (8.24)$$

The pulse train $Y_н(n\Delta t)$ (Fig. 8.12c) reaches the threshold device where it is compared with the threshold $u_{по\ 1}$. If an excess is determined, $Y_н(n\Delta t) \geq u_{по\ 1}$, the resolving unit fixes the detection of the signal in the frequency channel in question. The corresponding detection pulses are shown in Fig. 8.12d. The best detection characteristics in a device of this kind are secured by setting optimum values for the first and second threshold $u_{по}$ and $u_{по\ 1}$. The methods for selecting the threshold values and analyzing the detection characteristics have been reviewed in [37, 43].

The time quantification interval Δt in noncoherent processing is selected on the basis of the purpose of the device.

When the signal is noncoherently processed merely for the purpose of its detection and the determination of the frequency channel number, the time quantification interval may be selected

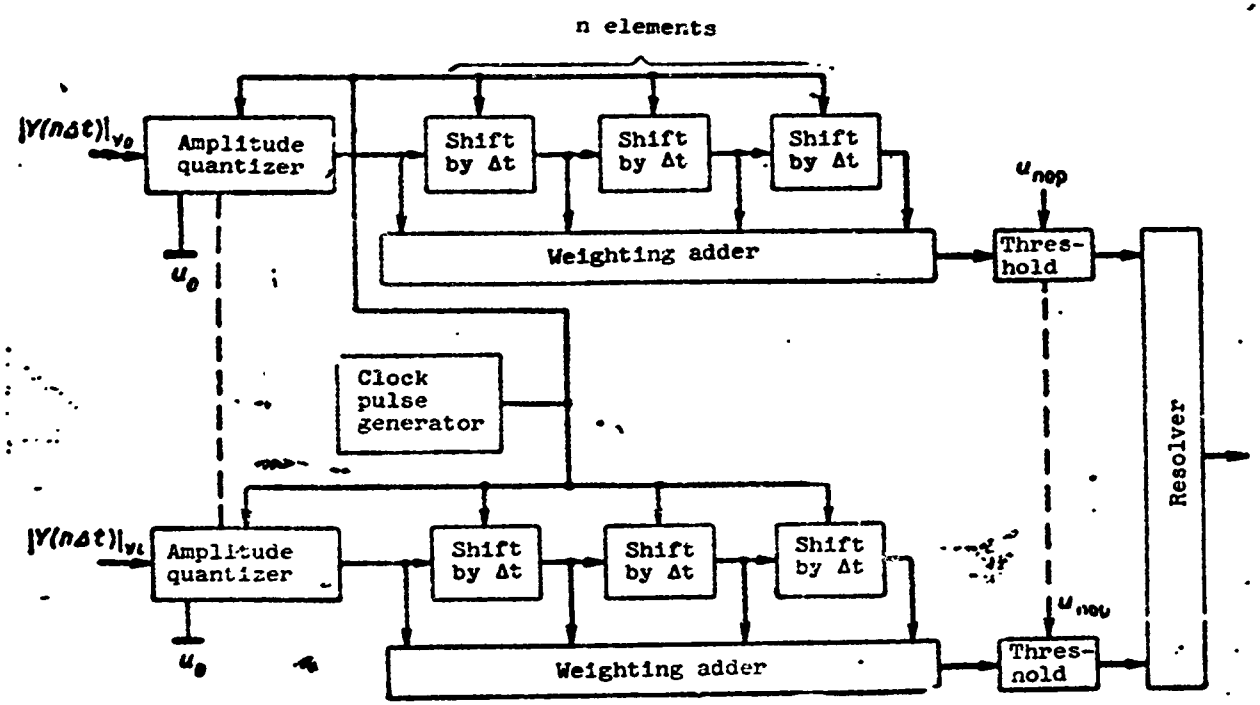

Fig. 8.11. Block diagram of digital noncoherent signal-processer with binary amplitude quantification.

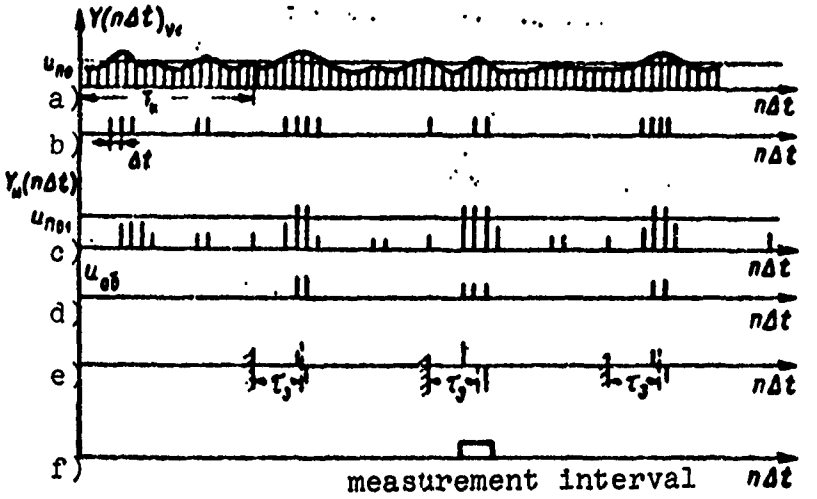

Fig. 8.12. Diagrams of signals in the digital noncoherent signal processor.

as equal to the correlation interval of the signal as it leaves the coherent filter circuit. On the other hand, in the measurement of signal delay time, when the task is one of high-accuracy measurement, the interval of time quantification must be taken in accordance with dependence (4.26):

$$\Delta t \leq \sigma_{\tau\,\text{min}}.$$

Following digital coherent filtration according to the diagram in Fig. 8.11, the signal delay time is measured by determining the center of the pulse burst obtained when the threshold u_{rol} is exceeded by the signal $Y(n\Delta t)$ (Fig. 8.12c, d, e). At this point, the maximum equipment error in the measurement will corespond to one-half the interval Δt; to ensure the least noise error, values are used which correspond to the moment of time when the signal/noise ratio is maximum. This moment is selected in Fig. 8.11 according to the greatest number of pulses exceeding the second threshold (Fig. 8.12f). If the value of Δt is small enough and the time interval for noncoherent signal processing large enough, the number of storage elements in the

shift-registers of each of the device's frequency channels (Fig. 8.11) becomes very sizable: $M = T_{обр}/\Delta t$.

To reduce the total number of storage elements in the noncoherent digital processor with binary amplitude quantification, when the number of useful signals is small, the method of the "independent" memory may be employed. With this approach, the number of memory elements is selected according to the number of probable instances involving crossing of the first threshold $u_{по}$ and equals the number of ones $1_n(n\Delta t)$. Since this number is considerably smaller than the value of n, a significant economy of storage elements is secured. The delay-time code of the pulses $1_n(n\Delta t)$ is recorded in each storage element, and from the output of these elements those pulses having close code values are added.

A possible configuration for this kind of noncoherent processor with the signals taken from a single frequency channel is shown in Fig. 8.13. The input oscillation $Y_н(n\Delta t)$ reaches the threshold circuit, where, similarly to Fig. 8.12b, it is converted into a series of unit pulses $1_n(n\Delta t)$ characterizing a crossing of the threshold. In the encoding circuit, to each pulse of this series there is assigned a code value corresponding to the delay time of the pulse. This time code is stored across recording (writing) selectors which successively unblock the free memory elements. These memory elements are periodically interrogated by a resolving device in which an analysis is made of the code values and where codes with close values are discriminated. The value describing the number of these codes is compared with the threshold. Signal detection is established when this value exceeds the threshold.

The method for designing these circuits and determining their characteristics is discussed in [59].

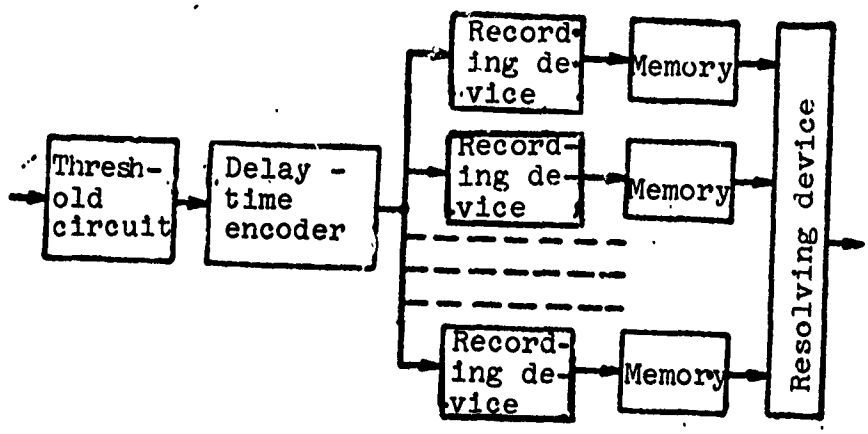

Fig. 8.13. Block diagram of immediate-access storage device.

9. OPTICAL FILTERS

9.1. General Description of Electron-Optical Signal Processors

Electron-optical devices constitute a relatively new engineering development trend in the area of signal filtration and processing. With respect to a great many parameters, the technical characteristics of electron-optical devices are superior to those of electronic equipment.

Specifically, as compared to purely electronic instrumentation, these devices afford considerably higher operating speed (broadbandedness), while making possible, in a relatively simple fashion, the multichannel and multifunctional processing of signals as well as the execution of a variety of two-dimensional operations on them. Optical filters provide rather a simple synthesis of virtually any required frequency-phase characteristic, which, should the need arise, can also be converted into any other. Electron-optical devices are employed at all stages in the signal-processing chain, including the filtering stage, the primary and

secondary processing stage, and the data-display stage.

Both analog and discrete electron-optical devices are used for these purposes [11, 19, 29, 46, 52, 64, 74]; however, the greatest opportunities for optical methods are to be found in the area of signal filtration and radar-information extraction, where they can be combined with comparatively simple systems to provide multichannel filtering of complex, high-information signals and to ensure the solution of a variety of multidimensional algorithms. As requirements increase with respect to the operating speed and multifunctionality of signal-processing systems, ever-greater importance attaches to the advantages of electron-optical devices for wider application in equipment of this kind.

9.2. Optical Signal-Filtration Methods

As follows from expression (5.2), the formation of a correlation function requires the execution of an operation of multiplication and integration. Both these operations can be easily performed in optics. For the multiplication operation there is employed the property involving the change in the amplitude and phase of light as it tranverses an optically inhomogeneous medium.

In the case of constant polarization, a light wave can be characterized by the electrical field-intensity component as defined in a system of coordinates (Fig. 9.1) in the form

$$S_{cв}(x, y) = A_{cв}(x, y) \exp[j\varphi_{cв}(x, y)] \exp[j\omega_{cв} t], \qquad (9.1)$$

where $A_{cв}(x, y)$ is the amplitude of the light wave;

$\omega_{cв}$ is the light frequency;

$\phi_{cв}(x, y)$ is the light-wave phase.

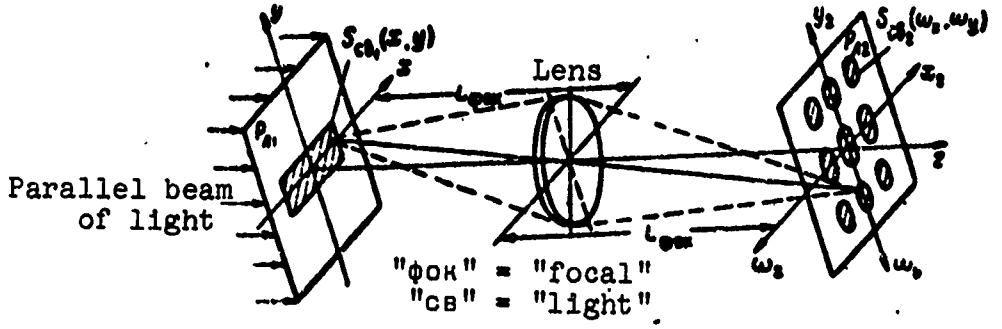

Fig. 9.1. Spatial conversion of light.

For coherent optical systems the factor exp $[\omega_{св} t]$ describing the instantaneous phase change can be dropped since for these systems the mutual phase relations of the light waves at different points in space are not time-dependent. The analytical expression for the light wave in this case assumes the form

$$S_{св}(x, y) = A_{св}(x, y) \exp [j\varphi_{св}(x, y)]. \qquad (9.2)$$

For a semi-transparent diapositive (transparency) attenuating the light intensity $a^2_{тр}(x, y)$ times ($0 < a_{тр} < 1$) and having an optical thickness of l_0, the light transmission characteristic will be expressed as

$$T(x, y) = a_{тр}(x, y) \exp [j a_{тр}(x, y)], \qquad (9.3)$$

where

$$a_{тр} = \frac{j 2\pi n_{пр} l_0}{\lambda_{св}};$$

$n_{пр}$ is the index of the refraction of the light by the transparency.

Having passed through a transparency with the transmission characteristic (9.3), the light wave (9.2) is modulated according to the expression

$$S_{св}(x, y)_1 = S_{св}(x, y)\,T(x, y) =$$
$$= A_{св}(x, y)\,a_{тр}(x, y)\exp\{j[\varphi_{св}(x, y) + a_{тр}(x, y)]\}. \qquad (9.4)$$

From this last expression it is clear that as a result of the passage of the light wave $S_{св}(x, y)$ through the optical transparency $T(x, y)$ there has been a multiplication of its optical characteristics. It follows from expression (9.4), in particular, that in the passage of a stream of light of constant amplitude $S_{св\ 0}$ through two superimposed transparencies having the characteristics $T_1(x, y)$ and $T_2(x, y)$ the distribution of the light $S_{св}(x, y)$ exiting from the transparencies will be determined by a product of the kind

$$S_{св}(x, y)_{вых} = S_{св\,0}T_1(x, y)\,T_2(x, y). \qquad (9.5)$$

The optical integration operation is accomplished by a lens. In effect, the light waves in the focal planes of a spherical lens (Fig. 9.1) are related by the dependence

$$S_{св}(\omega_x, \omega_y)_2 = \int_{-\infty}^{+\infty}\int S_{св}(x, y)_1 \exp[-j(\omega_x x + \omega_y y)]\,dx dy, \qquad (9.6)$$

where $\omega_x = -\frac{2\pi x_2}{\lambda_{св} L_{об}}$; $\omega_y = -\frac{2\pi y_2}{\lambda_{св} L_{об}}$ are spatial frequencies.

As is evident from expression (9.6), the light wave in the $P_{п2}$ plane is a two-dimensional Fourier transform of the distribution of the modulation function of the wave in the $P_{п1}$ plane. The integration of the light image of plane $P_{п1}$ will occur on the optical axis of the lens at point $\omega_x = 0$, $\omega_y = 0$.

In order that correlation operation (5.2) take place, the signal S(t) is recorded on the transparency $T_1(x)$ - in such a way, for example, that its transmittance in the interval $d_т$ changes according to the signal amplitude (Fig. 9.2). Now, if two such

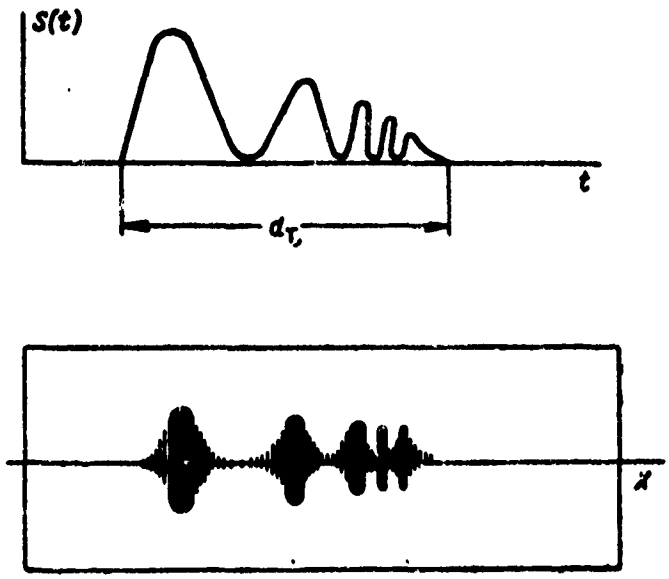

Fig. 9.2. Optical signal transparency.

transparencies are superimposed one on the other, shifted along the x axis by the amount x_0, and placed in the forward focal plane $P_{л1}$ of the lens (Fig. 9.1), then, when they are illuminated by coherent light $S_{св\ 0}$ there will be formed on the optical axis of the lens in the $P_{л2}$ plane a light wave whose amplitude $S_{св2}$ will be described by the expression

$$S_{св2}(x_0) = S_{св0} \int_0^{d_T} T_1(x) \cdot T_1(x - x_0)\, dx. \tag{9.7}$$

This operation may also be accomplished with the use of noncoherent light; in this case, however, at point $\omega_x = 0$, $\omega_y = 0$ of plane $P_{л2}$ there will be an addition of the intensity of the light propagating on plane $P_{л1}$, that is, the accomplishment of operation

$$S_{св2}(x_0) = S'_{св\,0} \int_0^{d_T} T_1^2(x) T_1^2(x - x_0)\, dx. \tag{9.8}$$

Thus, with noncoherent illumination the transmittance of the transparencies must be proportional to $\sqrt{S(t)}$. As a consequence of the fact that the transmittance cannot assume negative values, in accordance with Fig. 9.2 a transparency $T_1(x)$ can be produced only for video signals whose amplitude is always positive. Radio signals are bipolar, wherefore their recording on the transparency requires the introduction of an additonal constant biasing of the signal level, that is, the recording on the transparency of the sum

$$S(t)_{\text{пр}} = B_0 + S(t). \tag{9.9}$$

The introduction of the additional bias B_0 results in the fact that, along with the useful component of the correlation interval (9.7), the light wave $S_{\text{св}2}(x_0)$ will contain a spurious background causing a deterioration in the filtering result. In effect, if the transmittance functions of transparencies $T_1(x)$ and $T_2(x)$ have the form

$$\begin{aligned} T_1(x) &= B_{01} + S(x), \\ T_2(x) &= B_{02} + S(x), \end{aligned} \tag{9.10}$$

then, following (9.5) and (9.6), the amplitude of the light at point $\omega_x = 0$, $\omega_y = 0$ of plane P_{n2} will correspond, with accuracy to within a constant factor, to

$$\begin{aligned} S_{\text{св}2}(x_0) = S_{\text{св}0} B_{01} B_{02} + S_{\text{св}0} B_{01} \int_0^{d_x} S(x - x_0)\, dx + \\ + S_{\text{св}0} B_{02} \int_0^{d_x} S(x)\, dx + S_{\text{св}0} \int_0^{d_x} S(x) S(x - x_0)\, dx. \end{aligned} \tag{9.11}$$

From this last expression (9.11) it will be clear that only the final term of the sum is useful, with the remaining terms containing a noise background.

Since additional selection of the effective component from the sum (9.11) is not possible with the use of noncoherent light, the applicability of noncoherent optical methods for the filtering of bipolar signals is severely limited.

When coherent light is employed, special measures may be taken to permit a considerable attenuation of the constant constituent of the reference level. This may be accomplished through the rejection of its spectral components. For this purpose, the transparency with the radio signal inscribed on it - in the form, for example, of

$$T(x) = B_0 + A(x)\cos[\omega_{x_0}x + \varphi(x)]$$

for

$$0 < x \leqslant d_T \tag{9.12}$$

is located in the forward focal plane of the lens $P_{л1}$ (Fig. 9.1), and illuminated with coherent light. In keeping with dependence (9.6), in the rear focal plane of lens $P_{л2}$ function (9.12) will undergo a Fourier transform on axis x_2. As a result of this transform, the spectral components of signal (9.12) will be laid off along axis x_2. The origin of the coordinates will disclose the spectrum of the constant component B_0, while in the region of space frequencies $\pm\omega_{x0}$ will be found the spectrum of signal $A(x)\cos[\omega_{x0}x + \phi(x)]$. Since the spectral width of the constant component B_0 is determined by the interval d_T, thus at signal frequencies for which the signal spectrum

$$\frac{1}{d_T} \leqslant \omega_{x_0}, \tag{9.13}$$

shows virtually no overlap with the spectrum of the constant component, the spectral components of the constant component $B_0(\omega)$ can be eliminated - through the use, for example, of a screen shading the frequency region at point $\omega_x = 0$. This operation affords a significant attenuation of the effect of the

constant component during the further filter processing of the signal $A(x) \cos [\omega_{x0}x + \phi(x)]$.

9.3. Synthesis of Optical Filters

A variety of optical filters may be synthesized based on the properties of coherent optical systems. The fact that optical systems exhibit spatial two-dimensionality affords the possibility of realizing both two-dimensional and unidimensional multichannel filters. In the first instance, by analogy with (5.6), the filtering operation is expressed by a two-dimensional correlation integral

$$Y(x_0, y_0) = \int_{-\infty}^{+\infty}\int X(x_1, y_1) S^*(x_1 - x_0, y_1 - y_0)\, dx_1\, dy_1. \qquad (9.14)$$

In the case of unidimensional multichannel filtering the correlation integral is expressed in the form

$$Y_{y_1}(x_0) = \int_{-\infty}^{\infty} X_{y_1}(x_1) S^*(x_1 - x_0)\, dx_1, \qquad (9.15)$$

where $S^*(x_1)$ is a modulation function being the mirror and complex-conjugate function with respect to the filter response.

Two methods are distinguished for acquiring the required optical-filter characteristics:

a) the synthesis method in the space frequency region;

b) the synthesis method in the space-image region of the signal [33].

In case a) the structural arrangement of the filter will appear as indicated in Fig. 9.3. The transparency on which is inscribed the input oscillation $X(x_1, y_1)$ (this transparency will

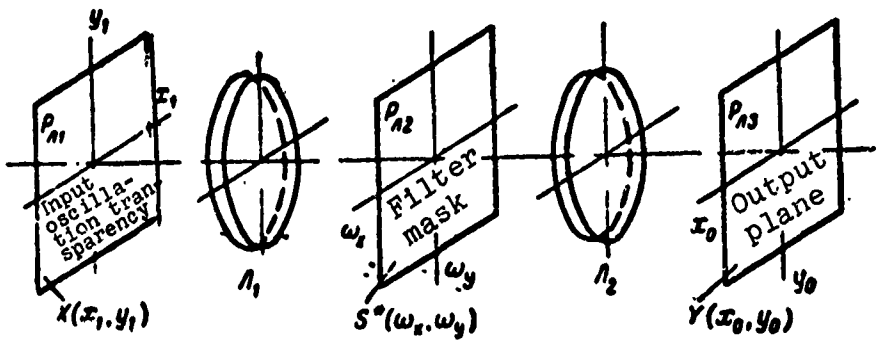

Fig. 9.3. Block diagram of an optical filter with a mask in the frequency region.

henceforth be referred to as the signal transparency) is located in plane $P_{л1}$. The two-dimensional spectrum $X(\omega_x, \omega_y)$ will be present in the focal plane of lens $Л_1(P_{л2})$. If there is placed in this plane a transparency with light transmittance $S^*(\omega_x, \omega_y)$, describing the frequency characteristic of the required filter (this transparency to be known as the optical filter mask), then in accordance with the properties of optical multiplication, the light wave leaving this transparency will have the following form:

$$X(\omega_x, \omega_y) S^*(\omega_x, \omega_y). \tag{9.16}$$

The subsequent two-dimensional Fourier space transform by lens $Л_2$ (9.6) will form in plane $P_{л3}$ a two-dimensional image of form (9.14).

The filter diagrammed in Fig. 9.4 provides for the location of the filter mask in plane $P_{л1}$ directly behind the signal transparency. Here the filter mask is a transparency carrying the reference signal $S^*(x_1, y_1)$. In this case, in the focal plane of the lens $Л_1(P_{л3})$ we shall have the image

$$Y(x_0, y_0) = \int_{-\infty}^{\infty}\int X(x_1, y_1) S^*(x_1 - x_0, y_1 - y_0) \exp[j(\omega_x x_1 + \omega_y y_1)]\, dx_1 dy_1, \tag{9.17}$$

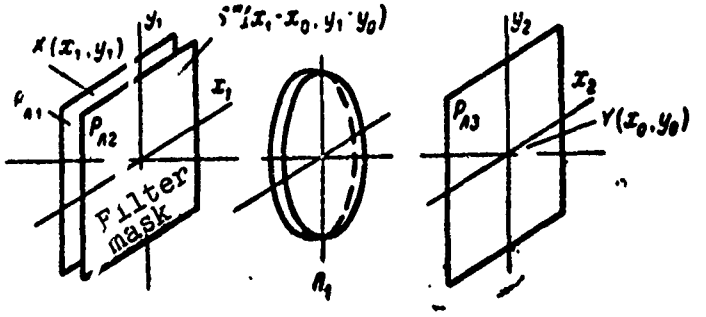

Fig. 9.4. Block diagram of an optical filter with signal plane mask.

where x_0, y_0 is the displacement of the filter mask coordinates in plane $P_{л1}$ relative to the input-oscillation transparency $X(x_1, y_1)$.

For point $\omega_x = 0$, $\omega_y = 0$ expression (9.17) is transformed to (9.14).

In the majority of cases, the filter circuit shown in Fig. 9.3 is to be preferred in that it performs correlation operation (9.14) in plane $P_{л3}$ for a wide range of parameters x_0, y_0. On the other hand, the arrangement shown in Fig. 9.3 [sic] performs the correlation operation only on a successive time basis for each shift in the parameters of the filter mask relative to the signal transparency. [Translator's Note - There is obviously a misprint in the last two sentences. The author has mistakenly twice referred to Fig. 9.3, when one reference should clearly be to Fig. 9.4.]

For the design of multichannel filters implementing the correlative integration operation for only one of the coordinates simultaneously over many channels, one may employ the same circuitries shown in Figs. 9.3 and 9.4 by replacing the spherical lens $Л_1$ and $Л_2$ by a lens system containing one cylindrical and one spherical lens [33].

The unidimensional signals to be filtered are written in the form $X_{y_i}(x_1)$ and arranged one above the other along the y_1 axis in plane P_{n1} in the arrangement shown in Fig. 9.3. The system of cylindrical and spherical lenses performs the Fourier transform for the x_1 coordinate only, with the signal not transformed for the y_1 coordinate, the result being that in the P_{n2} plane there is the simultaneous spectral transformation of the signals for each channel located along the y_1 axis separately. By placing an individual filter mask in each channel of plane P_{n2}, we obtain in plane P_{n3} along axis y_0 a multichannel image corresponding to the aggregate of correlation intervals of form (9.15).

By way of example, consider some practical block diagrams of unidimensional optical filters which provide filtering in both the signal and frequency plane. The arrangement of a unidimensional optical filter performing signal-plane filtration is shown in Fig. 9.5.

The x(t) input-oscillation transparency (139), having a transmittance function on the x_1 axis in the form

$$T_1(x_1) = B_0 + x(x_1) = B_0 + \\ + A_x(x_1)\cos[\omega_{x_0}x_1 + \varphi(x_1) + \varkappa_x(x_1) + \varphi_0], \qquad (9.18)$$

is located in the forward focal plane of lens $Л_1$ and is displaced with respect to the optical axis by the quantity x_0. In Figs. 9.5 and 9.6 the change in transmittance value is schematically represented in the formed of a darkened relief, with the hatched relief used to indicate the signal amplitude in the corresponding planes. In the rear focal plane of lens $Л_1$ the screen rejects the spectral components of the constant constituent B_0. Therefore, in accordance with the Fourier inversion, the amplitude of the light in the rear focal plane of lens $Л_2$ along the x_2 axis will reflect the input oscillation $S_{СВ0}x(x_2-x_0)$. Located in this same

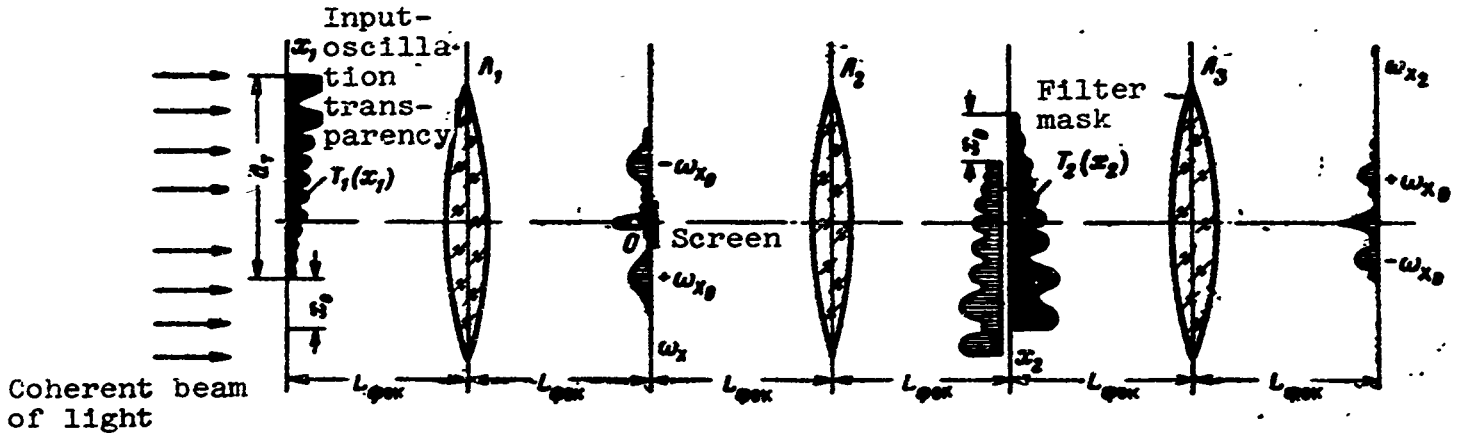

Fig. 9.5. Practical arrangement with signal-plane filtering.

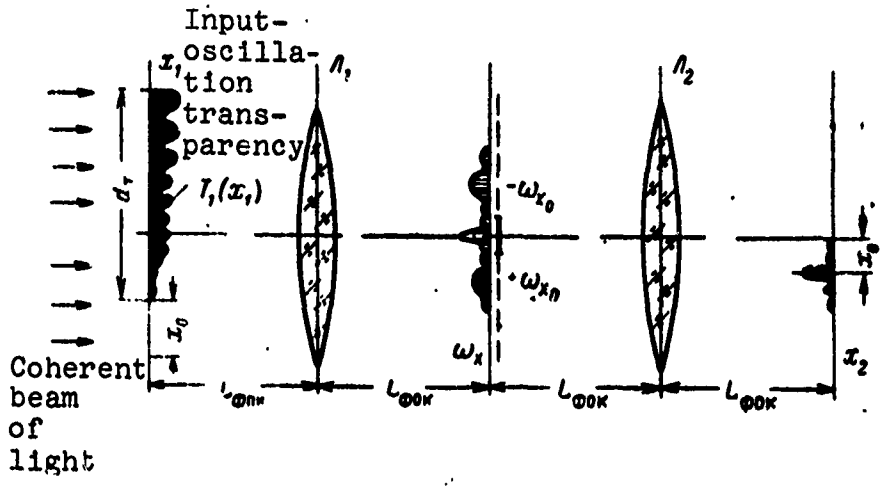

Fig. 9.6. Practical arrangement with frequency-plane filtering.

plane is an optical transparency with the transmittance function $T_2(x_2)$ corresponding to the filter mask

$$T_2(x_2) = A_0(x)\cos[\omega_{x_0}x_2 + \varphi(x_2)] + B_0. \tag{9.19}$$

The light amplitude leaving the mask will be expressed as

$$S_{св}(x_2) = S_{св\,0}x(x_2 - x_0)T_2(x_2). \tag{9.20}$$

The lens $Л_3$ produces the Fourier transform of function (9.20). Therefore, in the rear focal plane of lens $Л_3$ at point $\omega_{x_2} = 0$, following dependences (5.11), (9.6), (9.18), (9.19), and (9.20), we obtain

$$S_{св}(x_0)_{вых} = \frac{1}{2}S_{св\,0}\,\mathrm{Re}\exp[j(\omega_{x_0}x_0 + \varphi_0)] \times$$
$$\times \int_0^{d_T} S_x(x_2)S^*{}_0(x_2 - x_0)\,dx_2 + \frac{1}{2}B_0S_{св\,0}\int_0^{d_T} x(x_2 - x_0)\,dx_2. \tag{9.21}$$

Since $x(x_2-x_0)$ is a rapidly oscillating function, the final term in sum (9.21) has a value close to zero, and for this reason the amplitude of the light leaving the filter shown in Fig. 9.5 will be proportional to the required correlation integral, that is,

$$S_{cв}(x_0)=\frac{1}{2}S_{cв\,0}\,\mathrm{Re}\exp[j(\omega_{x_0}+\varphi_0)]\int_0^{d_T}S_x(x_2)S^*_0(x_2-x_0)\,dx_2. \tag{9.22}$$

With filtering in the frequency plane the block diagram of the optical filter has the appearance shown in Fig. 9.6. Just as in Fig. 9.5, lens $Л_1$ forms in its rear focal plane the spectrum of function (9.18), which, in accordance with (9.6) and (9.18), will be expressed in the form

$$S_{cв}(\omega_x)=S_{cв\,0}\left[B_0\frac{\sin\frac{d_T\omega_x}{2}}{\frac{d_T\omega_x}{2}}+\exp(-j\omega_x x_0)X(\omega_x)\right] \tag{9.23}$$

where $X(\omega_x)$ is the spectrum of signal $x(x_1)$.

Placed in the plane in question in the region of the optical axis is a screen which eliminates those spectral components which are caused by the constant part B_0, as well as a complex filter mask exhibiting a variation in the amplitude and phase of the light in conformity with the transmission factor $S^*_0(\omega)$. A correlation function is formed in the rear focal plane of lens $Л_2$ corresponding to

$$S_{cи}(x_2-x_0)_{вых}=\int_{-\omega_x}^{+\omega_x}X(\omega_x)S^*_0(\omega_x)\exp[j(x_2-x_0)\omega_x]\,d\omega_x=$$

$$=\int_0^{l_0}S_x(\xi)S^*_0(\xi-x_2+x_0)\,d\xi. \tag{9.24}$$

From this last expression it is clear that the shift of the transparency $T_1(x_1)$ along the x_1 axis does not lead to a distortion of the correlation function, but merely causes its displacement along the x_2 axis by the same quantity.

9.4. Optical Transparencies

In practical filtering and signal-processing systems the oscillation from the receiver channel output normally arrives in the form of an electrical voltage or current. The introduction of this kind of signal into an optical filter requires that it be converted into an optical transparency providing the required modulation of the light stream in the filter. An optical transparency is also required for the creation of the filter mask (Section 9.3).

According to their operating principles, optical transparencies are classed as static and dynamic.

The static transparency represents a comparatively long-term signal recording accomplished by varying the optical transmittance or phase thickness of some kind of optically transparent material such as photographic film, thermoplastic, and the like. The optical filtering and processing of the signal thus recorded is conducted in an altered time scale. Because they involve a variation of the transmittance factor and optical thickness, static transparencies permit both the amplitude and phase modulation of the light in accordance with expression (9.4).

The dynamic transparency modulates the light stream in conformity with an incoming electrical signal in an instantaneous time scale. The basic varieties of such optical transducers are the ultrasonic and electron-optical light modulator [20, 35, 46, 60, 64].

In practical optical filtering devices, photographic films are the most widely employed of the static transparencies and transparent ultrasonic delay lines of the dynamic variety. Let us consider in some detail the fundamental design principles of these transparencies.

A film-type optical transparency producing an amplitude signal recording of type (9.18) may be devised using the apparatus schematically represented in Fig. 9.7. The input oscillation $x(t)$ is summed in the control circuit with reference level v_0 and fed to the control electrode of a cathode-ray tube [CRT] (ЭЛТ). The control-electrode voltage modulates the brightness of the spot on the CRT screen. The relationship of spot brightness to the voltage across the control electrode of the CRT in the latter's working range of characteristics is expressed, in this case, in the following form:

$$I(t) = k_I i [v_0 + x(t)]^2, \tag{9.25}$$

where I(t) is the brightness of the spot on the CRT screen;

i is the current density of the CRT ray;

k_I is a proportionality factor.

From the screen of the cathode-ray tube the spot is projected onto a photosensitive film by means of the focusing lens. As the beam travels in time along the x axis, this being accomplishable either by sweeping the ray of the tube or physically moving the film, the spot brightness is recorded on the film and the time oscillation x(t) is inscribed in spatial coordinates along the x axis. The dependence of the film's optical density O(x) on the brightness of the incident spot within the linear segment of the film's sensitivity can be expressed by the relation

$$O(x) = \mu_k \lg \frac{I(x)}{I_0}, \tag{9.26}$$

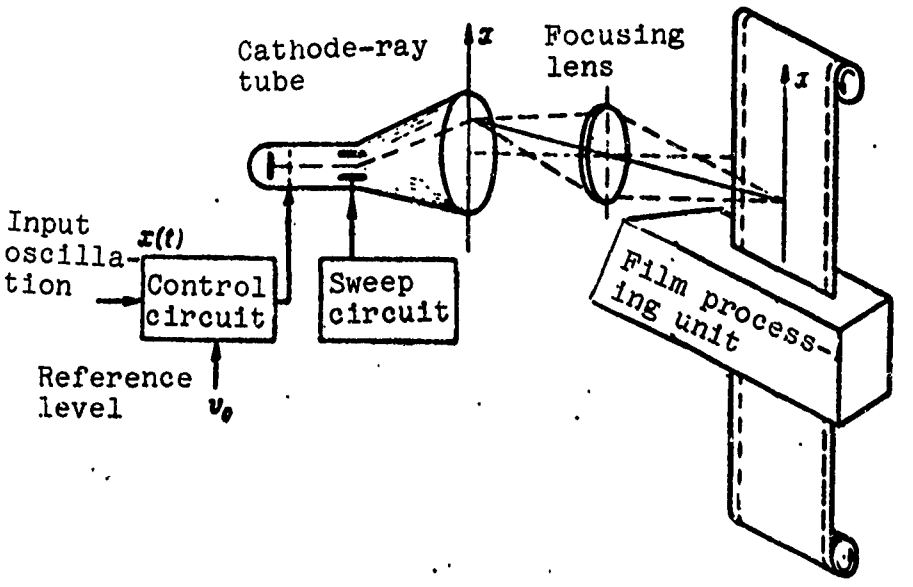

Fig. 9.7. Diagram of apparatus for producing a film-type transparency.

where μ_k is the film contrast;

I_n is the "inertia" coefficient of the film [96].

The optical transmittance of the transparency T(x) is related to the optical density of the film O(x) by the expression

$$T(x) = 10^{\frac{-O(x)}{2}} \tag{9.27}$$

or, taking into account Eq. (9.26),

$$T(x) = I_n^{\frac{\mu_k}{2}} I(x)^{-\frac{\mu_k}{2}}. \tag{9.28}$$

From expressions (9.25) and (9.28) it follows that in order to achieve for the transparency an optical transmittance proportional to the input oscillation x(t), the film must be inverted, that is, a positive with $\mu_k = -1$ must be produced from

the negative. However, this undesirable operation can be avoided, provided a sufficiently large displacement step v_0 is selected. In this case, the major weight in the expansion of relation (9.28) into a power series attaches to the first term, which ensures a dependence of the type

$$T(x) = k_1 \frac{\left(\frac{l_n^2}{l}\right)^{\mu_k}}{} [v_0^{-\mu_k} - \mu_k v_0^{-\mu_k - 1} x(x)]. \tag{9.29}$$

This latter expression can be converted to the form

$$T(x) = B_0 + mx(x), \tag{9.30}$$

where

$$B_0 = k_1 \left(\frac{l_n^2}{l}\right)^{\mu_k} v_0^{-\mu_k};$$

$$m = k_1 \mu_k \left(\frac{l_n^2}{l}\right)^{\mu_k} v_0^{-\mu_k - 1}.$$

The film carrying the time oscillation recording is chemically processed in a special unit shown in Fig. 9.7. This film processing requires considerable time - some 30-60 seconds - and for this reason the production of the phototransparency involves a time lag with respect to the incoming time oscillation.

This method of preparing the transparency can also be employed to produce a filter mask with an amplitude recording of the signal (9.19). In this case, a signal $S_0(t)$ is delivered to the control electrode of the cathode-ray tube.

Filtering in the frequency plane calls for a complex filter mask to vary the amplitude and phase of the transmitted light (9.24). There are certain practical difficulties in the design of a transparency with variable optical density and phase

thickness, and for this reason holographic techniques are normally used in the production of complex transparencies [74].

This method of preparing a complex transparency may be used together with the arrangement pictured in Fig. 9.8. In the x plane at a distance of d/2 from the optical axis is located a transparency with an amplitude recording of the signal T(x) of form (9.19) corresponding to the Fourier transform of the complex function of the required amplitude-phase transparency $T(\omega_x)$. Located in this same plane is a slot, also distant from the optical axis by the quantity d/2 (Fig. 9.8), through which is delivered a reference light beam, being a portion of the input light stream. A light wave will be present in the rear focal plane of the lens, whose modulation function is defined by the sum of the two spectra

$$T(\omega_x)\exp\left(-j\frac{\omega_x d}{2}\right) \quad \text{and} \quad O_1 \exp\left(j\frac{\omega_x d}{2}\right),$$

where O_1 is the amplitude of the reference light beam passing through the slot.

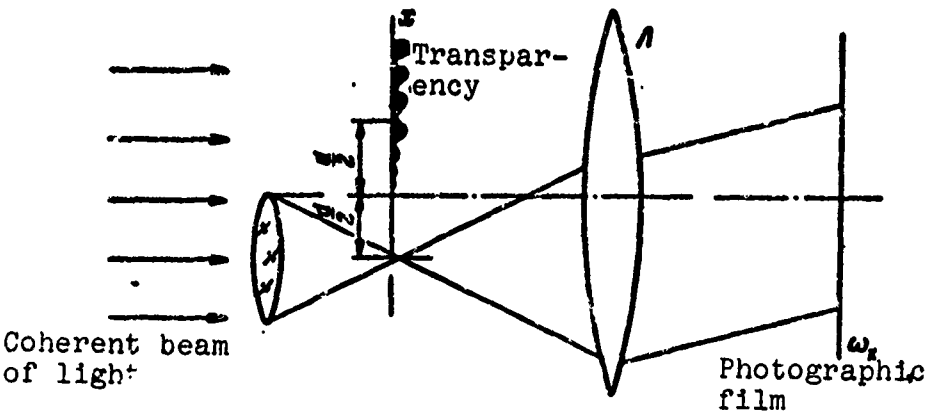

Fig. 9.8. Diagram showing the production of a filter for frequency-plane filtering.

Photographic film positioned in the same plane will record the brightness of the light image, that is

$$I(\omega_x) = \left| T(\omega_x) \exp\left(-j\frac{\omega_x d}{2}\right) + O_1 \exp\left(j\frac{\omega_x d}{2}\right) \right|^2 =$$
$$= |T(\omega_x)|^2 + O_1^2 + O_1 T(\omega_x) \exp(-j\omega_x d) +$$
$$+ O_1 T^*(\omega_x) \exp(j\omega_x d). \qquad (9.31)$$

Assuming a sufficiently intense reference beam, following (9.29) the transmittance function of the transparency $T_2(\omega_x)$ obtained on this film will be defined by the relation

$$T_2(\omega_x) = O^{-\mu_k} - \frac{\mu_k}{2} O_1^{-\mu_k - 2} |T(\omega_x)|^2 -$$
$$- \frac{\mu_k}{2} O_1^{-\mu_k - 1} T(\omega_x) \exp(-j\omega_x d) -$$
$$- \frac{\mu_k}{2} O_1^{-\mu_k - 1} T(\omega_x) \exp(j\omega_x d). \qquad (9.32)$$

It will be evident from this last expression that the transmittance function of the obtained transparency $T_2(\omega_x)$ is determined by the sum of the terms, one of which is proportional to the required complex function $T(\omega_x)$ of the transparency to be synthesized. Therefore, if a transparency of this kind is located in the frequency plane ω_x of the filter in Fig. 9.6, the required correlation integral will be formed in its output plane x_2. Because of the difference in their space frequency value, the additional terms occurring in the transmittance function $T_2(\omega_x)$ acquire a spatial displacement along the x_2 axis and are eliminated by virtue of the corresponding shading.

An optical transparency employing light modulation by means of ultrasound operates according to a somewhat different working principle than the film-type transparency. The reason for this

lies in the fact that in a transparency of this kind what is modulated is not the amplitude of the light, but its phase. On the other hand, however, under certain conditions, filtering devices employing ultrasonic light modulators exhibit the same characteristics as photo-transparency filter devices.

Let a signal $u(t) = A(t) \cos [\omega_0 t + \phi(t)]$ be delivered to the piezoelectric transducer of an optically transparent ultrasonic delay line (Fig. 9.9). In a UDL of this kind water, quartz, lithium niobate, etc., may be used as the acoustic line. The ultrasonic wave excited by the signal u(t), traveling over the acoustic line, changes its optical refractive index $n_{пр}(x, t)$ [8] according to the law

$$n_{\text{пр}}(x, t) = n_0 + \Delta n A(t) \cos \left[\omega_0 \left(t - \frac{x}{V_{\text{ак}}} \right) + \varphi \left(t - \frac{x}{V_{\text{ак}}} \right) \right], \quad (9.33)$$

where n_0 is the refractive index of light of an unexcited medium;

Δn is the amplitude of the specific change in the refractive index for the medium in question.

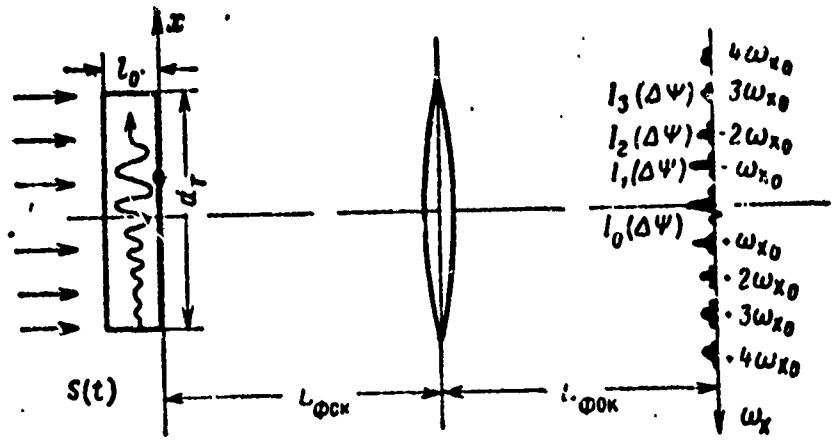

Fig. 9.9. Ultrasonic modulation of light.

In its passage through such an excited ultrasonic delay line, the coherent light (Fig. 9.9) acquires a phase modulation (9.3).

Thus, the complex amplitude of the light behind the UDL, over which propagates the acoustic wave generated by the signal u(t), is defined by the relation

$$S_{cn}(x,\ t)=S_{cn0}\exp j\left\{\psi_0+\Delta\psi A\left(t-\frac{x}{V_{ak}}\right)\times\right.$$
$$\left.\cos\left[\omega_0\left(t-\frac{x}{V_{ak}}\right)+\varphi\left(t-\frac{x}{V_{ak}}\right)\right]\right\}, \qquad (9.34)$$

where $\psi_0 = \frac{2\pi l_0 n_0}{\lambda_c^{\,B}}$ is the constant phase shift;

$\Delta\psi = \frac{2\pi l_0 \Delta n}{\lambda_c^{\,B}}$ is the phase modulation.

Disregarding the constant phase shift ψ_0, expression (9.24) can be represented by the series

$$S_{cn}(x,t),\ =S_{cn0}I_0[\Delta\psi A(x,\ t)]+2S_{cn0}\sum_{n=1}^{n=\infty}(j)^n\times$$
$$\times I_n[\Delta\psi A(x,\ t)]\cos\left\{n\left[\omega_0\left(t-\frac{x}{V_{ak}}\right)+\varphi\left(t-\frac{x}{V_{ak}}\right)\right]\right\}, \qquad (9.35)$$

where $I_n(z)$ is the n-th order Bessel function.

Expansion (9.35) indicates that the phase modulation is characterized by a set of harmonic components of different frequency, reflecting the amplitude modulation of the light. Therefore, if the lens of Fig. 9.9 is used to produce a Fourier transform of lightwave (9.35), there will be formed along the axis of space frequency ω_x the linear spectrum of series (9.35) with frequencies which are multiples of $\omega_{x0}=\frac{\omega_0}{V_{ak}}$ (Fig. 9.9). In the region of the fundamental frequency ω_{x0} an optical image is formed,

corresponding to a transparency with the transmittance function[1]

$$T(x, t) = I_1[\Delta\psi A(x, t)] \cos\left[\omega_0\left(t - \frac{x}{V_{ak}}\right) + \right.$$
$$\left. + \varphi\left(t - \frac{x}{V_{ak}}\right)\right]. \qquad (9.36)$$

Considering that the Bessel function of the first order

$$I_1(z) = \frac{z}{2} - \frac{z}{16} + \ldots \qquad (9.37)$$

when z << 1, can be represented by the first term only of sum (9.37), for small modulation indices relation (9.36) can be rewritten as follows:

$$T(x, t) \cong \frac{\Delta\psi}{2} A(x, t) \cos\left[\omega_0\left(t - \frac{x}{V_{ak}}\right) + \varphi\left(t - \frac{x}{V_{ak}}\right)\right]. \qquad (9.38)$$

It follows from this last expression that, at low modulation indices, ultrasonic light modulators, similarly to photographic film, permit the acquisition of optical signal transparencies with amplitude and phase modulation. A practical arrangement of an optical filtering device incorporating an ultrasonic light modulator may be seen in Fig. 9.10.

Input oscillation x(t) reaches the piezo-transducer of the optically transparent ultrasonic delay line. The illumination of the UDL by a coherent light stream permits the acquisition, in

[1]The factor j in expression (9.35) changes only the phase of the light oscillation, and may therefore be disregarded in the expressions for the amplitude of the light.

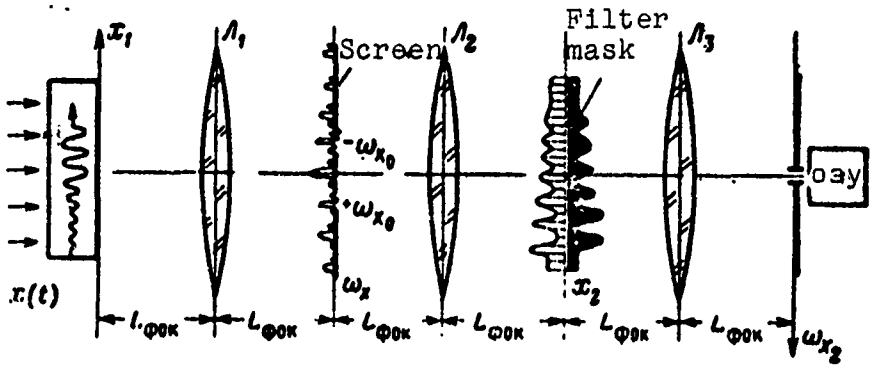

Fig. 9.10. Ultrasonic optical filtering device.

the rear focal plane of lens $Л_1$, of the spectral expansion (9.35). The screen placed in plane ω_x admits light only in the region of the fundamental frequencies $\pm\omega_{x0}$, whereupon, following (9.38), a light image of the input oscillation x(x, t) is formed along the x_2 axis in the rear focal plane of lens $Л_2$. Positioned in this plane is a filter mask consisting of a photographic film with the amplitude recording of a reference signal. Now, on the optical axis of lens $Л_3$ in its rear focal plane, similarly to Fig. 9.4, there will be formed a correlation integral of type (9.15). Since as a result of the propagation of the acoustic wave along the sound line there will be a time-continuous spatial displacement of the transmittance function of the transparency (9.38), all the values of the correlation integral will also be successively reproduced at the point $\omega_{x_2} = 0$. The operation of an optical filter with ultrasonic modulator takes place in an instantaneous time scale, a fact which makes it possible to employ such filters, unlike the static-transparency variety, for the filtering of rapidly changing signals.

9.5. Some Varieties of Practical Unidimensional Optic Filter Circuitries

Real optical filtering devices are designed for the most part using the circuit arrangements and methods discussed in Sections

9.3 and 9.4. In a number of instances, however, for special signal forms and processing systems it may be more expedient, in practical terms, to use circuitries exhibiting certain structural differences from those represented in Figs. 9.5 and 9.6. Let us consider, by way of example, the major varieties of these practical configurations, which offer the advantage of providing simpler hardware implementation.

Optical Filter with Photoelectronic Integration

A device of this kind was proposed in [76]. Its block diagram is shown in Fig. 9.11. The input signal $u(t) = A(t) \cos [\omega_0 t + \phi(t)]$ reaches the piezoelectric transducer of an optically transparent ultrasonic delay line, immediately following which is located a filter mask in the form of an optical transparency with a transmittance function $T_2(x)$ equal to

$$T_2(x) = B_0 + u\left(\frac{x}{V_{ax}}\right) = B_0 + A\left(\frac{x}{V_{ax}}\right) \cos\left[\frac{\omega_0 x}{V_{ax}} + \varphi\left(\frac{x}{V_{ax}}\right)\right]. \quad (9.39)$$

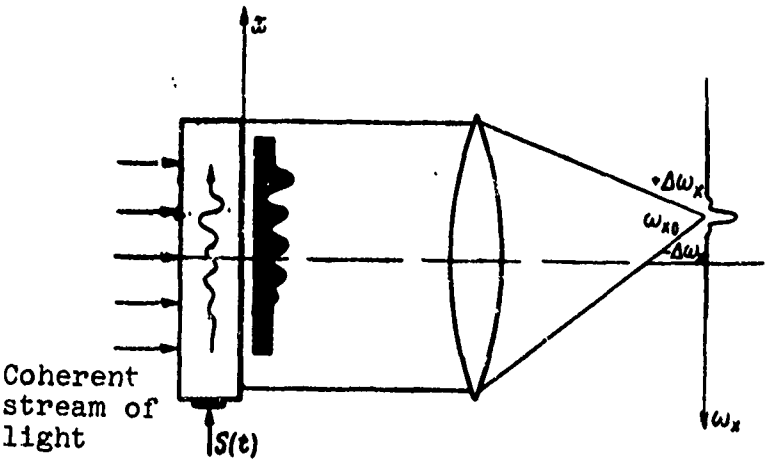

Fig. 9.11. Optical filtering device.

With the UDL illuminated by coherent light, the complex amplitude of the light wave $S_{св2}(x, t)$ behind the transparency is expressed in the form

$$S_{св\,2}(x, t) = S_{св\,1}(x, t)\,T_2(), \tag{9.40}$$

where $S_{св1}(x, t)$ is the complex amplitude of the light behind the UDL.

Excited by the input signal, the ultrasonic wave causes the phase modulation of the light transiting through the UDL in conformity with expression (9.35). Given low modulation indices, similarly to (9.38), the basic contribution to the region of the fundamental frequency ω_{x0} of the spectral expansion of the light $S_{св}(x, t)$ (plane ω_x) will be made by the two components of product (9.40), which will equal

$$S_{св\,2}(x, t)_{\omega_{x0}} = S_{св\,0}\,\mathrm{Re}\left\{S\left(\frac{x}{V_{зв}}\right)\exp\left(j\,\frac{\omega_0}{V_{зв}}\,x\right) + \right.$$
$$\left. + B_0\Delta\psi S\left(t + \frac{x}{V_{зв}}\right)\exp\left[j\omega_0\left(t + \frac{x}{V_{зв}}\right)\right]\right\}. \tag{9.41}$$

The spectral expansion of these components in the region of the frequency ω_{x0} can be represented by the relation

$$S_{св\,2}(\omega_x, t) = S_{св\,0}\int\limits_{-\frac{d_T}{2}}^{+\frac{d_T}{2}} S\left(\frac{x}{V_{зв}}\right)\exp(j\omega_{x_0}x)\exp(j\omega_x x)\,dx +$$

$$+ S_{св\,0}B_0\Delta\psi\exp(j\omega_0 t)\int\limits_{-\frac{d_T}{2}}^{+\frac{d_T}{2}} S\left(t + \frac{x}{V_{зв}}\right)\exp(j\omega_{x_0}x)\exp(j\omega_x x)\,dx. \tag{9.42}$$

If a photoelectric detector is located in the region of frequency ω_{x0}, then as a result of the fact that it reacts to the intensity of the light and sums it from a certain surface $\pm\Delta\omega_x$, the electric signal at the detector output will be defined by the expression

$$y(t) = \int_{-\Delta\omega_x}^{+\Delta\omega_x} |S_{\text{cu}\,3}(\omega_x, t)|^2 d\omega_x =$$

$$= S_{\text{cn}\,0}^2 \int_{-\Delta\omega_x}^{+\Delta\omega_x} \left| \int_{-\frac{d_T}{2}}^{+\frac{d_T}{2}} S\left(\frac{x}{V_{\text{ax}}}\right) \exp\left[j(\omega_x - \omega_{x0})x\right] dx \right|^2 d\omega_x +$$

$$+ S_{\text{cn}\,0}^2 B_0^2 \Delta\psi^2 \int_{-\Delta\omega_x}^{+\Delta\omega_x} \left| \int_{-\frac{d_T}{2}}^{+\frac{d_T}{2}} S\left(t + \frac{x}{V_{\text{ax}}}\right) \exp\left[j(\omega_x - \omega_{x0})x\right] dx \right|^2 d\omega_x + 2S_{\text{cn}\,0} B_0 \Delta\psi \operatorname{Re} \exp(-j\omega_0 t) \times$$

$$\times \int_{-\Delta\omega_x}^{\Delta\omega_x + \frac{d_T}{2} + \frac{d_T}{2}} \int_{-\frac{d_T}{2}}^{+\frac{d_T}{2}} \int_{-\frac{d_T}{2}}^{+\frac{d_T}{2}} S\left(\frac{x_1}{V_{\text{ax}}}\right) S^*\left(t + \frac{x_2}{V_{\text{ax}}}\right) \exp\left[j(x_1 - x_2)(\omega_x - \omega_{x0})\right] dx_1 dx_2 d\omega_x. \qquad (9.43)$$

The signal components described by the first two terms of the sum (9.43) fall within the low-frequency region and are filtered out in the frequency-selective amplifier following the photodetector. The component defined by the third term of the sum may be somewhat transformed. By extending to infinity the frequency integration range and considering that

$$\lim_{\Delta\omega\to\infty}\int_{-\Delta\omega_x}^{+\Delta\omega_x}\exp\left[j\omega(x_1-x_2)\right]d\omega=\delta(x_1-x_2),$$

then for the third component we obtain

$$y(l)\cong 2S_{cv_0}B_0\Delta\psi\,\mathrm{Re}\exp(-j\omega_0 l)\int_{-\frac{d_T}{2}}^{+\frac{d_T}{2}}S\left(\frac{x}{V_{ox}}\right)S^*\left(t+\frac{x}{V_{ox}}\right)dx. \quad (9.44)$$

If we compare this method of forming the correlation function with the one previously considered in the signal-plane filtering unit (9.22), it will be noted that the conversion of the light pattern by means of the photoelectric detector in case (9.22) forms the square of the modulus of the autocorrelation function, while this transformation (9.44) is characterized by the acquisition of the direct autocorrelation function value. This is true because here the photodetector plays a part in the integration operation.

This optical filter arrangement (Fig. 9.11) also offers a number of advantages over conventional optical filtering circuits in that it is simpler and does not require the elimination of the constant light component determined by the reference level.

Optical Filter Employing Space Focusing

For certain signal forms the optical filter can be designed without the use of masks. The approach in this case is through the space-focusing property of light vibrations. Similar optical filters can be designed, for example, for narrow-band, unmodulated radio signals (2.33) and signals with linear frequency modulation (2.37). The block diagram of this kind of filter with a dynamic transparency has been described in [20, 49] and is shown in Fig. 9.12.

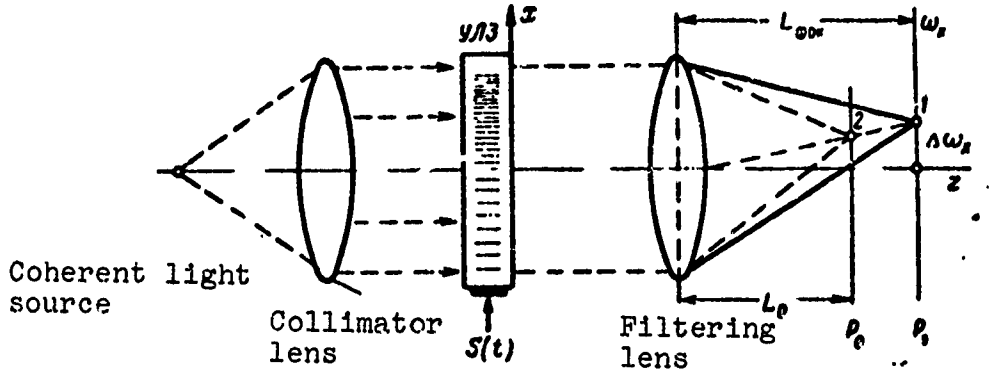

Fig. 9.12. Optical filter employing space light focusing.

The light stream, phase-modulated by the ultrasonic modulator, is focused by the filtering lens. When the input signal is represented by a radio pulse of form (2.33), the focusing of the beam occurs in plane $P_{л1}$, while in a certain region of the fundamental frequency ω_{x0} an image appears corresponding to the Fourier transform of the signal reaching the input of the ultrasonic modulator (9.38). As the frequency of the input oscillation varies, there is a shift in the light image relative to the point ω_{x0} by the amount Δx. Following (9.6), this shift is defined as

$$\Delta x = \frac{\Lambda_{св} L_{фок}}{\Lambda_{зв}}. \qquad (9.45)$$

If ahead of the photoelectric receiver at point 1 (Fig. 9.12) there is set up a narrow slot passing the spectral components determined only by the spectrum of the input signal, then the signal from the receiver output will characterize the envelope of the oscillation at the output of a matched filter tuned to the frequency of the radio pulse.

To create a set of filters overlapping the prescribed frequency band in plane $P_{л1}$, it is merely necessary to set up a series of photoelectric receivers having the appropriate slots.

With the arrival at the input of the ultrasonic modulator of Fig. 9.12 of a signal of type (2.37), frequency-modulated according to the linear law, the focusing of the beam behind the focusing lens shifts to the P_0 plane. Now

$$L_0 = L_{\phi ox}\left(1 - \frac{L_{\phi ox}}{Z_0}\right), \qquad (9.46)$$

where

$$Z_0 = \frac{V_{ak}^2 \Delta T}{\lambda_{ox} 2F_m}$$

Optical Filter with Dynamic Mask

A block diagram of this filter may be seen in Fig. 9.13. The filter is designed in conformity with the circuit of Fig. 9.5 or 9.11, in which the signal and filter transparencies are of the dynamic variety. Ultrasonic modulators may be used as dynamic transparencies of this kind [60]. With the delivery to the input of the first and second modulator of signals whose time characteristics mirror each other, the photoreceiver output produces a signal which describes in time either the square of the envelope of the correlation integral (9.22) or its direct value (9.44).

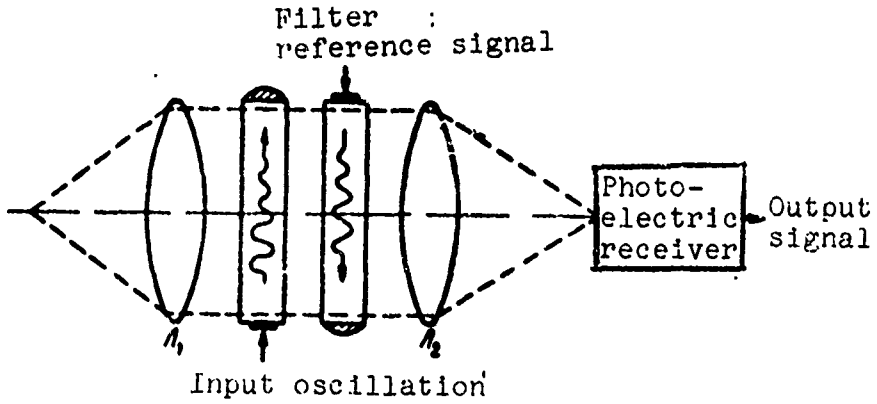

Fig. 9.13. Optical filter with dynamic mask.

For the purpose of altering the time scale of the filter reference signal and eliminating the need that it mirror the characteristics of the input signal, the circuit arrangement shown in Fig. 9.13 can be slightly modified to include an additional lens system (Fig. 9.14).

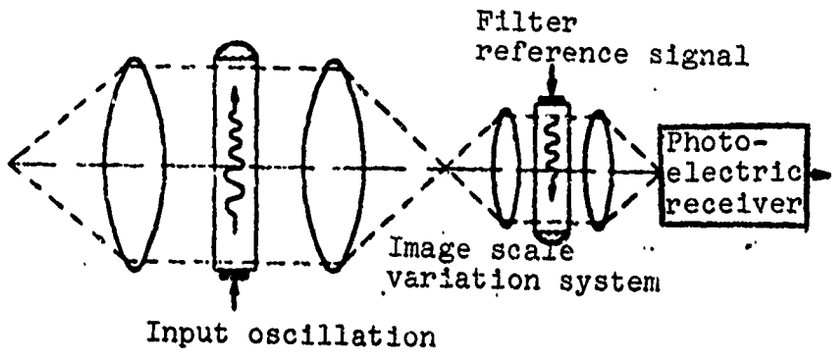

Fig. 9.14. Optical filter with dynamic mask and changing time scale.

BIBLIOGRAPHY

1. Альбац Н. Е. Справочник по расчету фильтров и линий задержки. Госэнергоиздат, 1963.
2. Антонов О. Е. Оптимальное обнаружение сигналов в негауссовых помехах. «Радиотехника и электроника», 1967, т. 12, вып. 5.
3. Бакулев П. А. Радиолокация движущихся целей. Изд-во «Советское радио», 1964.
4. Бакут П. А. и др. Вопросы статистической теории радиолокации. Изд-во «Советское радио», 1963.
5. Балабанян Н. Синтез электрических цепей. Госэнергоиздат, 1961.
6. Башаринов А. Е. Выделение радиолокационной информации при приеме сигналов в шумах. Учебное пособие по курсу «Основы радиолокации». Изд-во МЭИ, 1966.
7. Benjamin R. Modulation Resolution and Signal Processing in Radar Sonar and Related Systems. Pergamon Press, Oxford, 1966.
8. Бергман Л. Ультразвук. Изд-во иностранной литературы, 1956.
9. Bogoth S. E., Cook C. E. Effects of limiting on the Detectability of Partially Time Coincident Pulse Compression Signals. Trans. IEEE. MIL-9, № 1, 1965.
10. Босый Н. Д. Электрические фильтры. Гостехиздат УССР, 1960.
11. Brown R. Electrooptical Device. Electronical Equipm. News, № 8, 1965.

Bibliography (Continued)

12. Brockelsby C. F., Palfreemam I. E., Cilson R. W. Ultrasonic delay lines. London, Hill books Comp., 1963.
13. Вакман Д. Е. Сложные сигналы и принцип неопределенности. Изд-во «Советское радио», 1965.
14. Вендик О. Г. Антенны с немеханическим движением луча. Изд-во «Советское радио», 1965.
15. Волков В. М. Логарифмические усилители. Изд-во технической литературы, УССР, 1962.
16. Вудворд Ф. М. Теория вероятностей и теория информации с применениями в радиолокации. Пер. с англ., под ред. Г. С. Горелика. Изд-во «Советское радио», 1955.
17. Вузман П. М. Класс последовательностей для фазовой манипуляции сигналов. «Радиотехника», 1967, т. 22, № 9.
18. Вестерфильд Е. С. Способ подавления мешающих отражений путем использования согласованных фильтров. «Зарубежная радиоэлектроника», 1961, № 3.
19. Гауфер Я. Оптическая обработка сигналов импульсно-доплеровских РЛС. «Зарубежная радиоэлектроника», 1963, № 4.
20. Геринг, Монтагю. Простой оптический фильтр для РЛС, использующий сигнал с линейной частотной модуляцией. ТИИЭР, 1964, № 12.
21. Гитис Э. М. Преобразователи информации для электронных цифровых вычислительных устройств. Госэнергоиздат, 1961.
22. Глозман П. А. Пьезокерамические материалы в электронной технике. Изд-во «Энергия», 1965.
23. Гуткин Л. С. Теория оптимальных методов радиоприема при флюктуационных помехах. Изд-во «Советское радио», 1961.
24. Гоноровский И. С. Радиотехнические цепи и сигналы, ч. I и II. Изд-во «Советское радио», 1966—1967.
25. Джоунс Д. Идеальное ограничение процесса, состоящего из двух синусоидальных сигналов и случайного шума. Сб. «Некоторые проблемы обнаружения сигнала, маскируемого флюктуационной помехой», под ред. П. И. Шпер. Изд-во «Советское радио», 1965.
26. Davenport W. Signal-to-noise ratios in band — pass limiter J. Appl. Phys., v. 24, № 6, 1953.
27. Дифранко Ж. В., Рубин В. Л. Анализ искажений при обработке радиолокационного сигнала. «Зарубежная радиоэлектроника», 1961, № 1.
28. Дроздов Е. А., Пятибратов А. П. Автоматическое преобразование и кодирование информации. Изд-во «Советское радио», 1964.
29. «Оптическая обработка информации». Под ред. С. П. Ерковича. Изд-во «Мир», 1966.
30. Зиберт В. Общие закономерности обнаружения целей при помощи радиолокации. «Вопросы радиолокационной техники», 1957, № 2.
31. Kaiteris C., Rubin W. L. A Noncoherent signal Design Technique for Achieving a Low Residue Ambiguity Function. Trans. IEEE, AES-2, № 4, 1966.
32. Кейтерис, Рубин. Импульсные последовательности с низким остаточным уровнем поверхности неопределенности, минимизирующие подавления перекрывающихся отраженных сигналов от целей в приемниках с ограничением. ТИИЭР, 1966, № 3.
33. Катрона Л. Я. Оптические системы фильтрации и обработки сигналов. «Зарубежная радиоэлектроника», 1962, № 10.

Bibliography (Continued)

34. Клреев Б. Б., Неупокоев Б. А. Полупроводниковые элементы ЭЦВМ. Расчеты и схемы. Изд-во «Советское радио», 1964.
35. King M., William R. Real Time Electrooptical Signal Processors with coherent Detection. Applied Optics, № 8, 1967.
36. Klassen R. W. Comparison of Frequency Shift keyed and phase shift klyed pulse compression Systems. IEEE Int. Conv. Rec. Pt. 4, 1966.
37. Клюев Н. Ф. Обнаружение импульсных сигналов с помощью накопителей дискретного действия. Изд-во «Советское радио», 1963.
38. Кпарр Г. В. An Application of Nonlinear programming to Mismatched Filters. Trans. IEEE, CT-12, № 2, 1965.
39. Коганов Н. С. Основы синтеза, линейных электрических цепей во временной области. Изд-во «Связь», 1967.
40. Coguin G. A., Tiersten H. F. Analysis of the Excitation and Detection of Piezoelectric Surface Waves in Quartz by Means of Surface Electrodes. J. of the Acoustical Society of Amer. v. 41, № 4, Pt. 2, 1967.
41. Корф Ф. Импульсная УКВ станция, использующая шумоподобные сигналы. «Зарубежная радиоэлектроника», 1966, № 4.
42. Кривицкий Б. Х. Автоматические системы радиотехнических устройств. Госэнергоиздат, 1962.
43. Кузьмин С. З. Цифровая обработка радиолокационной информации. Изд-во «Советское радио», 1967.
44. Кук С. Функция предварительной корреляции сжатия импульса для уменьшения боковых лепестков в РЛС большой мощности. ТИИЭР, 1964, № 4
45. Cook C. E., Bernfeld M. Radar signals an introduction to theory and application. Academic Press, 1967.
46. Cooper D. C. Optical Signal processing. Radio & Electronical Eng., v. 32, № 1, 1966.
47. Кулаков В. К. К вопросу об отношении сигнал/шум на выходе стационарного линейного фильтра. «Вопросы радиоэлектроники», сер. общетехническая, вып. 10, 1968.
48. Куликов Е. И. О точности одного способа измерения параметра сигнала при дискретных значениях параметра опорного сигнала приемника. «Радиотехника и Электроника», 1962, № 7.
49. Lambert L. B. Wide — band instantaneous spectrum analyzers employing delay — line light modulators. IRE Int. Conv. Rec., Pt. 6, 1962.
50. Левин Б. Р. Теория случайных процессов и ее применение в радиотехнике. Изд-во «Советское радио», 1957.
51. Лезин Ю. С. Оптимальные фильтры и накопители импульсных сигналов. Изд-во «Советское радио», 1963.
52. Macdermott D. Optical data processing. Space Aeronautics, n. 1, 1963.
53. Мартин Т. Электронные цепи. Воениздат, 1958.
54. May I. E. Ultrasonic travelling wave devices for communications IEEE Spectrum, № 10, 1965.
55. Сб. статей «Физическая акустика», под ред. У. П. Мезон, часть А, т. 1. Методы и приборы ультразвуковых исследований. Изд-во «Мир», 1966.
56. Mintzer D. Y Advanced Radar Signal and Data processing. Space Aeronautics, № 6, 1962; № 4, 1963.
57. Mooney D., Ralston G. Performance in Clutter of Airborne Pulse MII. CW Doppler, and pulse Doppler Radar. IRE. Int. Conv. Rec., Pt. 5, 1961.

58. Мэзон С., Циммерман Г. Электронные цепи, сигналы и системы. Изд-во иностранной литературы, 1964.
59. Новосельцев Л. Я., Пугин Н. А. О некоторых особенностях устройства автосъема координат на основе накопителя бинарно-квантованных сигналов. «Известия высших учебных заведений МВ и ССО СССР», Радиотехника, 1967, т. 10, № 8.
60. Palfreeman J. S. An opto — acoustic cross — correlator in radar signal detection. Philips Technical Review, v. 28, № 5/6/7, 1967.
61. Pedmood M. Mechanical wavequides. Pergamon Press, London, 1962.
62. Пестряков В. Б. Фазовые радиотехнические системы. Изд-во «Советское радио», 1968.
63. Питерсон У. Коды, исправляющие ошибки. Изд-во «Мир», 1964.
64. Престон. Вычислительная машина, работающая со скоростью света. «Электроника», 1965, т. 38, № 18.
65. Rihaczek A. W. Radar waveforms for suppression of extended clutter. Trans. IEEE, AES-3, № 3, 1967.
66. Рихачек А. В. Синтез радиолокационных сигналов и улучшение разрешения целей. ТИИЭР, 1965, № 2.
67. Рихачек А. В. Разрешающие свойства импульсных последовательностей. ТИИЭР, 1964, т. 52, № 2.
68. Richard D. Microwave solid state delay. IEEE Int. Conv. Rec., Pt. 7, 1967.
69. Ричердс Р. К. Элементы и схемы цифровых вычислительных машин. Изд-во иностранной литературы, 1961.
70. Рытов С. М. Введение в статистическую радиофизику. Изд-во «Наука», 1966.
71. Rummler W. D. Clutter Suppression by Complex Weighting of Coherent Pulse Trains. Trans. IEEE, AES-2, № 6, 1966.
72. Скольник М. Введение в технику радиолокационных систем. Изд-во «Мир», 1966.
73. Соколинский А. Г., Сухаревский Ю. М. Магниевые ультразвуковые линии задержки. Изд-во «Советское радио», 1966.
74. Сорока Л. М. Лекции по голографии. Изд. Объединенного института ядерных исследований, Дубна, 1966.
75. Slobodin L. Optical correlation technique. Proc. IEEE, № 12, 1963.
76. Стратанович Р. Л., Сосулин Ю. Г. Оптимальный прием сигналов на фоне негауссовых помех. «Радиотехника и Электроника», 1966, т. 11, № 4.
77. Тафт В. А. Основы методики расчета линейных электрических цепей по заданным их частотным характеристикам. Изд-во АН СССР, 1954.
78. Тихонов В. И. Статистическая радиотехника. Изд-во «Советское радио», 1966.
79. Urkowitz H. Delay line sacondaries in Phase modulated sweep integrators. Trans. IEEE, MIL-9, № 3, 1965.
80. Уэстерфильд Л. Цифровые корреляторы со сжатием во времени и согласованные фильтры для активной гидролокации. «Зарубежная радиоэлектроника», 1964, № 12.
81. Фалькович С. Е. Прием радиолокационных сигналов на фоне флуктуационных помех. Изд-во «Советское радио», 1961.

82. Фаунер К. А. Обработка сигналов обзорного радиолокатора. «Зарубежная радиоэлектроника», 1962, № 3.
83. Felstead E. B. A simple real-time incoherent optical correlator. Trans. IEEE. AES-3. № 6, 1967.
84. Финкельштейн М. И. Гребенчатые фильтры. Изд-во «Советское радио», 1969.
85. Флек В. Спектр шума, прошедшего через ограничитель. ТИИЭР, 1966, № 1.
86. Фриз Е. А., Азарх С. Х. Пьезокерамические фильтры. Изд-во «Энергия», 1967.
87. Харкевич А. А. Теория преобразователей. Изд-во Госэнергоиздат, 1948.
88. Харли Р. Б. Логические схемы на транзисторах. Изд-во «Мир», 1965.
89. Хелстром К. Статистическая теория обнаружения сигналов. Изд-во «Советское радио», 1963.
90. Hetrich G. R. Frequency modulation techniques as applied to pulse doppler radar. IRE Int. Conv. Rec., Pt. 5, 1962.
91. Черняк Ю. Б. Квантование фазы при обнаружении сигналов на фоне шумов. «Радиотехника и электроника», 1962, № 8.
92. Черняк Ю. Б. Чувствительность, точность и разрешающая способность многоканального приемника с широкополосным ограничителем. «Радиотехника и электроника», 1962, т. 12, вып. 8.
93. Черняк Ю. Б. О линейных свойствах систем широкополосный ограничитель — фильтр. «Радиотехника и электроника», 1962, т. 12, вып. 7.
94. Черняк Ю. Б. Непараметрические фазовые методы обнаружения сигналов. «Вопросы радиоэлектроники», сер. общетехническая, 1967, вып. 5.
95. Ширман Я. Д., Голиков В. Н. Основы теории обнаружения радиолокационных сигналов и измерения их параметров. Изд-во «Советское радио», 1963.
96. Шишловский А. А. Прикладная физическая оптика. Физматгиз, 1961.
97. Штагер В. В. Полупроводниковые приборы в импульсных и коммутационных схемах. Госэнергоиздат, 1963.
98. Эпелет Дж. Обзор по ультразвуковым линиям задержки, работающим на частотах ниже 100 *Мгц*. ТИИЭР, 1965, № 10.
99. Дугин В. В. Оптимальное обнаружение сигналов с неизвестным моментом прихода на фоне нормального шума с изменяющейся во времени интенсивностью. Известия высших учебных заведений. Радиоэлектроника, том XII, 2, 1969.
100. Spafford L. J. Optimum radar signal processing in clutter. IEEE Trans. IF-14, n. 5, 1968.